UNIVERSITAT DE
BARCELONA

Entendiendo la síntesis de ADN en patógenos bacterianos: nuevas estrategias para el tratamiento de enfermedades infecciosas

Alba Rubio Canalejas

UNIVERSITAT DE BARCELONA

FACULTAD DE FARMÀCIA I CIÈNCIES DE L'ALIMENTACIÓ

Entendiendo la síntesis de ADN en patógenos bacterianos: nuevas estrategias para el tratamiento de enfermedades infecciosas

Alba Rubio Canalejas

Barcelona, 2023

UNIVERSITAT DE BARCELONA

FACULTAT DE FARMÀCIA I CIÈNCIES DE L'ALIMENTACIÓ

Programa de Doctorado en Biotecnología

Entendiendo la síntesis de ADN en patógenos bacterianos: nuevas estrategias para el tratamiento de enfermedades infecciosas

Memoria presentada por Alba Rubio Canalejas para optar al grado de doctora por la Universitat de Barcelona

Director y Tutor de la Tesis
Dr. Eduard Torrents Serra

Doctoranda
Alba Rubio Canalejas

Alba Rubio Canalejas

Barcelona, 2023

I

A mi madre

Resumen

Las ribonucleótido reductasas (RNR) son enzimas esenciales que convierten los ribonucleótidos en desoxirribonucleótidos, los monómeros utilizados en la síntesis y reparación del ADN. Existen tres clases de RNR (clase I, II y III), que se clasifican en función de su estructura, mecanismo para formar el radical, cofactores que utilizan y requisitos específicos de oxígeno. El genoma de los organismos eucariotas codifica únicamente para la ribonucleótido reductasa de clase Ia, pero hay microorganismos cuyo genoma codifica para más de una RNR. Por ejemplo, el genoma de *Pseudomonas aeruginosa* contiene información para producir las tres clases de RNR, lo que le aporta una gran ventaja para adaptarse a distintos ambientes. *P. aeruginosa* es una bacteria Gram-negativa que puede crecer formando una biopelícula (biofilm) donde hay un gradiente de la concentración de oxígeno. *P. aeruginosa* forma biofilms en tejidos del organismo y dispositivos quirúrgicos, y también se ha encontrado en biofilms polimicrobianos en heridas. Las infecciones por biofilms se consideran infecciones crónicas y son difíciles de tratar, lo que conlleva un mal pronóstico. Esto, sumado a que las terapias actuales son ineficaces, pone de manifiesto la necesidad de encontrar nuevos enfoques terapéuticos para tratar eficazmente las infecciones por biofilms.

En nuestro estudio nos centramos en el desarrollo de nuevas terapias para tratar las infecciones por biofilm. En la búsqueda de nuevas dianas moleculares, estudiamos los factores de transcripción AlgR y NrdR. En esta tesis investigamos la relación entre AlgR, clave en la formación del biofilm, y las RNR de *P. aeruginosa*. Hemos demostrado que AlgR en su estado no fosforilado activa la transcripción de las RNR bajo condiciones de estrés oxidativo cuando *P. aeruginosa* crece en forma planctónica y formando un biofilm. También determinamos que la RNR de clase II, NrdJ, es esencial durante la infección en el modelo *in vivo Galleria mellonella.*

Asimismo, estudiamos el mecanismo de activación del factor de transcripción NrdR en *P. aeruginosa* y *Escherichia coli*. En esta tesis determinamos que NrdR regula los promotores de todas las RNR en *P. aeruginosa* y *E. coli.* Según nuestros estudios, NrdR se encontraría formando poblaciones oligoméricas dinámicas en función del cofactor nucleotídico que se le una. NrdR forma grandes estructuras oligoméricas que son inactivas cuando se une ATP y estructuras entre tetrámeros y octámeros que son activas y reprimen la transcripción de las RNR cuando se une dATP.

También hemos desarrollado una nueva técnica de biología molecular, llamada ReViTA, que se basa en la transcripción *in vitro* para medir la expresión de genes cuando están regulados por factores de transcripción, y que permite estudiar la función biológica del factor de transcripción de interés.

Finalmente, estudiamos la formación de biofilms polimicrobianos de *P. aeruginosa* y *Staphylococcus aureus* en un modelo de herida *in vitro* para identificar nuevos tratamientos. Analizamos varias terapias que combinan antibióticos y enzimas disgregadoras de la matriz del biofilm solubles o inmovilizadas en nanopartículas. Los resultados apuntan a que, dentro del biofilm, las bacterias de *S. aureus* están protegidas y que las terapias que combinan enzimas y antibióticos mejoran el tratamiento del biofilm.

En conclusión, las RNR y los factores de transcripción que las regulan son posibles dianas moleculares para desarrollar nuevos enfoques terapéuticos contra las infecciones por biofilm. La técnica ReViTA puede ser útil en la identificación de nuevos factores de transcripción y en la evaluación de su papel en la regulación génica. El estudio de biofilms polimicrobianos es fundamental para entender la interacción entre diferentes especies bacterianas y desarrollar tratamientos efectivos contra las infecciones crónicas.

Abstract

Ribonucleotide reductases (RNR) are essential enzymes that convert ribonucleotides into deoxyribonucleotides, the monomers used in DNA synthesis and repair. There are three classes of RNRs (class I, II, and III), which are classified according to their structure, the mechanism to form the radical, the cofactors used, and specific oxygen requirements. The genome of eukaryotic organisms encodes only for class Ia ribonucleotide reductase, but there are microorganisms whose genome encodes for more than one RNR. For example, *Pseudomonas aeruginosa* produces all three classes of RNR, which gives it a great advantage in adapting to different environments. *P. aeruginosa* is a Gram-negative bacterium that can grow by forming a biofilm where there is a gradient of oxygen concentration. *P. aeruginosa* forms biofilms in body tissues and surgical devices and has also been found in polymicrobial biofilms in wounds. Biofilm infections are considered chronic infections and are difficult to treat, leading to a poor prognosis. This, coupled with the fact that current therapies are ineffective, highlights the need to find new therapeutic approaches to effectively treat biofilm infections.

In our study, we focused on the development of new therapies to treat biofilm infections. In the search for new molecular targets, we studied the transcription factors AlgR and NrdR. In this thesis, we investigated the relationship between AlgR, key in biofilm formation, and *P. aeruginosa* RNR. We have shown that AlgR in its non-phosphorylated state activates RNR transcription under oxidative stress conditions when *P. aeruginosa* grows planktonically and in a biofilm. We also determined that the class II RNR, NrdJ, is essential during infection in the *in vivo* model *Galleria mellonella*.

We also studied the mechanism of activation of the transcription factor NrdR in *P. aeruginosa* and *Escherichia coli.* In this thesis, we determined that NrdR regulates the promoters of all RNR in *P. aeruginosa* and *E. coli*. According to our studies, NrdR forms dynamic oligomeric populations depending on the nucleotide cofactor attached to it. NrdR forms large inactive oligomeric structures when ATP binds, and forms tetramers and octamers that are active and repress RNR transcription when dATP binds.

We have also developed a new molecular biology technique, called ReViTA, which relies on *in vitro* transcription to measure gene expression when regulated by transcription factors, and which allows us to study the biological function of the transcription factor of interest.

Finally, we studied the formation of polymicrobial biofilms of *P. aeruginosa* and *Staphylococcus aureus* in an *in vitro* wound model to identify new treatments. We analyzed several therapies combining antibiotics and biofilm matrix-disintegrating enzymes soluble or immobilized on nanoparticles. The results suggest that, within the biofilm, *S. aureus* bacteria are protected and that therapies combining enzymes and antibiotics improve biofilm treatment.

In conclusion, RNR and the transcription factors that regulate them are potential molecular targets for developing new therapeutic approaches against biofilm infections. The ReViTA technique may be useful in identifying novel transcription factors and assessing their role in gene regulation. And, the study of polymicrobial biofilms is fundamental to understanding the interaction between different bacterial species and developing effective treatments against chronic infections.

Índice

Lista de tablas y figuras

Abreviaturas

(d)NDP	(Desoxi)rribonucleótido difosfato
(d)NTP	(Desoxi)rribonucleótido trifosfato
ADNc	ADN complementario
AdoCbl	5'-Adenosilcobalamina
AMPc	Adenosina monofosfato cíclica
AMPs	*Antimicrobial peptides*, péptidos antimicrobianos
Cys	Cisteína
DOPA	Dihidroxifenilalanina
eDNA	*Extracellular DNA*, ADN extracelular
EPOC	Enfermedad Pulmonar Obstructiva Crónica
EPS	*Extracellular polymeric substance*, sustancia polimérica extracelular
FnBPs	Proteína de unión a fibronectina
FQ	Fibrosis Quística
FT	Factor de transcripción
Gly	Radical glicilo
H2O2	Peróxido de hidrógeno
IVT	in vitro *transcription*, transcripción *in vitro*
LPS	Lipopolisacárido
MSCRAMMs	*Microbial Surface Components Recognizing Adhesive Matrix Molecules*
Phe	Fenilalanina
PNAG	Poli-N-acetilglucosamina
ReViTA	*Reverse* in vitro *transcription assay*, ensayo de transcripción reversa *in vitro*
RNAP	ARN polimerasa
RNR	Ribonucleótido reductasas
ROS	*Reactive oxygen species*, especies reactivas de oxígeno
SAM	S-adenosilmetionina
SARM	*Staphylococcus aureus* resistente a meticilina
SCV	*Small colony variants*, fenotipo de pequeñas colonias
SpA	Proteína estafilocócica A
T3SS	Sistema de secreción de tipo III
T6SS	Sistema de secreción de tipo VI
TNF-a	Factor de necrosis tumoral α
TSS	*Transcripcion starting site*, sitio de transcripción inicial
TSST1	Toxina-1 de síndrome de shock tóxico
Tyr	Tirosina
UTR	*Untranslated region*, región no traducida

vWbp	Proteína de unión al factor von-Willebrand
WSM	*Wound Simulating Media*, medio de simulación de la herida
EMSA	*Electrophoretic mobility shift assay*, ensayo de desplazamiento de movilidad electroforética
WLB	*Wound like biofilm*, biofilm en herida
AgNP	Nanopartículas de plata

Introducción

1. Ribonucleótido reductasas

1.1 Importancia

Hace aproximadamente 4 billones de años comenzó la vida en la Tierra. La hipótesis que más fuerza tiene en cuanto al origen y mantenimiento de la vida es la idea del "mundo de ARN", que defiende que la vida comenzó a partir de una molécula de ARN. El ARN es una molécula químicamente frágil porque el radical hidroxilo del carbono 2' del anillo de ribosa de los nucleótidos facilita su hidrólisis (1). Este problema está subsanado en las moléculas de ADN. La reducción del radical hidroxilo (-OH) de los ribonucleótidos que forman el ARN a hidrogeno (-H) en los desoxirribonucleótidos que forman el ADN fue esencial para aumentar la estabilidad molecular, y permitió que el ADN se convirtiera en la molécula utilizada para almacenar la información genética de forma estable (2). Las enzimas encargadas de catalizar la reducción de los ribonucleótidos di o trifosfato (NDPs o NTPs, monómeros del ARN) a sus correspondientes desoxirribonucleótidos di o trifosfato (dNDPs o dNTPs, monómeros del ADN) son las ribonucleótido reductasas (RNR) (Figura 1). **Las RNR sintetizan los dNTPs y, por tanto, son enzimas esenciales en la replicación y reparación del ADN, siendo indispensables en la división celular y reproducción de las especies** (3, 4).
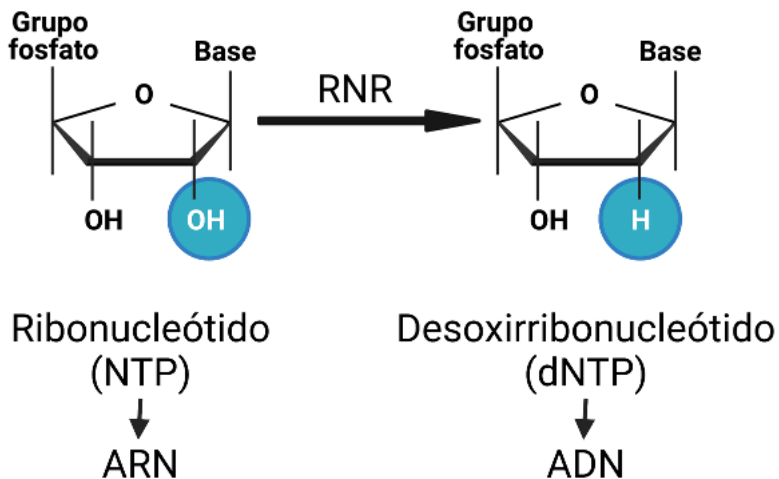
Figura 1. Versión simplificada de la actividad enzimática de las ribonucleótido reductasas. Imagen creada con Biorender.

1.2 Mecanismos de acción.

Las RNR son metaloproteínas que utilizan la química de los radicales para catalizar la reducción de todos los nucleótidos (ADP o ATP, CDP o CTP, GDP o GTP, UDP o UTP) (3, 4). La reacción está conservada y se produce mediante tres procesos: i) Primero se **genera un radical proteico a partir de un cofactor metálico**. El radical se transfiere a través de una cadena de transporte de electrones que finaliza con un radical tiílo en una cisteína (radical cisteinilo) en el centro activo de la enzima. ii) Después, **el ribonucleótido se reduce en el centro activo** de la RNR. Un único centro activo es capaz de reducir los cuatro ribonucleótidos. El radical cisteinilo activa el ribonucleótido y oxida el hidroxilo del carbono 3' de la ribosa, formando un radical de carbono 3', el hidroxilo en el carbono 2' se elimina generando una molécula de agua y finalmente el carbono 2' se reduce con dos electrones provenientes de dos cisteínas. Por tanto, la reducción del sustrato está acoplada a la oxidación de las cisteínas, formándose un puente disulfuro entre ellas (Figura 2). iii) Para terminar, **un donante de electrones externo vuelve a reducir el centro activo**. Los principales donadores de electrones son las tiorredoxinas y glutarredoxinas que dependen de tiol. Las tiorredoxinas se reducen a su vez mediante una tiorredoxina reductasa para acoplar su reducción al NADPH, y las glutarredoxinas utilizan una glutatión-reductasa para reducir el intermediario glutatión usando NADPH (3–6). Las enzimas de clase I y II (ver Tabla 1 y sección 1.3 de la introducción de esta tesis) utilizan tiorredoxina o glutarredoxina y las de clase III, utilizan formato directamente en la reacción catalítica sustituyendo a la cisteína ausente en dicha RNR, aunque hay algunas RNR de clase III que también utilizan tiorredoxinas (7, 8).
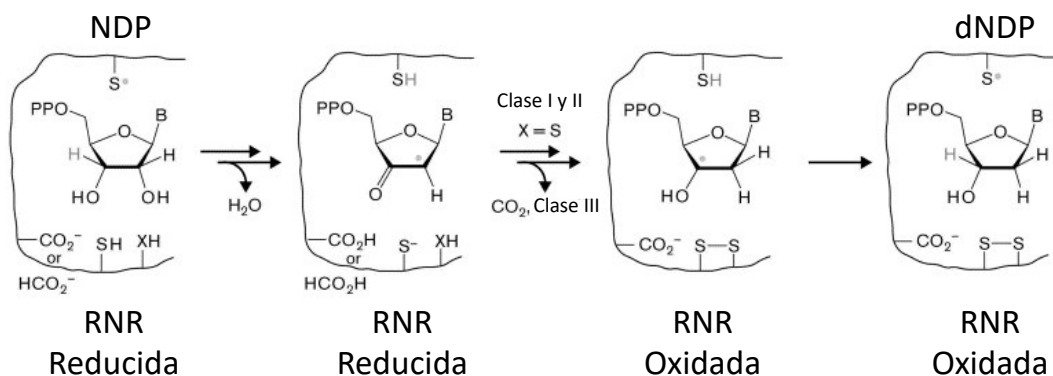
Figura 2. Mecanismo de acción de las ribonucleótido reductasas. Adaptada de (9).

1.3 Clases

Las RNR **se clasifican en tres clases (clase I, clase II y clase III)** según su estructura, la forma de generar el radical y por tanto su centro metálico, el tipo de cofactor que utilizan, el donante de electrones y su dependencia del oxígeno (3, 5). La Tabla 1 detalla Las principales diferencias entre las diferentes clases de RNR.

Aunque las distintas clases de RNR comparten menos del 20% de identidad en su estructura primaria, tienen una estructura tridimensional conservada y un mecanismo catalítico común, lo que sugiere un **mismo origen evolutivo** (4). Se cree que la primera RNR se originó durante la **transición del mundo de ARN al de ADN**, antes de la presencia de oxígeno en la Tierra, y probablemente se parecía más a la RNR de clase II o de clase III. A medida que comenzó la producción de oxígeno, surgieron las diferencias entre las distintas clases de RNR para adaptarse a las nuevas condiciones ambientales, siendo la RNR de clase I la más reciente (4).

Tabla 1. Características de las distintas clases de RNR. Adaptada de (4).

	Clase I					Clase II	Clase III
	Clase Ia	Clase Ic	clase Id	Clase Ib	Clase Ie		
Genes	***nrdAB***			***nrd(HI)EF***		***nrdJ***	***nrdDG***
Subunidad catalítica	NrdA (α)			NrdE (α)		NrdJ (α)	NrdD (α)
Subunidad activadora	NrdB (β)			NrdF (β)			
Proteína activadora				NrdI			NrdG (β)
Estructura	$\alpha_2\beta_2/\alpha_6\beta_6$			$\alpha_2\beta_2$		α/α_2	$\alpha_2 + \beta_2$
Radical	Tyr -> Cys	Phe -> Cys	Tyr -> Cys	Tyr -> Cys	DOPA -> Cys	AdoCbl -> Cys	AMet->Gly->Cys
Centro metálico	FeIII/FeIII	MnII/FeIII	MnIII/MnIV	FeIII/FeIII MnIII/MnIII		AdoCbl (Co)	SAM (FeIV-SIV)
Sustrato	NDPs					NDPs y NTPs	NTPs
Oxígeno	Dependiente					Independiente	Sensible
Donador electrones	Tiorredoxina/ Glutarredoxina			NrdH-Redoxina		Tiorredoxina	Formato/ Tiorredoxina

La diversidad de RNR permite a los organismos adaptarse a condiciones ambientales diversas. Mientras que el genoma de organismos eucariotas solo codifica para la RNR de clase Ia, el genoma de la mayoría de los procariotas tiene información para codificar al menos dos clases de RNR (4, 9). La capacidad de sintetizar distintas RNR les permiten adaptarse a diversas condiciones de oxígeno y a la presencia de distintos cofactores y donadores de electrones.

1.3.1 Clase I

La RNR de clase I es la primera que se descubrió. Se describió por primera vez en el organismo modelo *Escherichia coli* en 1960 y actualmente se considera el prototipo de RNR de clase Ia (10). Se han encontrado RNR de clase I en todos los organismos eucariota, en virus eucariotas, en especies de Archaea y Bacteria, así como en bacteriófagos. Las RNR de clase I utilizan NDPs como sustrato y, aunque pueden tener diferentes cofactores en su centro metálico, **dependen por completo del oxígeno** para realizar su proceso catalítico (5).

Estas enzimas están formadas por **dos subunidades homodiméricas:** la subunidad mayor α (o R1) y la subunidad menor β (o R2). **La subunidad mayor contiene el centro activo** y hasta dos sitios alostéricos diferentes que regulan la actividad global y la especificidad de la enzima. **La subunidad menor β (o R2) contiene la maquinaria necesaria para generar los radicales y es donde se sitúa el cofactor metálico** necesario para iniciar el proceso catalítico (Figura 3). El radical que inicia la reacción se produce inicialmente en un residuo de tirosina o fenilalanina en la subunidad β y se transfiere a un residuo de cisteína en el centro activo de la subunidad α. La estructura cuaternaria activa más común entre las RNR de clase I es la forma $\alpha_2\beta_2$, pero también se encuentra la forma $\alpha_6\beta_6$ (3, 11–13).
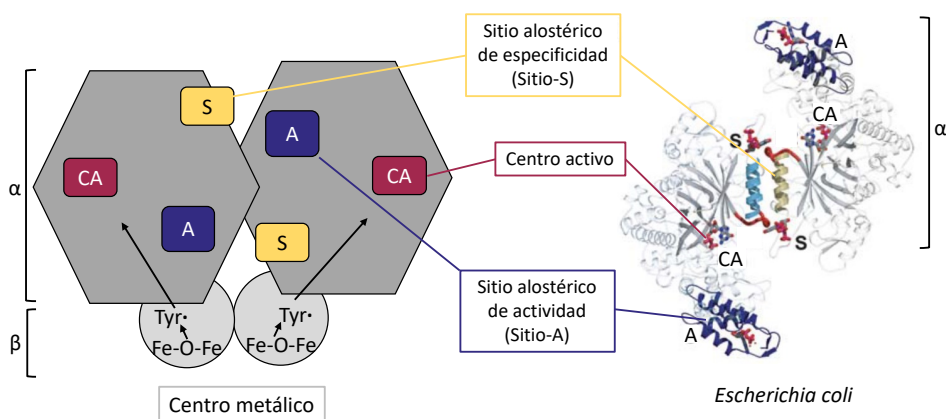
Figura 3. Estructura de la RNR de clase Ia de *E. coli*. Representación de las subunidades α y β de forma esquemática (izquierda) y tridimensional (derecha). El centro activo de la enzima (CA) se indica en color burdeos, el sitio alostérico de especificidad (S) se indica en color amarillo, el sitio alostérico de actividad (A) se indica en azul, y el centro metálico de la subunidad β (Fe-O-Fe) se indica en gris. Tyr· corresponde a radical tílo. Imagen adaptada de (13).

La clase I se subdivide, a su vez, en cinco subclases diferentes: Ia, Ib, Ic, Id y Ie, según la presencia o ausencia de sitios alostéricos, el cofactor metálico que utilizan y el aminoácido donde se genera el radical (5, 14–16). Todas las subclases, excepto la RNR de clase Ie, tienen un centro di-metálico en la subunidad β de la enzima (17). A continuación, se explica cada subclase con más detalle.

La **subclase Ia** es la primera RNR descubierta y se describió en *E. coli* en 1960 (10). En bacterias, los genes *nrdAB* codifican para las subunidades α (NrdA) y β (NrdB). Estas enzimas necesitan un centro diférrico (Fe^{III}-O-Fe^{III}) que se encuentra en la subunidad β para formar el radical tirosilo inicial, y dos sitios alostéricos de regulación: el de especificidad y el de actividad en la subunidad α (5, 12).

La **subclase Ib** solo se ha encontrado en bacterias y bacteriófagos y se describió por primera vez en *Salmonella typhimurium* (18). Está codificada por el operón *nrdHIEF*, donde los genes *nrdE* y *nrdF* codifican para la subunidad α y β, respectivamente. *nrdH* codifica para una proteína similar a la glutarredoxina, y *nrdI* para una flavodoxina necesaria en la síntesis y mantenimiento de su centro metálico (5, 11, 19). El cofactor metálico de la clase Ib es un centro dimanganeso (Mn^{II}/Mn^{II}) que se encuentra en NrdF, aunque la enzima también se mantiene activa con un centro Fe^{III}-O-Fe^{III} (20–23). La subunidad α de la clase Ib también tiene el centro activo de la enzima y el sitio alostérico de especificidad, pero no el de actividad global (4, 9).

La RNR de **clase Ic** está limitada a bacterias y se descubrió por primera vez en *Chlamydia trachomatis* (4, 24). Los genes *nrdA* y *nrdB* codifican para las subunidades α y β, respectivamente, igual que en la RNR de clase Ia, pero su cofactor metálico está formado por un centro de manganeso y hierro (Mn^{IV}-O-Fe^{III}) que forma un radical en una fenilalanina en lugar de la tirosina de las clases Ia y Ib (25, 26). Este radical se transfiere a la subunidad catalítica, NrdA, que es notablemente más grande que la de la clase Ia debido a una duplicación del sitio catalítico (24).

La nueva **subclase Id** se ha descrito recientemente en *Flavobacterium johnsoniae* y *Actinobacillus ureae* (14, 15). Los genes *nrdAB* codifican para las subunidades α y β, y al igual que en la subclase Ib, en la clase Id se conforma un centro Mn^{II}/Mn^{II} en su subunidad β. Este centro metálico se oxida utilizando anión superóxido (O$_2^{-}$) capturado del medio para general el primer radical (15).

La última subclase descrita hasta la fecha es la **clase Ie,** presente en algunas bacterias como *Streptococcus pyogenes* y *Aerococcus urinae*, y que análoga a la subclase Ib, ya que está codificada por los genes *nrdHIEF* (16, 17, 27)*.* La peculiaridad de esta nueva RNR es que su subunidad β no necesita metales para formar un radical estable, sino que la presencia de O_2 permite oxidar una tirosina modificada de manera postraducional para generar el radical. Esto proporciona una gran ventaja al patógeno durante la infección (16, 17, 27).

1.3.2 Clase II

La enzima de clase II se aisló por primera vez en *Lactobacillus leichmannii,* y está presente en bacterias, arqueas, bacteriófagos y algunos eucariotas como hongos y algas unicelulares (28–30)*.* Esta clase de RNR utiliza nucleótidos di- o trifosfato como sustrato y presenta un mecanismo catalítico diferente, ya que **su actividad es independiente de la presencia de O_2 y necesita el cofactor 5'adenosilcobalamina** (AdoCbl) para generar el radical proteico estable y ser activa en las rondas de catálisis (4, 9).

Estas enzimas están **formadas por un único polipéptido, la subunidad α** (NrdJ), codificado por el gen *nrdJ*, que en algunos organismos como *Pseudomonas aeruginosa* se encuentra dividido en dos unidades transcripcionales (*nrdJa* y *nrdJb*) formando parte del mismo operón (31, 32). **La estructura cuaternaria activa de la enzima puede ser** un monómero, como en *L. leichmannii*, o un dímero como en *Thermotoga maritima* (**α o α$_2$**, Figura 4) (28, 33).

Tanto el centro activo como el sitio alostérico de la enzima se encuentran en la proteína. Algunos organismos, como *Thermoplasma acidophilum*, tienen una enzima que también presenta un sitio alostérico de actividad, pero la mayoría solo contienen el de especificidad (4, 13, 32). Durante la catálisis, el metalocofactor 5'-desoxiadenosilcobalamina, una modificación de la vitamina B_{12}, se sitúa cerca del centro activo y el átomo de cobalto que tiene se utiliza para generar el radical 5'-desoxiadenosil (34–36). Este radical genera posteriormente el radical tiílo en las cisteínas conservadas del centro activo que al reducir el sustrato se oxidan formando un puente disulfuro (37). El centro activo de NrdJ se regenera gracias a la acción de tiorredoxinas y glutarredoxina (13, 38).
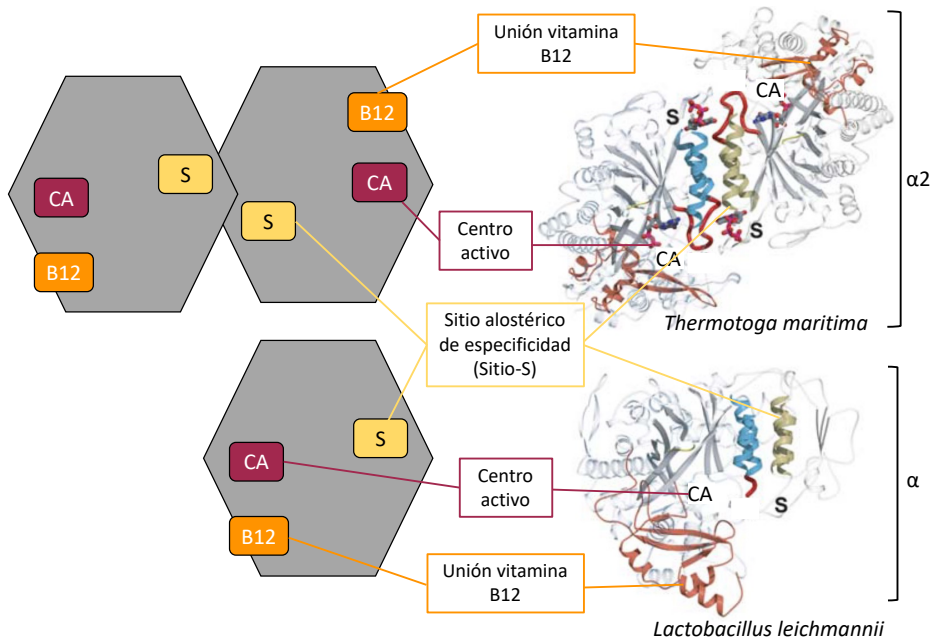
Figura 4. Estructura de la RNR de clase II de *Thermotoga marítima* y *Lactobacillus leichmanni*. Representación de la subunidad α de forma esquemática (izquierda) y tridimensional (derecha). El centro activo de la enzima (CA) se indica en color burdeos, el sitio alostérico de especificidad (S) se indica en color amarillo y el sitio de unión a la vitamina B_{12} se indica en naranja. Imagen adaptada de (13).

1.3.3 Clase III

La última clase de RNR se descubrió en 1989 en cultivo anaeróbicos estrictos de *E. coli.* Desde entonces, se han encontrado en otras bacterias, arqueas y algunos bacteriófagos, siendo las enzimas del bacteriófago T4 (*Escherichia virus* T4, Figura 5) y de *Lactococcus lactis* las más estudiadas en la actualidad (39–43). **La enzima de clase III es sensible al oxígeno y requiere S-adenosilmetionina (SAM) como cofactor** para reducir los NDPs y NTPs que utiliza como sustrato (4, 9, 44).

Las RNR de clase III necesitan dos proteínas independientes, NrdD y NrdG, codificadas por el operón *nrdDG*, para ser realizar su actividad catalítica (4, 9, 13). **La proteína catalítica α** es el polipéptido NrdD, y en ella **se encuentra el centro activo y los dos sitios de regulación alostérica** para especificidad y actividad global (4). NrdD **depende de la activasa β**, NrdG, para ser activa (45). Estas proteínas se encuentran *in vivo* como **dos homodímeros independientes** (**α₂ + β₂**) que se unen para realizar la reducción de los nucleótidos.

NrdG contiene en su centro metálico un clúster 4Fe-4S que rompe SAM para generar el radical 5'-desoxiadenosil (46–49). Este radical se transfiere a una glicina de la proteína NrdD formando un radical glicilo que es altamente sensible al oxígeno (Figura 5) (50). Además, el centro metálico de NrdG se oxida y desordena en presencia de oxígeno (13, 51–53). Debido a estos dos factores es imprescindible que la reacción catalítica se lleve a cabo en condiciones anaeróbicas estrictas. El radical glicilo se transfiere a una cisteína de NrdD para formar el radical tiílo y reducir el ribonucleótido (50). El centro activo se regenera al oxidar una molécula de formato, a diferencia de las clases I y II que utilizan tiorredoxinas y glutarredoxinas (50, 54).
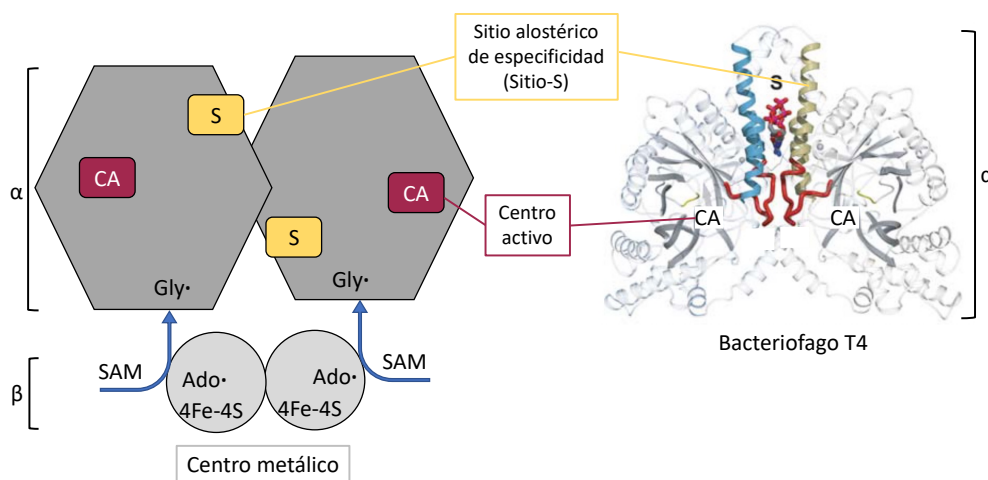
Figura 5. Estructura de la RNR de clase III del bacteriófago T4. Representación de la subunidad α de forma esquemática (izquierda) y tridimensional (derecha). El centro activo de la enzima (CA) se indica en color burdeos, el sitio alostérico de especificidad (S) se indica en color amarillo y el centro metálico de la subunidad β (4Fe-4S) se indica en gris. SAM corresponde a S-adenosilmetionina, Gly· a radical glicilo y Ado· a radical 5'-desoxiadenosil. Imagen adaptada de (13).

1.4 Regulación

Es importante que las RNR estén regulada a nivel transcripcional y de actividad enzimática para **mantener un equilibrio entre ribonucleótidos y desoxirribonucleótidos**, y que la **reserva de los cuatro dNTPs esté equilibrada**. De esta forma, se evita un aumento de las tasas de mutación y se mantiene la fidelidad a la hora de replicar el ADN (55–57). La actividad de las RNR se puede regular de forma alostérica o durante la transcripción. En la introducción de esta tesis nos centraremos en más detalle en la regulación transcripcional de las RNR bacterianas (58).

1.4.1 Regulación alostérica

Además del centro activo donde se pueden reducir los cuatro NDPs/NTPs a sus correspondientes dNDPs/dNTPs, las RNR presentan en su estructura sitios específicos para regular de forma alostérica la síntesis de desoxirribonucleótidos y así mantener la reserva de dNTPs equilibrada (3, 55, 59). Esta regulación se lleva a cabo mediante **moléculas efectoras** que, al unirse a los sitios alostéricos, **provocan cambios conformacionales en las RNR, modificando su actividad** (60). Los sitios de regulación alostérica regulan la especificidad del sustrato y la actividad global de la enzima.

Todas las RNR tienen en su estructura un **sitio alostérico de especificidad (sitio-S).** Cuando un nucleótido específico (efector) se une al sitio-S, se producen cambios estructurales en la proteína para adaptar su centro activo a un sustrato concreto. Se ha descrito que cuando ATP o dATP se unen al sitio-S, la enzima reduce CDP o CTP y UDP o UTP; cuando se une dGTP, la enzima reduce ADP o ATP; y, cuando se une dTTP, la enzima reduce GDP o GTP (Figura 6) (4, 60). De esta forma, se controla que la reserva de los cuatro dNTPs esté equilibrada. El mecanismo del sitio alostérico de especificidad es muy similar para todas las RNR (clase I, II y III) (60, 61).
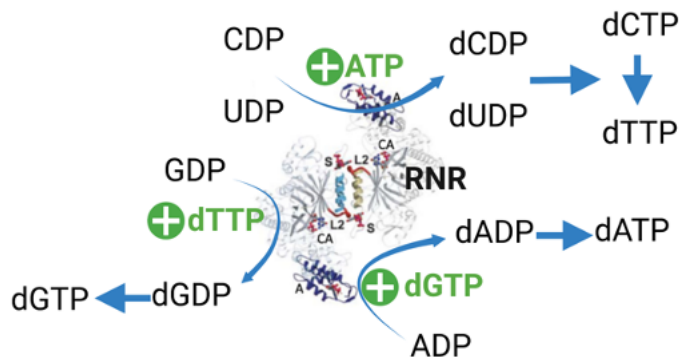
Figura 6. Modelo de la regulación alostérica de la RNR de clase Ia. En función del nucleótido que se une al sitio de especificidad de la enzima (signo positivo verde), se promueve la reducción de los NDPs a sus correspondientes dNDPs, y posteriormente éstos se pueden convertir en dNTPs (líneas azules). Imagen creada con Biorender.

El segundo sitio alostérico es el **sitio de actividad global (sitio-A),** que se encuentra en las RNR de clase I y es el responsable de regular la actividad catalítica global de la enzima y que utiliza ATP y dATP como efectores (62). El sitio-A se encuentra en el extremo N-terminal

de la proteína, en el dominio estructural denominado cono-ATP (63). La unión del efector (ATP o dATP) al cono-ATP provoca un cambio estructural en la enzima que afecta a la estructura cuaternaria de ésta, modificando directamente su actividad global (64, 65). La unión de ATP aumenta la actividad enzimática y la unión de dATP la disminuye (66). La afinidad del dATP por el sitio-A es menor que por el sitio-S para evitar que la enzima se bloquee por completo (65). De esta forma se controla la reserva global celular de dNTPs. El sitio-A está presente en la algunas RNR de clase I (47%), en pocas RNR de clase II (7%) y en la mayoría de RNR de clase III (76%) (67).

1.4.2 Regulación transcripcional

1.4.2.1 General

La regulación transcripcional se encarga de **ajustar la expresión génica de las RNR en dos momentos principales: cuando hay gran demanda de dNTPs**, por ejemplo, en las primeras etapas de la división celular o si hay daño en el ADN; **y cuando el organismo codifica para más de una clase de RNR**, como ocurre en la mayoría de las especies bacterianas (4, 9, 58). En estos organismos, es habitual que haya una RNR predominante cuya expresión esté regulada por el ciclo celular y que la transcripción del resto de RNR se active ante condiciones específicas, como cambios metabólicos o frente a la ausencia de algún metabolito, para que así el crecimiento celular se pueda adaptar a las distintas condiciones ambientales (4, 9). En este trabajo, nos centramos en la regulación transcripcional de las RNR de *E. coli* y *P. aeruginosa*.

El genoma de *E. coli* codifica para dos RNR de la clase I (Ia y Ib). El operón *nrdAB*, que codifica para **la RNR de clase Ia**, está regulado por varios factores transcripcionales conocidos, incluyendo DnaA, Fis, IciA, CRP, H-NS y NrdR (68). **DnaA** es el principal iniciador de la replicación en bacterias y su expresión aumenta durante la replicación o ante daños en el ADN, ya que está regulado por el ciclo celular (58, 69–72). El complejo DnaA-ATP se une a dos cajas en las posiciones -48 pb y -36 pb con respecto al sitio de inicio de la transcripción (TSS), favoreciendo la expresión de *nrdAB* (58, 68, 73, 74). **Fis** es otra proteína relacionada con la iniciación de la replicación, y actúa induciendo la transcripción de *nrdAB* mediante su unión en varios puntos del promotor (68, 75). **IciA** es un inhibidor de la iniciación de la replicación del ADN (70, 76). **CRP** es la proteína receptora del AMP cíclico (AMPc) que, tras acoplarse a AMPc, se une en una en la posición -136 pb (71). Finalmente, la proteína **H-NS** es un represor transcripcional global de genes regulados por el medio

ambiente (72). El regulador **NrdR** es un represor global de la transcripción de las RNR en bacterias que se detalla en la sección 1.4.2.2 de la introducción de esta tesis. Estos factores de transcripción se muestran en la Figura 7-A.

También se ha descubierto que las **RNR de clase Ia pueden estar reguladas a nivel post-transcripcional por riboswitches.** En el caso de *Streptomyces coelicolor*, la RNR de clase Ia está regulada por un riboswitch controlado por la vitamina B_{12} en la región 5' UTR del mRNA *nrdABS* (77)*.*

La regulación transcripcional de la RNR de **clase Ib** no está tan bien estudiada como la de la clase Ia, pero se ha descrito que su operón, *nrdHIEF*, está reprimido por **NrdR** y por la proteína **Fur** en presencia de hierro. En consecuencia, es probable que la expresión de esta RNR se active en condiciones de privación de hierro, cuando hay limitación de nutrientes y en momentos de alto estrés oxidativo, ya que su cofactor metálico es un centro de di-manganeso en lugar de di-hierro (78). La Figura 7-B muestra de forma esquemática el promotor de *nrdE* con sus factores de transcripción identificados.

Por último, la **RNR de clase III** se encuentra codificadas por *nrdDG* en *E. coli.* Además de por **NrdR**, están reguladas el regulador del metabolismo anaeróbico **Fnr**, que se une al promotor de *nrdDG* en las posiciones -65 pb y -35 pb desde el TSS (Figura 7-C) (79, 80). Esta proteína es responsable de que aumente la expresión de la clase III bajo anaerobiosis y en la fase estacionaria.
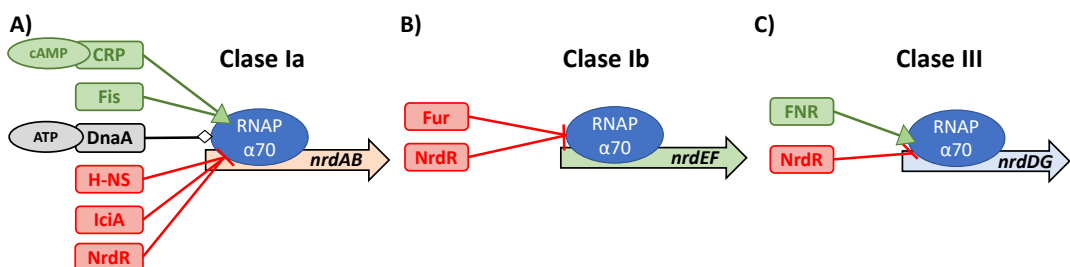
Figura 7. Regulación transcripcional de las RNR de *E. coli.* Los factores de transcripción (FT) que se muestran en verde activan la transcripción de la RNR. En cambio, los FT en rojo la inhiben y en gris, activan o reprimen la transcripción en función de otros factores.

Uno de los pocos microorganismos cuyo genoma codifica para las tres clases diferentes de RNR es *P. aeruginosa* (4). Su genoma codifica para la **RNR de clase Ia, II y III.** La expresión de la **RNR de clase I**, cuyo operón *nrdAB* produce las proteínas NrdA y NrdB, está regulada

por los factores transcripcionales **NrdR y AlgR** (81, 82). Hablaremos con más detalle de NrdR y AlgR en las secciones 1.4.2.2 y 3.1.2.1 de la introducción de esta tesis, respectivamente. Además, en la región promotora de *nrdA* también se encuentra una región larga no traducida (UTR). Estos factores se indican en la Figura 8-A. Cabe destacar que la proteína NrdA de *P. aeruginosa* presenta una duplicación del cono-ATP involucrado en la regulación alostérica que puede intervenir en la unión NrdA-NrdB y que hace que su secuencia codificante sea 202 residuos más larga que la secuencia de *E. coli* (83)*.*

P. aeruginosa también codifica para la **RNR de clase II**, cuya regulación transcripcional no está muy detallada hasta la fecha. Los factores transcripcionales que se han descrito hasta ahora y que se unen al promotor de *nrdJ* son **NrdR**, AlgR y Anr (Figura 8-B) (81, 84, 85). **AlgR** Se une al promotor de *nrdJ* y activa su transcripción durante la fase estacionaria y en la formación de biofilm (81). **Anr/Dnr** activa la transcripción de la RNR de clase II en condiciones de privación de oxígeno y durante la formación de biofilm (85).

Finalmente, la **RNR de clase III** también se codifica por *nrdDG* en *P. aeruginosa.* Esta RNR de clase III está regulada por **NrdR** y **Anr/Dnr**, que es un factor transcripcional involucrado en el metabolismo anaeróbico (Figura 8-C). Por lo tanto, la falta de oxígeno activa la transcripción de esta enzima (86). Cabe destacar que el promotor de la clase III de *P. aeruginosa* PAO1 presenta una mutación en la caja Anr/Dnr, por lo que la producción de esta enzima en esta cepa es más ineficiente que en otras cepas de *P. aeruginosa* (86).
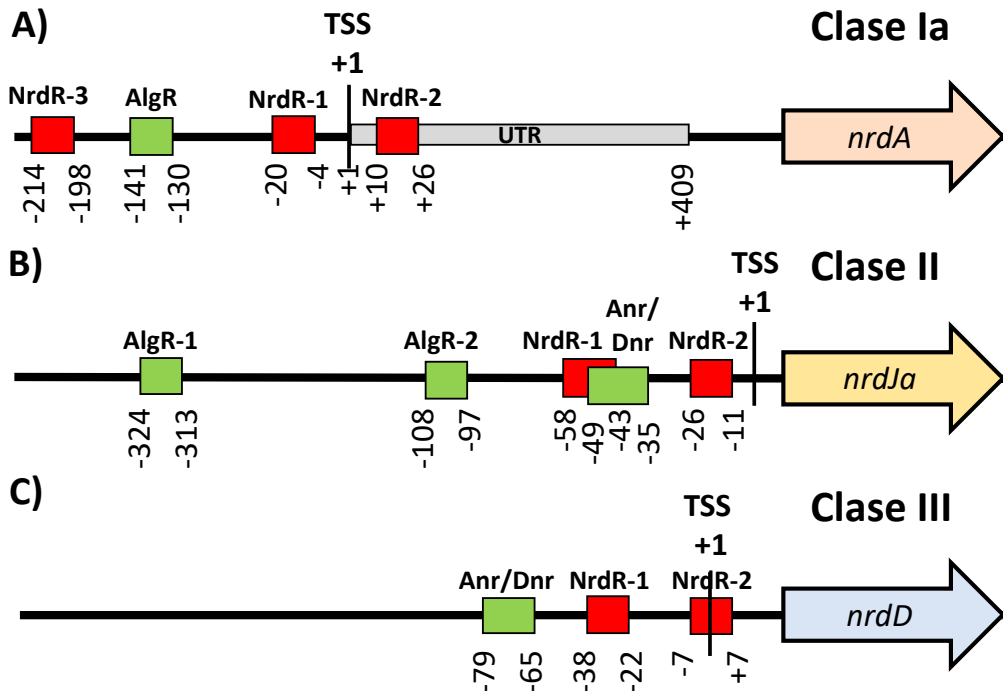
Figura 8. Esquema de las regiones promotoras de las RNR de *P. aeruginosa*. Los cuadrados indican las zonas de unión (cajas) de los factores de transcripción que regulan las RNR. Las cajas en verde activan la transcripción de la RNR, y las cajas en rojo la inhiben. Los números indican la posición de las cajas en los promotores en relación con el sitio de inicio de la transcripción (TSS, +1).

1.4.2.2 NrdR

El NrdR es un factor de transcripción que se detectó por primera en un estudio computacional en 2005. No fue hasta más adelante cuando se realizaron los experimentos en *S. coelicolor*, en cuyo genoma *nrdR* se encuentra junto al gen *nrdJ* (87, 88). **NrdR reprime la transcripción de todas las RNR de bacterias** y está ausente en arqueas y eucariotas (4). La proteína funciona como un **sensor de dNTPs para regular y ajustar la red de RNR** y mantener equilibradas las reservas de NTPs y dNTPs de la célula (89).

La proteína NrdR se une a las regiones promotoras de todas las RNR reconociendo **secuencias repetidas palindrómicas de 16 pb denominadas "cajas NrdR"** (90). Además, las cajas NrdR están normalmente localizadas interfiriendo con las secuencias consenso del promotor basal, lo que permite reprimir transcripcionalmente la expresión de las RNR (90–93). La función de NrdR se elucidó mediante análisis mutacionales y ensayos de gen reportero en *E. coli* (92).

La estructura tridimensional de NrdR está compuesta por un **dominio dedo de Zn en el extremo N-terminal, una cola ácida en el extremo C-terminal y un cono-ATP en la región central** (4, 91, 94). El dominio dedo de Zn tiene cuatro residuos de cisteína que se unen a átomos de zinc y que permiten reconocer las secuencias de ADN para que se genere el complejo ADN-proteína (95). La estructura del cono-ATP es muy similar al sitio de regulación alostérica de las RNR de clase I y II, lo que sugiere que la función de NrdR se lleva a cabo mediante un tipo de regulación alostérica simple (Figura 9) (91, 96).

Además de la estructura terciaria, NrdR puede encontrarse en **distintas formas oligoméricas**, y el grado de oligomerización depende en gran medida del nucleótido unido al domino del cono-ATP (92, 94). Recientemente se ha publicado un estudio en el que se resuelve la estructura cuaternaria de la proteína NrdR en *S. coelicolor* (89). En este trabajo se sugiere que la forma activa de la proteína se genera cuando se forma un octaedro al que se une una molécula de dATP y de ATP en cada monómero. A partir de este octaedro se genera un tetraedro que se une al ADN reprimiendo a las RNR. Cuando la cantidad de dATP baja, la proteína forma un dodecaedro cargado con dos moléculas de ATP que no puede unirse al ADN. De esta forma, mediante un mecanismo alostérico que mide los cambios en la reserva global de dNTP/NTP, se regula la transcripción de las RNR (89).
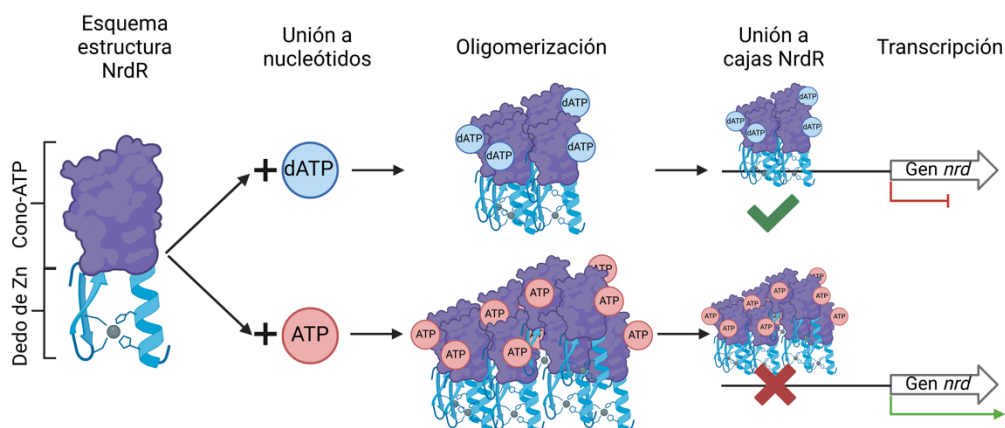
Figura 9. Mecanismo de acción hipotético de NrdR. En función del nivel celular de dNTPs y NTPs se desarrollaría un cambio conformacional en NrdR, haciendo que se una al promotor de los genes *nrd* reprimiendo su expresión, o se libere favoreciendo su transcripción. Imagen creada con Biorender.

Debido a que el factor **NrdR puede reprimir todas las RNR de una bacteria**, es importante que su **expresión esté cuidadosamente regulada** para evitar la falta total de dNTPs.

La regulación de NrdR sigue siendo objeto de investigación y hasta el momento se han localizado dos sitios de unión a NarL en la región promotora de NrdR, situados en las posiciones -18 pb y -40 pb desde el TSS (82). NarL es un factor transcripcional involucrado en metabolismo del nitrógeno que es fundamental para la respiración en condiciones anaeróbicas. Se ha demostrado que NarL es responsable de la expresión del gen *nrdR* en condiciones anaeróbicas (82). Aunque se cree que debe haber otros factores involucrados en su regulación, actualmente no se conocen todos los mecanismos que regulan NrdR.

2. Biofilm

El Dr. John William Costerton acuñaría el término biopelícula (biofilm) para definir **comunidades bacterianas, a menudo polimicrobianas, que pueden utilizar una superficie biológica o inerte, para adherirse y crecer** (97, 98). Para que una comunidad de bacterias sea considerada un biofilm es necesario que las células se encuentren **embebidas dentro de una matriz extracelular** hidratada producida por los microorganismos que lo habitan y formada principalmente por proteínas, polisacáridos y ADN extracelular (eDNA) (99). La matriz protege a las bacterias de agresiones externas como la desecación, cambios de temperatura u osmolaridad en los biofilms que se forman en la naturaleza; y del sistema inmune del huésped (fagocitosis, anticuerpos y estrés oxidativo) y de la mayoría de los antibióticos en los biofilms clínicos (99–102). En las bacterias que forman un biofilm se desencadenan cambios transcriptómicos que desembocan en cambios fenotípicos, como la eliminación de fimbrias y flagelos; y de metabolismo que les permiten adaptarse a las nuevas condiciones de crecimiento (103, 104). Por ejemplo, debido a la alta densidad celular, la difusión de moléculas se ve dificultada y se generan varios **gradientes de concentración de nutrientes, oxígeno y otros productos metabólicos**; por tanto, es necesario tener un metabolismo adaptado a las diferentes capas del biofilm (98). Además, la **baja penetración de los compuestos antimicrobianos** a través de la matriz y las **bajas tasas de crecimiento y metabólicas otorgan tolerancias antimicrobianas** a las bacterias que se encuentran embebidas en él, haciendo que se necesiten **concentraciones de antibiótico hasta 1000 veces superiores** en comparación a las bacterias que viven de forma libre (105). Los biofilms en el entorno clínico pueden producirse sobre los tejidos del huésped, generando colitis, uretritis, vaginitis, en heridas formando úlceras diabéticas y en pulmones de pacientes generando bronquiectasias como la Fibrosis Quística (FQ) y la Enfermedad Pulmonar Obstructiva Crónica (EPOC) (106, 107). También pueden encontrarse sobre dispositivos médicos como implantes, catéteres, etc (108). Así mismo, el desarrollo de biofilm durante las infecciones crónicas se asocia a un **mal pronóstico, un empeoramiento de la enfermedad y un aumento de la mortalidad** (107).

2.1 Formación

La formación del biofilm comienza en **respuesta a estímulos ambientales** como cambios en el contenido nutricional, temperatura, pH, oxigeno, e incluso el estrés producido por concentraciones subinhibitorias de antibióticos en el entorno clínico (102, 109). La formación del biofilm es un proceso complejo que engloba las siguientes fases: 1)

adhesión inicial y posteriormente irreversible mediante la producción de matriz extracelular, 2) desarrollo y maduración del biofilm y 3) dispersión (110, 111). Aunque tradicionalmente se ha ligado la formación de biofilms a la adhesión sobre superficies, recientes estudios indican que **la presencia de una superficie viva o inerte no es determinante para el crecimiento en forma de biopelículas**. La propia agregación bacteriana sería suficiente para que comience la producción de la matriz extracelular característica (Figura 10) (112).

1)   La **adhesión inicial** conlleva la formación de una monocapa de bacterias que se adhieren mediante polímeros específicos a la especie microbiana. Al finalizar la fase, la adhesión es tan fuerte que se considera irreversible (113, 114).

2)   El **biofilm completo se desarrolla** conforme se produce la matriz extracelular, lo que permite la unión entre los microorganismos y la formación de capas para generar microcolonias, que son agregados bacterianos compactos rodeados de matriz extracelular (113). El biofilm adquiere la arquitectura tridimensional típica a partir de las microcolonias, utilizando los canales líquidos entre ellas para obtener nutrientes y oxígeno, y eliminar los desechos (115). En este punto los sistemas de quorum sensing cobran mucha relevancia, ya que permiten la comunicación bacteriana para coordinar la expresión genética en función de parámetros como la densidad celular (116). De esta forma se consigue un biofilm maduro.

3)   En la **fase de dispersión** se destruye parte de la estructura del biofilm mediante enzimas y surfactantes para liberar bacterias otros microorganismos y que éstos colonicen una nueva superficie. Así comenzaría de nuevo el proceso de formación del biofilm (102). Además, los surfactantes matan a los leucocitos evitando que se pueda generar inmunidad (117).
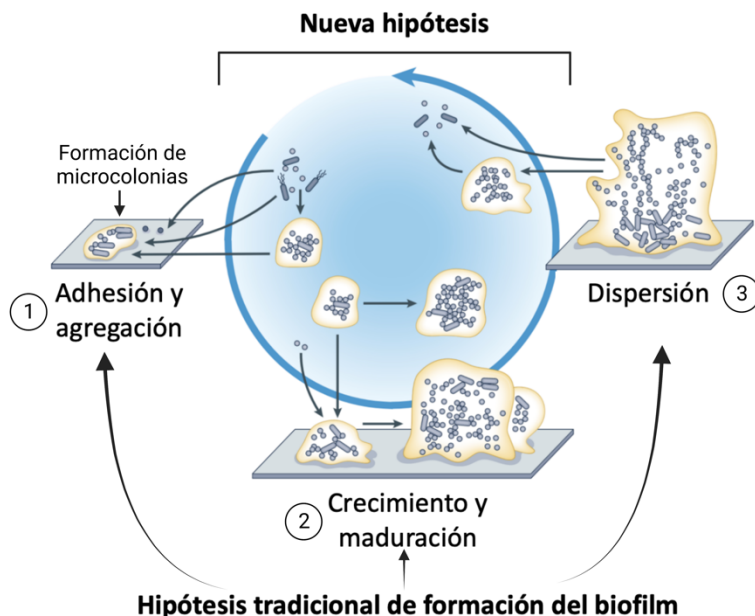
Figura 10. Fases de la formación del biofilm en las hipótesis propuestas hasta el momento. Se distinguen tres fases: 1) Adhesión y agregación, 2) Crecimiento y maduración, y 3) Dispersión del biofilm maduro. Imagen adaptada en Biorender de (112).

2.2 Matriz

Un biofilm está compuesto por células microbianas, que corresponden al 10% de la biomasa total del biofilm, y una mezcla de biopolímeros que forman la matriz, también conocida como sustancia polimérica extracelular (EPS), que representa el 90% de la masa total del biofilm (118). La EPS está formada principalmente por exopolisacáridos, proteínas, eDNA, lípidos y agua (Figura 11) (119).

Los **exopolisacáridos** son polímeros de monosacáridos que se secretan para formar parte de la matriz y son esenciales para el correcto desarrollo de la estructura del biofilm (120, 121). La composición de los exopolisacáridos dentro del biofilm depende de cada especie microbiana que lo forma.

La mayoría de las **proteínas** de la matriz son enzimas involucradas en la degradación de los polímeros de la EPS, como glucosidasas, proteasas, desoxiribonucleasas y lipasas. La degradación de los polímeros es importante para proporcionar una fuente de energía y carbono, así como durante la fase de dispersión del biofilm (122, 123). También se encuentran en este grupo proteínas que intervienen en la adhesión a superficie y entre microorganismos.

El **eDNA** desempeña una función estructural importante dentro del biofilm debido a su capacidad de adhesión entre microorganismos y a superficies (124). También participa en la patogenicidad bacteriana al evitar que los agentes antimicrobianos catiónicos se transporten dentro de la EPS gracias a su carga negativa, lo que favorece la resistencia antibiótica (125). La hipótesis más respaldada sobre el origen del eDNA *in vitro* es que se obtiene a partir de la lisis bacteriana dentro del biofilm (126). En los biofilms *in vivo*, puede provenir de la lisis de células del sistema inmune, acumulándose en las zonas más externas (127).

Los **lípidos** de la matriz actúan como surfactantes para dispersar las sustancias hidrofóbicas y permitir que los microorganismos puedan aprovecharlas. También pueden intervenir en la adhesión celular (128).

El **agua** es el componente más abundante. Mantiene el biofilm hidratado y protege a las bacterias contra la desecación (118).

La EPS es responsable de la unión entre microorganismos y superficies, y actúa como barrera protectora protegiendo a las células de agentes externos, del sistema inmune del huésped, y de procesos de desnutrición o desecación. Dependiendo de la especie y de la disposición nutricional los componentes de la matriz cambian, haciendo que se adopten diferentes estructuras. Este hecho, sumado a la gran plasticidad del biofilm permite a los microorganismos adaptarse a multitud de ambientes.
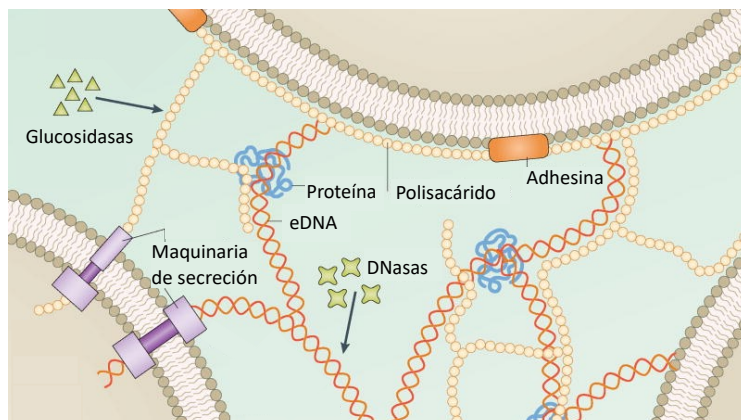
Figura 11. Componentes de la EPS del biofilm en la que varias células están interconectadas. Entre los componentes se pueden observar polisacáridos, eDNA y proteínas involucradas en la estructura. También observamos enzimas que disgregan el biofilm como glucosidasas y DNasas entre otras proteínas que favorecen la adhesión como las adhesinas. Imagen adaptada de (119).

3. Organismos modelo utilizados en este estudio

3.1 *Pseudomonas aeruginosa*

P. aeruginosa **es una bacteria Gram-negativa con forma de bacilo que pertenece al filo de las γ-proteobacterias** (129). Se encuentra como organismo de vida libre en el suelo, agua e infectando animales y plantas (130). Esta bacteria infecta humanos y otros animales, y es una de las principales causas de infecciones nosocomiales, provocando graves infecciones en personas con FQ, EPOC, cáncer, SIDA y quemaduras (131–134). Este patógeno también es la causa de neumonías, infecciones urinarias y gastrointestinales, queratitis, otitis externa, infecciones en huesos y articulaciones (osteomielitis), en tejidos blandos y tras intervenciones quirúrgicas en los dispositivos clínicos implantados (Figura 12) (135, 136).
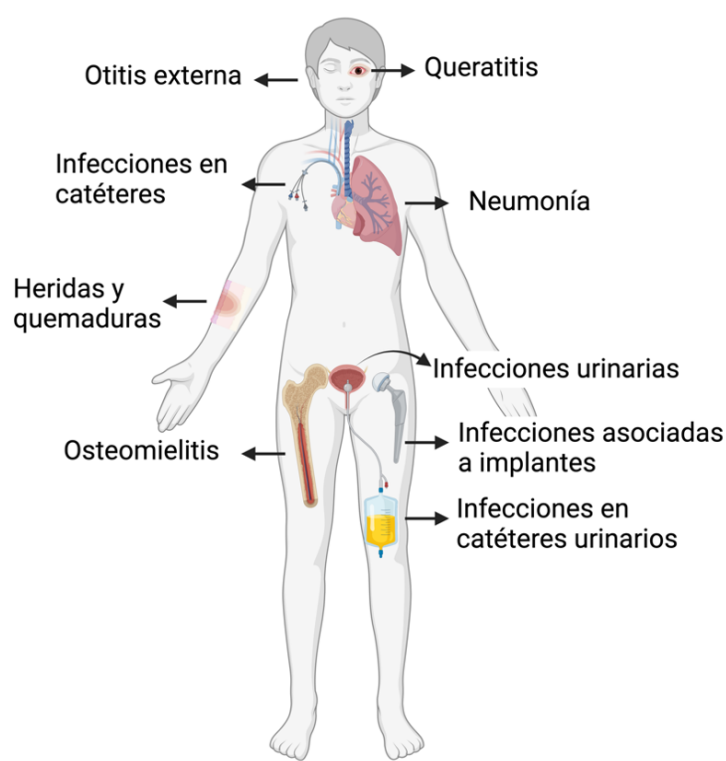
Figura 12. Infecciones asociadas a *P. aeruginosa* en el ser humano como hospedador. Imagen creada con Biorender.

Su genoma con más de 6.3 millones de pares de bases le confiere diversas ventajas, como la **resistencia natural a muchos antibióticos** como aminoglucósidos, quinolonas y β-lactámicos mediante la producción de bombas de eflujo, porinas de alta restricción,

enzimas inhibidoras de antibióticos (β-lactamasas) y enzimas modificadoras de aminoglucósidos (137, 138). También **puede adquirir resistencias a otros fármacos** (cefalosporinas, fluoroquinolonas y carbapenemas) de forma progresiva mediante elementos móviles como los plásmidos y por mutaciones en las dianas antimicrobiales. Todos estos mecanismos hacen que puedan aparecer cepas multirresistentes (135, 139).

El genoma de *P. aeruginosa* también le permite codificar más de 690 factores de transcripción, creando una **compleja red de regulación génica que le otorga una gran capacidad para adaptarse a diversos entornos** (137, 140). Por ejemplo, *P. aeruginosa* es capaz de vivir en ambientes con distintas concentraciones de oxígeno. En presencia de oxígeno, *P. aeruginosa* utiliza la respiración aeróbica, que es una vía compleja de transferencia de electrones que utiliza hidrogenasas respiratorias y oxidasas terminales y en la que el oxígeno se utiliza como receptor final de electrones (141). En ausencia de oxígeno, la bacteria cambia a respiración anaeróbica y utiliza el nitrato o nitrito como aceptor final de electrones, lo que se conoce como desnitrificación (142). También pueden realizar fermentación, pero de manera más limitada (143). El metabolismo anaeróbico es indispensable en procesos infecciosos en los que la bacteria forma un biofilm grueso con limitación de oxígeno en las capas más profundas (141, 144).

3.1.1 Factores de virulencia

P. aeruginosa es capaz de producir una gran variedad de factores de virulencia que permiten que la bacteria colonice e invada los tejidos del hospedador causando daño celular (136). La producción de estos factores varía en función del momento de la infección, y puede agravar la enfermedad. **Las infecciones por *P. aeruginosa* pueden ser agudas o crónicas**, con aislados fenotípicamente distintos en cada uno de estos estadios (145). La Figura 13 resume los factores de virulencia secretados por *P. aeruginosa.*

En las infecciones agudas, las cepas aisladas de *Pseudomonas* expresan un amplio abanico de factores de virulencia, como adhesinas (flagelo polar y pili de tipo IV), lipopolisacáridos (LPS) y el sistema de secreción de tipo III (T3SS) (133). Las adhesinas desempeñan un papel esencial en la motilidad bacteriana, la adhesión celular y la formación de biofilm, así como en el inicio de la respuesta inflamatoria (136). El LPS es un glicolípido complejo que forma parte de la membrana externa en bacterias Gram-negativas y las protege del sistema inmunitario del huésped, aumentando la inflamación (146). El T3SS permite la transferencia de toxinas al interior de las células del huésped (147).

En cambio, **en los aislados de infecciones crónicas, se observa que los factores inflamatorios y de virulencia están atenuados** (148). Por el contrario, se fomentan los mecanismos de formación de biofilm y producción de exopolisacáridos como el alginato, lo que hace que las cepas obtengan un fenotipo mucoide muy característico (149).

Otros factores de virulencia codificados por el genoma de *P. aeruginosa* son las proteasas, lipasas y fosfolipasas, que rompen membranas celulares; la exotoxina A, que inhibe la síntesis proteica; la piocianina, que produce estrés oxidativo; y la pioverdina, un sideróforo que secuestra el hierro del hospedador (133, 136). *P. aeruginosa* **también codifica para factores relacionados con el quorum sensing, un sistema de comunicación entre bacterias** para coordinar la expresión de genes relacionados con factores de virulencia, formación de biofilm y motilidad (150). En *P. aeruginosa*, hay tres sistemas de quorum sensing interconectados: Las, Rhl, IQS y PQS. Todos estos factores contribuyen a la patogenicidad de la bacteria y el agravamiento de la enfermedad (138).
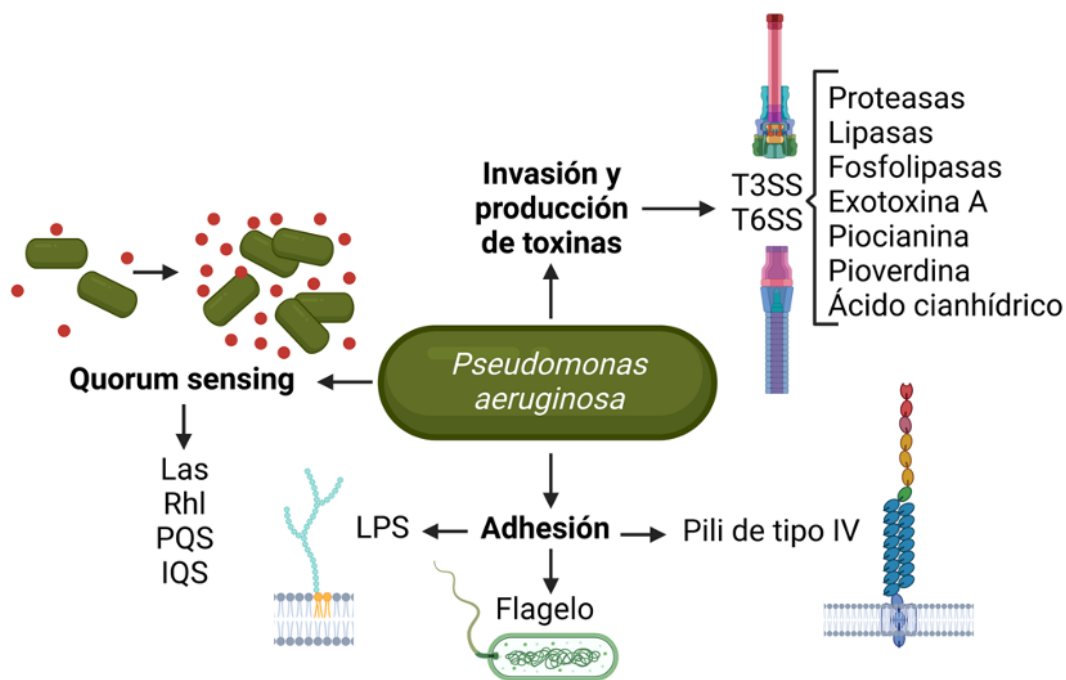
Figura 13. Factores de virulencia producidos por *P. aeruginosa*. Imagen creada con Biorender.

3.1.2 Biofilm de *P. aeruginosa*

Ante señales ambientales, *P. aeruginosa* desencadena cascadas moleculares que cambian su morfología para formar el biofilm. Entre estos cambios, encontramos la

inhibición de la capacidad natatoria del flagelo y el desarrollo del pili de tipo IV para comenzar la adhesión intercelular y a superficie (151). Los cambios suelen estar coordinados por el sistema de quorum sensing y dan como resultado un biofilm maduro formado por exopolisacáridos, proteínas y eDNA, además de lípidos y agua como se explicó con anterioridad (ver sección 2.2 de la introducción).

1) **Los exopolisacáridos son esenciales para la matriz del biofilm**. *P. aeruginosa* es capaz de sintetizar tres polisacáridos diferentes: **PsI, Pel y alginato**. Mientras que el PsI es un polisacárido no cargado formado por D-manosa, D-glucosa y L-ramnosa, el Pel está cargado positivamente y formado por N-acetilglucosamina y N-acetilgalactosamina (152). Ambos polímeros son importantes durante las fases iniciales en la formación de biofilm para adherir a las células entre sí y con la superficie (152). El alginato es un polisacárido cargado negativamente y compuesto por el ácido α-L-gulurónico y el β-D-manurónico, con O-acetilaciones en algunos residuos de manuronato (153). Su función principal es estabilizar el biofilm maduro, creando una capa mucosa. De esta forma, se crea una barrera que protege frente a la fagocitosis, la desecación y al estrés oxidativo (138, 154). La producción de alginato está estrechamente regulada en *P. aeruginosa* por el factor transcripcional AlgR y el factor sigma AlgU, dando lugar al fenotipo mucoide de la bacteria, tal y como se explicará en la sección 3.1.2.1 de la introducción de esta tesis (155, 156). En los pacientes con este tipo de cepas, se encuentran biofilms crónicos y recalcitrantes, y es común que tengan una mala prognosis.

2) Entre las **proteínas** que se encuentran en los biofilms de *P. aeruginosa* destacan la **CdrA**, una adhesina de unión a Psl, y **las lectinas LecA y LecB**, que se unen a los polisacáridos promoviendo la agregación bacteriana (103, 157). El **pili de tipo IV** entra dentro de esta categoría por su función estructural y de adhesión al unirse al eDNA (158). También encontramos **enzimas disgregadoras** como la alginato liasa (159).

3) **El eDNA es uno de los componentes más abundantes en el biofilm** de *P. aeruginosa* y es clave en su estructura (126)*.* Forma una red en la que interactúa físicamente con el Psl, aportando estabilidad y aumentando la tolerancia a antibióticos gracias a su carga negativa y a que induce el sistema de secreción de tipo VI (T6SS) (160, 161). Aunque el eDNA es clave en las primeras etapas de la formación del biofilm, se ha observado que tratamientos con DNasa I pueden disgregar biofilms maduros (162).

4) **Entre los lípidos destacan los ramnolípidos**, que participan en la adherencia a superficie, colonización y motilidad bacteriana (163).

El desarrollo de un biofilm durante una infección de *P. aeruginosa* agrava la enfermedad y el pronóstico de los pacientes en los que se localiza (164). Asimismo, teniendo en cuenta que la composición del biofilm cambia en función de los nutrientes disponibles, su eliminación se dificulta (165).

3.1.2.1 AlgR

AlgR es un factor transcripcional que actúa como regulador global en *P. aeruginosa*, interviniendo en procesos como la **síntesis del pili de tipo IV, quorum sensing, metabolismo anaeróbico, T3SS, producción de cianida y la producción de factores de virulencia** (166). Se descubrió por primera vez formando parte de la red de regulación de la producción de alginato. El alginato es un polisacárido esencial que forma parte de la matriz del biofilm y cuya secreción favorece la aparición del fenotipo mucoide de *P. aeruginosa* (155, 167, 168). Como se ha descrito anteriormente, en la síntesis de alginato están implicadas un gran número de enzimas y sustratos, y es un proceso estrechamente regulado por su elevado gasto energético (156, 168). Entre los **reguladores más importantes implicados en la producción de alginato** se encuentra el factor sigma **AlgU**, que en condiciones normales está secuestrado por el factor anti-sigma transmembrana **MucA**; y el factor transcripcional **AlgR**, que forma parte del sistema de dos componentes AlgR-FimS (104, 154, 155, 166, 169). AlgR y AlgU regulan los operones *algD844KEGXLI* y *algC-argB*, que codifican las principales enzimas implicadas en la producción de alginato (104, 154, 155, 166, 169). El modo de actuación de AlgU y AlgR durante la producción de alginato está reflejado en la Figura 14.

AlgU activa la producción de alginato al unirse a promotores específicos después de ser liberado del factor anti-sigma MucA. Esta liberación suele ocurrir en las fases más tardías de una infección. Durante una infección, la respuesta del sistema inmunológico y el tratamiento con antibióticos pueden provocar mutaciones en la bacteria para en un intento de eliminarla. Sin embargo, cuando se producen mutaciones en genes reguladores como *mucA*, lo que se ocurre es la liberación de AlgU, que regula positivamente su expresión y favorece la producción de alginato, dando lugar al fenotipo mucoide (104, 154, 155, 166, 169).
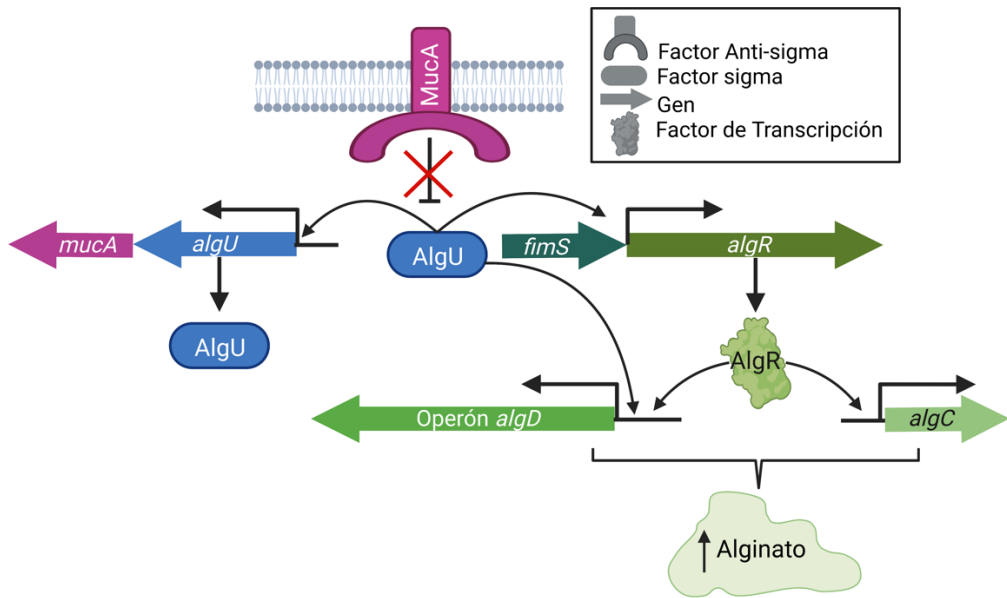
Figura 14. Regulación transcripcional de la producción de alginato. El factor sigma AlgU se libera de la proteína transmembrana MucA a través de mutaciones espontaneas o tras su degradación por proteasas. AlgU activa su propia expresión, la expresión de AlgR y del operon *algD*. AlgR también coordina la activación del operón *algD* y el gen *algC* para fomentar la producción de alginato. Imagen creada con Biorender.

AlgR **es un regulador transcripcional que forma parte del sistema de dos componentes AlgR-FimS**, codificados por los genes *algR* y *fimS*. El gen *fimS*, que codifica para una quinasa transmembrana, se encuentra aguas arriba de *algR*. La expresión de *algR* está regulada por dos promotores: uno en la posición -160 pb y otro en la posición -73 pb. El primer promotor (-160 pb), que está activo de forma constitutiva, produce tanto la proteína FimS como la proteína AlgR, mientras que el segundo promotor (-73 pb) produce únicamente AlgR (170, 171). Los factores sigma que **regulan la expresión de AlgR** a partir del segundo promotor incluyen **RpoS**, involucrado en la transición de fase exponencial a estacionaria, y **AlgU**, cuya expresión también aumenta en la fase estacionaria (171). Se ha observado que la síntesis de AlgR es mayor en la fase estacionaria de la célula, coincidiendo con la síntesis de las enzimas AlgA, AlgC y AlgD, que son esenciales en la producción de alginato (172).

FimS, también conocido como AlgZ, es una **quinasa transmembrana** que modula la fosforilación de AlgR después de recibir una señal ambiental desconocida hasta el momento (173). El estado de fosforilación de AlgR funciona como un interruptor para mediar los

procesos regulados por AlgR. Por ejemplo, la síntesis del pili de tipo IV, que es esencial en la colonización de tejidos, y la síntesis de factores de virulencia, requieren que AlgR esté fosforilado en el aminoácido D54. Por otro lado, la producción de alginato para formar el biofilm, está regulada por AlgR no fosforilado (174, 175). Finalmente, también se ha observado que **AlgR forma parte de la red de regulación de las RNR y su estado de fosforilación influye en su activación** (81).

3.2 *Staphylococcus aureus*

S. aureus **es una bacteria Gram-positiva, anaerobia facultativa, con forma esférica que crece formando agregados y pertenece al filo Firmicutes.** Se encuentra en la piel, mucosas y el tracto gastrointestinal de seres humanos y otros animales sanos (176). Puede causar infecciones agudas y superficiales en la piel y tejidos blandos, como impétigo, foliculitis e infecciones en heridas; infecciones crónicas más invasivas como bacteriemia, endocarditis infecciosa, neumonía e infecciones urinarias; o enfermedades producidas por toxinas como meningitis y síndrome de shock tóxico (177–180). La mayoría de las infecciones producidas por *S. aureus* ocurren en pacientes inmunodeprimidos, con altas tasas de mortalidad. *S. aureus* también puede formar biofilms en prótesis, catéteres e implantes articulares, lo que hace que las infecciones producidas por *S. aureus* sean difíciles de eliminar y puedan desembocar en el torrente sanguíneo (Figura 15) (181–183). La formación de biofilms en *S. aureus* está regulada por el sistema de quorum sensing a través de la señalización Arg (184, 185).

Finalmente, *S. aureus* también tiene gran relevancia en el ámbito agrícola, ya que la infección por *S. aureus* de animales de granja puede causar enfermedades como mastitis en las ubres de vacas lecheras (186).
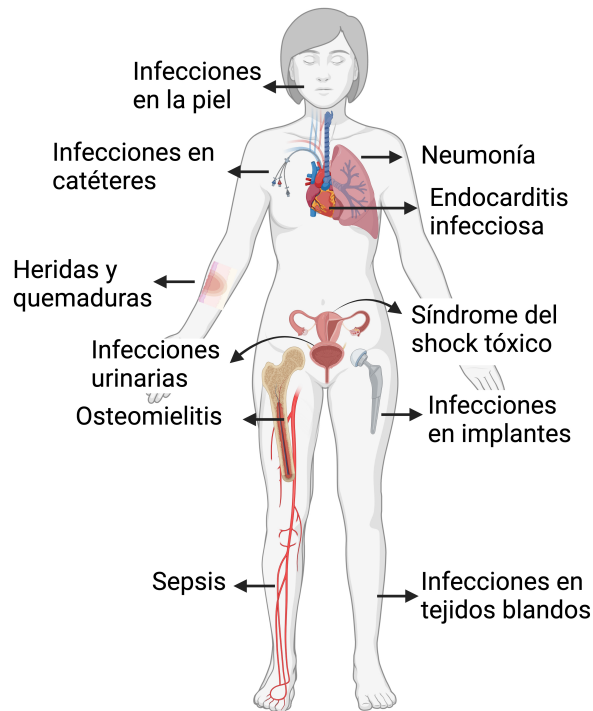
Figura 15. Infecciones asociadas a *S. aureus* en el ser humano como hospedador. Imagen creada con Biorender.

3.2.1 Virulencia y patogenicidad

S. aureus produce un amplio abanico de factores de virulencia y toxinas que fomentan la lisis celular, la destrucción de tejidos humanos y la modificación de la respuesta inmune del huésped (187–189). Entre los factores de virulencia y toxinas encontramos la **proteína estafilocócica A** (SpA) que aumenta la adhesión de las bacterias a las plaquetas, reduce el TNF-α y la señalización proinflamatoria (190); la **toxina-α** que forma poros en eritrocitos y monocitos (191); la **toxina-1** de síndrome de shock tóxico (TSST1), que induce la proliferación de los linfocitos T y suprime la producción de inmunoglobulinas (192); las **adhesinas**, como las proteínas de unión a la fibronectina y fibrinógeno (FnBP-A, ClfA) que favorecen la adhesión a la matriz extracelular y a las proteínas del hospedador para colonizar y diseminar las bacterias (193); y las **coagulasas Coa** y la **proteína de unión al factor von-Willebrand** (vWbp) que promueven la polimerización del fibrinógeno del huésped en fibrina generando coágulos de sangre (194). Las bacterias quedan embebidas dentro de la fibrina que genera una red que las protege frente a las células del sistema inmune.

Además de las toxinas, *S. aureus* también produce **proteínas específicas para evitar el sistema inmune del hospedador**. Entre estas proteínas encontramos la estafiloquinasa, que evita el efecto bactericida de los neutrófilos al unirse a las α-defensinas que secretan (195); la aureolisina, que rompe la catelicidina LL-37, un péptido bactericida con una potente actividad contra *Staphylococcus* (196); la catalasa, para reducir el H_2O_2 producido por neutrófilos (197); y el inhibidor del complemento estafilocócico, que interactúa con las convertasas C3 del sistema del complemento bloqueándolo (198). Los factores de virulencia de *S. aureus* se resumen en la Figura 16.
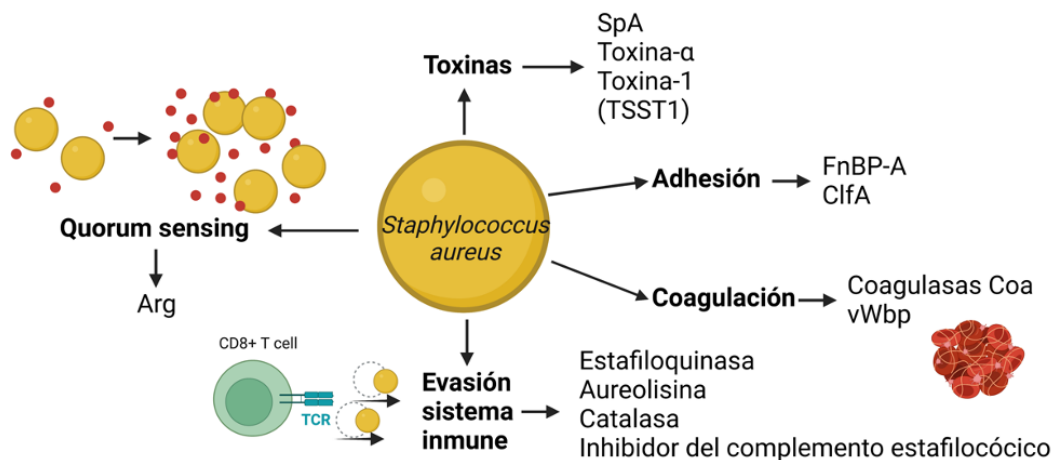
Figura 16. Factores de virulencia producidos por *S. aureus*. TSST1: toxina-1 de síndrome de shock tóxico. Imagen creada con Biorender.

Asimismo, ***S. aureus* tiene gran facilidad para desarrollar resistencia a antibióticos**. Es importante destacar que fue una cepa de *S. aureus* la primera que desarrollo resistencia a β-lactámicos, primero a la penicilina en la década de 1940, y después a la meticilina en los 1960, apareciendo las cepas altamente virulentas de SARM (*S. aureus* resistente a meticilina) (199). El tratamiento de las infecciones por SARM con vancomicina durante largos periodos de tiempo desencadenó la aparición de bacterias con resistencia a la vancomicina (200). La facilidad con la que *S. aureus* puede adquirir resistencias pone de manifiesto la necesidad de desarrollar nuevas opciones de tratamiento.

3.2.2 Biofilm de *S. aureus*

S. aureus crece formando agregados y cuando las condiciones ambientales son las adecuadas, se activa su sistema de quorum sensing para comenzar la producción de

exopolisacáridos, eDNA y proteínas que darán lugar a la matriz extracelular del biofilm (201).

1) **Entre los polisacáridos producidos por *S. aureus* destaca la adhesina intercelular PIA o poli-N-acetilglucosamina (PNAG),** cuyo papel principal es la adhesión entre células, contribuyendo en los primeros momentos de la formación del biofilm y en su estabilidad (202). Este polisacárido está cargado positivamente, lo que le ayuda a interaccionar con el eDNA del biofilm, reforzando su estructura (203).

2) Hay un **amplio abanico de proteínas** formando parte de la EPS de *S. aureus.* Encontramos adhesinas de unión a superficie, proteínas extracelulares y enzimas que degradan el biofilm. Las proteínas **MSCRAMMs** (Microbial Surface Components Recognizing Adhesive Matrix Molecules) son adhesinas que participan en la unión inicial de la bacteria a la superficie, como puede ser el tejido del huésped (204). Dentro de estas proteínas encontramos la SpA, las proteínas de unión a fibronectina (FnBPs) y las proteínas de superficie SasC y SasG (204, 205). *S. aureus* también secreta proteínas a la EPS que participan en la estabilización del biofilm cuando se unen al eDNA al estar cargadas positivamente (206). Algunas de las enzimas secretadas degradan el biofilm y promueven su dispersión, entre estas proteínas encontramos la proteasa SpI y la termonucleasa (207). Además, *S. aureus* también secreta factores de virulencia como hemolisinas, lipasas y coagulasas que actúan sobre las células del huésped. En concreto, las coagulasas Coa y vWbp coagulan el fibrinógeno en fibrina, que pasa a formar parte del biofilm de *S. aureus* (194, 208)*.*

3) **El eDNA es un componente esencial y mayoritario en el biofilm de *S. aureus*** (203)*.* Su presencia en la EPS está mediada por procesos de autolisis en el que se libera ADN cromosómico. El eDNA tiene varias funciones dentro del biofilm. Por un lado, está implicado en la adhesión inicial a superficies, junto con algunas adhesinas específicas (209). Por otro, su carga negativa le permite interaccionar con polisacáridos y proteínas cargadas positivamente, lo que le confiere una gran relevancia en el mantenimiento de la estructura del biofilm de *Staphylococcus* (209)*.* Además, se ha observado que el tratamiento de estos biofilms con DNasa disminuye la biomasa de éste e impide la adhesión inicia (203).

4. Heridas crónicas infectadas

La piel es el órgano más extenso del cuerpo humano y actúa como barrera para proteger al organismo de agentes externos, como los daños físicos, químicos y biológicos, como patógenos (210). Para proteger al cuerpo de los patógenos, la piel cuenta con su propio microbioma, formado por una gran diversidad de microorganismos, como Actinobacterias, Proteobacterias y Firmicutes. De esta manera, se evita la proliferación de microorganismos perjudiciales (211).

Cuando la piel se rompe, pierde su función protectora y se genera una herida. En este momento, se activan los **mecanismos fisiológicos para curar la herida**, que generalmente implican cuatro etapas: **respuesta inmediata, inflamación, proliferación y remodelación y cierre** (Figura 17) (212). Durante la respuesta inmediata, las plaquetas colonizan la zona de la herida, forman un coágulo de fibrina y liberan protrombina para detener el flujo de sangre. En la inflamación, las células del sistema inmunológico liberan anticuerpos, factores ... ción de las células de la piel.

Las heridas que no cicatrizan se consideran heridas crónicas y están asociadas a patologías como la diabetes, las enfermedades cardiovasculares, la obesidad o la hipertensión (214). Estas heridas se conocen como úlceras de pie diabético, úlceras por presión y úlceras venosas y arteriales (215). La inflamación desmedida que se observa en estos casos está caracterizada por una liberación exacerbada de ROS, enzimas citotóxicas y citoquinas por parte de los leucocitos polimofonucleares, lo que provoca graves daños en los tejidos (216). **Las heridas crónicas tienen una mayor probabilidad de ser infectadas**, lo que dificulta su cicatrización. Asimismo, las heridas que se producen por quemaduras o por intervenciones quirúrgicas también soy muy susceptibles de ser infectadas, aumentando la morbilidad y mortalidad de los pacientes (108, 217).

En la mayoría de las heridas crónicas infectadas encontramos una gran variedad de microorganismos como hongos, *Candida spp.*, *Curvularia spp.* y *Cladosporium spp.*; y bacterias, *Staphylococcus spp. Pseudomonas spp*, *Peptoniphilus spp*, *Enterococcus spp*, *Enterobacter spp*, *Stenotrophomonas spp*, y *Serratia spp* (218, 219). Cabe destacar que *S. aureus, P. aeruginosa* y *Enterococcus faecalis* son, a su vez, las especies bacterianas más frecuentes en heridas crónicas (220, 221). **El 90% de las bacterias que infectan las heridas crecen formando un biofilm polimicrobiano** (Figura 18) (222). El desarrollo del biofilm aporta ventajas a las bacterias, por ejemplo, favorece el desarrollo de interacciones sinérgicas y mutualistas entre ellas, lo que favorece su adaptabilidad al medio (219). El desarrollo de la matriz también dificulta el paso de agentes antimicrobianos, impidiendo la proliferación celular (223). Esto dificulta la eliminación de la infección y agrava el daño que se produce en los tejidos debido a la sobreestimulación continua de la respuesta inflamatoria (219).
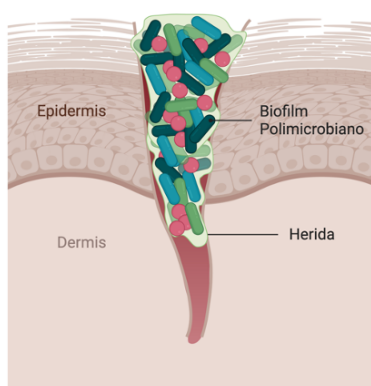
Figura 18. Biofilm en una herida crónica. Imagen creada con Biorender.

4.1 Coinfección por *P. aeruginosa* y *S. aureus* en heridas

En heridas crónicas y en pacientes con bronquiectasias, es común encontrar infecciones producidas por *P. aeruginosa* y *S. aureus* (220, 224). La relevancia clínica de estas coinfecciones pone de manifiesto la necesidad de estudiar la compleja relación entre ambas bacterias.

En condiciones naturales, *P. aeruginosa* y *S. aureus* se relacionan de forma competitiva, ya que algunos de los compuestos secretados por *P. aeruginosa* como proteasas, exotoxinas y el HQNO inhiben el crecimiento de *S. aureus*, favoreciendo la aparición del fenotipo de pequeñas colonias (SCV) (225, 226). Además, el co-cultivo de *P. aeruginosa* y *S. aureus* aumenta la sensibilidad de *S. aureus* a varios antibióticos como vancomicina, gentamicina y ciprofloxacina (226–229). Por el contrario, también se han identificado algunos metabolitos secretados por *S. aureus*, como adhesinas, enzimas, otras proteínas como la SpA y algunos polisacáridos, que inhiben el crecimiento de *P. aeruginosa* y aumentan su susceptibilidad a ciprofloxacina y a los aminoglucósidos (229–231).

Sin embargo, cuando ambas bacterias conviven en un biofilm su relación pasa a ser sinérgica favoreciendo su cooperación, virulencia y resistencia a antibióticos (229). La relación entre las bacterias también se ve influenciada por su localización dentro del biofilm, ya que de eso dependerá la disponibilidad de nutrientes y, por consiguiente, la composición de la EPS. Es importante estudiar la localización espacial de las distintas especies bacterianas en un biofilm polimicrobiano, porque **el efecto de muchos agentes antimicrobianos depende de su capacidad para atravesar la matriz del biofilm**. Entender la organización bacteriana y comprender las interacciones entre los compuestos y la EPS ayuda a diseñar terapias más efectivas (125).

También se ha estudiado la localización de *P. aeruginosa* y *S. aureus* dentro del biofilm en las heridas crónicas infectadas para comprender las interacciones entre ambas bacterias. Muchos autores describen que ambas bacterias crecen de forma segregada, formando agregados de una única especie rodeados de matriz (232–235). Estos patrones en los que las bacterias se encuentras segregadas por especies proponen una interacción bacteriana competitiva (236). A pesar de todos los estudios realizados hasta el momento, no hay un acuerdo sobre la localización de estos agregados dentro del biofilm. Hay estudios que indican que los agregados de *P. aeruginosa* se localizan en las zonas más profundas del biofilm y los de *S. aureus* en la región más cerca de la superficie (232, 233). En cambio, otros

autores han observado agregados de *P. aeruginosa* en las partes más superficiales del biofilm (234, 235, 237). **La baja frecuencia con la que se encuentra *P. aeruginosa* y *S. aureus* cohabitando la misma región puede indicar que su relación es competitiva dentro de la herida** y, por tanto, que la separación física de las especies impide que se inhiba su crecimiento por los metabolitos secretados.

Los nutrientes presentes en el entorno de la herida también influyen en la interacción entre bacterias de distintas especies, ya que pueden alterar la liberación de factores de virulencia. Por ejemplo, la albumina es una proteína sanguínea que bloquea las señales de quorum sensing de *P. aeruginosa*, impidiendo la secreción de toxinas que afectan negativamente a *S. aureus* (238)*.* También se ha observado que el alginato secretado por *P. aeruginosa* protege a *S. aureus* facilitando la coexistencia de las dos bacterias (239). Además de los nutrientes, la concentración de oxígeno presente en un biofilm también influye en la interacción interbacteriana. En condiciones anóxicas se inhiben los factores de virulencia de *P. aeruginosa*, lo que facilita la coexistencia de *P. aeruginosa* y *S. aureus*. Esto puede ser muy beneficioso para el desarrollo de infecciones polimicrobianas en entornos en los que la concentración de oxígeno es baja, como los biofilms o las heridas profundas (240).

Para estudiar las heridas crónicas infectadas por *P. aeruginosa* y *S. aureus* se utilizan modelos *in vitro* e *in vivo*. Los modelos *in vitro* deben parecerse al entorno de la herida. Para ello, el medio de crecimiento debe contener nutrientes similares a los que se encuentran en una herida, y los componentes de la matriz deben estar formados por polímeros que se encuentren en el huésped. Teniendo en cuenta que una herida *in vivo* es un entorno dinámico, un modelo *in vitro* debería tener un suplemento frecuente de nutrientes, estar infectado por más de una especie bacteriana y debería generar un gradiente de nutrientes y de oxígeno para que el biofilm sea heterogéneo (241). Entre los modelos *in vitro* destaca el diseñado por Sun et al., en 2008, en el que *P. aeruginosa* y *S. aureus* coexisten y que se ha usado para distintos estudios de interacción entre bacterias (237, 242, 243). Pero existen otros modelos, como los modelos de perfusión, el modelo de herida microfluídica, el modelo semi-sólido, el biofilm en gel o el modelo 3D (244–248). La figura 19 muestra una visión general de los modelos de infección de herida *in vitro* en función de distintos parámetros. Entre las ventajas que presentan los modelos *in vitro* destaca la ausencia de limitaciones éticas, su accesibilidad, la facilidad para replicarlos, la rapidez de producción y el hecho de que las condiciones de temperatura, humedad y pH

son controlables. Sin embargo, también presentan varias limitaciones, ya que no pueden imitar completamente una herida real debido a la falta de flujo sanguíneo, la ausencia de regeneración del tejido y la falta de respuesta por parte del sistema inmune (241). Esto hace que los modelos *in vitro* sean adecuados para estudiar interacciones simples entre dos o tres factores, pero para llegar a conclusiones más completas son necesarios los modelos *in vivo*.

Visión general de los modelos de infección de herida *in vitro*								
Modelo ↓ Características →	**WSM**	**Matriz**	**Nutrientes**	**Especies**	**3D grad.**	**Flow**	**Medio**	**Superficie**
Sun *et al.* 2008 **"Lubbock Chronic Wound Biofilm Model (LCWB)"**	🩸	🦠		🦠	🔴	〰️		◢
"Modelo de perfusión"	🩸		➡️			〰️	🌿	▭
"Modelo de herida microfluídica"		🦠	➡️	🦠	🔴	〰️	🌿	◢
"Modelo semi-sólido"	🩸				EXPECTED		🌿	
"Biofilm en gel"					🔴		🌿	
"Modelo 3D"				🦠	🔴		🌿	

Figura 19. Visión general de algunos modelos de herida *in vitro.* Se han clasificados en base a los criterios positivos que deben estar presentes (en azul) como el WSM ("Wound simulating media", medio de crecimiento utilizado), la matriz del hospedador, la adición continuada de nutrientes, la presencia de una o varias especies, y el establecimiento de un gradiente de nutrientes y oxígeno dentro del biofilm. También se tienen en cuenta características que no deben estar presentes (en rosa) como el movimiento (Flow), la presencia de medio o matriz no humano, y el crecimiento en superficies sólidas. Los recuadros sombreados y con símbolos indican que la característica está presente, y los recuadros a medio sombrear indican que hay variantes del modelo que pueden incluir o excluir partes concretas. Imagen adaptada de (241).

En cuanto a los modelos *in vivo*, destacan las infecciones producidas en la piel de ratones. Los ratones presentan diferencias en el panículo carnoso de la piel y algunas células epiteliales en comparación con los tejidos y células humanas, pero es un buen modelo preclínico para la investigación traslacional y para probar posibles tratamientos (237, 249, 250). Otros animales como conejos, ratas, cerdos e incluso peces cebra también han sido sujetos para la investigación clínica de heridas crónicas (251).

4.2 Tratamientos

Las heridas crónicas infectadas contribuyen a un mayor deterioro tisular empeorando la salud física y mental del paciente lo que conduce a una mala prognosis, y además acarrean unos elevados costes médicos. El tratamiento de las infecciones en heridas crónicas presenta varios problemas. Por un lado, la aplicación tópica de antibióticos en las heridas infectadas aumenta la aparición de bacterias con resistencia a antibióticos (252). Además, las bacterias que crecen embebidas dentro del biofilm presentan un metabolismo ralentizado, por lo que adquieren tolerancia a los compuestos microbianos utilizados (ver sección 2 de la introducción). Y, además, se dificulta la penetración de los antimicrobianos hacia las zonas internas de las heridas debido a las características físicas que encontramos en el biofilm (253). Por lo tanto, es esencial encontrar estrategias terapéuticas para tratar las heridas infectadas.

En la actualidad, se utilizan altas concentraciones de antibiótico en combinación con otros compuestos para tratar las infecciones producidas por biofilm. Entre los antibióticos más utilizados destacan las cefalosporinas de quinta generación, como el ceftolozán y el tazobactamo, y los inhibidores de β-lactamasas, como la ureidopenicilina, para combatir las cepas de *P. aeruginosa* resistentes a múltiples antibióticos, y la colistina para tratar las infecciones de *S. aureus* (254, 255)

Hay **compuestos que se administran junto con los antibióticos** en forma de terapia combinada para aumentar su eficacia. Entre estos agentes se encuentran los péptidos antimicrobianos (AMPs), las enzimas disgregadoras del biofilm, los inhibidores de quorum sensing y los aceites esenciales (254).

Los **AMPs** son pequeñas proteínas que pueden disolver membranas plasmáticas para inhibir el crecimiento bacteriano. Por ejemplo, se ha observado que la prolina-novispirina G10 y el PXL150 inhiben el crecimiento de *S. aureus* y *P. aeruginosa*, respectivamente (256).

Las **enzimas que degradan el biofilm**, como las hidrolasas o las nucleasas, atacan directamente a los componentes de la EPS e impiden su formación, favoreciendo la penetración de los antibióticos (223, 257).

El uso de **agentes inhibidores de quorum sensing** como la furanona halogenada, es una estrategia alternativa para impedir la formación del biofilm (258). Estos agentes pueden actuar impidiendo la síntesis de las moléculas de señalización, degradándolas o

actuando como sus competidores. De esta forma, se rompe la red de comunicación entre las bacterias y se consigue aumentar la eficacia de los antimicrobianos (259, 260). Por ejemplo, se ha observado que la utilización del tanino hamamelitanino hidrolizable aumenta la eficacia de la vancomicina, tobramicina y cefalosporinas en un biofilm de *S. aureus* (261).

Finalmente, los **aceites esenciales**, como el aceite de jengibre y la curcumina, también están relacionados con la inhibición del quorum sensing, por lo que tendrían un gran potencial como agentes antibiofilm utilizándolos en combinación con otros antibióticos (254).

El desarrollo de nuevas terapias que contribuyan a la eliminación de las heridas infectadas es esencial. Entre los tratamientos más novedosos que se han estudiado, destaca la **terapia con bacteriófagos,** que son los predadores naturales de las bacterias. Pueden utilizarse para tratar heridas crónicas infectadas debido a la proximidad de las células dentro del biofilm, lo que favorece su uso, como se observó en una quemadura de ratón (262). Sin embargo, se observan problemas a la hora de usar bacteriófagos, como la posible obstaculización de su penetración debido a la estructura y composición del biofilm, así como el desarrollo de resistencias. Para evitar esto último, es conveniente utilizar un cóctel de fagos (263–265). Además, se ha estudiado la posibilidad de utilizar **luz azul** para estimular la producción de ROS y así eliminar las bacterias del biofilm (266). Finalmente, el uso de nanopartículas es una estrategia ampliamente utilizada para inhibir la formación del biofilm. Se ha observado que el uso de **nanopartículas de plata** junto con antibióticos, como gentamicina y cloranfenicol, produce un efecto sinérgico en la inhibición del biofilm (267).

Aunque se han realizado avances significativos en la comprensión de las infecciones polimicrobianas, todavía se necesitan numerosos estudios para identificar los factores que influyen en la interacción bacteriana en estos casos, así como para entender cómo la coexistencia de múltiples patógenos puede contribuir a la cronificación de las heridas. Sólo a través de una comprensión más profunda de estos procesos será posible diseñar tratamientos efectivos capaces de eliminar las infecciones en las heridas.

Objetivos

En este trabajo nos hemos centrado en el estudio del patógeno *P. aeruginosa* para desarrollar nuevas estrategias antibacterianas utilizando distintos enfoques. Por un lado, hemos estudiado como los factores de transcripción AlgR y NrdR regulan la expresión de las distintas clases de RNR en *P. aeruginosa*. Por otro lado, hemos evaluado distintas terapias que combinan enzimas degradadoras de la matriz del biofilm con la acción de los antibióticos para tratar las heridas crónicas infectadas.

Los objetivos concretos se enumeran a continuación:

1. Estudiar la expresión génica de las RNR en distintas cepas de *P. aeruginosa* para explorar el mecanismo de activación de las RNR mediante el factor transcripcional AlgR en condiciones de estrés oxidativo y comprobar si el estrés oxidativo influye en la expresión de las RNR durante la formación de biofilm y en infección.
2. Establecer una nueva técnica de transcripción *in vitro* para estudiar la expresión de genes cuando están regulados por factores transcripcionales.
3. Estudiar el factor transcripcional NrdR como nueva diana antibacteriana y la interacción entre los diferentes factores transcripcionales regula la expresión génica de las distintas RNR.
4. Estudiar la colocalización de *P. aeruginosa* y *S. aureus* en un modelo *in vitro* de herida infectada y el efecto de diferentes terapias antimicrobianas y antibiofilm para el tratamiento de una herida infectada por *P. aeruginosa* y *S. aureus* en un modelo *in vitro*.
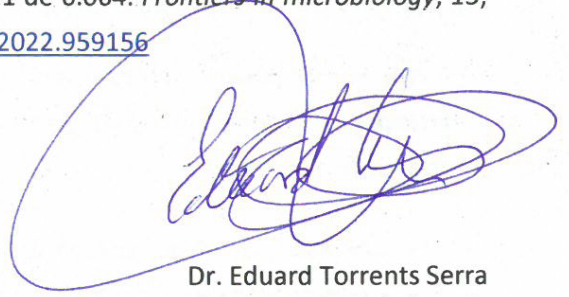
Informes

Informe sobre el factor de impacto

Yo, el Dr. Eduard Torrents, declaro que los artículos publicados que constituyen esta tesis doctoral han sido publicados en revistas científicas internacionales dentro del Journal Citation Reports, que son relevantes en la línea de investigación que se ha desarrollado en mi laboratorio y que pertenecen al primer cuartil (Q1) en sus áreas de conocimiento. El factor de impacto de los artículos presentados en esta tesis en la fecha de su presentación se detalla en cada uno. Un cuarto artículo se presenta en forma de manuscrito.

- **El artículo 1, "*Pseudomonas aeruginosa* nonphosphorylated AlgR induces ribonucleotide reductase expression under oxidative stress infectious conditions"**, Rubio-Canalejas, A., Admella, J., Pedraz, L., & Torrents, E., fue publicado en 2023 en la revista *mSystems* que se encuentra en el Q1 en la categoría "Microbiology" y presenta un factor de impacto en 2021 de 7.328. *mSystems*, e0100522. Advance online publication. https://doi.org/10.1128/msystems.01005-22.

- **El artículo 2, "ReViTA: A novel *in vitro* transcription system to study gene regulation"**, Rubio-Canalejas, A., Pedraz, L., & Torrents, E., se presenta como manuscrito y ha sido enviado a la revista *New biotechnology* que se encuentra en el Q1 en la categoría "Biotechnology" y presenta un factor de impacto en 2021 de 6.490.

- **El artículo 3, "Regulon and mechanism of action of NrdR, a global regulator of ribonucleotide reduction",** Pedraz, L., Szura, A., Rubio-Canalejas, A., Calo, A., Santella, A., Gual, N., Solà, M., Gomila, G., & Torrents, E., se presenta como manuscrito.

- **El artículo 4, "3D spatial organization and improved antibiotic treatment of a *Pseudomonas aeruginosa–Staphylococcus aureus* wound biofilm by nanoparticle enzyme delivery",** Rubio-Canalejas, A., Baelo, A., Herbera, S., Blanco-Cabra, N., Vukomanovic, M., & Torrents, E., fue publicado en 2022 en la revista *Frontiers in Microbiology* que se encuentra en el Q1 en la categoría "Microbiology"

y presenta un factor de impacto en 2021 de 6.064. *Frontiers in microbiology, 13*, 959156. https://doi.org/10.3389/fmicb.2022.959156

Dr. Eduard Torrents Serra
Director y tutor de la tesis

Informe de participación en los artículos

Yo, el Dr. Eduard Torrents, declaro que la doctoranda Alba Rubio Canalejas ha participado en todos los artículos que forman parte de su tesis como se detalla a continuación:

- **Artículo 1, "*Pseudomonas aeruginosa* nonphosphorylated AlgR induces ribonucleotide reductase expression under oxidative stress infectious conditions"**. Rubio-Canalejas, A., Admella, J., Pedraz, L., & Torrents, E. (2023). *mSystems*, e0100522. Advance online publication. https://doi.org/10.1128/msystems.01005-22. Alba es la primera autora de este artículo y participó activamente en el diseño y supervisión de todos los experimentos. Fue parte fundamental en la realización del proceso experimental y análisis de los datos obtenidos en los estudios de expresión génica en condiciones planctónicas y de biofilm (Figuras 1, 2, 3, 4, 5 y 7). Alba lideró la escritura de esta publicación y participó en su revisión.

- **Artículo 2, "ReViTA: A novel *in vitro* transcription system to study gene regulation"**. Rubio-Canalejas, A., Pedraz, L., & Torrents, E. Alba comparte el primer lugar del artículo junto con el Dr. Lucas Pedraz. Alba participó activamente en el diseño y supervisión experimental y el análisis de los datos para obtener las Figuras 1, 2 y 3 de este estudio. La doctoranda escribió el manuscrito de esta futura publicación y participó en el proceso de revisión.

- **Artículo 3, "Regulon and mechanism of action of NrdR, a global regulator of ribonucleotide reduction"**. Alba participó en el diseño y el análisis de los datos para obtener la Figura 5 de este estudio. También ha colaborado en la redacción del artículo. Una versión muy preliminar de este manuscrito se utilizó en la tesis doctoral presentada por el Dr. Lucas Pedraz en enero de 2020, aunque el trabajo de Alba es fundamental para su publicación. Como las contribuciones de Alba están relacionadas con el Objetivo 3 de esta tesis, considero adecuado incluir este artículo en el conjunto del compendio de publicaciones.

- **Artículo 4, "3D spatial organization and improved antibiotic treatment of a *Pseudomonas aeruginosa–Staphylococcus aureus* wound biofilm by nanoparticle enzyme delivery".** Rubio-Canalejas, A., Baelo, A., Herbera, S., Blanco-

Cabra, N., Vukomanovic, M., & Torrents, E. (2022). *Frontiers in microbiology*, *13*, 959156. https://doi.org/10.3389/fmicb.2022.959156. Alba es la primera autora de este artículo, participó en el diseño experimental, supervisión y análisis de los experimentos relacionados con el análisis de la actividad antimicrobiana y antibiofilm de las terapias combinatorias de antibióticos y nanopartículas y/o enzimas del estudio (Figuras 1, 3, 4, 5, 6 y 7). La doctoranda escribió el manuscrito de la publicación y participó en su revisión.

Dr. Eduard Torrents Serra
Director y tutor de la tesis

Artículos

Artículo 1: *Pseudomonas aeruginosa* nonphosphorylated AlgR induces ribonucleotide reductase expression under oxidative stress infectious conditions

Alba Rubio-Canalejas, Joana Admella, Lucas Pedraz and Eduard Torrents

Resumen

P. aeruginosa es una bacteria Gram-negativa que causa numerosas infecciones, siendo especialmente dañina en las infecciones pulmonares. Durante una infección, *P. aeruginosa* produce alginato, uno de los polímeros esenciales en la estructura y formación del biofilm. La producción de alginato está estrechamente regulada por diversos reguladores, entre los que se encuentra el factor de transcripción AlgR. AlgR forma parte del sistema de dos componentes FimS-AlgR, siendo FimS una quinasa transmembrana que fosforila a AlgR en respuesta a señales desconocidas hasta el momento (ver sección 3.1.2.1. de la introducción de esta tesis para más detalle) (81). En función del estado de fosforilación de AlgR, este activará o inhibirá rutas de regulación específicas (166).

AlgR también forma parte de la red de regulación de las RNR. Las RNR son enzimas que catalizan la reducción de los NTPs a dNTPs, y que son esenciales en la replicación celular y en procesos de reparación del ADN, por ejemplo, tras sufrir daños por estrés oxidativo (3, 81). Las RNR se clasifican en tres clases, la clase I, III y III (3, 81). El genoma de *P. aeruginosa* codifica para los tres tipos de RNR, lo que le aporta una gran versatilidad para vivir en distintos ambientes. La expresión de las RNR está muy regulada para que se active la enzima adecuada en función de la fase de crecimiento o de diferentes condiciones ambientales (3). En estudios anteriores se describió que la regulación de las RNR de clase I y II depende del estado de fosforilación de AlgR, y, de manera provisional, que AlgR es el factor responsable de activar la expresión de la RNR de clase I y II en condiciones de estrés oxidativo (81).

El objetivo principal de este proyecto es estudiar en profundidad la regulación de las RNR de clase I y II por el factor de transcripción AlgR en condiciones de estrés oxidativo cuando *P. aeruginosa* PAO1 crece en cultivo plantónico, formando un biofilm y durante una infección en *Galleria mellonella.* También estudiamos la expresión de las RNR en otras cepas de *P. aeruginosa*, el aislado de laboratorio PA14 y el aislado clínico de una infección pulmonar crónica PAET1. De esta forma, en esta publicación se recogen los resultados que abordan el Objetivos 1 de esta tesis.

En esta tesis se investiga el mecanismo de activación de las RNR mediante el factor transcripcional AlgR bajo condiciones de estrés oxidativo. En primer lugar, se estudió la expresión de *algR* en cuando *P. aeruginosa* crecía junto con el oxidante H_2O_2. El gen *algR* se encuentra en el genoma aguas abajo del gen *fimS* y se expresa a partir de dos promotores diferentes, P*fimS* que activa la expresión de *fimS* y *algR*, y P*algR* que activa únicamente la expresión de *algR*(171)*.* Ambos promotores se fusionaron transcripcionalmente de forma independiente a *gfp* y se estudió la expresión de *algR* en presencia de H_2O_2 como inductor del estrés oxidante en fase de crecimiento exponencial y estacionaria. Se observó que en fase exponencial y bajo condiciones de estrés oxidativo, la expresión de *algR* aumentaba ligeramente. En fase estacionaria, sin embargo, el nivel basal de P*algR* era mayor que la de P*fimS*, y solo aumentó la expresión de *algR* con H_2O_2 a partir del promotor P*algR* (Figura 1 del Artículo 1).

Una vez descifrada la relación existente entre AlgR y el estrés oxidativo, se estudió el mecanismo de activación de las RNR de clase II (*nrdJ*) y de clase I (*nrdA*) de *P. aeruginosa* mediante AlgR en presencia de H_2O_2. Los resultados mostraron que ambas RNR inducían su expresión tanto en fase exponencial como estacionaria y que esta inducción se eliminaba en una cepa de *P. aeruginosa* PAO1 Δ*algR* y de la misma manera cuando se mutaban las cajas AlgR en las regiones promotoras de *nrdJ* y *nrdA.* Esto pone de manifiesto que hay una regulación directa de las RNR por AlgR en condiciones de estrés oxidativo. La deleción del gen *algR* se complementó con la proteína salvaje (AlgR) y con la proteína mutada en el aminoácido D54 (AlgR-D54N). Esta mutación impide la fosforilación de AlgR (81). La complementación de Δ*algR* con AlgR y AlgR-D54N restableció la expresión de *nrdJ* y *nrdA*, obteniendo una expresión mayor tras la complementación con AlgR-D54N. Esto parece indicar que es la forma no fosforilada de la proteína la encargada de activar la expresión de las RNR en *P. aeruginosa* PAO1 en condiciones de estrés oxidativo (Figuras 2 y 3 del Artículo 1).

Asimismo, se estudió la expresión de *nrdJ* y *nrdA* en el aislado de la cepa salvaje de laboratorio *P. aeruginosa* PA14 y en el aislado clínico *P. aeruginosa* PAET1, para estudiar cómo afectaba el contesto genético de cada una en la expresión de las distintas RNR.

En la cepa salvaje de *P. aeruginosa* PA14, se observó un nivel de expresión basal de *nrdJ* similar a PAO1, en cambio la expresión de *nrdA* era menor, mostrando variabilidad genética en función de la cepa. Al inducir estrés oxidativo añadiendo H_2O_2 al medio, aumentó la expresión de *nrdJ* y *nrdA*. Este aumento de expresión es debido a AlgR, ya que, un mutante de la cepa de *P. aeruginosa* PA14 Δ*algR* o al mutar las cajas AlgR en los promotores de *nrdJ* y *nrdA*, esta inducción se eliminaba. La expresión de *nrdJ* se reestableció al complementar la mutación de Δ*algR* con AlgR en fase exponencial, y con AlgR-D54N en fase estacionaria. En cambio, la expresión de *nrdA* se reestableció únicamente al complementar con la proteína AlgR no fosforilada (Figuras 2 y 3 del Artículo 1).

Asimismo, al cuantificar la expresión de las RNR de clase I y II en el aislado clínico *P. aeruginosa* PAET1, observamos que la expresión basal de *nrdJ* y *nrdA* era menor que en la cepa de laboratorio PAO1. La expresión de ambas RNR también fue menor en comparación a PAO1 al añadir H_2O_2 en fase exponencial y estacionaria. Lo que se mantuvo en PAET1 al comparar con PAO1 es que la expresión de las RNR se elimina en la cepa mutante de *P. aeruginosa* PAET1 Δ*algR* o al mutar las regiones de unión a AlgR en los promotores de *nrdJ* y *nrdA*, lo que indica que la regulación de las RNR se produce de forma directa por AlgR. La inducción de *nrdJ* se reestableció al complementar con la proteína AlgR en su estado no fosforilado, y la expresión de *nrdA* se restableció al complementar con AlgR en fase exponencial y AlgR-D54N en fase estacionaria (Figuras 2 y 3 del Artículo 1).

Seguidamente, se estudió la expresión de las RNR en presencia de H_2O_2 cuando la cepa *P. aeruginosa* PAO1 crecía formando biofilm e infectado el modelo de infección *in vivo* de *G. mellonella.* La expresión de *nrdJ* y *nrdA* se indujo en el biofilm al añadir H_2O_2, y esta inducción se eliminó al utilizar una cepa con las cajas AlgR mutadas en los promotores de las RNR, lo que indica la relación directa que hay entre la expresión de las RNR y AlgR en condiciones de estrés oxidativo al crecer en un biofilm. Cuando utilizamos una cepa mutante Δ*algR* y ésta se complementa con las proteínas AlgR y AlgR-D54N, observamos que la expresión de *nrdJ* se reestablece, destacando que es mayor al utilizar la proteína no fosforilada (AlgR-D54N). La expresión de *nrdA* también se reestablece, pero en menor

medida. Además, es remarcable el aumento de la expresión de *nrdJ* en comparación a *nrdA* bajo estas condiciones de crecimiento (Figuras 4 y 5 del Artículo 1)*.*

Finalmente, al estudiar la expresión de las RNR en una infección en *G. mellonella* a 14, 16 y 18 h tras la infección observamos que la expresión de P*algR* fue mayor que la de P*fimS* en todos los puntos tomados, encontrando la mayor diferencia a las 18h. Esto parece indicar que durante una infección en *G. mellonella* la mayor parte de la proteína AlgR producida no estaría fosforilada También medimos la expresión de *nrdJ* y *nrdA*, con los promotores salvajes y con las cajas AlgR de los promotores mutadas. Observamos que, a las 18h, la expresión de *nrdJ* prácticamente desaparecía al mutar las cajas AlgR, mientras que la expresión de *nrdA* cuando se mutaba la caja AlgR era menor que la cepa salvaje pero no llegando a valores tan bajos como los de *nrdJ.* Este hecho indica que *nrdJ* cumple una importante función durante la infección y formación de biofilm, ya que su inducción es mucho mayor que la de *nrdA* (Figura 6 del Artículo 1).

Todos estos resultados ayudan a comprender la regulación de las RNR mediante el factor transcripcional AlgR, dilucidando la interacción entre distintos factores transcripcionales en función de la condición de crecimiento (Objetivo 1).

Publicación

Check for updates

Pseudomonas aeruginosa Nonphosphorylated AlgR Induces Ribonucleotide Reductase Expression under Oxidative Stress Infectious Conditions

Alba Rubio-Canalejas,[a] Joana Admella,[a] Lucas Pedraz,[a] Eduard Torrents[a,b]

[a]Bacterial Infections and Antimicrobial Therapies Group, Institute for Bioengineering of Catalonia (IBEC), Barcelona Institute of Science and Technology (BIST), Barcelona, Spain
[b]Microbiology Section, Department of Genetics, Microbiology and Statistics, Faculty of Biology, University of Barcelona, Barcelona, Spain

ABSTRACT Ribonucleotide reductases (RNRs) are key enzymes which catalyze the synthesis of deoxyribonucleotides, the monomers needed for DNA replication and repair. RNRs are classified into three classes (I, II, and III) depending on their overall structure and metal cofactors. *Pseudomonas aeruginosa* is an opportunistic pathogen which harbors all three RNR classes, increasing its metabolic versatility. During an infection, *P. aeruginosa* can form a biofilm to be protected from host immune defenses, such as the production of reactive oxygen species by macrophages. One of the essential transcription factors needed to regulate biofilm growth and other important metabolic pathways is AlgR. AlgR is part of a two-component system with FimS, a kinase that catalyzes its phosphorylation in response to external signals. Additionally, AlgR is part of the regulatory network of cell RNR regulation. In this study, we investigated the regulation of RNRs through AlgR under oxidative stress conditions. We determined that the nonphosphorylated form of AlgR is responsible for class I and II RNR induction after an H_2O_2 addition in planktonic culture and during flow biofilm growth. We observed similar RNR induction patterns upon comparing the *P. aeruginosa* laboratory strain PAO1 with different *P. aeruginosa* clinical isolates. Finally, we showed that during *Galleria mellonella* infection, when oxidative stress is high, AlgR is crucial for transcriptional induction of a class II RNR gene (*nrdJ*). Therefore, we show that the nonphosphorylated form of AlgR, in addition to being crucial for infection chronicity, regulates the RNR network in response to oxidative stress during infection and biofilm formation.

IMPORTANCE The emergence of multidrug-resistant bacteria is a serious problem worldwide. *Pseudomonas aeruginosa* is a pathogen that causes severe infections because it can form a biofilm that protects it from immune system mechanisms such as the production of oxidative stress. Ribonucleotide reductases are essential enzymes which synthesize deoxyribonucleotides used in the replication of DNA. RNRs are classified into three classes (I, II, and III), and *P. aeruginosa* harbors all three of these classes, increasing its metabolic versatility. Transcription factors, such as AlgR, regulate the expression of RNRs. AlgR is involved in the RNR regulation network and regulates biofilm growth and other metabolic pathways. We determined that AlgR induces class I and II RNRs after an H_2O_2 addition in planktonic culture and biofilm growth. Additionally, we showed that a class II RNR is essential during *Galleria mellonella* infection and that AlgR regulates its induction. Class II RNRs could be considered excellent antibacterial targets to be explored to combat *P. aeruginosa* infections.

KEYWORDS ribonucleotide reductase, biofilm, oxidative stress, AlgR, *Galleria mellonella*, *nrdJ*

Pseudomonas aeruginosa is a versatile Gram-negative opportunistic pathogen which causes acute and chronic illness in immunocompromised patients and people with cystic fibrosis (CF), chronic obstructive pulmonary disease, and other diseases. In

Artículo 1: *Pseudomonas aeruginosa* nonphosphorylated AlgR induces ribonucleotide reductase expression under oxidative stress infectious conditions

AlgR Induces Ribonucleotide Reductase Gene Expression   mSystems

addition, it is known as one of the major sources of pulmonary health care-associated infections and the primary cause of morbidity and mortality (1). Once infection begins, *P. aeruginosa* colonizes the lungs in its nonmucoid form. However, as the infection course continues, *P. aeruginosa* switches into a mucoid phenotype involving massive alginate production, increasing lung deterioration and leading to a poor prognosis (2).

One of the leading players involved in the production of alginate and thus in the chronicity of infection is the *algD* operon, which encodes the main enzymes responsible for alginate production. The *algC* gene, located within the *algC-argB* operon, encodes an enzyme required for alginate biosynthesis and LPS production (3). Alginate production is a very advantageous form of bacterial protection because it prevents phagocytosis, antibiotic penetration, and desiccation. The metabolic process of alginate production is highly regulated because it is highly energy consuming (4).

One of the most significant regulators of alginate production is the *algU/mucABCD* operon. AlgU is an alternative sigma factor (σ^E) which, in the nonmucoid phenotype, is sequestered by the anti-sigma factor MucA. During an infection, the cellular stress produced by the immune system induces the proteolytic degradation of MucA, releasing AlgU and therefore activating the transcription of several genes, such as the *algD* operon, promoting alginate synthesis (5) and the expression of *algR* (6).

AlgR is a transcription factor that is part of the two-component system FimS-AlgR with FimS, a membrane kinase which, in response to external signals, can phosphorylate AlgR. AlgR is a transcription factor which functions as a global regulator, controlling several metabolic pathways depending on its phosphorylation state. It is known that phosphorylated AlgR activates rhamnolipid formation, cyanide production, and type IV pili, which are important for twitching motility. It seems that the biological pathways activated by phosphorylated AlgR are related to the first phases of infection, regulating functions related to cell attachment and initial biofilm formation (3). On the other hand, nonphosphorylated AlgR activates important pathways of biofilm formation, such as the production pathway of the polymer alginate (7). Thus, the metabolic pathways triggered by AlgR in its nonphosphorylated state are related to late biofilm formation, including alginate biosynthesis and the mucoid phenotype which lead to chronic infections (3).

In addition, we and other authors have linked the *algR* system with the *P. aeruginosa* ribonucleotide reductase (RNR) network (8). RNRs are key enzymes which catalyze the reduction of ribonucleotides (NTPs) to deoxynucleotides (dNTPs), which are essential for DNA repair and *de novo* synthesis (9). RNRs are classified into three different classes (I, II, and III) based on their three-dimensional structure, use of cofactors and metals, dependence on oxygen, and radical generation. Class I RNRs are encoded by *nrdAB*, and the enzymes produced are only active under aerobic conditions. Class I is subsequently classified into subclasses Ia, Ib, Ic, Id, and Ie based on the metal center requirement to form the protein radical (10). Class II RNRs, encoded by *nrdJ*, require vitamin B$_{12}$ to be enzymatically active, and their activity is oxygen-independent (11). Class III RNRs, encoded by *nrdDG*, require anaerobic conditions to be active (12). *P. aeruginosa* encodes all three RNR classes, which is very advantageous for its survival in different environmental conditions (9, 13). Depending on the growth and infection phase, specific RNRs are activated; for example, we previously showed that *nrdJ*, encoding class II RNRs, is highly expressed under anaerobic conditions and during biofilm growth (11, 12, 14).

The macrophages and neutrophils of the host immune system try to remove the pathogen by producing reactive oxygen species (ROS) which cause oxidative stress (15). ROS can cause damage to DNA, lipids, proteins, and nucleic acids; thus, bacteria have several ways to protect themselves from oxidative stress (15). *P. aeruginosa* has two superoxide dismutases, three catalases (KatA, KatB, and KatC), and four alkyl hydroperoxide reductases to eliminate the ROS that produce oxidative stress (15). A biofilm formed with alginate protects the bacteria from antibiotics and the host immune system (4). Additionally, bacteria embedded within a biofilm acquire protection from oxidative stress (16).

Previous studies have revealed the relationship between FimS-AlgR and the RNR. We previously described that the AlgR regulation of class I and II RNRs depends on its phosphorylation state (8). Additionally, AlgR is linked with the oxidative stress response system (17), and it is known that the expression of the *Escherichia coli* RNR is activated under oxidative stress conditions (18). We have also discovered that AlgR is the transcription factor responsible for the induction of *P. aeruginosa* class I and II RNRs under oxidative stress (8).

In this study, we delved into the regulation of class I and II RNRs by AlgR in the presence of H_2O_2 in different biological growth stages, in a planktonic culture, in a biofilm, and during *G. mellonella* infection. To determine gene regulation variability, we measured RNR expression in other *P. aeruginosa* strains (laboratory and clinical isolates). To obtain a clinical perspective on RNR expression under oxidative conditions, one of the strains used was a clinical strain isolated from a CF patient (12). In this work, we confirmed that AlgR, in its nonphosphorylated state, is responsible for class I and II RNR transcriptional induction under oxidative stress conditions. We demonstrated that AlgR is essential for *nrdA* and *nrdJ* expression in biofilms under stress conditions. Finally, we observed that ROS are produced during *G. mellonella* infection and that *nrdJ* is the principal RNR expressed, with AlgR being essential for its induction. The different *nrdJ* and *nrdA* induction patterns help to elucidate the essential role of NrdJ in ensuring bacterial survival and suggest a molecular pathway used by *P. aeruginosa* during bacterial infection to restore the dNTP pool and repair damaged DNA.

RESULTS

AlgR expression is induced under oxidative stress conditions. AlgR is a transcription factor that is part of the *fimS-algR* operon. FimS-AlgR is a two-component system of *P. aeruginosa* that can regulate several metabolic pathways in response to external signals. However, the expression of *algR* can be activated through two different promoter regions, P*fimS* and P*algR* (7). Figure 1A shows a scheme of the two promoters in *fimS-algR*. The first promoter is located upstream of *fimS*; when it is transcriptionally activated, the transcript produced encodes the FimS and AlgR proteins. The second promoter is located upstream of *algR* within the *fimS* coding region. This second promoter responds to specific sigma factors, such as AlgU and RpoS, to activate its transcription, and the mRNA obtained encodes only the protein AlgR (7).

Previous studies have linked AlgR with the bacterial response system to oxidative stress (8, 19). However, the specific mechanism by which AlgR is activated under oxidative stress conditions has not been clarified. In this work, we aimed to examine the direct link between AlgR and oxidative stress. First, we transcriptionally fused the P*fimS* promoter and the P*algR* promoter to *gfp*, obtaining pETS-P*fimS* and pETS-P*algR*, respectively (see Materials and Methods). Our goal was to determine whether the expression of *algR* was induced under oxidative stress conditions and, if so, which promoter was responsible for this specific activation. Figure 1B shows that during the exponential phase (OD_{600} [optical density at 600 nm] = 0.5), *algR* expression slightly increased after H_2O_2 was added. When *algR* expression was measured in the stationary growth phase ($OD_{600} > 2.5$), P*algR* had a higher basal expression level (2.7 times higher) than P*fimS*. In addition, only pETS-P*algR* displayed significantly increased *algR* expression after the addition of H_2O_2. To test our system and as a control, we transcriptionally fused the promoter regions of two *P. aeruginosa* catalases, *katA* and *katB*, to *gfp* and analyzed whether the H_2O_2 concentration used was suitable for generating oxidative stress. The catalases *katA* and *katB* are part of the oxidative stress response system in *P. aeruginosa*. *katA*, the main catalase of *Pseudomonas*, is constitutively expressed to remove the H_2O_2 produced in the bacterial respiratory network. When ROS levels are high, other proteins, such as KatB, are expressed to remove excess oxidative stress (15). Figure 1C shows that both catalases, pETS-P*katA* and pETS-P*katB*, were transcriptionally induced when 1 mM H_2O_2 was added for 30 min during the exponential and stationary growth phases. This clearly indicated that the conditions used in this study created enough ROS to generate oxidative stress growth conditions.
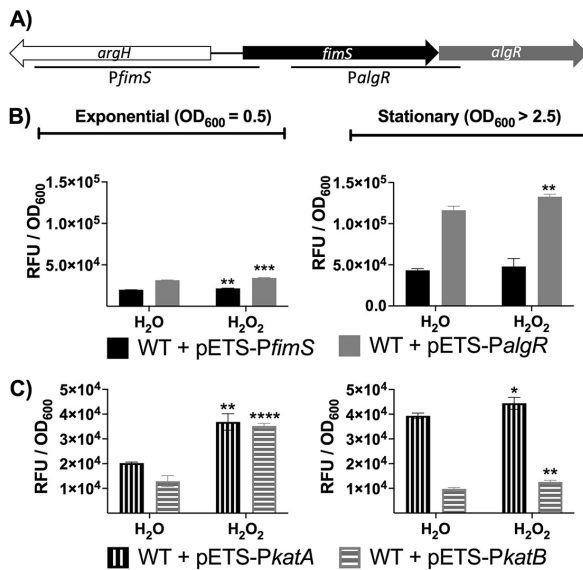
FIG 1 Induction of *algR* and catalases in *Pseudomonas aeruginosa* under oxidative stress. (A) Scheme of the *algR* genetic background. The *algR*-specific promoters are indicated with lines. (B) Gene expression of the two different promoter regions of *algR*, P*fimS-algR* and P*algR*, which were transcriptionally fused to *gfp* (pETS-P*fimS* and pETS-P*algR*, respectively), in the exponential (OD_{600} [optical density at 600 nm] = 0.5) and stationary phases ($OD_{600} > 2.5$) after the addition of 1 mM H_2O_2 or the equivalent volume of water for 30 min. (C) The promoter regions of *katA* and *katB* were transcriptionally fused to *gfp* (pETS-P*katA* and pETS-P*katB*, respectively). The strains were incubated with 1 mM H_2O_2 or an equivalent volume of water for 30 min in the exponential ($OD_{600} = 0.5$) and stationary phases ($OD_{600} > 2.5$). Three independent experiments were performed; error bars indicate standard deviation. Statistical analysis to determine significant differences between the H_2O_2 and their H_2O counterpart samples was performed using Student's unpaired *t* test (**, $P < 0.01$; ***, $P < 0.001$).

Nonphosphorylated AlgR controls the expression of class II (*nrdJ*) and Ia (*nrdA*) RNRs under oxidative stress conditions. Crespo et al. (8) reported that during the exponential growth phase, RNR expression increases under oxidative stress conditions because the master transcriptional regulator AlgR directly binds to an AlgR box in the promoter region of each RNR. We aimed to elucidate how oxidative stress regulates the different RNR genes more deeply via AlgR. Additionally, because regulation by AlgR is linked to the AlgR phosphorylation state, we studied how the phosphorylated form of AlgR modulates *nrd* expression (8).

The promoter regions of *nrdA* and *nrdJ* were transcriptionally fused to the reporter gene *gfp* to obtain pETS-P*A* and pETS-P*J*, respectively. In the promoter region of *nrdA*, one AlgR box was found upstream from the coding region. In the *nrdJ* promoter region, two AlgR boxes were found (8). The RNR promoter regions with their respective mutated AlgR boxes were transcriptionally fused to *gfp* as well, yielding pETS-P*A*-Δ*box1* and pETS-P*J*-Δ*box1+2*. These plasmids were transformed into different *P. aeruginosa* strains: PAO1 and PAO1 Δ*algR*, PA14 and PA14 Δ*algR*, and the clinical *P. aeruginosa* CF isolate PAET1 and PAET1 Δ*algR* (Fig. 2 and 3). The Δ*algR* strains were complemented with pUCP-AlgR, which encodes the wild-type (WT) AlgR protein, or with pUCP-D54N, which encodes the AlgR protein with a mutation in amino acid 54 (D54N) to prevent phosphorylation (3).

To study the expression of RNRs under oxidative stress conditions, we treated the bacterial cultures with 1 mM H_2O_2 for 30 min when the cultures reached the exponential ($OD_{600} = 0.5$) and stationary ($OD_{600} > 2.5$) growth phases. We observed that *nrdJ* (class II RNR) was transcriptionally induced in both the exponential and stationary growth phases (Fig. 2A). Moreover, *nrdJ* induction was eliminated in a *P. aeruginosa* PAO1 Δ*algR* strain
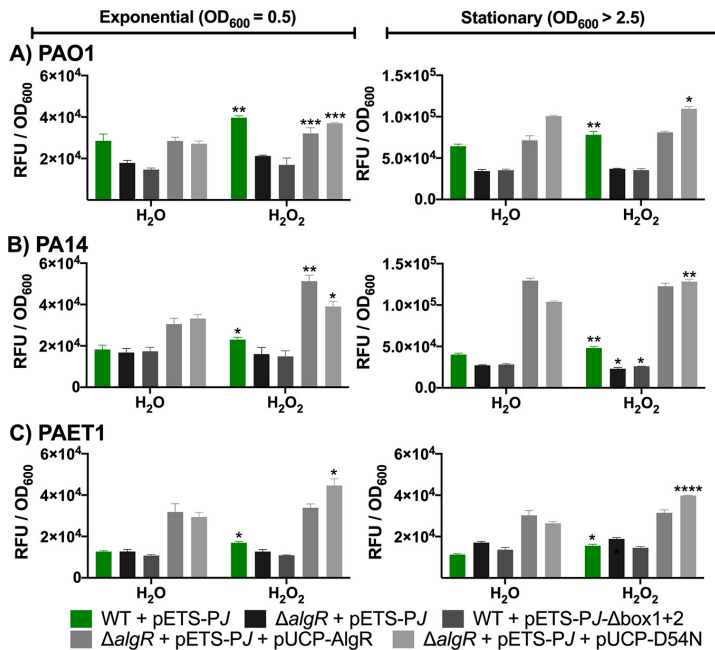
FIG 2 Oxidative stress conditions induce *nrdJ* expression through nonphosphorylated AlgR in different *P. aeruginosa* strains. The promoter region of *nrdJ* (P*J*) was transcriptionally fused to *gfp* (pETS-P*J*). The laboratory strains PAO1 (A) and PA14 (B) and the clinical isolate PAET1 (C) were used to monitor gene expression at different time points ($OD_{600} = 0.5$ and $OD_{600} > 2.5$). The strains were incubated with 1 mM H_2O_2 or an equivalent volume of water for 30 min. Three independent experiments were performed, and standard deviation is indicated with error bars. Statistical analysis to determine significant differences between the samples treated with H_2O_2 and their counterpart samples treated with H_2O was performed using Student's unpaired *t* test (*, $P < 0.05$; **, $P < 0.01$; ***, $P < 0.001$; ****, $P < 0.0001$).

and when the plasmid pETS-P*J*-Δ*box1+2* was used (Fig. 2A), indicating the specific dependence on AlgR during transcription. In addition, the complementation of the *algR* deletion with pETS-D54N restored *nrdJ* induction under oxidative stress conditions in the exponential growth phase. Both the pETS-AlgR and pETS-D54N plasmids complemented the *algR* deletion in the stationary phase. However, the induction was significant only when AlgR was not phosphorylated.

To unravel the molecular mechanism involved in the transcriptional gene induction of class I and II RNRs in strains other than the laboratory strain PAO1, we measured the expression of *nrdJ* and *nrdA* in the laboratory strain *P. aeruginosa* PA14 and the clinical strain *P. aeruginosa* PAET1. We observed that the promoter region of *nrdJ* was conserved with 99% identity, while that of *nrdA* was conserved with 100% identity, among the three strains (Fig. S1). Thus, we surmised that measurement of *nrdA* and *nrdJ* expression would provide information on how the genetic background of each strain affects the expression of class I and II RNRs under oxidative stress conditions.

When using the laboratory strain *P. aeruginosa* PA14, we observed that the basal expression level of *nrdJ* was similar to that of *nrdJ* in PAO1 (Fig. 2B). Figure 2B shows that the oxidative stress generated after incubation with 1 mM H_2O_2 for 30 min induced *nrdJ* expression during the exponential and stationary growth phases. AlgR caused this gene induction, as indicated by the finding that the increased *nrdJ* expression was eliminated in a PA14 Δ*algR* strain and when using the plasmid pETS-P*J*-Δ*box1+2*. Expression was restored when the gene deletion was complemented with AlgR. In the exponential phase, the induced expression of *nrdJ* was higher when pETS-AlgR was used than when pETS-
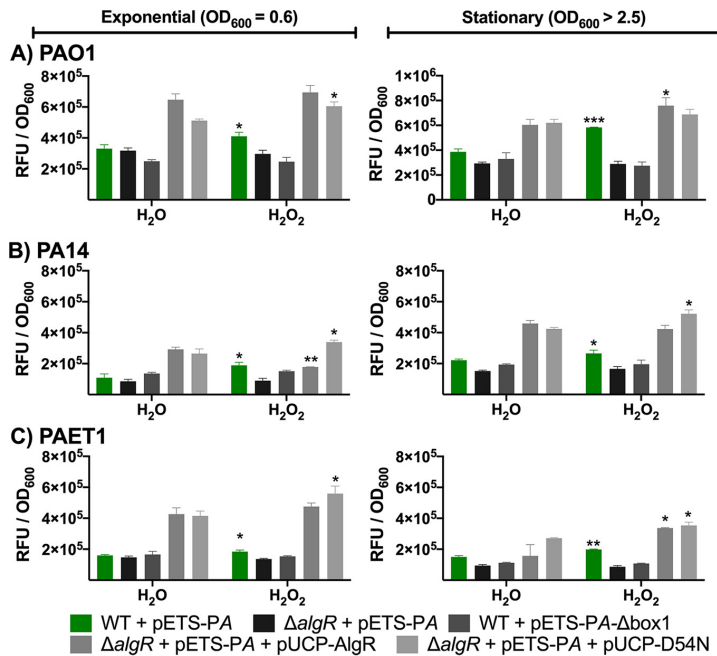
FIG 3 *nrdA* expression is AlgR-dependent under oxidative stress conditions in several *P. aeruginosa* strains. The promoter region of *nrdA* (P*A*) was transcriptionally fused to *gfp* (pETS-P*A*). Gene expression was monitored in the laboratory strains PAO1 (A) and PA14 (B) and the clinical isolate PAET1 (C) at different time points ($OD_{600} = 0.6$ and $OD_{600} > 2.5$). The strains were incubated with 1 mM H_2O_2 or an equivalent volume of water for 30 min. Three independent experiments were performed, and the standard deviation is indicated with error bars. Statistical analysis to determine significant differences between the counterpart samples treated with H_2O_2 or H_2O was performed using Student's unpaired t test (*, $P < 0.05$; **, $P < 0.01$; ***, $P < 0.001$).

D54N was used. In the stationary phase, the induction of *nrdJ* was reestablished after AlgR-D54N was used.

We also measured RNR expression in the clinical strain *P. aeruginosa* PAET1, isolated from a chronic CF patient. Figure 2C shows the basal *nrdJ* expression in the clinical isolate PAET1 and *nrdJ* induction under incubation with 1 mM H_2O_2 for 30 min. The graphs show that *P. aeruginosa* PAET1 *nrdJ* expression was lower than that in the laboratory strain PAO1. *nrdJ* expression increased after the addition of H_2O_2 in the exponential and stationary phases. The induction was abolished in the Δ*algR* strain or when the AlgR boxes of the promoter region were mutated. When the *algR* deletion was complemented with AlgR and AlgR-D54N, *nrdJ* induction was restored. When AlgR-D54N was used, the expression of *nrdJ* was higher than that when AlgR was used. This may imply that *nrdJ* induction under oxidative stress is due to nonphosphorylated AlgR.

The same type of regulation pattern was found when the general transcription of *nrdA* (class I RNR) under oxidative stress conditions was analyzed. The strains were incubated for 30 min with 1 mM H_2O_2 when they reached exponential and stationary growth phases. Figure 3A shows that *nrdA* expression increased during the exponential and stationary phases in *P. aeruginosa* PAO1. This induction was abolished in PAO1 Δ*algR*, and when we used the plasmid pETS-P*A*-ΔAlgR*box1*, which carries a mutation in its AlgR binding box, the transcriptional induction was found to be specific to the transcription factor AlgR. The *algR* deletion was complemented with AlgR-D54N, restoring *nrdA* expression.

nrdA showed lower basal expression in the *P. aeruginosa* laboratory strain PA14 than in PAO1 (Fig. 3B), demonstrating its strain variability. *nrdA* expression was also induced after 1 mM H_2O_2 was added (by 1.7 times in the exponential growth phase and 1.2 times in the stationary phase). This induction was abolished in the Δ*algR* strain and when using the plasmid pETS-P*A*-ΔAlgR*box1*, again showing that AlgR was responsible for *nrdA* induction. The induction was restored when Δ*algR* was complemented with the nonphosphorylated AlgR.

Finally, the expression of *nrdA* in the clinical isolate PAET1 is shown in Fig. 3C. The overall expression of *nrdA* was lower in PAET1 than in the PAO1 laboratory strain (by 26 times in the exponential phase and 2.5 times in the stationary phase). Even so, the induction pattern observed in the strains PAO1 and PA14 was also observed in PAET1. When 1 mM H_2O_2 was added, *nrdA* was induced in the exponential and stationary phases, and this induction was abolished in both the Δ*algR* strain and when the AlgR binding box was removed in the plasmid pETS-P*A*-ΔAlgR*box1*. *nrdA* induction was reestablished when the Δ*algR* strain was complemented with AlgR-D54N in the exponential phase and with AlgR and AlgR-D54N in the stationary phase.

During biofilm growth, class II and I RNR expression under oxidative stress conditions is AlgR-dependent. The different environmental characteristics inside a biofilm also affect the transcriptional activation of RNRs. While *nrdA* expression is activated in the upper layers of the biofilm, where oxygen is available, the class II (*nrdJ*) and III (*nrdD*) RNRs are activated in the deeper biofilm layers. Additionally, we previously demonstrated the essential role of *nrdJ* during biofilm development in *P. aeruginosa* PAO1 (8, 11, 14).

We used flow-cell chambers to grow different *P. aeruginosa* strain biofilms and measured RNR gene expression under oxidative stress conditions (see Materials and Methods). Luria-Bertani (LB) medium supplemented with 4 mM H_2O_2 was added to a mature biofilm (96 h) to generate oxidative stress. Negative controls were treated with LB medium. Following an incubation period of 4 h, the biofilm was dyed and imaged under a confocal microscope (see Materials and Methods). The biofilm biomass was stained with SYTO60, which appears gray in the images (Fig. 4 and 5); the DNA damage due to the oxidative stress present in the biofilm was dyed with CELLRox Orange, shown in magenta; and the RNR-specific expression was measured using green fluorescent protein (GFP) fluorescence (*nrdJ* and *nrdA*), shown in green (Fig. 4 and 5).

Figure 4A shows that *nrdJ* expression (pETS-P*J*) was transcriptionally induced under oxidative stress conditions and almost completely eliminated when the AlgR boxes 1 and 2 were mutated (pETS-P*J*-Δ*box1+2*) (Fig. 4A). This may indicate that during biofilm infection, AlgR is the primary transcription factor that regulates *nrdJ* expression under oxidative stress conditions. In addition, because biofilms show oxygen gradient heterogenicity, we wanted to study their pleiotropic regulation with the Anr transcriptional regulator. Anr is a transcription factor regulating several pathways related to oxygen tension and NO (20, 21). We previously mutated the Anr box in *nrdJ* (14) and, because it is an important regulator of oxygen-depletion conditions, we wanted to determine its involvement in *nrdJ* expression in biofilms under oxidative stress conditions. *nrdJ* expression was similar when the single AlgR boxes were mutated and when a double mutation was present in the AlgR and Anr binding sites (pETS-P*J*-Δ*box1+2*-Δ*Anrbox*), thus demonstrating that Anr does not play an important role during oxidative stress conditions (Fig. 4A).

Figure 4B shows that when the *P. aeruginosa* PAO1 Δ*algR* strain was complemented with AlgR or AlgR-D54N under oxidative stress conditions, *nrdJ* expression increased to the wild-type level. Furthermore, *nrdJ* induction was higher than that in the wild-type strain when the nonphosphorylated AlgR protein was used (Fig. 4B). These results indicate that AlgR plays a key role in *nrdJ* regulation during biofilm infection under oxidative stress conditions. *nrdJ* expression was quantified using COMSTAT software and plotted on a graph as shown in Fig. 4C.

The same expression pattern was observed when the expression of *nrdA* (class Ia RNR) was examined during biofilm formation (Fig. 5). Figure 5A shows images of
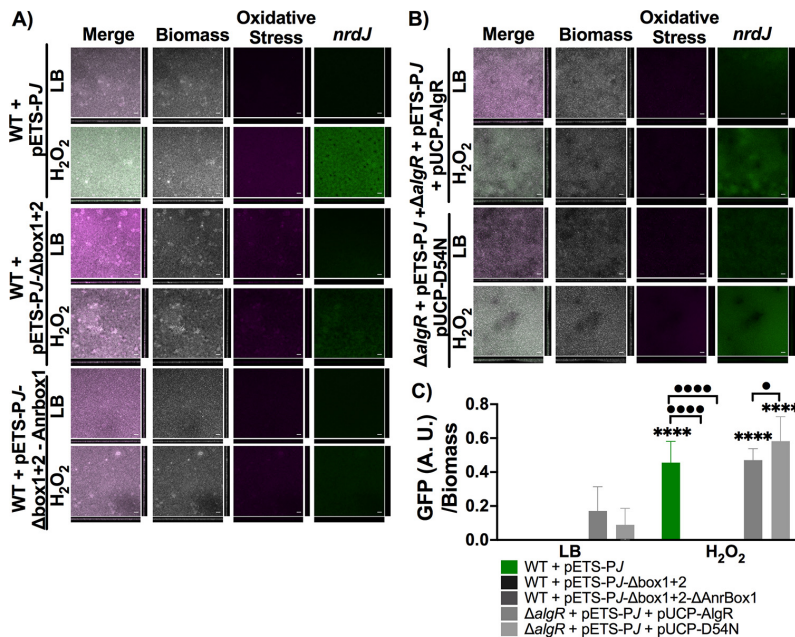
FIG 4 *nrdJ* expression under oxidative stress conditions in a biofilm of *P. aeruginosa* PAO1. (A) Expression in the biofilm of *nrdJ* with the wild-type promoter, the AlgR boxes mutated, and the AlgR boxes and the Anr box mutated (PJ, PJ-Δbox1+2, and PJ-Δbox1+2-ΔAnrbox, respectively). (B) Expression of *nrdJ* in a PAO1 Δ*algR* strain complemented with AlgR and AlgR-D54N. The samples were induced with 4 mM H_2O_2 or an equivalent volume of Luria-Bertani (LB) medium for 4 h. The biofilm was dyed with SYTO60 (gray) and CellROX Orange (magenta), and *gfp* is shown in green. Scale bars = 20 μM. (C) Data show the mean and standard deviation of *gfp* expression normalized by biomass. Student's unpaired *t* test was used to determine significant differences between the samples treated with H_2O_2 and their counterpart samples treated with LB medium (****, $P < 0.0001$) and significant differences between the strains induced with oxidative stress (•, $P < 0.05$; ••••, $P < 0.0001$).

P. aeruginosa PAO1 with pETS-P*A* and PAO1 with pETS-P*A*-Δ*box1* after the addition of LB medium supplemented with 4 mM H_2O_2 or pure LB medium. The images show that *nrdA* expression was induced under oxidative stress conditions during biofilm growth (Fig. 5C). The induction was removed when a promoter with a mutated AlgR box (pETS-PA-Δ*box1*) was used, demonstrating a direct role of AlgR in its transcriptional activation (Fig. 5A). When *P. aeruginosa* PAO1 Δ*algR* was complemented with AlgR or AlgR-D54N, it was observed that *nrdA* expression was restored after addition of H_2O_2 (Fig. 5B). The *nrdA* expression was not restored to the wild-type level but was closer when AlgR-D54N was used for complementation (Fig. 5C).

nrdJ plays an important role during *Galleria mellonella* infection in response to oxidative stress. *Galleria mellonella* is an outstanding alternative *in vivo* model to study bacterial infections because its innate response mimics that of mammals (22). *G. mellonella* has been previously used to study RNR expression during infection (23). Because *Galleria* larvae have autofluorescence, plasmids which produce GFP cannot be used to monitor gene expression during infection. Thus, the promoter regions used in this study were transcriptionally fused to *luxCDABE* genes that produce bioluminescence (23). After injecting the *Galleria* larvae, we made relative luminescence (RL) measurements for each larval group at 8, 14, 16, and 18 h postinfection. We determined the expression induction of each gene by comparing its expression at 14, 16, and 18 h with its expression at 8 h postinfection (the initial stage of infection).

Figure 6A shows the induction of *katA* and *katB* expression during infection. It was determined that the expression of *katA* (pLUX-P*katA*) was induced at 14, 16, and 18 h (113-, 865-, and 2,449-fold induction, respectively). In addition, *katB* (pLUX-P*katB*) was
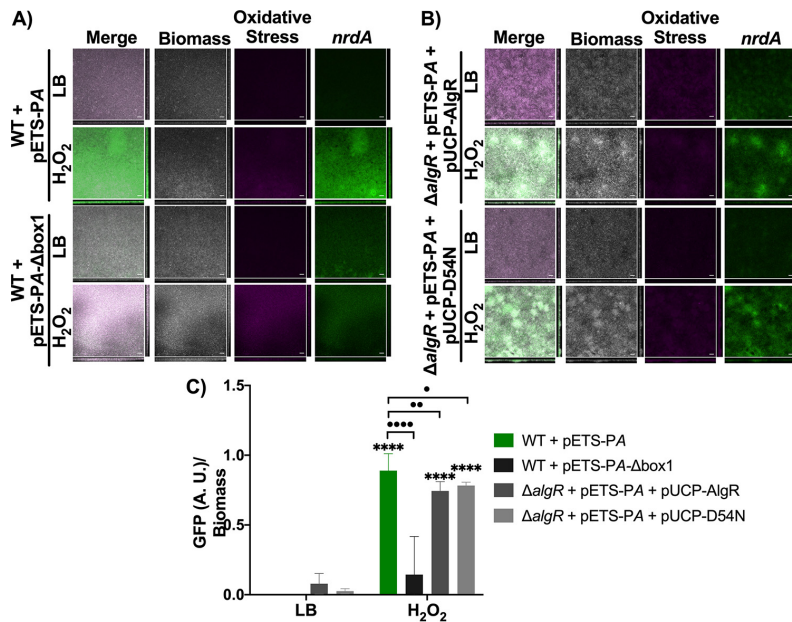
FIG 5 *nrdA* expression under oxidative stress conditions in a biofilm. (A) Expression of the *nrdA* promoter and the *nrdA* promoter with the AlgR box mutated (P*A* and P*A*-Δ*box1*, respectively) in biofilm. (B) Expression of *nrdA* in a PAO1 Δ*algR* strain complemented with AlgR and AlgR-D54N. The samples were induced with 4 mM H_2O_2 or an equivalent volume of LB medium for 4 h. The biofilm was dyed with SYTO60 (gray) and CellROX Orange (magenta), and *gfp* is shown in green. Scale bars = 20 μM. (C) Data show the mean and standard deviation of *gfp* expression normalized by biomass. Student's unpaired *t* test was used to determine significant differences between the counterpart samples treated with H_2O_2 or LB medium (****, $P < 0.0001$) and significant differences between the strains induced with oxidative stress (●, $P < 0.05$; ●●, $P < 0.01$; ●●●●, $P < 0.0001$).

induced at 14, 16, and 18 h, but its expression was lower than that of *katA* (51-, 85-, and 1,220-fold induction, respectively). These results may indicate that as the amount of ROS increases during infection, the expression of bacterial catalases increases as well to protect the bacteria from damage.

The induction of *algR* from the two promoters (pLUX-P*fimS* and pLUX-P*algR*) was measured (Fig. 6B). We found that the expression of P*algR* was higher than that of P*fimS* throughout the whole infection course, with the highest difference at 18 h post-infection (3,579- and 6,098-fold induction for P*fimS* and P*algR*).

We measured the expression of *nrdJ* (pLUX-P*J*), *nrdJ* with the AlgR boxes 1 and 2 mutated (pLUX-P*J*-Δ*box1+2*), *nrdJ* with the Anr box mutated (pLUX-P*J*-ΔAnrbox), and *nrdJ* with AlgR boxes 1 and 2 mutated and the Anr box mutated (pLUX-P*J*-Δ*box1+2*-ΔAnrbox) (Fig. 6C). The results showed that *nrdJ* expression was highly induced during infection, with *nrdJ* showing the highest induction at 18 h postinfection (130,257-fold induction). The expression of *nrdJ* decreased significantly when the AlgR boxes were mutated and when the Anr box was mutated (3,519- and 2,669-fold induction at 18 h, respectively). However, the most dramatic decrease in *nrdJ* expression was observed when both the AlgR and Anr boxes were mutated (825-fold induction). The expression observed when the AlgR boxes and the AlgR and Anr boxes were mutated was 158 times lower than that of the wild-type promoter, revealing the importance of both transcription factors during infection.

Finally, we measured the expression of the class I RNR gene *nrdA* with the WT pro-moter (pLUX-P*A*) and the promoter with the AlgR box mutated (pLUX-P*A*-Δ*box1*). The graph in Fig. 6D shows that the highest induction in *nrdA* expression occurred at 18 h
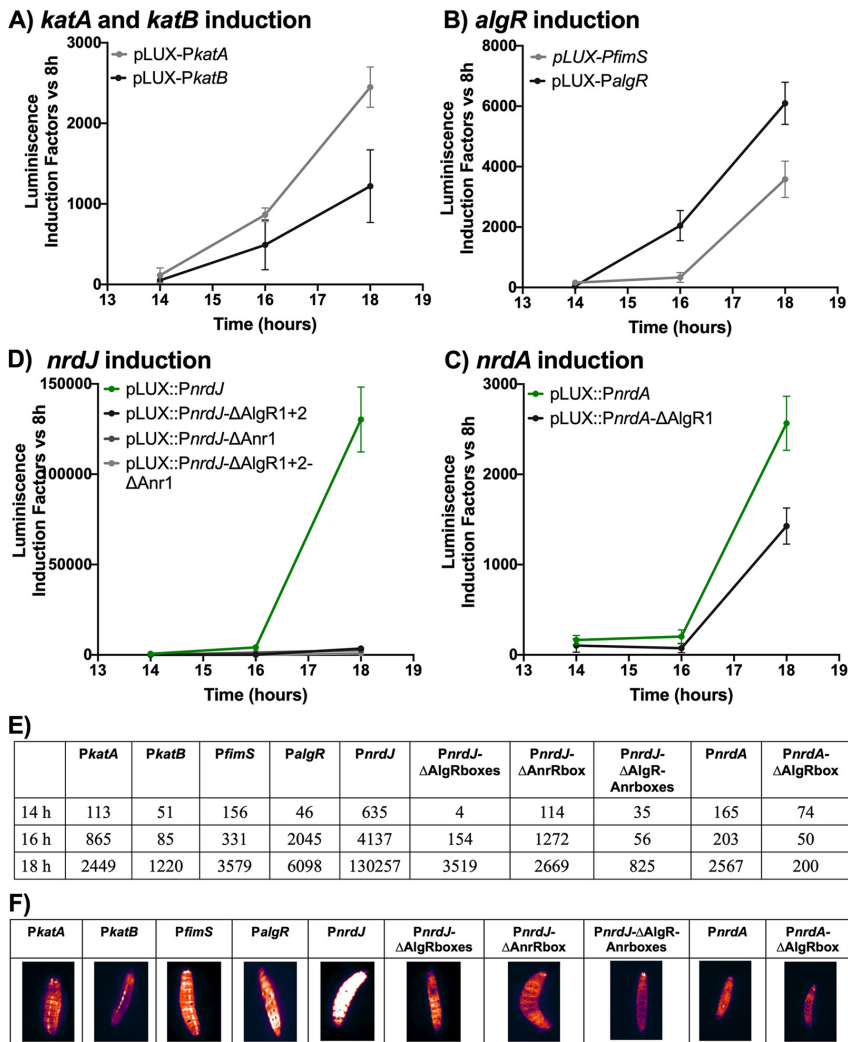
FIG 6 Gene expression in *Galleria mellonella* larvae infection. Bioluminescence induction factors of expression in (A) *kat*, (B) *algR*, (C) *nrdJ*, and (D) *nrdA* promoters at different time points (14, 16 and 18 h postinfection). (E) Table listing bioluminescence induction factors. (F) Images of *G. mellonella* larvae bioluminescence taken with a ImageQuant LAS 4000 mini-imager.

postinfection (2,567-fold induction). At that time, the expression of *nrdA* with the AlgR box mutated was decreased by 13 times (200-fold induction).

Notably, the induction of *nrdJ* expression was much larger than that of *nrdA* expression (37 and 13 times, respectively, compared with that of the AlgR box mutant promoter counterpart), which demonstrates the key role of the class II RNR gene *nrdJ*, compared to *nrdA*, which was not the primary RNR gene activated during the infection of *G. mellonella*.

The bioluminescence produced by the different promoters was visualized using the ImageQuant LAS 4000, and images were taken at 18 h postinfection (Fig. 6E). The amount of bioluminescence shown in the images of the larvae depends on the expression of each gene, which is in accordance with the results shown in Fig. 6A to D.

DISCUSSION

RNRs are essential enzymes in the life of any cell. Bacterial genomes commonly encode several RNRs to facilitate adaptation to different environmental conditions; thus, the expression and activation of each RNR class are tightly regulated. One of the main RNR transcriptional regulators is AlgR, which is part of the two-component system FimS-AlgR. AlgR is a global regulator, and FimS catalyzes its phosphorylation (8). The phosphorylation state of AlgR determines which regulatory pathways are activated or inactivated (3). We previously demonstrated that while *nrdA* is activated by phosphorylated AlgR in planktonic growth, *nrdJ* needs nonphosphorylated AlgR to be activated during early biofilm formation (8, 12).

The transcription of *algR* is carried out through two different promoters regulated by specific transcription factors (7). Environmental signals activate *algR* transcription through a specific promoter. In this study, we found that the expression of *algR* was induced under oxidative stress conditions, especially during the stationary growth phase (Fig. 1). The *algR* expression levels were not very high, probably due to its role as a global bacterial regulator. Global regulators are tightly regulated because dramatic changes in their expression can modify several metabolic pathways in the cell. However, although the activation was low, it was mainly observed through P*algR*, whose transcription is carried out after the binding of sigma factors such as RpoS and AlgU (7). The activation through the P*algR* promoter may indicate that AlgR does not depend on FimS when ROS are produced; thus, it may be nonphosphorylated or simply found in small amounts. Thus, new experiments using *rpoS* and *algU* mutant strains should be performed in the future to unravel their exact roles under oxidative stress conditions. Other studies have linked AlgR to the oxidative stress defense system in *P. aeruginosa*, but its role is not yet clear (19). It is possible that one of the main roles that AlgR plays against ROS is activating the *algD* operon to produce alginate, as it is known that alginate scavenges ROS, protecting bacteria (15). Due to this, studying *algD* or *algC* when ROS are present could be another acceptable way to delve into the roles of AlgR and alginate under oxidative stress conditions.

AlgR is a key factor in the regulation of class II (*nrdJ*) and class I (*nrdA*) RNRs and is involved in the control of the total dNTP pool in the cell. We determined that AlgR is responsible for inducing *nrdJ* expression under oxidative stress conditions (Fig. 2). It seems that *nrdJ* depends directly on AlgR binding, as its induction was removed when the AlgR binding boxes of the *nrdJ* promoter region were mutated and in a Δ*algR* strain (8). *nrdJ* induction was restored in a higher expression pattern when the *algR* mutation was complemented with the protein AlgR in its unphosphorylated state (pUCP-D54N). Using a *fimS* mutant strain could have been another acceptable way to study the phosphorylation state of AlgR under oxidative stress conditions. In the laboratory *P. aeruginosa* PA14 strain and the clinical isolate *P. aeruginosa* PAET1, we observed similar patterns of expression. *nrdJ* was induced when H_2O_2 was present, and this induction was abolished in a Δ*algR* strain and when using P*nrdJ*-Δ*box1+2*. AlgR-D54N restored *nrdJ* induction, indicating that AlgR was not phosphorylated. We observed that the basal expression of *nrdJ* in *P. aeruginosa* PA14 and PAET1 was lower than that in the PAO1 laboratory strain. We hypothesize that the reduced expression values observed may be due to differences in the genetic contexts of the three strains. However, the experiments confirmed that nonphosphorylated AlgR was the factor responsible for inducing *nrdJ* under oxidizing conditions.

When we measured the expression of *nrdA* under oxidative stress conditions, we found that class I RNRs were transcriptionally induced in *P. aeruginosa* PAO1, PA14, and PAET1 (Fig. 3) (8). This induction was absent in a Δ*algR* strain and when the AlgR binding box in the *nrdA* promoter was mutated (P*nrdA*-Δ*box1*). As shown in Fig. 2, *nrdA* expression in *P. aeruginosa* PA14 and in the clinical isolate *P. aeruginosa* PAET1 was lower than that in the laboratory strain PAO1. However, the experiments were useful enough to confirm that AlgR in its nonphosphorylated state was the factor responsible for inducing *nrdA* expression when H_2O_2 was present.

During infection, the production of ROS is one of the main defensive mechanisms against bacteria (15). To evaluate whether AlgR regulates RNR expression under oxidative

stress conditions during infection, we measured RNR induction in a continuous biofilm, which can simulate an infection-like situation (24). Other studies have already measured ROS in biofilms and have shown the importance of this growth condition during infection (25). In our experiments, we used a continuous flow biofilm to measure *nrdJ* and *nrdA* expression under oxidizing conditions (Fig. 4). The results showed that *nrdJ* expression was transcriptionally induced when H_2O_2 was present and that this induction was completely abolished when the AlgR boxes on the promoter region were mutated. When the Anr box found in the *nrdJ* promoter was mutated together with the AlgR boxes, we showed that *nrdJ* expression was even lower. These results demonstrate the critical role of AlgR in regulating *nrdJ* during biofilm formation. Anr is a transcription factor which regulates genes involved in anaerobic conditions (21), and it was shown to have a role in the regulation of *nrdJ* during biofilm formation (Fig. 4). However, the use of an *anr* mutant strain or a *nrdJ* promoter with the Anr box mutated could contribute to a better understanding of the role of Anr on its own. Because the complementation of Δ*algR* with AlgR and AlgR-D54N restored *nrdJ* expression under oxidative stress conditions, we determined that AlgR in its nonphosphorylated state was responsible for inducing *nrdJ* during biofilm formation. These results agree with those of previous studies showing that while phosphorylated AlgR regulates the initial steps of infection, nonphosphorylated AlgR controls the later steps, such as the production of alginate (7, 8).

In addition, we observed that the expression of *nrdA* was transcriptionally induced under oxidative stress conditions and that this induction was abolished when the AlgR box was mutated, confirming that AlgR is responsible for *nrdA* induction in biofilms. When we evaluated whether AlgR bound to the promoter in its phosphorylated or nonphosphorylated state, we observed that *nrdA* expression did not reach WT levels; however, AlgR-D54N produced slightly higher expression than wild-type AlgR (Fig. 5).

Finally, we used the *in vivo* model *G. mellonella* to measure the expression of several genes (Fig. 6). Other authors have linked the hemocytes of *G. mellonella* with the production of ROS inside the larvae (26). To test whether the bacteria inside the larvae could sense the oxidative stress produced during infection, we measured the expression of the *P. aeruginosa* catalases *katA* and *katB*. We observed that during *G. mellonella* infection, the expression of the constitutive catalase *katA* was increased at all the time points measured, and the expression of *katB*, the catalase whose expression is activated only when large amounts of ROS are detected (15), was activated at 16 and 18 h postinfection. After confirming that *P. aeruginosa* sensed the oxidative stress produced, we measured the expression of the remaining genes. We observed that *algR* expression was induced throughout the infection process, with higher levels of induction factors observed with P*algR* than with P*fimS*. When measuring the expression of the RNR, we observed that *nrdJ* showed the highest induction at 18 h postinfection, but its expression was completely eliminated when the AlgR boxes and the Anr box were mutated, confirming the remarkable roles of these transcription factors during infection (8, 21). The high induction of *nrdJ* at the latest time point suggests the important role of class II RNR in infections. However, when investigating the expression of *nrdA*, we observed that it decreased when the AlgR box was mutated, but it was not completely eliminated; thus, other factors may regulate the expression of *nrdA*. These results highlight the essential role of *nrdJ* in *G. mellonella* infection as the principal transcriptionally active RNR gene.

It is important to mention that all the experiments were conducted using plasmid constructions, which may not reflect the endogenous expression levels inside the cell and could yield certain modifications of the final levels depending on the system studied. However, our goal was not to investigate the specific amount of RNR production but to understand all actors taking place in their transcriptional regulation.

We have designed a schematic diagram to summarize the steps followed by *P. aeruginosa* under oxidative stress conditions (Fig. 7). Under nonoxidative conditions and after specific signals are sensed, the transmembrane protein FimS is autophosphorylated and phosphorylates the regulatory protein AlgR (3). Phosphorylated AlgR induces the

Artículo 1: *Pseudomonas aeruginosa* nonphosphorylated AlgR induces ribonucleotide reductase expression under oxidative stress infectious conditions

AlgR Induces Ribonucleotide Reductase Gene Expression   mSystems
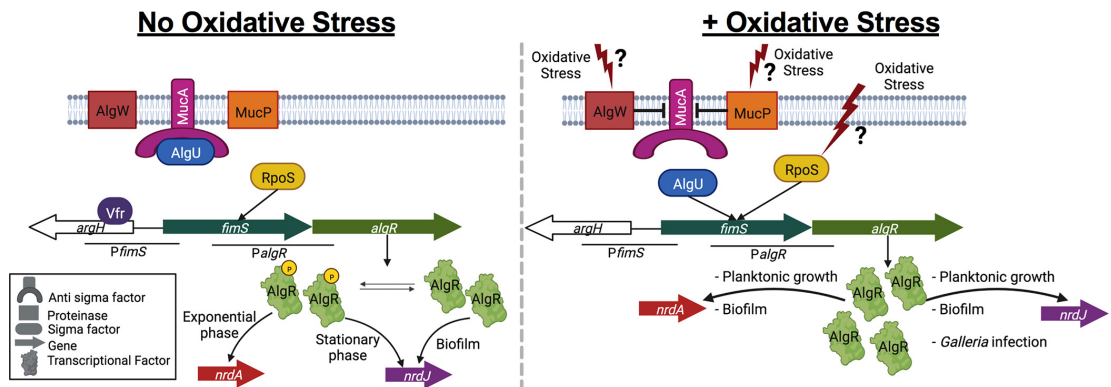
FIG 7 Schematic representation of AlgR regulation with and without oxidative stress. Hypothetical regulatory model of the molecular pathway used by *P. aeruginosa* with or without oxidative stress conditions. Question marks indicate the putative pathways that oxidative stress may follow to induce *algR* expression and consequently class I (*nrdA*) and class II (*nrdJ*) ribonucleotide reductase (RNR) expression under specific growth conditions. Sources of information for each event are indicated in the manuscript. Artwork created with www.biorender.com.

expression of *nrdA* during the exponential growth phase and in the initial stages of biofilm colonization (8).

During the stationary growth phase, the sigma factors AlgU and RpoS bind to the promoter region of *algR*. AlgU is a sigma factor (σ^{22}) that is usually sequestered by the anti-sigma factor MucA. AlgU regulates genes important for alginate formation (27). RpoS is a sigma factor (σ^{38}) whose expression is cell cycle-dependent. It is regulated by cell density, and it regulates the transition to stationary phase (28). Once AlgU and RpoS bind to P*algR*, most of the AlgR protein produced is not phosphorylated (7). The nonphosphorylated AlgR favors the expression of *nrdJ* in the stationary phase of a planktonic culture and in biofilm.

Under oxidative stress conditions, AlgR expression is generated from P*algR*, and class I and class II RNRs are induced by nonphosphorylated AlgR in planktonic, biofilm and infection conditions (Fig. 1–6). These results suggest that AlgU and/or RpoS are the factors responsible for sensing ROS when they are present. AlgU has been linked with the oxidative stress defense system in *P. aeruginosa* (29). In addition, other proteins related to AlgU and MucA, such as AlgW and MucP, have been related to oxidative stress. We hypothesize that under oxidative conditions, AlgW or MucP cleaves MucA, freeing AlgU (15). The freed AlgU may activate *algR* expression, and AlgU and AlgR together may activate the transcription of their target genes. In addition, the RNR NrdA and NrdJ would produce the dNTPs needed to repair the damaged DNA. Once the ROS are eliminated by the multifaceted system of *P. aeruginosa*, AlgU would be sequestered by MucA again. On the other hand, the RpoS counterpart in *E. coli*, in addition to being involved in the transition to stationary phase, plays a role in the sensing of several stresses, including oxidative stress. However, no conclusive studies have confirmed a notable role of RpoS in oxidative stress-sensing in *P. aeruginosa* beyond a slight relationship (30). Taking all of this into account, we believe that AlgU is the sigma factor involved in the activation of *algR* under oxidative stress conditions. However, there are still many gaps that need to be filled. Experiments using Δ*algU* and Δ*rpoS* strains would help to shed light on the oxidative stress defense system and its relationship with the RNR regulatory network.

Conclusion. In conclusion, these results indicate that *algR* expression is induced after the addition of H_2O_2 in exponential and stationary phases and that *algR* expression under oxidative stress conditions is mostly obtained through the promoter P*algR*. These results may help unravel the role of AlgR in the oxidative stress response system. Additionally, we observed that under planktonic and biofilm conditions with oxidative stress, the expression of *nrdJ* and *nrdA* was transcriptionally induced by AlgR in its nonphosphorylated state in all *P. aeruginosa* strains tested. Finally, we showed that during

G. mellonella infection, the ROS produced by the larvae can be sensed by the bacteria and that *nrdJ* plays a major role in the production of dNTPs during an infection.

MATERIALS AND METHODS

Bacterial strains, plasmids, and growth conditions. The bacterial strains and plasmids used are listed in Table S1. *E. coli* and *P. aeruginosa* strains were routinely grown in Luria-Bertani (Scharlab, Spain) medium at 37°C. Liquid cultures were shaken at 200 rpm. When necessary, antibiotics were added at the following concentrations: 50 μg/mL ampicillin and 10 μg/mL gentamicin for *E. coli*; and 100 μg/mL gentamicin, 40 μg/mL tetracycline, and 300 μg/mL carbenicillin for *P. aeruginosa*.

DNA manipulation and plasmid construction. Recombinant DNA manipulations were performed using standard protocols (31). The molecular biology kits and enzymes used in this study were purchased from Thermo Fisher Scientific (Spain) except as otherwise stated and were used following the manufacturers' instructions. DNA fragments were amplified using Phusion High-Fidelity DNA polymerase or DreamTaq Green PCR MasterMix with the primers listed in Table S2. DNA fragments were isolated from agarose gels using a GeneJet Gel Extraction kit. Plasmid DNA was extracted using a GeneJET Plasmid Miniprep kit and transferred into *P. aeruginosa* cells via electroporation using a Gene Pulser XCell electroporator (Bio-Rad) as previously described (32). All the constructs obtained were verified with DNA sequencing by Eurofins Genomics.

The plasmids pETS-P*katA* (pETS229), pETS-P*katB* (pETS230), and pETS-P*algR*-2 (pETS231) were constructed. Briefly, the *katA* (PA4236, 748 bp), *katB* (PA4613, 492 bp), and *algR* (PA5261, 878 bp) promoter regions were first amplified from *P. aeruginosa* PAO1 genomic DNA using primers 1 to 6, listed in Table S2. Each fragment was gel-purified, cloned into the pJET1.2b vector, and transformed into the *E. coli* DH5α strain. The resulting plasmids and the pETS130-GFP plasmid were digested with the corresponding restriction enzymes (BamHI-SmaI), and ligation was performed using the enzyme T4 ligase. These plasmids were electroporated into *P. aeruginosa* PAO1.

The Anr binding box in the *nrdJ* promoter region was mutated using PCR-based site-directed mutagenesis. The primer pairs 7/8 and 9/10 were used to amplify two fragments of the templates pETS-P*J* (pETS180) and pETS-P*J*-Δ*box1+2* (pETS211) to generate the DNA fragments P*nrdJ*-Δ*Anrbox* and P*nrdJ*-Δ*AlgRbox1+2*-Δ*Anrbox*, respectively. Each fragment was gel-purified and used as a template for a second round of PCR with the primers 7/10. The resulting amplicons were ligated into the pJET1.2b vector. The resulting plasmids and the pETS130-GFP plasmid were digested with BamHI-SmaI, and ligation was performed using the enzyme T4 ligase to obtain the plasmids pETS-P*J*-Δ*Anrbox* (pETS232) and pETS-P*J*-Δ*box1+2*-Δ*Anrbox* (pETS233). These plasmids were electroporated into *P. aeruginosa* PAO1. Each construct was verified by DNA sequencing.

The promoter regions of the genes used in this study were cloned into the *lux* promoter vector pETS220. The plasmids pETS-P*A*-Δ*box1* (pETS208), pETS-P*J*-Δ*box1+2* (pETS211), pETS-P*J*-Δ*Anrbox* (pETS232), pETS-P*J*-Δ*box1+2*-Δ*Anrbox* (pETS233), pETS-P*katA* (pETS229), pETS-P*algR*-1 (pETS207), and pETS-P*algR*-2 (pETS231) were digested using the enzymes SmaI and SacI. The fragments obtained were gel-purified and ligated using the enzyme T4 ligase into the digested SmaI-SacI pLUX (pET220) to obtain the plasmids pLUX-P*A*-Δ*box1* (pETS234), pLUX-P*J*-Δ*box1+2* (pETS235), pLUX-P*J*-Δ*Anrbox* (pETS236), pLUX-P*J*-Δ*box1+2*-Δ*Anrbox* (pETS237), pLUX-P*katA* (pETS238), pLUX-P*algR*-1 (pETS240), and pLUX-P*algR*-2 (pETS241). The plasmid pETS-P*katB* (pETS230) was digested with the enzymes SmaI and SpeI, and the digested fragment was gel purified and ligated with the enzyme T4 ligase into the digested SmaI-SpeI pLUX to obtain pLUX-P*katB* (pETS239). These plasmids were electroporated into *P. aeruginosa* PAO1.

Deletion of the algR gene in *P. aeruginosa* strain PA14 and the clinical PAET1 strains. The plasmid pEX100Tlink was used to obtain *P. aeruginosa* PA14 and PAET1 *algR* mutant strains. First, we performed PCR to amplify the upstream and downstream regions of *algR* using the primer pairs 11/12 and 13/14 and the chromosomal DNA of PA14 and PAET1 as the templates. The amplified fragments were gel-purified and ligated into pJET1.2b using the enzyme T4 ligase. The plasmids obtained and the vector pEX100Tlink were digested using the restriction enzymes HindIII-BamHI and BamHI-SacI. The gel-purified fractions were ligated with the digested pEX100Tlink plasmid to obtain pEX100Tlink::*algR'*-'*algR* (pETS242) and pEX100Tlink::*algR'*-'*algR* (pETS243) for PA14 and PAET1, respectively. Afterward, the plasmids pETS242, pETS243, and pUCGmlox were digested with the restriction enzyme BamHI. The digested fractions were gel-purified and ligated with the enzyme T4 ligase to obtain the plasmids pEX100Tlink::*algR'*-Gmlox-'*algR* (PA14; pETS244) and pEX100Tlink::*algR'*-Gmlox-'*algR* (PAET1; pETS245). These final constructs were transformed into the *E. coli* S17.1 helper strain.

The PA14 Δ*algR*Gmlox mutant (pETS131) and PAET1 Δ*algR*Gmlox mutant (pETS133) of *P. aeruginosa* were generated by introducing pETS244 and pETS245, respectively, from *E. coli* S17.1 by conjugation. LB medium supplemented with 5% sucrose was used to counterselect the gentamicin-resistant transconjugants PA14 Δ*algR*Gmlox and PAET1 Δ*algR*Gmlox. Next, the plasmid pCM157 was electroporated into PA14 Δ*algR*Gmlox and PAET1 Δ*algR*Gmlox. The mutant strains were grown on LB broth supplemented with tetracycline to remove the gentamicin resistance cassette via the expression of the *cre* recombinase (33). The pCM157 was then removed from the mutant strains by three successive growth cycles in LB broth without tetracycline. The selected PA14 Δ*algRlox* mutant (pETS132) and PAET1 Δ*algRlox* mutant (pETS134) of *P. aeruginosa* were sensitive to gentamicin and tetracycline.

Green fluorescent protein gene reporter assay. *P. aeruginosa* bacterial cultures were grown on LB without antibiotics at 37°C and 200 rpm to OD$_{550}$ = 0.5 (exponential phase) and OD$_{550}$ > 2 (stationary phase). Upon reaching the desired OD$_{550}$, three independent 1-mL samples of each strain were collected. The samples were centrifuged for 10 min at 5,000 rpm, and the cell pellets were fixed with 1 mL of freshly prepared phosphate-buffered saline (PBS) solution containing 2% formaldehyde and stored in

the dark at 4°C for 10 min. The samples were centrifuged again, and the pellets were resuspended in 1 mL PBS. The fluorescence of the samples was measured in 96-well plates (Costar 96-Well Black Polystyrene plate, Corning) in an Infinite 200 Pro Fluorescence Microplate Reader (Tecan, Switzerland). Three measurements were performed for each independent sample.

Biofilm in flow cell chambers, microscopy, and image analysis. Different bacterial cultures of *P. aeruginosa* were adjusted to an OD$_{550}$ of 0.3 and inoculated into a three-channel flow cell (DTU Systems Biology, Technical University of Denmark). LB medium supplemented with 0.2% glucose was pumped through the flow cells at a constant flow rate of 42 μL/min and channel using an Ismatec ISM 943 pump (Ismatec, Wertheim, Germany). After 96 h of growth, the *P. aeruginosa* biofilms were treated with H$_2$O$_2$ at 4 mM for 4 h. The biofilm was stained with 10 μM SYTO60 reagent (Thermo Fisher Scientific, Spain) for 30 min at room temperature to visualize the total biofilm biomass and with 5 μM CellROX Orange reagent (Thermo Fisher Scientific) for 20 min at room temperature to detect oxidative stress.

A Zeiss LSM 800 confocal laser scanning microscope with excitation wavelengths of 488, 561, and 640 nm was used to generate the images. Microscope images were processed using ImageJ, and COMSTAT 2 software was used to quantify biofilm biomass as previously described (4, 34).

Galleria mellonella maintenance and injection. *G. mellonella* larvae were fed a diet of 15% corn flour, 15% wheat flour, 15% infant cereal, 11% powdered milk, 6% brewer's yeast, 25% honey, and 13% glycerol and raised at 34°C in darkness as previously described (35). Before injection, the bacterial cultures of the different strains were centrifuged at 4,000 rpm for 10 min. The supernatant was discarded, and the pellet was washed three times in 5 mL PBS (Thermo Fisher Scientific, Spain). The culture was set to a final OD$_{590}$ of 1. Afterward, 10-fold serial dilutions of the equalized cultures were made with PBS. A total of 20 to 40 CFU of the bacteria were injected into groups of 6 *G. mellonella* larvae through the top right proleg using a 26-gauge microsyringe (Hamilton, NV, USA). The larvae were then kept at 37°C during the infection course.

Bioluminescence measurements. The relative luminescence of infected larvae was measured using a 6-well microtiter plate (Caplugs Evergreen, NY, USA) in an Infinite 200 Pro Fluorescence Microplate Reader (Tecan, Switzerland) with an integration time of 1,000 ms. GraphPad Prism 9.0 software (GraphPad Software, San Diego, CA, USA) was used to analyze the results obtained, and an ImageQuant LAS 4000 mini-imager (GE Healthcare, IL, USA) was used to obtain images of the chemiluminescence of the larvae at different time points postinfection with an exposure time of 30 s. The images were edited with ImageJ FIJI (version 1.52p, NIH, USA). Before each measurement, the larvae were anesthetized for 10 min on ice.

Promoter alignment. The T-COFFEE multiple sequence alignment server was used to align and compare the promoter regions of *nrdJ* and *nrdA* from the *P. aeruginosa* PAO1, PA14, and PAET1 strains (36).

Statistical analysis. GraphPad Prism 9.0 (GraphPad Software) was used to perform statistical analyses. Single comparisons were performed with unpaired or paired Student's *t* tests depending on the experiment type. The data values are expressed as the mean $\pm$ standard deviation.

SUPPLEMENTAL MATERIAL

Supplemental material is available online only.

FIG S1, PDF file, 1.8 MB.

TABLE S1, PDF file, 0.1 MB.

TABLE S2, PDF file, 0.1 MB.

ACKNOWLEDGMENTS

The manuscript was written by A.R.-C. E.T., L.P., and J.A. conducted the experiments. E.T. directed the research and revised the experimental data. All authors have approved the final version of the manuscript.

REFERENCES

1. Govan JR, Deretic V. 1996. Microbial pathogenesis in cystic fibrosis: mucoid *Pseudomonas aeruginosa* and *Burkholderia cepacia*. Microbiol Rev 60:539–574. https://doi.org/10.1128/mr.60.3.539-574.1996.

2. Mohr CD, Hibler NS, Deretic V. 1991. AlgR, a response regulator controlling mucoidy in *Pseudomonas aeruginosa*, binds to the FUS sites of the algD promoter located unusually far upstream from the mRNA start site. J Bacteriol 173:5136–5143. https://doi.org/10.1128/jb.173.16.5136-5143.1991.

3. Okkotsu Y, Little AS, Schurr MJ. 2014. The *Pseudomonas aeruginosa* AlgZR two-component system coordinates multiple phenotypes. Front Cell Infect Microbiol 4:82. https://doi.org/10.3389/fcimb.2014.00082.

4. Blanco-Cabra N, Paetzold B, Ferrar T, Mazzolini R, Torrents E, Serrano L, LLuch-Senar M. 2020. Characterization of different alginate lyases for dissolving *Pseudomonas aeruginosa* biofilms. Sci Rep 10:9390. https://doi.org/10.1038/s41598-020-66293-2.

5. Damron FH, Goldberg JB. 2012. Proteolytic regulation of alginate overproduction in *Pseudomonas aeruginosa*. Mol Microbiol 84:595–607. https://doi.org/10.1111/j.1365-2958.2012.08049.x.

6. Darzins A, Chakrabarty AM. 1984. Cloning of genes controlling alginate biosynthesis from a mucoid cystic fibrosis isolate of *Pseudomonas aeruginosa*. J Bacteriol 159:9–18. https://doi.org/10.1128/jb.159.1.9-18.1984.

7. Pritchett CL, Little AS, Okkotsu Y, Frisk A, Cody WL, Covey CR, Schurr MJ. 2015. Expression analysis of the *Pseudomonas aeruginosa* AlgZR two-component regulatory system. J Bacteriol 197:736–748. https://doi.org/10.1128/JB.02290-14.

8. Crespo A, Pedraz L, Van Der Hofstadt M, Gomila G, Torrents E. 2017. Regulation of ribonucleotide synthesis by the *Pseudomonas aeruginosa* two-component system AlgR in response to oxidative stress. Sci Rep 7:17892. https://doi.org/10.1038/s41598-017-17917-7.

9. Torrents E. 2014. Ribonucleotide reductases: essential enzymes for bacterial life. Front Cell Infect Microbiol 4:52. https://doi.org/10.3389/fcimb.2014.00052.

10. Ruskoski TB, Boal AK. 2021. The periodic table of ribonucleotide reductases. J Biol Chem 297:101137. https://doi.org/10.1016/j.jbc.2021.101137.

11. Crespo A, Blanco-Cabra N, Torrents E. 2018. Aerobic vitamin B12 biosynthesis is essential for *Pseudomonas aeruginosa* class II ribonucleotide reductase activity during planktonic and biofilm growth. Front Microbiol 9:986. https://doi.org/10.3389/fmicb.2018.00986.

12. Crespo A, Gavalda J, Julian E, Torrents E. 2017. A single point mutation in class III ribonucleotide reductase promoter renders *Pseudomonas aeruginosa* PAO1 inefficient for anaerobic growth and infection. Sci Rep 7:13350. https://doi.org/10.1038/s41598-017-14051-2.

13. Sjöberg BM, Torrents E. 2011. Shift in ribonucleotide reductase gene expression in *Pseudomonas aeruginosa* during infection. Infect Immun 79:2663–2669. https://doi.org/10.1128/IAI.01212-10.

14. Crespo A, Pedraz L, Astola J, Torrents E. 2016. *Pseudomonas aeruginosa* exhibits deficient biofilm formation in the absence of class II and III ribonucleotide reductases due to hindered anaerobic growth. Front Microbiol 7:688. https://doi.org/10.3389/fmicb.2016.00688.

15. da Cruz Nizer WS, Inkovskiy V, Versey Z, Strempel N, Cassol E, Overhage J. 2021. Oxidative stress response in *Pseudomonas aeruginosa*. Pathogens 10:1187. https://doi.org/10.3390/pathogens10091187.

16. Cochran WL, Suh SJ, McFeters GA, Stewart PS. 2000. Role of RpoS and AlgT in *Pseudomonas aeruginosa* biofilm resistance to hydrogen peroxide and monochloramine. J Appl Microbiol 88:546–553. https://doi.org/10.1046/j.1365-2672.2000.00995.x.

17. Katharios-Lanwermeyer S, Koval SA, Barrack KE, O'Toole GA. 2022. The diguanylate cyclase YfiN of *Pseudomonas aeruginosa* regulates biofilm maintenance in response to peroxide. J Bacteriol 204:e0039621. https://doi.org/10.1128/JB.00396-21.

18. Monje-Casas F, Jurado J, Prieto-Alamo MJ, Holmgren A, Pueyo C. 2001. Expression analysis of the *nrdHIEF* operon from *Escherichia coli*. Conditions that trigger the transcript level *in vivo*. J Biol Chem 276:18031–18037. https://doi.org/10.1074/jbc.M011728200.

19. Malhotra S, Limoli DH, English AE, Parsek MR, Wozniak DJ. 2018. Mixed communities of mucoid and nonmucoid *Pseudomonas aeruginosa* exhibit enhanced resistance to host antimicrobials. mBio 9:e00275-18. https://doi.org/10.1128/mBio.00275-18.

20. Trunk K, Benkert B, Quack N, Munch R, Scheer M, Garbe J, Jansch L, Trost M, Wehland J, Buer J, Jahn M, Schobert M, Jahn D. 2010. Anaerobic adaptation in *Pseudomonas aeruginosa*: definition of the Anr and Dnr regulons. Environ Microbiol 12:1719–1733. https://doi.org/10.1111/j.1462-2920.2010.02252.x.

21. Pedraz L, Blanco-Cabra N, Torrents E. 2020. Gradual adaptation of facultative anaerobic pathogens to microaerobic and anaerobic conditions. FASEB J 34:2912–2928. https://doi.org/10.1096/fj.201902861R.

22. Moya-Anderico L, Vukomanovic M, Cendra MDM, Segura-Feliu M, Gil V, Del Rio JA, Torrents E. 2021. Utility of *Galleria mellonella larvae* for evaluating nanoparticle toxicity. Chemosphere 266:129235. https://doi.org/10.1016/j.chemosphere.2020.129235.

23. Moya-Anderico L, Admella J, Fernandes R, Torrents E. 2020. Monitoring gene expression during a *Galleria mellonella* bacterial infection. Microorganisms 8:1798. https://doi.org/10.3390/microorganisms8111798.

24. Blanco-Cabra N, Lopez-Martinez MJ, Arevalo-Jaimes BV, Martin-Gomez MT, Samitier J, Torrents E. 2021. A new BiofilmChip device for testing biofilm formation and antibiotic susceptibility. NPJ Biofilms Microbiomes 7:62. https://doi.org/10.1038/s41522-021-00236-1.

25. Rossi F, Catto C, Mugnai G, Villa F, Forlani F. 2021. Effects of the quinone oxidoreductase WrbA on *Escherichia coli* biofilm formation and oxidative stress. Antioxidants 10:919. https://doi.org/10.3390/antiox10060919.

26. Grizanova EV, Semenova AD, Komarov DA, Chertkova EA, Slepneva IA, Dubovskiy IM. 2018. Maintenance of redox balance by antioxidants in hemolymph of the greater wax moth *Galleria mellonella* larvae during encapsulation response. Arch Insect Biochem Physiol 98:e21460. https://doi.org/10.1002/arch.21460.

27. Wozniak DJ, Ohman DE. 1994. Transcriptional analysis of the *Pseudomonas aeruginosa* genes *algR*, *algB*, and *algD* reveals a hierarchy of alginate gene expression which is modulated by *algT*. J Bacteriol 176:6007–6014. https://doi.org/10.1128/jb.176.19.6007-6014.1994.

28. Potvin E, Sanschagrin F, Levesque RC. 2008. Sigma factors in *Pseudomonas aeruginosa*. FEMS Microbiol Rev 32:38–55. https://doi.org/10.1111/j.1574-6976.2007.00092.x.

29. Yu H, Boucher JC, Hibler NS, Deretic V. 1996. Virulence properties of *Pseudomonas aeruginosa* lacking the extreme-stress sigma factor AlgU (sigmaE). Infect Immun 64:2774–2781. https://doi.org/10.1128/iai.64.7.2774-2781.1996.

30. Hou S, Zhang J, Ma X, Hong Q, Fang L, Zheng G, Huang J, Gao Y, Xu Q, Zhuang X, Song X. 2021. Role of *rgsA* in oxidative stress resistance in *Pseudomonas aeruginosa*. Curr Microbiol 78:3133–3141. https://doi.org/10.1007/s00284-021-02580-z.

31. Sambrook J, Fritsch ER, Maniatis T. 1989. Molecular cloning: a laboratory manual, 2nd ed. Cold Spring Harbor Laboratory Press, Cold Spring Harbor, NY.

32. Chuanchuen R, Narasaki CT, Schweizer HP. 2002. Benchtop and microcentrifuge preparation of *Pseudomonas aeruginosa* competent cells. Biotechniques 33:760, 762–3. https://doi.org/10.2144/02334bm08.

33. Marx CJ, Lidstrom ME. 2002. Broad-host-range *cre-lox* system for antibiotic marker recycling in Gram-negative bacteria. Biotechniques 33:1062–1067. https://doi.org/10.2144/02335rr01.

34. Heydorn A, Nielsen AT, Hentzer M, Sternberg C, Givskov M, Ersboll BK, Molin S. 2000. Quantification of biofilm structures by the novel computer program COMSTAT. Microbiology 146:2395–2407. https://doi.org/10.1099/00221287-146-10-2395.

35. Moya-Anderico L, Admella J, Torrents E. 2021. A clearing protocol for G*alleria mellonella* larvae: visualization of internalized fluorescent nanoparticles. N Biotechnol 60:20–26. https://doi.org/10.1016/j.nbt.2020.08.002.

36. Erb I, Gonzalez-Vallinas JR, Bussotti G, Blanco E, Eyras E, Notredame C. 2012. Use of ChIP-Seq data for the design of a multiple promoter-alignment method. Nucleic Acids Res 40:e52. https://doi.org/10.1093/nar/gkr1292.

Material Suplementario

Fig. S1. Multiple alignment of the class II and I RNR promoter regions. Alignment of the promoter regions of A) *nrdJ* and B) *nrdA* from the *P. aeruginosa* PAO1, PA14, and PAET1 strains. The AlgR binding box sites found in the promoter regions of the RNR are indicated with black rectangles.

Table S1. Bacterial strains and plasmids used in this study

Name	Reference name	Description	Source
Plasmids			
pJET1.2/blunt	pJET1.2b	Blunt-end vector; AmpR	Thermo Scientific
pETS130-GFP	pETS130	Broad host range, promoterless GFP; GmR	(1)
pETS134	pETS-P*A*	pETS130 derivative carrying *nrdA* promoter; GmR	(1)
pETS208	pETS-P*A*-Δbox1	pETS130 derivative carrying AlgR-box1 mutation in P*nrdA*, GmR	(2)
pETS180	pETS-P*J*	pETS130 derivative carrying *nrdJ* promoter; GmR	(3)
pETS211	pETS-P*J*-Δbox1+2	pETS130 derivative carrying AlgR-box1+2 mutation in P*nrdJ*, GmR	(2)
pET229	pETS-P*katA*	pETS130 derivative carrying *katA* promoter; GmR	This work
pETS230	pETS-P*katB*	pETS130 derivative carrying *katB* promoter; GmR	This work
pETS203	pUCP-AlgR	pUCP20T derivative carrying the *algR* gene; CbR	(2)
pETS204	pUCP-D54N	pUCP20T derivative carrying the *algR*D54N gene; CbR	(2)
pETS207	pETS-P*fimS*	pETS130 derivative carrying *fimS-algR* promoter; GmR	(2)
pETS231	pETS-P*algR*	pETS130 derivative carrying *algR* promoter; GmR	This work
pETS232	pETS-P*J*-ΔAnrbox	pETS130 derivative carrying Anr-box mutation in P*nrdJ*, GmR	This work
pETS233	pETS-P*J*-Δbox1+2-ΔAnrbox	pETS130 derivative carrying AlgR-box1+2 and Anr-box mutation in P*nrdJ*, GmR	This work
pETS220	pLUX	Broad host range, promoterless luxCDABE; GmR	(4)
pETS221	pLUX-P*A*	pETS220 derivative carrying *nrdA* promoter; GmR	(4)
pETS234	pLUX-P*A*-Δbox1	pETS220 derivative carrying AlgR-box1 mutation in P*nrdA*, GmR	This work
pETS222	pLUX-P*J*	pETS220 derivative carrying *nrdJ* promoter; GmR	(4)
pETS235	pLUX-P*J*-Δbox1+2	pETS220 derivative carrying AlgR-box1+2 mutation in P*nrdJ*, GmR	This work
pETS236	pLUX-P*J*-ΔAnrbox	pETS220 derivative carrying AnrR-box mutation in P*nrdJ*, GmR	This work
pETS237	pLUX-P*J*-Δbox1+2-ΔAnrbox	pETS220 derivative carrying AlgR-box1+2 and Anr-box mutation in P*nrdJ*, GmR	This work
pETS238	pLUX-P*katA*	pETS220 derivative carrying *katA* promoter; GmR	This work
pETS239	pLUX-P*katB*	pETS220 derivative carrying *katB* promoter; GmR	This work
pETS240	pLUX-P*algR*-1	pETS220 derivative carrying *fimS-algR* promoter; GmR	This work
pETS241	pLUX-P*algR*-2	pETS220 derivative carrying *algR* promoter; GmR	This work
pETS225	pLUX-*anr*	pETS220 derivative carrying *anr* gene fragment; GmR	(4)
pEX100Tlink	pEX100Tlink	pEX100T with a MCS; AmpR	(5)
pETS242	pEX100Tlink::*algR*´-`*algR* (PA14)	pEX100Tlink containing 5′ and 3′ flanking sequences of *algR* of *P. aeruginosa* PA14; AmpR	This work
pETS243	pEX100Tlink::*algR*´-`*algR* (PAET1)	pEX100Tlink containing 5′ and 3′ flanking sequences of *algR* of *P. aeruginosa* PAET1; AmpR	This work
pETS244	pEX100Tlink::*algR*´-Gm*lox*-`*algR* (PA14)	pEX100Tlink containing 5′ and 3′ flanking sequences of *algR* :: Gm*lox* of *P. aeruginosa* PA14; AmpR, GmR	This work
pETS245	pEX100Tlink::*algR*´-Gm*lox*-`*algR* (PAET1)	pEX100Tlink containing 5′ and 3′ flanking sequences of *algR* :: Gm*lox* of *P. aeruginosa* PAET1; AmpR, GmR	This work
pUCGmlox	pUCGmlox	pUC18-based vector containing the *lox* flanked *aacC1* gene	(5)
pCM157	pCM157	*cre* expression vector; TcR	(6)

	(PA14)	PA14; AmpR	
pETS243	pEX100Tlink::*algR′*-`*algR* (PAET1)	pEX100Tlink containing 5′ and 3′ flanking sequences of *algR* of *P. aeruginosa* PAET1; AmpR	This work

pETS245	pEX100Tlink::*algR′*-Gm*lox*-`*algR* (PAET1)	pEX100Tlink containing 5′ and 3′ flanking sequences of *algR* :: Gm*lox* of *P. aeruginosa* PAET1; AmpR, GmR	This work
pUCGmlox	pUCGmlox	pUC18-based vector containing the *lox* flanked *aacC1* gene	(5)
pCM157	pCM157	*cre* expression vector; TcR	(6)

Strains

E. coli			
DH5α	DH5α	*recA1 endA1 hsdR17 supE44 thi-1 relA1 Δ(lacZYA-argF)U169 deoR Φ80dlacZM15*	Laboratory
S17.1	S17.1	*recA thi pro hsdR- M+RP4::2-Tc::Mu::Km Tn7 Tpr Smr Xpir*	(7)
P. aeruginosa			
PAO1	PAO1 WT	Wild-type (ATCC 15692 / CECT 4122) - Spanish Type Culture Collection	Laboratory
PW9855	PAO1 Δ*algR*	*P. aeruginosa* PAO1 algR::ISphoA/hah; TcR	(8)
PA14	PA14 WT	*P. aeruginosa* PA14 wild-type strain	Laboratory
pETS131	PA14 Δ*algR*Gm*lox*	*P. aeruginosa* PA14Δ*algR*::Gm*lox*	This work
pETS132	PA14 Δ*algR*	*P. aeruginosa* PA14Δ*algR*::*lox*	This work
PAET1	PAET1 WT	*P. aeruginosa* clinical isolated from CF patient strain	(9)
pETS133	PAET1 Δ*algR*Gm*lox*	*P. aeruginosa* PAET1Δ*algR*::Gm*lox*	This work
pETS134	PAET1 Δ*algR*	*P. aeruginosa* PAET1Δ*algR*::*lox*	This work

1. Sjöberg BM, Torrents E. 2011. Shift in ribonucleotide reductase gene expression in *Pseudomonas aeruginosa* during infection. Infect Immun 79:2663-9.

2. Crespo A, Pedraz L, Van Der Hofstadt M, Gomila G, Torrents E. 2017. Regulation of ribonucleotide synthesis by the *Pseudomonas aeruginosa* two-component system AlgR in response to oxidative stress. Sci Rep 7:17892.

3. Crespo A, Pedraz L, Torrents E. 2015. Function of the *Pseudomonas aeruginosa* NrdR Transcription Factor: Global Transcriptomic Analysis and Its Role on Ribonucleotide Reductase Gene Expression. PLoS One 10:e0123571.

4. Moya-Anderico L, Admella J, Fernandes R, Torrents E. 2020. Monitoring Gene Expression during a *Galleria mellonella* Bacterial Infection. Microorganisms 8.

5. Quenee L, Lamotte D, Polack B. 2005. Combined *sacB*-based negative selection and cre-lox antibiotic marker recycling for efficient gene deletion in *Pseudomonas aeruginosa*. Biotechniques 38:63-7.

6. Marx CJ, Lidstrom ME. 2002. Broad-host-range *cre-lox* system for antibiotic marker recycling in Gram-negative bacteria. Biotechniques 33:1062-7.

7. de Lorenzo V, Cases I, Herrero M, Timmis KN. 1993. Early and late responses of TOL promoters to pathway inducers: identification of postexponential promoters in *Pseudomonas putida* with *lacZ-tet* bicistronic reporters. J Bacteriol 175:6902-7.

8. Jacobs MA, Alwood A, Thaipisuttikul I, Spencer D, Haugen E, Ernst S, Will O, Kaul R, Raymond C, Levy R, Chun-Rong L, Guenthner D, Bovee D, Olson MV, Manoil C. 2003. Comprehensive transposon mutant library of *Pseudomonas aeruginosa*. Proc Natl Acad Sci U S A 100:14339-44.

9. Crespo A, Gavalda J, Julian E, Torrents E. 2017. A single point mutation in class III ribonucleotide reductase promoter renders *Pseudomonas aeruginosa* PAO1 inefficient for anaerobic growth and infection. Sci Rep 7:13350.

Table S2. Primers and probes used in this study.

Primers

Number	Name	Sequence (5' -> 3')	Application
1	PkatA_BamHI_Fw	GGATCCGAATTGAACCATGCGCCATC	P*katA* promoter cloning/Sequencing
2	PkatA_SmaI_Rv	CCCGGGTCTGCACGTTCTGGTTA	P*katA* promoter cloning/Sequencing
3	PkatB_BamHI_Fw	GGATCCCAGATGCCGGAAGTTGAAGT	P*katB* promoter cloning/Sequencing
4	PkatB_SmaI_Rv	CCCGGGTCGAAACGTTGCAACTTC	P*katB* promoter cloning/Sequencing
5	fimS_SacI_Fw	GAGCTCCTGTTCTGCCGCCTG	P*algR* promoter cloning/Sequencing
6	fimS_BamHI_Rv	GGATCCCATCGACAATCAGGACATTCA	P*algR* promoter cloning/Sequencing
7	PnrdJ_PAO_BamHI_up_new	GGATCCCGCGCCCAGCTGAAGG	Mutagenesis P*nrdJ* Anrbox/Sequencing
8	PJ mut ad low	TATCCGTACCTGCGTGGAATCAATA	Mutagenesis P*nrdJ* Anrbox
9	PJ mut ad up	TATTGAGGACACGCAGGTACGGA	Mutagenesis P*nrdJ* Anrbox
10	PnrdJ_SmaI_Rv	CCCGGGGACTGCGTGCGTCTGTC	Mutagenesis P*nrdJ* Anrbox/Sequencing
11	fimS_HindIII_Fw	AAGCTTGCAGGTCGAGGCGGTTTAT	Deletion *algR* gene
12	fimS_BamHI_Rv	GGATCCCATCGACAATCAGGACATTCA	Deletion *algR* gene
13	HemC_BamHI_Fw	GGATCCGCATTTCCAGCTCTACCT	Deletion *algR* gene
14	HemC_SacI_Rv	GAGCTCGATGGTGTAGAGGCCGA	Deletion *algR* gene
15	pJET 1.2 fw	CGACTCACTATAGGGAGAGCGGC	Check cloning/Sequencing
16	pJET 1.2 rv	AAGAACATCGATTTTCCATGGCAG	Check cloning/Sequencing
17	pUCP20T-up	CCTCTTCGCTATTACGCCAG	Check cloning/Sequencing

Artículo 2: ReViTA: A novel *in vitro* transcription system to study gene regulation.

Alba Rubio-Canalejas, Lucas Pedraz and Eduard Torrents

Resumen

La transcripción *in vitro* (IVT) es una técnica de biología molecular que permite la síntesis de ARN a partir de una molécula de ADN utilizando un complejo formado por ARN polimerasa (RNAP) y el factor σ purificado previamente. Hasta ahora, la IVT se ha utilizado para estudiar la función de promotores, los factores σ, los ARN antisentido, entre otras. Además de la RNAP y factor σ, hay otros reguladores que intervienen en la transcripción de un promotor. Entre estos reguladores encontramos los factores de transcripción (FT), que son proteínas con dominios de unión a ADN y que regulan la expresión génica activando o inhibiendo el posicionamiento y/o actividad de la RNAP (268, 269).

El objetivo principal de este estudio coincide con el Objetivo 2 de la tesis y consiste en diseñar un sistema basado en la IVT para estudiar la expresión transcripcional de genes cuando están regulados por FT y comprender la función de los reguladores implicados. Hemos denominado a este sistema como ReViTA (**Re**verse *in* ***Vitro*** **T**ranscription **A**ssay, ensayo de transcripción reversa *in vitro*).

En este trabajo hemos desarrollado un sistema que utiliza una RNAP de *E. coli* saturada con el factor σ70, y que por tanto solo puede reconocer promotores con sitios de unión σ70; y un plásmido (pReViTA) que incluye las regiones promotoras de dos genes. Una de estas regiones pertenece al gen de interés que se quiere estudiar y que es donde se une el FT a estudiar. La otra región corresponde a un gen control a cuya región transcripcional no se une el FT a estudiar y que sirve para estandarizar la metodología y el número de transcritos generados. Una vez clonado el promotor de interés en el plásmido, hay que incubar el plásmido con el FT que se quiere estudiar. El tiempo, temperatura y buffer de incubación ADN-FT es recomendable que sea determinado de forma experimental previamente. Tras la incubación se añade la RNAP y comienza la IVT. La producción de ARN

que estará influenciada por el FT, si el FT es un activador se producirá más ARN y si es un represor se producirá menos. El ADN molde se elimina y el ARN generado se retrotranscribe a ADN complementario (ADNc). Mediante qRT-PCR se puede medir la amplificación de ADNc y así calcular la cantidad de ARN de cada muestra para dilucidar si los FTs utilizados son represores o activadores transcripcionales (Figura 1 del Artículo 2).

Como prueba de concepto, en este trabajo hemos utilizado el sistema ReViTA con dos FT de *P. aeruginosa*, un activador (AlgR) y un represor (LexA) junto con los promotores de los genes que regulan. AlgR activa la transcripción del gen de la RNR de clase Ia (*nrdA*) y LexA inhibe la transcripción del gen *dinB*, que codifica para una polimerasa de tipo IV (81, 270). Ambos FT se evaluaron con ensayos de desplazamiento de movilidad electroforética (EMSA) para comprobar que se unían al promotor de interés y no a la región control. Mientras que con AlgR se cumplían estos requisitos de unión únicamente al promotor de interés (*nrdA*), con LexA se observó una unión débil a la región control además de al promotor de *dinB* (Figura 2 del Artículo 2). Al realizar el ensayo de IVT utilizando el sistema ReViTA observamos que la expresión de *nrdA* aumentó entre un 29 y 55% cuando se ponía en contacto con AlgR en comparación con la muestra sin AlgR. Al utilizar las bandas lineares de PCR el aumento de transcripción fue menor, entre un 17 y un 40%. Al estudiar la expresión de *dinB* tras la incubación con LexA se observó que su transcripción disminuyó un 27% utilizando el sistema ReViTA y un 30% con las bandas lineares. Al aumentar la cantidad de LexA, la represión disminuyó, observando una inhibición del 10% con el sistema ReViTA y un 11% con las bandas lineares de PCR (Figura 3 del Artículo 2).

Con todo esto, estos resultados ayudaron a confirmar que con el sistema ReViTA se puede estudiar la regulación transcripcional de genes mediante FT, ya que los resultados obtenidos con el plásmido pReViTA son comparables a los obtenidos con los fragmentos linearles de ADN que se usan de forma tradicional, validando el Objetivo 2 de esta tesis.

Manuscrito

ReViTA: A novel *in vitro* transcription system to study gene regulation

Alba Rubio-Canalejas[1,&], Lucas Pedraz[2,&], Eduard Torrents[1,3,*]

[1]Bacterial infections and antimicrobial therapies group, Institute for Bioengineering of Catalonia (IBEC), The Barcelona Institute of Science and Technology (BIST). Baldiri Reixac 15-21. 08028 Barcelona, Spain.

[2]Centre for Microbial Diseases and Immunity Research. University of British Columbia. Vancouver BC V6T1Z4, Canada.

[3]Microbiology Section, Department of Genetics, Microbiology and Statistics, Faculty of Biology, University of Barcelona, 643 Diagonal Ave., 08028, Barcelona, Spain.

*Corresponding author:

Dr. Eduard Torrents: etorrents@ibecbarcelona.eu / eduard.torrents@ub.edu

Institute for Bioengineering of Catalonia (IBEC)

Ed. Helix | C/ Baldiri Reixac, 15-21 | 08028 Barcelona | (+ 34) 934034756

[&] These authors contributed equally to this work

Graphical Abstract
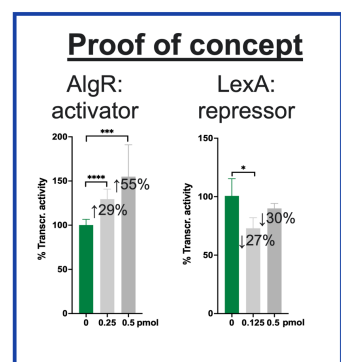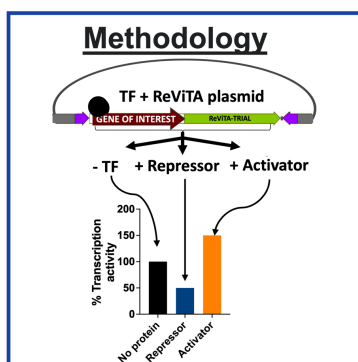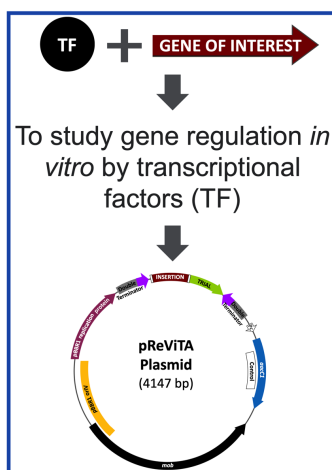
ReViTA: A novel *in vitro* transcription system to study gene regulation

Abstract

ReViTA (**Re**verse *in **Vitro** **T**ranscription **A**ssay) is a novel *in vitro* transcription-based method to study gene expression under the regulation of specific transcription factors. The ReViTA system uses a plasmid with a control sequence, the promoter region of the studied gene, the transcription factor of interest, and an RNAP saturated with σ^{70}. The main objective of this study was to evaluate the method; thus, as a proof of concept, we used two different transcription factors, a transcriptional inducer, AlgR, and a repressor, LexA, from *Pseudomonas aeruginosa*. After the promoters were incubated with the transcription factors, the plasmid was transcribed into RNA and reverse transcribed to cDNA. Gene expression was measured using qRT–PCR. Using the ReViTA plasmid, we observed transcription induction of 55% when AlgR protein was added and a 27% transcription reduction when the repressor LexA was used compared with the samples without transcription factors. Our results demonstrated the correct functioning of ReViTA as a novel method to study transcription factors and gene expression. Therefore, we believe that ReViTA could be a rapid and accessible *in vitro* method to evaluate genes and regulators of various species.

Keywords

Abbreviations:

ReViTA, Reverse *in Vitro* Transcription Assay; RNAP, RNA polymerase; qRT–PCR, quantitative Real Time-Polymerase Chain Reaction; IVT, *in vitro* transcription; TF, Transcription Factor; RNR, ribonucleotide reductase; IMAC, immobilized metal affinity chromatography; EMSA, Electrophoretic mobility shift assay; sspDNA, salmon sperm DNA; BSA, bovine serum albumin; D3-PA, D3-phosphoramidite.

Introduction

Gene transcription *in vivo* starts when RNA polymerase (RNAP) binds to DNA and catalyzes RNA production from the DNA template. Bacterial RNAP is an enzyme composed of five different subunits ($\alpha_2\beta\beta'\omega$) that additionally binds to a dissociable sigma (σ) factor in initiating the transcription process [1]. The σ factors bind to specific promoters to facilitate promoter recognition by RNAP and to activate the expression of a particular group of genes [2].

In vitro transcription (IVT) is a well-known technique that allows the synthesis of RNA in a laboratory test tube. It has been used to study the function of gene promoters, RNAP, σ factors, ribozyme biochemistry studies, antisense RNA and RNAi experiments, microarray analysis, *in vitro* translation, RNA vaccines [3], transcription inhibitors [4], and transcription factors [5], among others. In addition, it is a widespread methodology being used to study different organisms [6–9].

Over the years, IVT assays have evolved from using radiolabeled nucleotides[8] to developing nonradioactive PCR-based methods[9]. Additionally, in traditional IVT assays, the RNAP of the organism under study had to be purified and free of σ factors, which can be a limitation, especially when large amounts of pathogenic microorganisms need to be grown to obtain the RNAP [6–8,10,11]. This problem is easily solved by using the commercially available *Escherichia coli* RNAP. The RNAP holoenzyme from *E. coli* is saturated with the σ^{70} factor; thus, it can recognize only promoters with σ^{70} binding sites; however, it is an excellent solution to tackle the study of transcription regulators. Additionally, in addition to the RNAP and σ factors, many other regulators are involved in the modulation of gene expression during transcription.

Transcription factors (TFs) are proteins with DNA-binding domains that recognize specific DNA sequences and regulate the expression of genes under specific conditions. TFs are essential to modulate genetic transcription. By binding to their promoter region, they can transcriptionally activate or repress gene expression [12,13]. Several TFs can regulate a specific gene, and one TF can regulate more than one gene. Thus, it is crucial to consider TFs when studying transcription procedures [14]. Other investigators have already developed IVT systems to detect regulons modulated by a specific transcription regulator [11].

In this study, we described an IVT-based system called ReViTA (**Re**verse *in **Vi**tro* **T**ranscription **A**ssay), whose aim is to understand and study how specific TFs affect RNAP activity over certain promoters to modulate the overall transcription process. This approach represents a previously unexplored application of IVT assays. The ReViTA system uses RNAP from *E. coli* saturated with σ^{70} and a plasmid (pReViTA) that includes two gene promoter regions. One of them is used to study the promoter of interest to which the TF binds, and the other promoter is used as a control gene to which the TF does not bind and is specifically used to standardize the methodology. As a proof of concept, in this study we used the ReViTA system to measure the expression of two genes of *Pseudomonas aeruginosa* PAO1 after incubation with specific TFs. We worked with *nrdA*, which encodes class Ia ribonucleotide reductase (RNR) and its transcriptional inducer AlgR [15], and *dinB*, a type IV polymerase transcriptionally repressed in the presence of the protein LexA [16,17]. Using ReViTA, we determined that specific concentrations of AlgR and LexA transcriptionally induce and repress the expression of *nrdA* and *dinB*, respectively. In addition, we confirmed that the ReViTA system produced comparable results to those obtained using traditional linear DNA fragments, making it a novel system to use in the study of *in vitro* gene regulation.

Materials and Methods

Bacterial strains, plasmids, and growth conditions.

The bacterial strains and plasmids used in this study are listed in Table S1. The different *Pseudomonas aeruginosa* and *Escherichia coli* strains were routinely grown in Luria-Bertani (LB; Scharlab, Barcelona, Spain) medium at 37 °C. Liquid cultures were shaken at 200 rpm. Antibiotics were added to the culture medium, when necessary, at the following concentrations: 50 µg/mL ampicillin, 10 µg/mL gentamicin, 50 µg/mL kanamycin, and 34 µg/mL chloramphenicol for *E. coli*, and 100 µg/mL gentamicin for *P. aeruginosa*.

ReViTA cassette design

The ReViTA cassette (see Figure 1A) was synthesized as a GeneArt gene synthesis product cloned into the pMK-RQ vector (Thermo Fisher Scientific, Waltham, MA, USA), generating pMK-RQ::ReViTA (pETS251). The cassette was designed as a sequence of random DNA with 65% GC (ReViTA-INSERTION) and a sequence of DNA corresponding to the internal region of *gyrB* (*E. coli* K12 MG1655) with single nucleotide modifications to reduce the chance of internal promoters (ReViTA-TRIAL). Two double terminators flank ReViTA-INSERTION and ReViTA-TRIAL sequences, the terminator rrnBT1-T7TE forward (Registry of Standard Biological Parts #BBa_B0015) upstream, and the bidirectional T7TE-LuxIA double terminator (Registry of Standard Biological Parts #BBa_B0014) downstream.

DNA manipulation and plasmid construction.

Recombinant DNA manipulations were performed using standard protocols [18]. The manufacturer's instructions were followed in using the molecular biology kits and enzymes in this study. DNA amplifications were performed with the primers listed in Table S2 and using Phusion High-Fidelity DNA Polymerase (Thermo Fisher Scientific) or DreamTaq Green PCR MasterMix (Thermo Fisher Scientific). DNA fragments were isolated from agarose gels using the GeneJet Gel Extraction Kit (Thermo Fisher Scientific). The plasmids constructed throughout the work were extracted from *E. coli* DH5α using the GeneJET Plasmid Miniprep Kit (Thermo Fisher Scientific). The constructs obtained were verified via DNA sequencing by Eurofins Genomics. All the enzymes used in this study were purchased from Thermo Scientific except those indicated otherwise.

To construct the pReViTA (pETS252) plasmid, the backbone of pBBR1MSC5 was amplified with PCR using primers 1 and 2 listed in Table S2[19]. The fragment was gel purified, cloned into pJET1.2b, and transformed into *E. coli* DH5α to obtain pJET1.2b::[pETS130]bb (pETS250). Then, the plasmids pMK-RQ::ReViTA (pETS251) and pJET1.2b::[pETS130]bb (pETS250) were digested with *Xba*I-*Aat*II. The fragments obtained were gel purified, ligated using the T4 ligase enzyme, and transformed into *E. coli* DH5α. The sequence of the plasmid pReViTA has the GenBank accession no. **OP909926.**

The AlgR overproducer plasmid (pETS28a-AlgR) was built previously by our group and transformed into the *E. coli* Rosetta (DE3) strain [15]. The LexA overproducer plasmid was constructed by cloning the *lexA* gene from *P. aeruginosa* PAO1 (PA3007) into the pET28a overexpression system (Sigma-Aldrich, St. Louis, MO, USA). The primer pairs 3/4 listed in Table S2 were used to amplify a PCR band of 615 bp. Afterward, the amplified PCR band and the plasmid pETS were digested using the restriction enzymes *Nco*I and *Xho*I. The bands were gel purified, ligated using the T4 ligase enzyme, and transformed into *E. coli* DH5α, generating the plasmid pET28a-LexA (pETS255). The constructed plasmid was subsequently transformed into the *E. coli* Rosetta (DE3) strain.

Overexpression and purification of transcription factors (TFs)

The protein AlgR-His was overproduced and purified, as we indicated previously [15]. The protein LexA-His in the C-terminal end of the protein was overproduced in the Rosetta (DE3) strain and induced with IPTG 1.0 mM for 4 h at 37 °C. Afterward, the cells were centrifuged, and the pellet was resuspended in LexA buffer lysis buffer (20 mM Tris-HCl, 300 mM NaCl, 5 mM imidazole, and 1 mM DTT) to prepare the crude protein extract. The suspension was sonicated, and the crude extract was obtained by centrifuging the sonicated suspension for 30 min at 15000 g at 4 °C.

We used an FPLC system (BioLogic DuoFlow System, Bio-Rad, Hercules, CA, USA) to purify the LexA protein with a 5 ml His-Trap™ HP column (GE Healthcare, Chicago, IL, USA) by immobilized metal affinity chromatography (IMAC). Different volumes of buffer A (20 mM Tris-HCl, 300 mM NaCl, 5 mM imidazole, and 1 mM DTT) and buffer B (20 mM Tris-HCl, 300 mM NaCl, 500 mM imidazole, and 1 mM DTT) were used to generate specific imidazole concentrations. The purified protein was visualized with SDS–PAGE (12% acrylamide protein gel, Bio-Rad) and stored at -80 °C. Bradford reagent (Bio-Rad) was used to

determine the protein concentration using bovine serum albumin (BSA, Bio-Rad) as a standard.

Electrophoretic mobility shift assay (EMSA)

The promoter regions of the genes *nrdA* and *dinB* and the control were used in this assay to check TF binding. To produce the DNA probes used in EMSA, the primer pairs 5/6 and 8/9 listed in Table S2 were used to amplify the promoter regions of *nrdA* (491 bp) and *dinB* (242 bp), respectively, from the genomic DNA of *P. aeruginosa* PAO1. Primers 1 and 10 listed in Table S2 were used to amplify the promoter of the control sequence using the plasmid pReViTA (pETS252) as the template (264 bp). The primer M13 added the arbitrary sequence 5'-CTGGGCGTCGTTTTAC-3' at the 3' end of every probe. The bands obtained in the first PCR were used as templates for a second PCR that used the WellRED dye-labeled oligo (Sigma-Aldrich) coupled to the near-infrared fluorophore D3-phosphoramidite (D3-PA) to obtain the EMSA probes.

The promoters of *nrdA* and the control sequence were used at 50 fmol per reaction. The purified AlgR protein was added at 0, 0.5, and 1 pmol in each binding reaction. The DNA bands and the AlgR protein were mixed with binding buffer containing 20 mM Tris-HCl (pH 7.8 at 25 °C), 120 mM KCl, 2 mM MgCl$_2$, 2 mM DTT, 10% glycerol, 50 ng/μl sspDNA (salmon sperm DNA), and 12.5 ng/μl BSA. AlgR-*nrdA* reactions were incubated for 20 min at RT before gel electrophoresis.

The purified LexA protein was used in binding reactions at 0, 0.125, or 0.5 pmol per reaction. The DNA bands, *dinB* and control, were used at 50 fmol per reaction. The binding reactions also contained 50 ng/μl BSA, 50 ng/μl sspDNA, 20 mM Tris-HCl (pH 8.0 at 25 °C), 50 mM KCl, 2 mM MgCl2, 1 mM EDTA, 2 mM DTT, and 5% glycerol. LexA-*dinB* reactions were incubated for 30 minutes at 37 °C before gel electrophoresis.

EMSA was performed in 4% acrylamide gels using 37.5:1 acrylamide:bis-acrylamide (Sigma-Aldrich), 5% triethylene glycol (Sigma-Aldrich) and 2 mg/ml ammonium persulfate (Sigma-Aldrich). The running buffer was 40 mM TAE (pH 7.8 or 8.0 at 25 °C) for the proteins AlgR and LexA, respectively. Images were obtained by scanning the gels in the 700-nm channel of the Odyssey Imaging System (LI-COR Biosciences, Lincoln, NE, USA).

Construction of promoter carrying ReViTA for in vitro transcription

The plasmids pReViTA-P*nrdA* (pETS253) and pReViTA-P*dinB* (pETS254) were constructed as follows. First, the promoter regions of *nrdA* (P*nrdA*, 786 bp) and *dinB* (P*dinB*, 504 bp) were amplified by PCR using the primer pairs 5/7 and 14/15 listed in Table S2, and the genomic DNA from *P. aeruginosa* PAO1 was used as the template. The fragments were gel purified, ligated into the vector pJET1.2b with the enzyme T4 ligase, and transformed into *E. coli* DH5α. The resulting plasmids and the plasmid pReViTA were digested with *Bam*HI/*Spe*I, and the fragments were gel purified and ligated with the enzyme T4 ligase, generating pReViTA-P*nrdA* and pReViTA-P*dinB*. The primers ReViTA-Test-fw and ReVita-Test-rv were used to verify the insertion of P*nrdA* and P*dinB* into the ReViTA cassette through PCR and sequencing.

Construction of promoter-carrying PCR bands for in vitro transcription

The genes used in this study were amplified via PCR using primers 12/13 to amplify *nrdA* (P*nrdA*-PCR-IVT, 1045 bp) and 14/16 to amplify *dinB* from genomic DNA of *P. aeruginosa* PAO1, obtaining a PCR band of 954 bp (P*dinB*-PCR-IVT). Simultaneously, the promoter region of the control sequence was amplified using primers 1/17 listed in Table S2 using the plasmid pReViTA as the DNA template, obtaining an amplified band of 869 bp (CTRL-PCR-IVT). The *in vitro* transcription fragments were extracted using the Gel Extraction Kit.

In vitro transcription assay

The RNAP used in the *in vitro* transcription assay was the commercially available *E. coli* RNA polymerase (New England Biolabs, Ipswich, MA, USA). This holoenzyme is saturated with the σ^{70} factor, which recognizes specific σ^{70} promoters to initiate RNA transcription. The *E. coli* RNAP Reaction Buffer 5 X (New England Biolabs) was used in the experiment.

First, the promoter templates (ReViTA-P*nrdA*, ReViTA-P*dinB*, and their linear PCR transcription fragment counterparts mixed with the control sequence) were incubated with the transcription factor and the reaction buffer (New England Biolabs) of RNApol for 30 min at RT using AlgR and 37 °C using LexA. In each reaction, 25 fmol of the template (25 nM) per reaction was used. A specific protein concentration was tested in each reaction.

The *in vitro* transcription buffer was composed of 1X reaction buffer, 0.5 mM NTP mix (ATP, UTP, CTP, and GTP, Sigma-Aldrich), 1 mM spermidine (Sigma-Aldrich), 0.06 U pyrophosphatase (Sigma-Aldrich), and 20 U Ribolock RI (Thermo Fisher Scientific). The *in vitro* transcription buffer was mixed with the protein–DNA complex and incubated at RT or 37 °C for 30 min. Subsequently, 0.5 U of *E. coli* RNAP was added to each reaction. The *in vitro* transcription reaction was performed at 37 °C for 30 min. All the incubations were carried out using the T100 Thermal Cycler (Bio-Rad).

The samples were diluted 1:2 with Milli-Q water and mixed with 1X Turbo DNase I buffer and Turbo DNase I (Thermo Fisher Scientific) to remove the DNA template. DNase treatment was performed at 37 °C for 1 h with gentle shaking. The DNase inactivation reagent (Thermo Fisher Scientific) at 1X was added to each sample, and the mix was incubated for 5 min at room temperature with occasional mixing. After centrifuging the samples for 90 s at 10000 g, the supernatant was recovered. We performed a PCR using specific primers as DNA absence test to ensure that the samples were DNA free. The control sequence was used as the positive control.

Reverse transcription, qPCR, and data analysis

The mRNA produced from the *in vitro* transcription reaction was reverse transcribed using 200 U Maxima Reverse Transcriptase (Thermo Fisher Scientific), 0.5 mM dNTPs mix (dATP, dTTP, dCTP, and dGTP, Sigma, Spain), 1 X Thermo RT buffer (Thermo Fisher Scientific), 20 U Ribolock RI, and gene-specific primers. The primers ReViTA_TRIAL_rt and ReViTA_ctrl_rt were used to reverse transcribe the plasmid pReViTA; the primers qRTgreen_IVT_PAO-nrdA_rv, IVT_dinB-PAO1_rt and ReViTA_ctrl_rt were used to reverse transcribe the PCR band templates of *nrdA*, *dinB*, and the control, respectively. The mixture was incubated following the manufacturer's instructions. The cDNA obtained was quantified by qRT–PCR with the StepOne-Plus 96-well real-time PCR system (Thermo Fisher Scientific). Samples were mixed with 1X PowerUp SYBER green Master Mix (Thermo Fisher Scientific) and 200 nM specific amplification primers. The primers used are specified in Table S2. Additionally, calibration curves of the tested amplicons were prepared. These standards were used to determine the number of copies of DNA in each reaction and to calculate the percentage of transcription activity in each sample.

Promoter prediction

The software phiSITE (with predetermined matrices) was used to predict σ^{70} promoters in the studied genes (http://www.phisite.org/main/index.php?nav=tools&nav_sel=hunter) [20]. The promoter regions that were cloned into the plasmid pReViTA (P*nrdA*, 786 bp and P*dinB*, 504 bp) were submitted *in silico* to the software and analyzed.

Statistical analysis

GraphPad Prism 9.0 (GraphPad Software, Boston, MA, USA) was used to perform statistical analyses. Single comparisons were performed with unpaired Student's *t* tests. The data values are expressed as the mean and standard deviation.

Results

ReViTA system: characterization and functioning

The ReViTA system was developed to address the need to study transcription factors and their specific roles and functions *in vitro*. The ReViTA cassette is a synthetic sequence explicitly designed to facilitate the study of regulators and their regulons using the widely known *in vitro* transcription technique (Fig. 1). Fig. 1A shows a representative scheme of the ReViTA cassette. It is composed of a random DNA sequence (ReViTA-INSERTION) where the promoter of interest will be cloned using the *Spe*I-*Bam*HI restriction sites. Downstream of the INSERTION site, the ReViTA-TRIAL sequence corresponds to an internal region of *gyrB* (*E. coli* K12 MG1655). This sequence is used to measure and quantify the expression of the promoter to be studied, and the primers used in the assay are designed to bind specifically to it. Double terminators flank the ReViTA-INSERTION and ReViTA-TRIAL sequences to stop transcription in both directions, with the expression measurements being gene specific. Finally, the ReViTA cassette also includes a control sequence that corresponds to the *aacC1* gene to standardize the reaction, as further described.

The ReViTA cassette was integrated into a pBBR1MSC5 plasmid backbone, as shown in the representative scheme in Fig. 1B[19]. The pBBR1MSC5 backbone sequence was amplified by PCR and cloned into pJET1.2b. The plasmid pJET1.2b::[pETS130]bb and the ReViTA cassette were digested with *Aat*II-*Xba*I and ligated, generating the pReViTA (pETS252) vector (see Materials and Methods). In this plasmid, the gene *aacC1* encodes a gentamicin 3-N-acetyltransferase, which confers resistance to gentamicin. Part of the *aacC1* sequence is used in the IVT assay as the control sequence. *aacC1* has its promoter (Pc), a class 1 integron promoter, and should not be recognized by the studied TF. In addition, pReViTA includes a *mob* gene for mobilization functions and the pBBR1 oriV and pBBR1 replication protein used in various microorganisms for plasmid maintenance and replication.

Any promoter of interest can be cloned into the ReViTA-INSERTION site, and the IVT assay can be performed to evaluate the function of the studied TF. An experiment with the ReViTA system will encompass five different steps: 1) DNA template preparation, 2) *in vitro* transcription, 3) cDNA synthesis, 4) qRT–PCR, and 5) data analysis (Fig. 1C).

1) DNA template preparation.

This step includes the cloning of the promoter of interest into pReViTA. The final plasmid concentration was set to 25 nM to have 25 fmol of plasmid in each IVT transcription reaction. To ensure that the DNA template was high quality, the DNA was extracted from *E. coli* DH5α (see Materials and Methods).

2) *In vitro* transcription (IVT)

The commercially available RNA polymerase holoenzyme from *E. coli* (RNAP, New England Biolabs, USA) was used to generate the RNA from the DNA templates used. To carry out IVT, the TF of interest was first incubated with the DNA template (plasmid or free DNA fragment). The time and temperature for DNA-transcription factor incubation may vary depending on the TF used.

The buffer composition for the TF-DNA incubation and the IVT assay was determined empirically by trial and error. When choosing a buffer, it is crucial to bear in mind the salt concentration present in the buffer, such as NaCl, $MgCl_2$, or KCl, which can dramatically alter the transcription reaction. We tried different buffers, and the one that worked best was the buffer of RNAP itself mixed with additives such as spermidine, pyrophosphatase, and Ribolock RI (see Materials and Methods).

The amount of RNA transcribed from the DNA template will depend on the strength of the promoter and TF binding. We hypothesize that when testing a transcriptional repressor, the amount of RNA transcribed from the sample incubated with the protein will be less than that from the sample without protein. Simultaneously, we believe that if the TF is an activator, the amount of RNA transcribed from the DNA template incubated with the protein will be higher than that in the sample without protein. In all cases, the amount of RNA obtained with the transcription of the control sequence should not vary, as the TF would not bind to this DNA region.

After transcription, the DNA template was eliminated using Turbo DNase I for 1 h at 37 °C. A DNA absence test using the control sequence as the positive control was performed to ensure that the DNA template was eliminated.

3) cDNA synthesis

The mRNA obtained from the tested promotor and the control sequence, independent of whether they were incubated with the TF, was reverse transcribed to cDNA using specific transcription primers (listed in Table S2) and Maxima Reverse Transcriptase. The primer used to reverse transcribe the RNA from the tested promoter binds to the TRIAL sequence. We assumed that for each RNA molecule, a cDNA molecule was obtained.

4) qRT–PCR

We used qRT–PCR to measure cDNA amplification. Specific primers (listed in Table S2) and the PowerUP SYBR Green Master Mix (1 X) were used to amplify DNA copies. With the ReViTA system, primers used to measure transcription of the promotor of interest bind to the TRIAL sequence; thus, they are independent of the tested promotor cloned into the plasmid. The amplicons from the ReViTA-TRIAL and the control sequence were designed to have similar lengths to obtain the same PCR efficiencies and comparable results.

5) Data analysis

As the signal intensity in qRT–PCR is proportional to the number of amplified DNA copies, a calibration curve of each amplicon was used to calculate the number of DNA copies in each reaction. Assuming that every RNA molecule was reverse transcribed into a DNA molecule, we calculated the original number of RNA copies in each sample and the percentage of transcription activity in each reaction.

To determine whether a TF is a transcriptional repressor or an activator, it is necessary to compare the transcriptional activity of the pReViTA incubated with the protein and the plasmid with no TF. The transcription values of the control sequence were used to normalize the data for analysis, facilitating the comparison between samples.
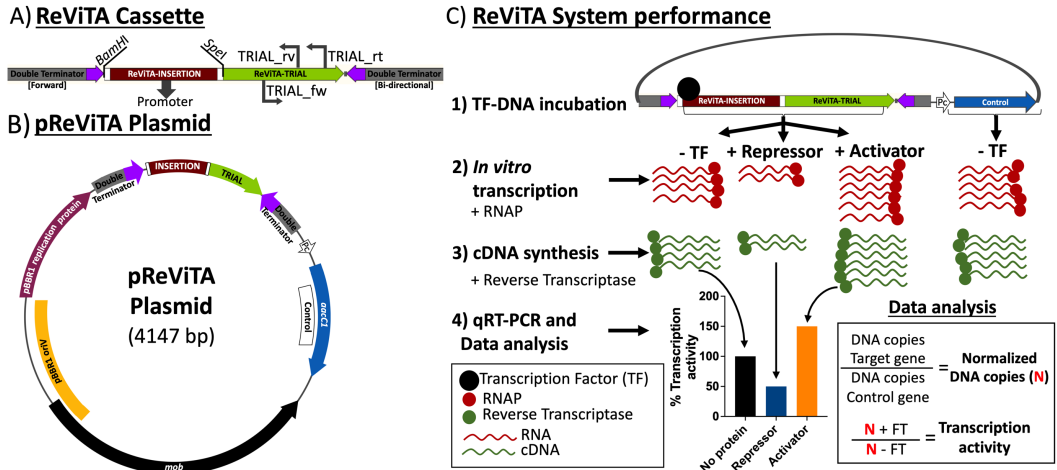
Fig. 1. Overview of the ReViTA system. A) Schematic representation of the ReViTA cassette. The cassette includes a random DNA sequence where the promoter to be studied would be inserted (ReViTA-INSERTION) and a specific sequence to measure gene expression (ReViTA-TRIAL). Double terminators flank the sequences ReViTA-INSERTION and ReViTA-TRIAL; one of them stops transcription in one direction (Forward), and the other in both directions (Bidirectional). The primers to reverse transcribe the RNA from the promoter into cDNA (TRIAL_rt) and to perform qRT–PCR (TRIAL_fw and TRIAL_rv) bind to the ReViTA-TRIAL sequence. B) Map of the pReViTA plasmid, which includes the ReViTA cassette inserted into the pBBR1MSC5 backbone vector, the *aacC1* gene, which confers resistance to gentamicin and was used as a control sequence for the *in vitro* transcription (IVT) assay, the *mob* gene for mobilization functions, pBBR1 *oriV* as a replication origin (used for broad-host-replication range), and finally the pBBR1 replication protein[19]. C) pReViTA system performance. The ReViTA system is based on the IVT methodology to measure gene expression. The study transcription factor (TF), which can be a transcriptional repressor or an activator, binds to the promoter region of the target gene and does not bind to the promoter of the control sequence. Once the plasmid is incubated with the TF, the RNA polymerase (RNAP) binds to the promoters and transcribes the genes. Depending on the presence or absence of the TF, the transcription levels of the genes are different. Afterward, the reverse transcriptase catalyzes the conversion of RNA into cDNA. The cDNA levels of each sample were measured using qRT–PCR. The data obtained in the qRT–PCR were analyzed using the formulas found in the bottom right square of the image to obtain the transcription activity of each sample. If the TF is a repressor, the samples with protein will show less transcription activity than samples with no protein, and if the TF is an activator, the samples with protein will show higher transcription levels than the no-protein sample.

*Use of the ReViTA system to measure transcription of P*nrdA *and P*dinB P. aeruginosa *promoters after specific TF binding*

As proof of concept, we used the ReViTA system to measure the expression of the well-known *P. aeruginosa* genes *nrdA* with the transcriptional activator AlgR [15] and *dinB* in the presence of the transcriptional repressor LexA [16,17]. The gene *nrdA* is part of the operon *nrdAB,* which encodes the class Ia ribonucleotide reductase constitutively active in *P. aeruginosa.* Different TFs tightly regulate the transcription of this promoter. One of them is AlgR, which transcriptionally induces the expression of *nrdA* through an AlgR binding box in its promoter [15].

The other gene analyzed in this work is *dinB*, which encodes a DNA polymerase IV with no proofreading activity that is transcriptionally repressed by LexA and it is part of the SOS-response system [21]. The promoter region of *dinB* (P*dinB*) has one LexA-binding sequence.

The genes used in the IVT assay need a σ^{70}-dependent promoter to be recognized by the RNAP used in the assay. The transcription of *dinB* has been thoroughly studied in *E. coli*, and it was determined that *dinB* presents a single promoter that can be transcribed using σ^{70} (RpoD, constitutive) or σ^{38} (RpoS, stationary phase, and stress) [22]. However, there were no data available for its counterpart in *Pseudomonas*.

In the case of *P. aeruginosa* PAO1, there was no evidence that σ^{70} bound to the promoter regions of *nrdA* and *dinB*. After bioinformatic prediction, we detected several putative σ^{70} binding regions in the promoter sequences of *nrdA* and *dinB* (Fig. S1)*.* In the *nrdA* promoter region, three putative σ^{70} binding sites were found, two of which were downstream of the AlgR binding box, overlapping with the TF NrdR binding sites[23]. In the *dinB* promoter region, the experimentally demonstrated LexA box was found to overlap one of the σ^{70} binding sites; two more were found upstream (and thus could still be controlled by LexA), and the last two were found downstream of the LexA box (Fig. S1). Therefore, we hypothesized that *nrdA* and *dinB* would have a σ^{70}-dependent promoter.

The TFs used in this work are shown on a 12% SDS–PAGE gel (Fig. 2A-B), which corresponded to a His-tagged AlgR protein (27 kDa) and a His-tagged LexA protein (23 kDa). When purifying AlgR, some nonspecific bands were observed; however, AlgR was found

mainly as a monomer (signaled in the gel with a m). LexA was found as both a monomer (m, 23 kDa) and a dimer (indicated in the gel with a d, 46 kDa).

The purified proteins were used in electrophoretic mobility shift assay (EMSA) to confirm specific AlgR-P*nrdA*[15] and LexA-P*dinB* binding [21] and verify that the AlgR-Control and LexA-Control complexes did not form (Fig. 2C-D). It was observed that the highest concentration of TF increased the amount of shifted P*nrdA* and P*dinB*, with the highest shift observed when using 1 and 0.5 pmol of protein, respectively. The control region used in these assays was not bound to the protein AlgR (Fig. 2C). However, it was bound lightly to LexA when using 1 pmol of protein (Fig. 2D), indicating that there may be some competitivity among *dinB* and the control when using LexA.
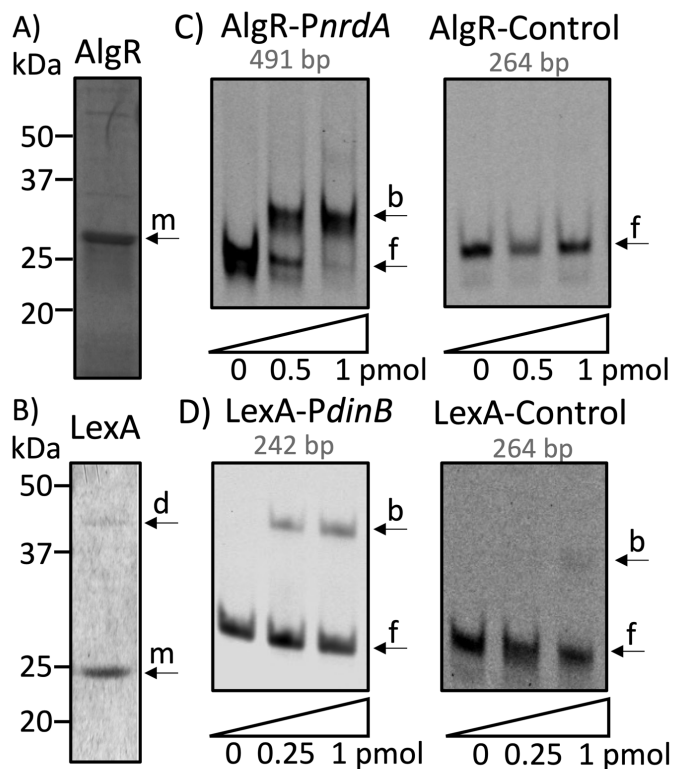
Fig. 2. Study of TF binding to promoter regions. SDS–PAGE (12%) gel of *P. aeruginosa* PAO1 A) purified AlgR-His (27 kDa), and B) LexA-His (23 kDa). The bands indicated with arrows on the gel correspond to the protein monomer (m) and dimer (d). C) EMSA experiments using the promoter region of *nrdA* (P*nrdA*, 491 bp) from *P. aeruginosa* and the promoter control sequence of the ReViTA plasmid (264 bp) and the AlgR protein. D) EMSA using the promoter of *dinB* (P*dinB*, 242 bp) from *P. aeruginosa* and the control sequence (264 bp). Fifty femtomoles of each probe was used per

reaction. The number of picomoles of AlgR-His or LexA-His used is labeled. f, free DNA; b, bound DNA.

AlgR transcriptionally *induces* nrdA *expression, and LexA* transcriptionally *represses* dinB *expression via* in vitro *transcription*

To evaluate the performance of our ReViTA system and as a proof of concept, we conducted an IVT assay using the ReViTA plasmid or linear DNA fragments as DNA templates (see Materials and Methods) and Fig. 3. We cloned the promoter region of *nrdA* and *dinB* in the ReViTA-INSERTION sequence of the ReViTA plasmid (pReViTA-P*nrdA* and pReViTA-P*dinB,* Fig. 3A and C). The linear DNA fragments were obtained by PCR amplification of P*nrdA,* P*dinB* and the control sequence, which were 1045 bp, 954 bp, and 869 bp, respectively (Fig. 3B and D).

Fig. 3A and B show that *nrdA* expression increased by 29 and 55% after adding 0.25 and 0.5 pmol of AlgR, respectively, when using the ReViTA system and by 17 and 40% when using the PCR bands. The increase in both cases was similar and consistent with the higher *nrdA* expression as the protein concentration increased. The raw data of a representative experiment using the ReViTA system and the PCR bands can be found in Fig. S2A.

Fig. 3C and D show that the expression of *dinB* decreases by 27% when using the plasmid pReViTA and by 30% with the PCR bands after incubation with 0.125 pmol of LexA. However, when the protein concentration was increased to 0.5 pmol, P*dinB* expression decreased only by 10 and 11% in the ReViTA system and PCR bands, respectively although the tendency is clear but not statistically significant. Fig. S2B shows the raw data of a representative experiment when the FT LexA is used with the ReViTA plasmid and with PCR bands.
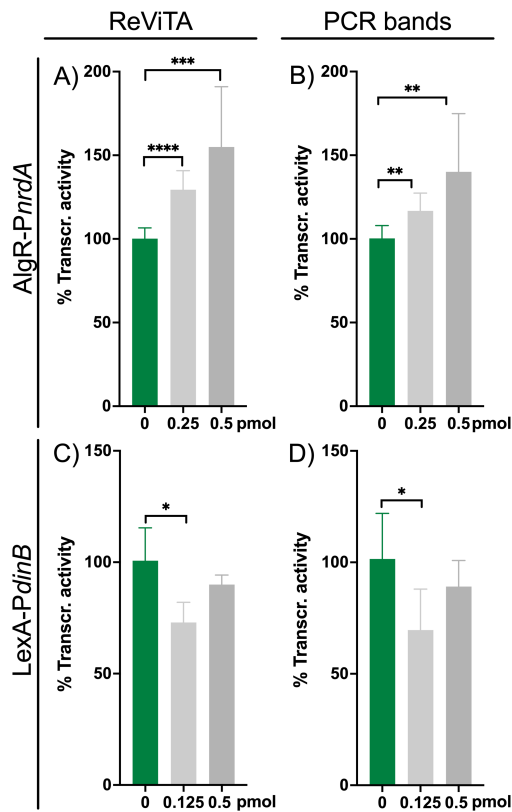
Fig. 3. *In vitro* transcription (IVT) assays. IVT assay using 25 fmol of A) the plasmid pReViTA-P*nrdA* with the promoter region of *nrdA*, B) the PCR bands of P*nrdA* (1045 bp) and the control sequence (P*aacC1-aacC1*, 869 bp), C) the plasmid pReViTA-P*dinB*, with P*dinB*, and D) the PCR bands of P*dinB* (954 bp) and control gene (P*aacC1-aacC1*, 869 bp) promoter regions. The Y-axis of the graphs represents the percentage of transcription of the template. The numbers below the X-axis represent the pmol of AlgR (A and B) or LexA (C and D) used in the assays. The data are expressed as the mean ± standard deviation. Student's unpaired *t* test was used to determine significant differences between samples with protein (0.125, 0.5, and 2.5 pmol) and the sample without protein (0 pmol) (*, *p* value < 0.05; **, *p* value < 0.01; ***, *p* value < 0.001; ****, *p* value < 0.0001).

Discussion

In vitro transcription assays are a widely used technique to produce RNA from DNA templates in the laboratory. Here, we designed a novel IVT system called ReViTA, which stands for Reverse *in Vitro* Transcription Assay, to measure gene expression after a TF binds to a promoter of broad-spectrum organisms. The ReViTA system uses the plasmid pReViTA to transcribe the promoter of interest and the control gene into RNA in the presence of a given TF. The main goal of ReViTA is to evaluate TF activity by measuring gene expression under the binding of a specific TF. Different TFs can be studied with the ReViTA system, and quantifying RNA expression changes can reveal whether these TFs inhibit or activate gene expression (Fig. 1).

The use of ReViTA offers several advantages over traditional IVT techniques. First, there is no need to genetically modify the host organism, which is highly useful in organisms whose genome is difficult to manipulate and when studying genes that cannot be mutated. Second, when studying a TF *in vitro*, the specific outcome from the regulator-regulon binding is obtained. *In vivo*, however, due to the complexity of the system, other unknown factors, proteins, or sRNA may modulate gene expression in an unknown way. Thus, the gene expression measured *in vivo* may not be as clear as the specific gene expression measured *in vitro.* Third, no radiolabeling is needed, as the ReViTA system method is based on quantifying the RNA produced in the reactions by qRT–PCR, which prevents health concerns [9]. Finally, the DNA template is protected in a plasmid, preventing degradation by 5'-exonucleases. It is known that using supercoiled plasmids as DNA templates offers advantages compared to linear DNA fragments [24]. The signals from the transcripts of promoters in supercoiled plasmids are higher than the signals from transcripts of linear templates, whose signal is weaker and can lead to misinterpretations. Even though it is easier for linear fragments to form the RNAP-DNA complex, these complexes tend to be less stable than specific promoter-RNAP complexes [25].

However, the use of ReViTA presents some disadvantages as well. First, the RNAP used in the assay is the commercial *E. coli* RNAP saturated with σ^{70}; thus, only promoters recognized by the σ^{70} factor can be used. Therefore, our methodology would be limited when studying promoters with alternative sigma factors or promoters from other species if the promoter cannot be recognized by heterologous RNAP[8]. However, this problem can be solved by using the specific σ, if available, or with a combination of purified RNAP and σ factor complexes [11,26]. Second, RNAP-promoter complex formation is affected by several

parameters, such as salt concentration, temperature, template topology, and RNAP concentration. These IVT conditions depend on the TF and promoter used and must be optimized empirically [24]. Finally, to perform IVT, the TF needs to be purified, with associated challenges. Using a TF whose *in vitro* conditions are very different from the RNAP conditions may limit the use of ReViTA.

Considering the above points, we evaluated whether the ReViTA system is a good option for studying gene expression after TF binding. We cloned the *nrdA* and *dinB* promoter regions from *P. aeruginosa* into pReViTA and measured their expression after incubating them with the transcriptional inducer AlgR and transcriptional repressor LexA, respectively. AlgR and LexA from *P. aeruginosa* were purified using *E. coli* Rosetta (DE3) as overproducing cells (Fig. 2A-B). The AlgR protein was purified as a monomer, and the rest of the bands found in the gel may correspond to nonspecific proteins, as there is no evidence of AlgR being active as a dimer. LexA was found to be present as both a monomer and a dimer. Some studies claim that LexA is active in its dimeric form in *E. coli*, *Bacillus subtilis*, and *Mycobacterium tuberculosis* [27–29]. When this dimer is cleaved by RecA, LexA loses its transcription repression function. As only one LexA-binding box has been experimentally found in the promoter region of *dinB* [21], the presence of a protein dimer may indicate that in *P. aeruginosa,* LexA needs to form a dimer to be active; however, more experiments should be performed to confirm this hypothesis. The protein AlgR, on the other hand, was found to be a single monomer, which may indicate that it is the active form of the TF (Fig. 2A).

When studying AlgR and LexA binding to P*nrdA* and P*dinB*, respectively, and the control sequence, we experimentally demonstrated that small concentrations of the TF, 0.5 pmol of AlgR, and 0.25 pmol of LexA bound to P*nrdA* and P*dinB*, respectively, shifting the bands in the EMSA gel (Fig. 2C-D). When studying the binding of the TF to the control sequence, band shifting was not observed when using AlgR (Fig. 2C), but a slight shift was seen when using 1 pmol of LexA (Fig. 2D), which indicates that there may be some promoter competition when using the transcriptional repressor LexA.

To evaluate whether the ReViTA system is suitable for studying gene regulation, we conducted IVT assays using the plasmid pReViTA and linear PCR fragments with the promoter region of *nrdA* or *dinB* and the control sequence (Fig. 3). It was observed that in both types of experiments, the incubation of the TF with its specific promoter changed the transcriptional activity. The use of 0.25 or 0.5 pmol of AlgR increased the transcription of

nrdA by 29 and 55% when using the ReViTA system and by 17 and 40% when using the PCR bands. These results are consistent, as an increased protein concentration led to higher *nrdA* expression, as can be observed in the raw data shown in Fig. S2A.

Additionally, using 0.125 pmol of LexA decreased the transcription of *dinB* by 27 and 30% when using the ReViTA plasmid and the linear PCR bands, respectively. However, a higher concentration of LexA (0.5 pmol) did not result in lower expression; in contrast, the expression of *dinB* seemed to decrease by only 10 and 11% when using the ReViTA plasmid or the PCR bands, respectively. Although the tendency is clear, it did not show statistical significance. We believe that the nonspecific binding of LexA to the control region observed in Fig. 2D, and thus the competition among promoters, may be the reason for not finding a higher repression of *dinB* when using an increased protein concentration of LexA. The reasoning behind this hypothesis is shown in the raw data of Fig. S2B. The Ct values of the control sample without FT show a slight increase when adding 0.5 pmol of the protein LexA (for example in the PCR bands samples, the control Ct changes from 25.34 to 26.57), which may indicate that its transcription is been slightly repressed. While this outcome may suggest that performing an EMSA before using the ReViTA system is necessary, we are confident that, due to the high sensibility of ReViTA, it is not completely essential to carry out the EMSA. Still, it is helpful to test whether the TF to be studied is a good candidate or be used in a high throughput method to determine binding to a specific promoter region.

Moreover, as the data in Fig. S2 shows, there is some variability among experiments. Thus, it is important to normalize the data before comparing between experiments. To normalize the data, first, we compared the %Act (percentage of activity) of the DNA sequences with protein with the %Act of the DNA sequences without protein. Afterward, we compared the test with the control samples obtaining the %Act nor (percentage of activity normalized) with corresponds to the transcriptional activity of the IVT experiment.

Although, it seems that the unspecific TF-promoter binding could be avoided by performing the experiment using the test sequence with and without the TF, we believe that it is important to run the control along with the TF to assure that the transcription activity obtained in the experiment is due to the specific binding between the promoter and the protein and not due to non-specific DNA interactions.

Nonetheless, the results obtained with pReViTA and linear PCR bands are similar, which may indicate the correct functioning of the plasmid pReViTA. We also observed that this system is specific enough to differentiate between a transcriptional activator and a repressor; thus, it could be used to study the specific unknown function of a TF.

Therefore, the ReViTA system is as a novel technique to measure gene expression and study TF regulation, whose benefits outweigh its disadvantages. In addition, the results obtained from the experiments conducted with pReViTA and the linear PCR fragments as DNA templates are very similar, which confirms its specificity and functionality.

Conclusion

ReViTA is a novel system to study transcriptional regulation of genes from broad-spectrum organisms as it consists of a plasmid to study transcription factors *in vitro.* Its simplicity and easy functioning offer many advantages over traditional techniques, overcoming its disadvantages. The transcription factors used as proof of concept were a transcription activator and repressor. The transcription activator increased gene expression and the transcription repressor decreased gene expression after comparing with the samples with no protein, showing the right functioning of the system ReViTA.

Acknowledgments

Author Contribution

ARC and ET wrote the manuscript. ARC and LP designed the plasmid and performed the biological assays. ET directed the research and revised the experimental data. All authors have approved the final version of the manuscript.

References

[1] Gruber TM, Gross CA. Multiple sigma subunits and the partitioning of bacterial transcription space. Annu Rev Microbiol 2003;57:441–66. https://doi.org/10.1146/annurev.micro.57.030502.090913.

[2] deHaseth PL, Zupancic ML, Record Jr. MT. RNA polymerase-promoter interactions: the comings and goings of RNA polymerase. J Bacteriol 1998;180:3019–25. https://doi.org/10.1128/JB.180.12.3019-3025.1998.

[3] Pardi N, Hogan MJ, Porter FW, Weissman D. mRNA vaccines - a new era in vaccinology. Nat Rev Drug Discov 2018;17:261–79. https://doi.org/10.1038/nrd.2017.243.

[4] Yang X, Ma C. *In Vitro* Transcription Assays and Their Application in Drug Discovery. J Vis Exp 2016. https://doi.org/10.3791/54256.

[5] Kanwal F, Chen T, Zhang Y, Zhang Y, Simair A, Rujie C, et al. Large-Scale *in Vitro* Transcription, RNA Purification and Chemical Probing Analysis. Cell Physiol Biochem 2018;48:1915–27. https://doi.org/10.1159/000492512.

[6] Fujita M, Sagara Y, Aramaki H. *In vitro* transcription system using reconstituted RNA polymerase (Esigma(70), Esigma(H), Esigma(E) and Esigma(S)) of *Pseudomonas aeruginosa*. FEMS Microbiol Lett 2000;183:253–7. https://doi.org/10.1111/j.1574-6968.2000.tb08967.x.

[7] Holatko J, Silar R, Rabatinova A, Sanderova H, Halada P, Nesvera J, et al. Construction of *in vitro* transcription system for *Corynebacterium glutamicum* and its use in the recognition of promoters of different classes. Appl Microbiol Biotechnol 2012;96:521–9. https://doi.org/10.1007/s00253-012-4336-1.

[8] Jacques JF, Rodrigue S, Brzezinski R, Gaudreau L. A recombinant *Mycobacterium tuberculosis in vitro* transcription system. FEMS Microbiol Lett 2006;255:140–7. https://doi.org/10.1111/j.1574-6968.2005.00071.x.

[9] Wibisono P, Liu Y, Sun J. A novel *in vitro Caenorhabditis elegans* transcription system. BMC Mol Cell Biol 2020;21:87. https://doi.org/10.1186/s12860-020-00332-8.

[10] Beaucher J, Rodrigue S, Jacques PE, Smith I, Brzezinski R, Gaudreau L. Novel *Mycobacterium tuberculosis* anti-sigma factor antagonists control sigmaF activity by distinct mechanisms. Mol Microbiol 2002;45:1527–40. https://doi.org/10.1046/j.1365-2958.2002.03135.x.

[11] Maclellan SR, Eiamphungporn W, Helmann JD. ROMA: an *in vitro* approach to defining target genes for transcription regulators. Methods 2009;47:73–7. https://doi.org/10.1016/j.ymeth.2008.10.009.

[12] Abril AG, Rama JLR, Sanchez-Perez A, Villa TG. Prokaryotic sigma factors and their transcriptional counterparts in Archaea and Eukarya. Appl Microbiol Biotechnol 2020;104:4289–302. https://doi.org/10.1007/s00253-020-10577-0.

[13] Martinez-Antonio A, Collado-Vides J. Identifying global regulators in transcriptional regulatory networks in bacteria. Curr Opin Microbiol 2003;6:482–9. https://doi.org/10.1016/j.mib.2003.09.002.

[14] Browning DF, Busby SJ. The regulation of bacterial transcription initiation. Nat Rev Microbiol 2004;2:57–65. https://doi.org/10.1038/nrmicro787.

[15] Crespo A, Pedraz L, van der Hofstadt M, Gomila G, Torrents E. Regulation of ribonucleotide synthesis by the *Pseudomonas aeruginosa* two-component system AlgR in response to oxidative stress. Scientific Reports 2017 7:1 2017;7:1–15. https://doi.org/10.1038/s41598-017-17917-7.

[16] Mercolino J, lo Sciuto A, Spinnato MC, Rampioni G, Imperi F. RecA and Specialized Error-Prone DNA Polymerases Are Not Required for Mutagenesis and Antibiotic Resistance Induced by Fluoroquinolones in *Pseudomonas aeruginosa*. Antibiotics 2022;11:325.

[17] Layton JC, Foster PL. Error-prone DNA polymerase IV is controlled by the stress-response sigma factor, RpoS, in *Escherichia coli*. Mol Microbiol 2003;50:549–61. https://doi.org/10.1046/j.1365-2958.2003.03704.x.

[18] Sambrook J, Fritsch ER, Maniatis T. Molecular Cloning: A Laboratory Manual. 2nd ed. NY, USA,: Cold Spring Harbor Laboratory Press: Cold Spring Harbor; 1989.

[19] Kovach ME, Elzer PH, Hill DS, Robertson GT, Farris MA, Roop 2nd RM, et al. Four new derivatives of the broad-host-range cloning vector pBBR1MCS, carrying different antibiotic-resistance cassettes. Gene 1995;166:175–6. https://doi.org/10.1016/0378-1119(95)00584-1.

[20] Klucar L, Stano M, Hajduk M. phiSITE: database of gene regulation in bacteriophages. Nucleic Acids Res 2010;38:D366-70. https://doi.org/10.1093/nar/gkp911.

[21] Sanders LH, Rockel A, Lu H, Wozniak DJ, Sutton MD. Role of *Pseudomonas aeruginosa dinB*-encoded DNA polymerase IV in mutagenesis. J Bacteriol 2006;188:8573–85. https://doi.org/10.1128/JB.01481-06.

[22] Storvik KA, Foster PL. RpoS, the stress response sigma factor, plays a dual role in the regulation of *Escherichia coli*'s error-prone DNA polymerase IV. J Bacteriol 2010;192:3639–44. https://doi.org/10.1128/JB.00358-10.

[23] Crespo A, Pedraz L, Torrents E. Function of the *Pseudomonas aeruginosa* NrdR Transcription Factor: Global Transcriptomic Analysis and Its Role on Ribonucleotide Reductase Gene Expression. PLoS One 2015;10. https://doi.org/10.1371/JOURNAL.PONE.0123571.

[24] Ross W, Gourse RL. Analysis of RNA polymerase-promoter complex formation. Methods 2009;47:13–24. https://doi.org/10.1016/j.ymeth.2008.10.018.

[25] Melancon P, Burgess RR, Record Jr. MT. Direct evidence for the preferential binding of *Escherichia coli* RNA polymerase holoenzyme to the ends of deoxyribonucleic acid restriction fragments. Biochemistry 1983;22:5169–76. https://doi.org/10.1021/bi00291a017.

[26] Douglas AL, Saxena NK, Hatch TP. Enhancement of in vitro transcription by addition of cloned, overexpressed major sigma factor of *Chlamydia psittaci* 6BC. J Bacteriol 1994;176:3033. https://doi.org/10.1128/JB.176.10.3033-3039.1994.

[27] Giese KC, Michalowski CB, Little JW. RecA-dependent cleavage of LexA dimers. J Mol Biol 2008;377:148–61. https://doi.org/10.1016/j.jmb.2007.12.025.

[28] Groban ES, Johnson MB, Banky P, Burnett PG, Calderon GL, Dwyer EC, et al. Binding of the *Bacillus subtilis* LexA protein to the SOS operator. Nucleic Acids Res 2005;33:6287–95. https://doi.org/10.1093/nar/gki939.

[29] Chandran A v, Srikalaivani R, Paul A, Vijayan M. Biochemical characterization of *Mycobacterium tuberculosis* LexA and structural studies of its C-terminal segment. Acta Crystallogr D Struct Biol 2019;75:41–55. https://doi.org/10.1107/S2059798318016066.

Material Suplementario

Fig. S1. Analysis of the Putative Sigma-70 (σ70) binding sites in *nrdA* and *dinB* promoter region of *P. aeruginosa* PAO1. Bioinformatical identification of putative σ70 binding sites by phiSITE and the genetic context of the putative σ70 promoters in the promoter region of A) *nrdA* and B) *dinB* genes of *P. aeruginosa* PAO1. The X-axis of PhiSITE correspond to the nucleotide (nt) numbering of the promoter region of each gene (P*nrdA*, 784 bp and P*dinB* 504 bp) PhiSITE web:

http://www.phisite.org/main/index.php?nav=tools&nav_sel=hunter
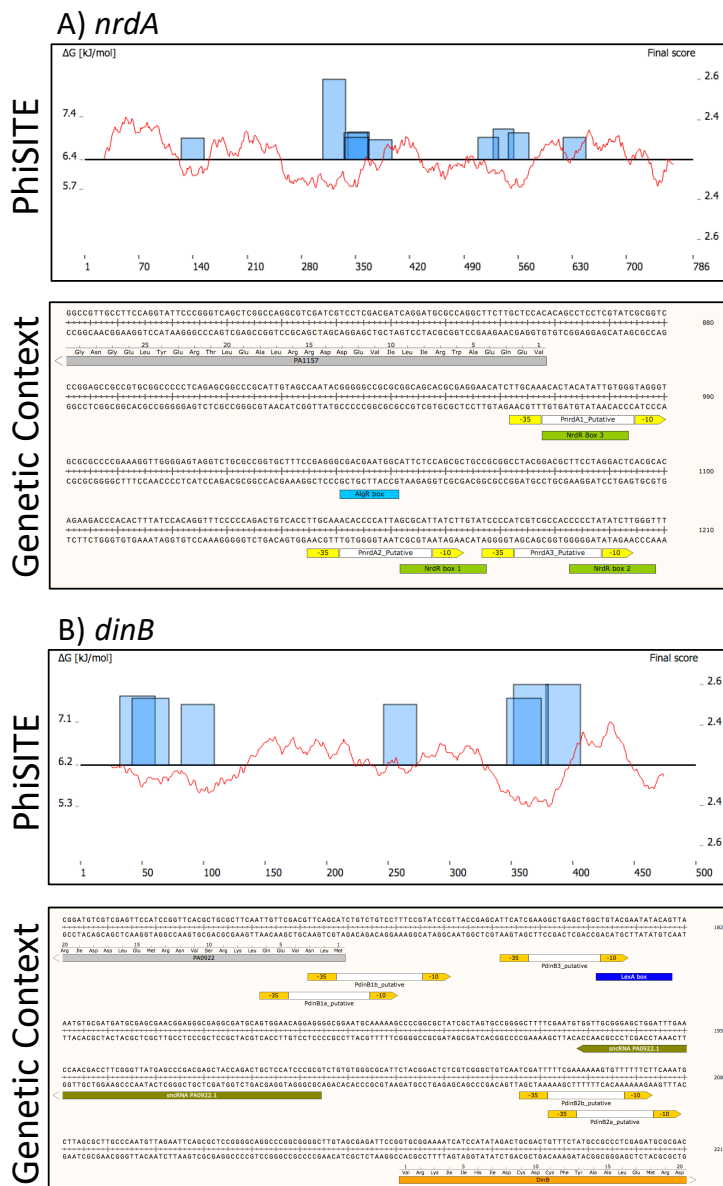
Fig. S2. Raw data of representative qRT-PCR experiments using the ReViTA system and the PCR bands as control. A) qRT-PCR data using the FT AlgR. B) qRT-PCR data using the FT LexA. The names of the columns correspond to: Ind, Individual; Ave, Average; C qRT, DNA copies in qRT reaction; C IVT, DNA copies in IVT reaction; %Act, Percentage of activity; C-nor, DNA copies normalized; %A nor, Percentage of activity normalized.

A) AlgR — ReViTA

Sample	Target	Ind Ct	Ind C qRT	Ind C IVT	Ind %Act	Ind C-nor	Ind %A nor	Ave Ct	Ave C qRT	Ave C IVT	Ave %Act	Ave C-nor	Ave %A nor
0 pmol	PA	26.180	49046.701	4.95E+08	101.80%	3.13	101.80%	26.207	48180.675	4.86E+08	100.00%	3.08	100.00%
0 pmol	PA	26.059	53220.256	5.37E+08	110.46%	3.40	110.46%	26.207	48180.675	4.86E+08	100.00%	3.08	100.00%
0 pmol	PA	26.381	42848.132	4.32E+08	88.93%	2.74	88.93%	26.207	48180.675	4.86E+08	100.00%	3.08	100.00%
0.25 pmol	PA	25.802	63239.206	6.38E+08	131.25%	5.18	168.31%	25.883	59900.700	6.04E+08	124.33%	4.91	159.42%
0.25 pmol	PA	25.846	61412.691	6.20E+08	127.46%	5.03	163.44%	25.883	59900.700	6.04E+08	124.33%	4.91	159.42%
0.25 pmol	PA	26.001	55341.529	5.58E+08	114.86%	4.53	147.29%	25.883	59900.700	6.04E+08	124.33%	4.91	159.42%
0.5 pmol	PA	25.539	75496.271	7.62E+08	156.69%	6.21	201.75%	25.723	66695.297	6.73E+08	138.43%	5.48	178.23%
0.5 pmol	PA	25.804	63172.393	6.37E+08	131.12%	5.19	168.82%	25.723	66695.297	6.73E+08	138.43%	5.48	178.23%
0.5 pmol	PA	25.827	62205.996	6.28E+08	129.11%	5.11	166.24%	25.723	66695.297	6.73E+08	138.43%	5.48	178.23%
0 pmol	CTRL	23.212	13914.155	1.40E+08	88.86%			23.044	15658.906	1.58E+08	100.00%		
0 pmol	CTRL	23.131	14731.287	1.49E+08	94.08%			23.044	15658.906	1.58E+08	100.00%		
0 pmol	CTRL	22.788	18732.086	1.89E+08	119.63%			23.044	15658.906	1.58E+08	100.00%		
0.25 pmol	CTRL	23.149	14542.252	1.47E+08	92.87%			23.399	12211.675	1.23E+08	77.99%		
0.25 pmol	CTRL	23.575	10795.507	1.09E+08	68.94%			23.399	12211.675	1.23E+08	77.99%		
0.25 pmol	CTRL	23.472	11599.782	1.17E+08	74.08%			23.399	12211.675	1.23E+08	77.99%		
0.5 pmol	CTRL	23.356	12584.040	1.27E+08	80.36%			23.405	12161.701	1.23E+08	77.67%		
0.5 pmol	CTRL	23.314	12961.161	1.31E+08	82.77%			23.405	12161.701	1.23E+08	77.67%		
0.5 pmol	CTRL	23.544	11028.534	1.11E+08	70.43%			23.405	12161.701	1.23E+08	77.67%		

A) AlgR — PCR bands

Sample	Target	Ind Ct	Ind C qRT	Ind C IVT	Ind %Act	Ind C-nor	Ind %A nor	Ave Ct	Ave C qRT	Ave C IVT	Ave %Act	Ave C-nor	Ave %A nor
0 pmol	PA	32.923	376.576	3.80E+06	95.81%	0.31	95.81%	32.861	393.032	3.97E+06	100.00%	0.32	100.00%
0 pmol	PA	32.517	496.678	5.01E+06	126.37%	0.41	126.37%	32.861	393.032	3.97E+06	100.00%	0.32	100.00%
0 pmol	PA	33.141	324.608	3.27E+06	82.59%	0.27	82.59%	32.861	393.032	3.97E+06	100.00%	0.32	100.00%
0.25 pmol	PA	32.704	437.293	4.41E+06	111.26%	0.47	147.46%	32.587	473.629	4.78E+06	120.51%	0.51	159.72%
0.25 pmol	PA	32.762	420.328	4.24E+06	106.94%	0.46	141.74%	32.587	473.629	4.78E+06	120.51%	0.51	159.72%
0.25 pmol	PA	32.503	501.374	5.06E+06	127.57%	0.54	169.07%	32.587	473.629	4.78E+06	120.51%	0.51	159.72%
0.5 pmol	PA	32.286	581.455	5.87E+06	147.94%	0.66	206.76%	32.365	551.060	5.56E+06	140.21%	0.63	195.95%
0.5 pmol	PA	32.326	565.819	5.71E+06	143.96%	0.65	201.20%	32.365	551.060	5.56E+06	140.21%	0.63	195.95%
0.5 pmol	PA	32.482	508.631	5.13E+06	129.41%	0.58	180.86%	32.365	551.060	5.56E+06	140.21%	0.63	195.95%
0 pmol	CTRL	27.363	1306.157	1.32E+07	106.82%			27.456	1222.736	1.23E+07	100.00%		
0 pmol	CTRL	27.409	1264.141	1.28E+07	103.39%			27.456	1222.736	1.23E+07	100.00%		
0 pmol	CTRL	27.595	1107.148	1.12E+07	90.55%			27.456	1222.736	1.23E+07	100.00%		
0.25 pmol	CTRL	27.833	935.087	9.43E+06	76.47%			27.852	922.561	9.31E+06	75.45%		
0.25 pmol	CTRL	27.767	979.816	9.89E+06	80.13%			27.852	922.561	9.31E+06	75.45%		
0.25 pmol	CTRL	27.956	857.015	8.65E+06	70.09%			27.852	922.561	9.31E+06	75.45%		
0.5 pmol	CTRL	27.972	847.562	8.55E+06	69.32%			27.927	874.890	8.83E+06	71.55%		
0.5 pmol	CTRL	27.923	877.634	8.85E+06	71.78%			27.927	874.890	8.83E+06	71.55%		
0.5 pmol	CTRL	27.887	900.276	9.08E+06	73.63%			27.927	874.890	8.83E+06	71.55%		

B) LexA — ReViTA

Sample	Target	Ind Ct	Ind C qRT	Ind C IVT	Ind %Act	Ind C-nor	Ind %A nor	Ave Ct	Ave C qRT	Ave C IVT	Ave %Act	Ave C-nor	Ave %A nor
0 pmol	dinB	30.889	30375.783	3.06E+08	117.34%	0.61	117.34%	31.175	25887.095	2.61E+08	100.00%	0.52	100.00%
0 pmol	dinB	31.376	23129.175	2.33E+08	89.35%	0.46	89.35%	31.175	25887.095	2.61E+08	100.00%	0.52	100.00%
0 pmol	dinB	31.259	24692.290	2.49E+08	95.38%	0.49	95.38%	31.175	25887.095	2.61E+08	100.00%	0.52	100.00%
0.125 pmol	dinB	31.418	22582.341	2.28E+08	87.23%	0.39	75.69%	31.494	21642.861	2.18E+08	83.60%	0.37	72.55%
0.125 pmol	dinB	31.313	23958.395	2.42E+08	92.55%	0.41	80.31%	31.494	21642.861	2.18E+08	83.60%	0.37	72.55%
0.125 pmol	dinB	31.751	18737.766	1.89E+08	72.38%	0.32	62.81%	31.494	21642.861	2.18E+08	83.60%	0.37	72.55%
0.5 pmol	dinB	31.968	16596.511	1.67E+08	64.11%	0.44	85.38%	31.876	17473.161	1.76E+08	67.50%	0.46	89.89%
0.5 pmol	dinB	31.862	17610.152	1.78E+08	68.03%	0.47	90.60%	31.876	17473.161	1.76E+08	67.50%	0.46	89.89%
0.5 pmol	dinB	31.798	18253.013	1.84E+08	70.51%	0.48	93.90%	31.876	17473.161	1.76E+08	67.50%	0.46	89.89%
0 pmol	CTRL	28.602	54036.141	5.45E+08	1.078			28.735	50144.700	5.06E+08	1.000		
0 pmol	CTRL	28.703	51061.658	5.15E+08	1.018			28.735	50144.700	5.06E+08	1.000		
0 pmol	CTRL	28.901	45697.862	4.61E+08	0.911			28.735	50144.700	5.06E+08	1.000		
0.125 pmol	CTRL							28.482	57789.224	5.83E+08	1.152		
0.125 pmol	CTRL	28.304	63864.464	6.44E+08	1.274			28.482	57789.224	5.83E+08	1.152		
0.125 pmol	CTRL	28.661	52291.848	5.28E+08	1.043			28.482	57789.224	5.83E+08	1.152		
0.5 pmol	CTRL	29.097	40954.936	4.13E+08	0.817			29.247	37651.964	3.80E+08	0.751		
0.5 pmol	CTRL	29.161	39499.370	3.99E+08	0.788			29.247	37651.964	3.80E+08	0.751		
0.5 pmol	CTRL	29.482	32996.289	3.33E+08	0.658			29.247	37651.964	3.80E+08	0.751		

B) LexA — PCR bands

Sample	Target	Ind Ct	Ind C qRT	Ind C IVT	Ind %Act	Ind C-nor	Ind %A nor	Ave Ct	Ave C qRT	Ave C IVT	Ave %Act	Ave C-nor	Ave %A nor
0 pmol	dinB	30.389	1334.624	1.35E+07	88.11%	0.01	88.11%	30.259	1514.648	1.53E+07	100.00%	0.01	100.00%
0 pmol	dinB	30.442	1266.702	1.28E+07	83.63%	0.01	83.63%	30.259	1514.648	1.53E+07	100.00%	0.01	100.00%
0 pmol	dinB	29.945	2055.417	2.07E+07	135.70%	0.02	135.70%	30.259	1514.648	1.53E+07	100.00%	0.01	100.00%
0.125 pmol	dinB	30.623	1062.305	1.07E+07	70.14%	0.01	62.55%	30.427	1285.199	1.30E+07	84.85%	0.01	75.67%
0.125 pmol	dinB	30.231	1555.194	1.57E+07	102.68%	0.01	91.57%	30.427	1285.199	1.30E+07	84.85%	0.01	75.67%
0.125 pmol	dinB	30.428	1284.927	1.30E+07	84.83%	0.01	75.66%	30.427	1285.199	1.30E+07	84.85%	0.01	75.67%
0 pmol	CTRL	27.624	123368.442	1.24E+09	106.07%			27.727	116303.899	1.17E+09	100.00%		
0 pmol	CTRL	27.809	111053.761	1.12E+09	95.49%			27.727	116303.899	1.17E+09	100.00%		
0 pmol	CTRL	27.750	114827.258	1.16E+09	98.73%			27.727	116303.899	1.17E+09	100.00%		
0.125 pmol	CTRL	27.394	140613.701	1.42E+09	120.90%			27.526	130412.897	1.32E+09	112.13%		
0.125 pmol	CTRL	27.651	121478.343	1.23E+09	104.45%			27.526	130412.897	1.32E+09	112.13%		
0.125 pmol	CTRL	27.534	129847.536	1.31E+09	111.65%			27.526	130412.897	1.32E+09	112.13%		

Sample	Target	Ind Ct	Ind C qRT	Ind C IVT	Ind %Act	Ind C-nor	Ind %A nor	Ave Ct	Ave C qRT	Ave C IVT	Ave %Act	Ave C-nor	Ave %A nor
0 pmol	dinB	26.398	32959.654	3.33E+08	101.55%	0.22	101.55%	26.420	32456.574	3.27E+08	100.00%	0.22	100.00%
0 pmol	dinB	26.442	31961.174	3.22E+08	98.47%	0.21	98.47%	26.420	32456.574	3.27E+08	100.00%	0.22	100.00%
0.5 pmol	dinB	27.749	12864.344	1.30E+08	39.64%	0.17	79.26%	27.694	13362.862	1.35E+08	41.17%	0.18	82.33%
0.5 pmol	dinB	27.639	13880.717	1.40E+08	42.77%	0.19	85.53%	27.694	13362.862	1.35E+08	41.17%	0.18	82.33%
0 pmol	CTRL	25.261	155793.105	1.57E+09	104.40%			25.338	149223.503	1.51E+09	100.00%		
0 pmol	CTRL	25.338	149198.246	1.51E+09	99.98%			25.338	149223.503	1.51E+09	100.00%		
0 pmol	CTRL	25.414	142955.283	1.44E+09	95.80%			25.338	149223.503	1.51E+09	100.00%		
0.5 pmol	CTRL	26.737	67971.779	6.86E+08	45.55%			26.571	74619.403	7.53E+08	50.01%		
0.5 pmol	CTRL	26.559	75129.584	7.58E+08	50.35%			26.571	74619.403	7.53E+08	50.01%		
0.5 pmol	CTRL	26.417	81360.715	8.21E+08	54.52%			26.571	74619.403	7.53E+08	50.01%		

Table S1. Bacterial strains and plasmids used in this study

Name	Reference name	Description	Source
Plasmids			
pJET1.2/blunt	pJET1.2b	Blunt-end vector; AmpR	Thermo Scientific
pBBR1MSC5	pBBR1MSC5	Broad-host-range cloning vector; GmR	[1]
pETS250	pJET1.2::[pETS130]bb	Backbone of plasmid pBBR1MSC5 in carrier pJET1.2; AmpR, GmR	This work
pETS251	pMK-RQ::ReViTA	Synthetic ReViTA cassette in carrier pMK-RQ; KnR	Thermo Scientific
pETS252	pReViTA	Synthetic ReViTA cassette in pBBR1MSC5 backbone; GmR	This work
pETS253	pReViTA-P*nrdA*	Synthetic ReViTA cassette in pBBR1MSC5 backbone with *nrdA* promoter; GmR	This work
pETS254	pReViTA-P*dinB*	Synthetic ReViTA cassette in pBBR1MSC5 backbone with *dinB* promoter; GmR	This work
pETS255	pET28a-LexA	pET28b derivative carrying lexA, LexA overproducer; KnR	This work
pETS28a	pETS28a	Vector for His6-tagged protein overexpression; KnR	Thermo Scientific [2]
pETS201	pET28a-AlgR	pET28a derivative carrying algR, AlgR overproducer, KnR	
Strains			
E. coli			
DH5α	DH5α	*recA1 endA1 hsdR17 supE44 thi-1 relA1 Δ(lacZYA-argF)U169 deoR Φ80dlacZM15*	Lab strain
Rosetta (DE3)	Rosetta (DE3)	*F- ompT hsdSB (rB ‾ mB‾) gal dcm (DE3) pRARE (CamR)*	Merck
P. aeruginosa			
PAO1	PAO1 WT	Wild-type (ATCC 15692 / CECT 4122) - Spanish Type Culture Collection	Lab strain

1   Kovach, M. E. *et al.* Four new derivatives of the broad-host-range cloning vector pBBR1MCS, carrying different antibiotic-resistance cassettes. *Gene* **166**, 175-176 (1995).

2   Crespo, A., Pedraz, L., Van Der Hofstadt, M., Gomila, G. & Torrents, E. Regulation of ribonucleotide synthesis by the *Pseudomonas aeruginosa* two-component system AlgR in response to oxidative stress. *Sci Rep* **7**, 17892, doi:10.1038/s41598-017-17917-7 (2017).

Table S2. Primers and probes used in this study

Primers

Number	Name	Sequence (5' -> 3')	Application
1	pETS130_backbone_XbaI_up	AATCTAGATGCCCATGGACGCACAC	Cloning pETS130 backbone/CTRL EMSA band/CTRL template for IVT
2	pETS130_backbone_XbaI_low	AATCTAGACGGGGAGGCAGACAAGGTATA	Cloning pETS130 backbone with ReViTA cassette
3	PAlexA-NcoI-up	ACCATGGAGAAGCTGACGCCC	*lexA* cloning into pET28b
4	PAlexA-XhoIHis-lw	ACTCGAGGCGCCGGATCACGCCGAC	*lexA* cloning into pET28b
5	PnrdA_GFP_up	AGGATCCGAATTCTTGCTCCACACAGCCTC	P*nrdA* promoter for EMSA and cloning
6	PnrdA_low_M13	CTGGGCGTCGTTTTACGGCTCCTTGCGATGAG	P*nrdA* promoter for EMSA
7	Nrda_SpeI_Rv	ACTAGTGGGCTCGCGTGTGGTGTCGG	P*nrdA* promoter cloning
8	dinB1-PAO1-dir	GAGTTCCATCCGGTTCACG	P*dinB* promoter for EMSA
9	DinB low M13	CTGGGCGTCGTTTTACCAGCTCCCGCAACCAC	P*dinB* promoter for EMSA
10	SPLIT_CTRL_M13-Short	CTGGGCGTCGTTTTACTGCTCCATAACATCAAACATCG	Control band for EMSA
11	Wellred M13	[D3-PA]GTCACTGGGCGTCGTTTTAC	Bands for EMSA
12	IVT_PAO-nrdA_fw	CAGCCTCCTCGTATCGC	P*nrdA* PCR template for IVT
13	IVT_PAO-nrdA_rv	ACCTGGTCCTGGATCTCTTC	P*nrdA* PCR template for IVT
14	REVITA_PdinB-PAO1_fw	GGATCCATGTCGTCGAGTTCCATCC	Cloning P*dinB* in ReViTA/ PCR template for IVT
15	REVITA_PdinB-PAO_rv	ACTAGTAAACAGTCGCAGTCTATATGG	Cloning P*dinB* promoter in ReViTA
16	IVT_dinB-PAO1_rv	GGGGTAATCACGAACAGCC	P*dinB* PCR template for IVT
17	pReViTA-SPLIT_CTRL-rv	GCGGCGTTGTGACAATTTA	PCR template of CTRL region for IVT
18	ReViTA-TEST_fw	AGCACAAGTTTTATCCGGCC	Checking insertion of test promoter into ReViTA
19	ReViTA-TEST_rv	CATATCACCAGCTCACCGTC	Checking insertion of test promoter into ReViTA
20	qRTgreen_IVT_PAO-nrdA_fw	TCCCCTACACCGATGACAAG	qRT-PCR of P*nrdA* with PCR templates
21	qRTgreen_IVT_PAO-nrdA_rv	CGCACGGTGTCATGGATAC	qRT-PCR of P*nrdA* with PCR templates
22	IVT_dinB-PAO1_rt	GTGATGTGCAGCTCCTCG	Reverse transcription of P*dinB*- PCR templates
23	qRT-IVT_dinB-PAO1_fw	CTCAAGCTGTGTCCCGATC	qRT-PCR of P*dinB* using PCR templates
24	qRT-IVT_dinB-PAO1_rv	GGTATAATCGCGGAAGATCG	qRT-PCR of P*dinB* using PCR templates
25	ReViTA-TRIAL_rt	CCAACCACGATTTTCGCGTC	Reverse transcription of P*dinB* using ReViTA
26	ReViTA-TRIAL_fw	GGACCCGAAATTCTCCTCCC	qRT-PCR of IVT using ReViTA
27	ReViTA-TRIAL_rv	TGCCAGCAGTTCGTTCATC	qRT-PCR of IVT using ReViTA
28	ReViTA_ctrl_rt	CGCCAACAACCGCTTCTTG	Reverse transcription of control gen - ReViTA
29	REVITA_ctrl_fw	TTTCGGTCGTGAGTTCGGAG	qRT-PCR of control gene using ReViTA
30	REVITA_ctrl_rv	GCAAGCGCGATGAATGTCTT	qRT-PCR of control gene using ReViTA

Artículo 3: Regulon and mechanism of action of NrdR, a global regulator of ribonucleotide reduction

Lucas Pedraz, Arkadiusz Szura, **Alba Rubio-Canalejas**, Annalisa Calo, Neus Gual, Maria Solà, Gabriel Gomila, Eduard Torrents

Manuscrito

Resumen

Las RNR son las enzimas encargadas de transformar los NTPs a dNTPs, por lo que son esenciales para producir y reparar el ADN. Hasta el momento se han descrito tres clases diferentes de RNR, la clase I, II y III, y todas ellas comparten el mismo mecanismo de reducción, por lo que su actividad debe estar estrechamente regulada mediante mecanismos alostéricos y transcripcionales, para más detalle se puede consultar la sección 1 de la introducción de esta tesis (3). La regulación alostérica de la actividad de las RNR se lleva a cabo mediante la unión de ATP o dATP en el cono-ATP de estas enzimas (4, 63). La regulación transcripcional permite controlar la expresión global de las enzimas y la expresión diferencial entre las diferentes RNR cuando una misma especie codifica para distintas clases de RNR. Se conocen numerosos FT que regulan la expresión de las RNR, siendo especialmente importante el represor global NrdR, un factor exclusivo de la regulación transcripcional en las RNR bacterianas. En la estructura tridimensional proteica de NrdR encontramos un dominio dedo de Zn que permite la unión a ADN y un cono-ATP similar al sitio alostérico de las RNR. En los promotores de los genes regulados por NrdR, se encuentran secuencia repetidas que corresponden a las zonas de unión de NrdR al ADN. Estas secuencias se conocen como "cajas NrdR" y la presencia de repeticiones sugiere que es necesaria la interacción entre varias moléculas de NrdR unidas a las cajas para que el FT sea activo (82). Otros estudios han demostrado la regulación alostérica de NrdR por ATP y dATP influye la oligomerización de NrdR (94). Los obstáculos encontrados en la producción y purificación de la proteína han dificultado el uso de NrdR en ensayos experimentales para determinar su funcionalidad.

El objetivo principal de este proyecto es comprender el mecanismo de acción y el papel biológico que desempeña NrdR en *E. coli* y *P. aeruginosa*. Para abordar este objetivo hemos

utilizado datos transcriptómicos, estudios *in vitro* utilizando la proteína purificada y técnicas como SEC, SEC-MALS y AFM para analizar la estructura cuaternaria de la proteína al unirse a diferentes cofactores nucleotídicos. Las estructuras cuaternarias se estudiaron a nivel de unión al ADN y a nivel funcional. Finalmente, se evaluó si NrdR puede ser considerada una nueva diana para terapias antimicrobianas estudiando la virulencia bacteriana al alterar la expresión de *nrdR*. Los resultados obtenidos se relacionan con el Objetivo 3 de esta tesis.

En este manuscrito hemos investigado el mecanismo de acción de NrdR. Utilizamos una búsqueda bioinformática de las cajas NrdR en el genoma de *E. coli* y *P. aeruginosa* y los datos transcriptómicos obtenidos en ensayos de crecimiento en los que se compara la expresión de las cepas salvajes de *E. coli* y *P. aeruginosa* con las cepas mutantes *E. coli* Δ*nrdR* y *P. aeruginosa* Δ*nrdR*. De esta forma se determinó que la regulación por NrdR estaba limitada únicamente a las RNR en *E. coli* y *P. aeruginosa* mediante la unión a cajas NrdR que se encuentran repetidas en sus regiones promotoras (Figura 1 del Artículo 3).

Para continuar con los ensayos experimentales, se purificó la proteína NrdR de *E. coli* y *P. aeruginosa* utilizando etiquetas de solubilización y purificación. La proteína de *P. aeruginosa* se marcó con His_6 y se purificaron pequeñas cantidades funcionales, ya que la mayor parte estaba en la parte insoluble formando cuerpos de inclusión. La proteína de *E. coli* no pudo obtenerse de manera soluble con el marcaje de histidina. Para mantener la estabilidad de la proteína y mantener su estabilidad se fusionó con la etiqueta SUMO, que favorece su solubilidad y que es fácilmente eliminable utilizando una proteasa para así obtener la proteína NrdR pura y sin etiquetas (Figura 2 del Artículo 3).

Las proteínas NrdR purificadas de *E. coli* y *P. aeruginosa* se analizaron con cromatografía de exclusión por tamaño (SEC), cromatografía de exclusión por tamaño acoplada a dispersión multiángulo de la luz (SEC-MALS) y microscopía de fuerza atómica (AFM) para estudiar su oligomerización, ya que de eso depende la funcionalidad de la proteína. Se observó que la incubación de NrdR con diversos nucleótidos modificaba de forma drástica su estructura cuaternaria. Tras la incubación 20:1 nucleótido:proteína con AMP o sin nucleótido se observó que el NrdR mostraba un peso molecular bajo que correspondería a una estructura di- o trimérica. En cambio, al unirse a dATP o ATP las formas oligoméricas tenían un mayor peso molecular. Se observaron tetrámeros y octámeros tras incubar la proteína NrdR con dATP y estructuras más grandes, como dodecámeros al incubar con ATP. La forma de los picos obtenidos con SEC-MALS parece

indicar que NrdR forma complejos débiles generando asociaciones dinámicas proteína-proteína (Figuras 3-5 del Artículo 3).

Tras caracterizar las estructuras cuaternarias obtenidas, utilizamos la técnica EMSA para estudiar la capacidad de unión al ADN de cada complejo NrdR-nucleótido. Tras incubar la proteína NrdR de *E. coli* con los distintos nucleótidos, se observó que cuando se incubaba la proteína con AMP o sin nucleótido el complejo ADN-proteína era inestable y solo causaba un pequeño desplazamiento de la sonda. La incubación NrdR-ATP no causó ningún desplazamiento significativo, pero, sin embargo, la incubación NrdR-dATP produjo un desplazamiento del ADN más claro e intenso (Figura 6 del artículo 3). La proteína homologa de *P. aeruginosa* mostró resultados análogos a la de *E. coli*.

Para estudiar el significado biológico de los complejos y determinar su actividad se utilizó el sistema ReViTA que se basa en la transcripción *in vitro* (esta técnica está extensamente detallada en el Artículo 2 de esta tesis). Estos experimentos mostraron que la capacidad de NrdR para reprimir la transcripción de los genes de las RNR dependía del nucleótido con el que se había incubado la proteína previamente. La proteína NrdR de *E. coli* tras unirse a dATP reprimió la transcripción de *nrdD* hasta 54.5% y 34.8% cuando la proteína estaba en una ratio 2:1 y 4:1, respectivamente. En cambio, NrdR-ATP no mostró represión. La proteína NrdR de *P. aeruginosa* reprimió la transcripción génica hasta 45.7% al unirse a dATP y no produjo represión cuando se incubó con ATP y AMP (Figura 7 del Artículo 3).

Finalmente se estudió la proteína NrdR como posible diana antibacteriana contra *P. aeruginosa* en infecciones *in vivo* en el modelo de infección *G. mellonella.* Los resultados mostraron que alteraciones en la producción de NrdR afectan a la virulencia de la bacteria. Se observó que la cepa *P. aeruginosa* salvaje mató a todas las larvas a las 18h. En cambio, una cepa con el gen *nrdR* mutado y otra con la correspondiente complementación necesitaron más de 24 h para acabar con todas las larvas (Figura 8 del artículo 3).

Manuscrito

Regulon and mechanism of action of NrdR, a global regulator of ribonucleotide reduction

Lucas Pedraz[1]*, Arkadiusz Szura[2], **Alba Rubio-Canalejas**[1], Annalisa Calo[3,4], Anthony Santella[5], Neus Gual[1], Maria Solà[2], Gabriel Gomila[3], Eduard Torrents[1,6]*.

1: Bacterial Infections: Antimicrobial Therapies, Institute for Bioengineering of Catalonia (IBEC), The Barcelona Institute of Science and Technology (BIST), Barcelona, Spain.
2: Structural Biology of Mitochondrial Macromolecules, Structural Biology Unit (SBU), Molecular Biology Institute of Barcelona (IBMB), Consejo Superior de Investigaciones Científicas (CSIC).
3: Nanoscale Bioelectrical Characterization, Institute for Bioengineering of Catalonia (IBEC), The Barcelona Institute of Science and Technology (BIST), Barcelona, Spain.
4: University of Barcelona, Department of Electronic and Biomedical Engineering, University of Barcelona (UB), Barcelona, Spain.
5: Molecular Cytology Core Facility, Memorial Sloan Kettering Cancer Center
6: Department of Genetics, Microbiology and Statistics, Faculty of Biology, University of Barcelona (UB), Barcelona, Spain.

Abstract

All living cells require deoxyribonucleotides (dNTPs) for DNA synthesis and repair. Ribonucleotide reductases (RNRs) form the only *de novo* pathway for dNTP synthesis. Numerous studies have explored the regulation of RNRs by known transcription factors. However, the RNR network is also controlled by its own master regulator, NrdR. NrdR is a nucleotide-binding, oligomeric, global repressor of RNRs encoded by almost all bacterial species but absent in *Eukarya* and *Archae*a. Despite its crucial role, the mechanism of action of NrdR remains fundamentally unknown due to, among other reasons, the challenge it supposes to obtain this transcription factor in a pure and stable form for *in vitro* studies.

In this work, we conducted a thorough exploration of the NrdR regulon and its mechanism of action. We performed RNA-seq and DNA microarray studies in *Escherichia coli* and *Pseudomonas aeruginosa* and correlated the data with whole-genome searches for NrdR-boxes to draw a global picture of the NrdR regulon. We designed a series of NrdR fusion proteins to improve their stability and facilitate their purification. Using these proteins, we conducted a series of tests aimed towards two purposes: first, analyzing the oligomerization of NrdR depending on the nucleotide cofactor it binds using size-exclusion chromatography, SEC-MALS, and atomic force microscopy; second, understanding the functional meaning of these oligomeric states using EMSAs and *in vitro* transcription.

Overall, we offer the first demonstration of a mechanism of action for NrdR. This transcription factor acts as a sensor of the nucleotide pool, modulating its oligomerization state and its repression of RNR operons depending on the nucleotide cofactor bound to its ATP-cone domain.

Introduction

Ribonucleotide reductases (RNRs) are the enzymes responsible for the reduction of ribonucleotides (NDPs or NTPs) to deoxyribonucleotides (dNDPs or dNTPs), thereby forming the building blocks for DNA synthesis and repair (1). Three different RNR classes have been described, namely class I (subclassified into Ia, Ib, Ic, Id, and Ie), class II, and class III. All ribonucleotide reductases can reduce all four ribonucleotides, and they all share a common, free-radical-based mechanism (1–3). The different classes, however, rely on distinct systems for the generation of the radical, use different electron donors and present various quaternary structures (1, 4). While complex eukaryotic organisms only encode for class Ia RNR, eubacteria and archaea make use of all RNR classes in any possible combination (3, 4). As all living cells require dNTPs, and a balanced supply of all four is critical to avoid increased mutation rates during DNA replication (2, 5, 6), RNR activity needs to be tightly regulated. This occurs at the allosteric level and the transcriptional level (1, 7–9).

The allosteric regulation of RNRs is responsible for two different aspects of nucleotide homeostasis: Firstly, keeping the balance of all four dNTPs, using the "specificity" allosteric site present in all RNRs (4, 10, 11). Secondly, keeping the balance of ribonucleotides and deoxyribonucleotides. For the latter, most class I and class III RNRs (and a small subset of class II RNRs) include a second allosteric site, the "activity" site. This allosteric element appears as a four-helix bundle covered by a three-stranded beta-sheet (12), forming a cone-shaped structure, for which it is called the ATP-cone domain (4, 12). The binding of ATP or dATP to the ATP-cone activates or inactivates the overall activity of the RNR (4, 12).

The transcriptional regulation of RNRs is responsible for two missions: Firstly, controlling the overall expression of RNR genes (e.g., increasing it in certain points of the cell cycle or upon DNA damage) (1). Secondly, controlling differential RNR expression in species encoding more than one class, i.e., activating or repressing different classes in response to changing events and environmental conditions (1). The transcriptional regulation of the RNR network in bacteria has been extensively studied, and many regulation events limited to particular species and RNR classes are known. In *E. coli*, for instance, class Ia RNR expression is controlled by DnaA, Fis, IciA and H-NS to couple its transcription to the cell cycle, class Ib RNR expression is controlled by Fur to derepress it

under iron deprivation, and class III RNR is controlled by the anaerobic master regulator Fnr to induce its expression under anaerobic conditions (4, 7). However, specifically in bacteria, there is also a global regulator of the RNR network, a transcription factor exclusive to this pathway named NrdR (4, 13, 14).

NrdR was first discovered in *Streptomyces coelicolor* (15). Structural analysis revealed that NrdR contains an N-terminal Zn-finger domain and a central ATP-cone domain, very similar to the "activity" allosteric site of ribonucleotide reductases (14–16). NrdR was immediately hypothesized to be a transcriptional regulator of RNR expression controlled by nucleotide binding (14). Additionally, a bioinformatic search identified orthologs of NrdR across the Bacteria domain and linked this regulator to the presence of a consensus 16 bp sequence in RNR promoters (13). In species encoding NrdR, two repeats of these "NrdR-boxes," always separated by an integer number of turns in the DNA helix, can be found in the promoters of all RNR operons, often overlapping with the base promoter sequences (13). These findings suggest that NrdR is a transcriptional repressor (13, 14, 16, 17) and that it relies on protein-protein interaction between NrdR molecules bound to both boxes (16). The distribution of *nrdR* genes and NrdR-boxes suggests that NrdR is present in most bacterial species and absent in *Eukarya* and *Archaea*, and that, when present, it controls all RNR classes (13).

The functionality of NrdR has been studied in different bacterial species, including *S. coelicolor* (14, 16), *E. coli* (17) and *P. aeruginosa* (18), always acting as a repressor of all RNR classes. It was demonstrated that NrdR contains zinc (14, 16), that it binds nucleotides (16), and that it is an oligomeric protein (14, 16, 17, 19, 20). Further studies concerning the nucleotide-binding capabilities of NrdR show that it uses a negative-cooperative mechanism to bind both dATP and ATP *in vivo* despite being present at very different concentrations (20), which supports the hypothesis of NrdR working as a sensor of the dATP-ATP balance. As expected, the oligomeric state of the protein is influenced by nucleotide binding (20). This hypothesis was tested recently by Grinberg et al., 2022 (26) who studied the influence of dATP and ATP in the oligomeric state of NrdR. They suggested that the binding of two ATP molecules to NrdR triggers the formation of a dodecamer, and that the binding of an ATP and a dATP molecule favors the formation of octamers. According to this study, only the octameric structures of NrdR could bind to DNA. Although this study clarifies the mechanism of action of NrdR, the biological role of NrdR still remains unknown.

One of the major challenges in the study of NrdR is the difficulty to express and purify it in a recombinant form. NrdR is reportedly unstable and tends to precipitate during and after purification (19–21). The functional effect of NrdR in *Chlamydia trachomatis* has been studied using *in vitro* transcription. However, protein instability made it impossible to conduct experiments to differentiate the effects of nucleotide cofactors (21).

Here, we report a study aimed towards a better understanding of the mechanism of action and the biological role of NrdR. We first explored the extent of the NrdR regulon in *E. coli* and *P. aeruginosa* using transcriptomics data and correlating it to the presence or absence of NrdR-boxes. To conduct *in vitro* studies with the protein, we then developed a series of recombinant NrdR fusion proteins designed for increased stability and easy purification. These proteins were used for SEC, SEC-MALS and AFM experiments to explore the effects of different nucleotide cofactors on the quaternary structure of NrdR. Then, we analyzed the meaning of these different quaternary structures both at a DNA-binding level (using EMSA) and at a functional level (using *in vitro* transcription). Finally, as a bacteria-exclusive protein able to fully repress an essential pathway may be a potential target for antimicrobial therapies, we explored the effects that altering *nrdR* expression causes on bacterial virulence and fitness. Overall, these results offer insight into the role of NrdR as a nucleotide sensor and provide a first description of the mechanism of NrdR regulation of RNR expression.

Materials and methods

Bacterial strains, plasmids, and growth conditions

Bacterial strains and plasmids are listed in Supplementary Table S1. Escherichia coli and Pseudomonas aeruginosa cells were routinely grown in Luria-Bertani broth (LB, Scharlab, Spain) at 37 ºC. When necessary, antibiotics were added at the following concentrations: for *E. coli*, 10 µg/ml gentamicin (Gm^R), 50 µg/ml ampicillin (Amp^R), 30 µg/ml kanamycin (Kn^R); for *P. aeruginosa*, 150 µg/ml gentamicin (Gm^R), 300 µg/ml carbenicillin (Amp^R). Liquid cultures were shaken on a horizontal shaker at 200 rpm.

Growth curves were conducted in 96-well plates. Overnight cultures (in LB medium, with the required antibiotics) of the desired strains were prepared. Cells were pelleted by centrifugation (5000 g, 10 minutes) and resuspended in sterile PBS, calculated for an OD$_{550}$ of 1.0. The cultures for the growth curves were prepared with LB medium, the required antibiotics, and cell suspension to a final OD$_{550}$ of 0.05. Plates were incubated at 37 ºC with orbital shaking and constant humidity in the SPARK Multimode Microplate Reader (TECAN, Switzerland) using the SPARK Small Humidity Cassette (TECAN, Switzerland). OD$_{550}$ was monitored every 20 minutes.

DNA manipulation and plasmid construction

Recombinant DNA manipulations were carried out according to published protocols. Plasmid DNA was prepared using the GeneJET Plasmid MiniPrep Kit (ThermoFisher, MA, USA), according to the manufacturer's instructions. Plasmid transformation into *P. aeruginosa* cells was done by electroporation, using a Gene Pulser Xcell electroporator (Bio-Rad, CA USA). Digestion reactions with restriction enzymes were performed according to the manufacturer's instructions (ThermoFisher, MA, USA). Ligations were performed with the T4 DNA ligase (ThermoFisher, MA, USA). DNA fragments for cloning were obtained by PCR using Phusion High-Fidelity DNA Polymerase (ThermoFisher, MA, USA). During all plasmid construction procedures, fragments synthesized by PCR and digested with restriction enzymes were first cloned via blunt-end cloning to pJET1.2b (CloneJET PCR Cloning Kit, ThermoFisher, MA, USA), according to the manufacturer's instructions, and then digested from the resulting carrier plasmid. Colony PCR reactions to test plasmid incorporation was carried out using DreamTaq Green PCR Master Mix (ThermoFisher, MA, USA). All PCR primers used in this study are listed in

Supplementary Table S2. PCR primers will be referred by their numbers as listed on the table.

Bioinformatic prediction of NrdR-boxes

To perform genome-wide searches for NrdR-boxes, we started by retrieving the sequence and annotation for the *E. coli* K-12 substr. MG1655 genome (NCBI Reference Sequence: NC_000913.3) and the *P. aeruginosa* PAO1 genome (NCBI Reference Sequence: NC_002516.2). We then extracted only the "gene" features from the annotation. Using gene features as reference, we retrieved the sequences starting 450 bp upstream and ending 20 bp downstream of every translation start codon in the genome using the SAMtools (22) suite and the BEDtools (23) functions flank, slop, and getfasta. A comprehensive shell script for this process is available upon request.

A consensus sequence for the NrdR-box was obtained using the γ-proteobacteria data published by Rodionov *et al.* (13), representing a total of 135 NrdR-box sequences. First, we used MEME (24) (MEME Suite (25) to produce a weight matrix. Then, FIMO (26) (MEME Suite (25) searches were performed, applying a 10^{-4} *p*-value threshold. Results were deduplicated and assigned to the gene with the closest translation start. Hits inside non-coding RNAs and low-complexity regions were ignored.

Transcriptomics and transcriptomics data treatment

To extract samples for RNA-seq, we used three independent cultures of *P. aeruginosa* PAO1 in 25 ml LB medium and three of its isogenic mutant strain PAO1 Δ*nrdR* in 25 ml LB medium supplemented with 40 μg/ml tetracycline. Cultures were grown to an OD_{550} of 0.5, and then stopped and fixed using RNAprotect Bacteria Reagent (QIAGEN, Germany), according to the manufacturer's instructions. Then, RNA was extracted using RNeasy Mini RNA Isolation Kit (QIAGEN, Germany), according to the manufacturer's instructions. Reverse transcription, library generation, and RNA sequencing were performed by Beckman Coulter Genomics (CA USA), according to the protocol "Illumina TruSeq Stranded Total RNA with Ribo-Zero rRNA Removal (Bacteria)". The platform used was Illumina 1.9, with library TruSeq3-PE-2. A total of 6 samples were analyzed, and a total of 362 million paired-end reads were generated (2 x 100 bp each).

RNA-seq data were received as untreated sequence+quality data (FASTQ). To remove adapter sequences and low quality bases, a first FASTQ trimming step was introduced using Trimmomatic version 0.36 (LEADING:5, TRAILING:5, SLIDINGWINDOW

4:15, MINLEN:25, LLUMINACLIP:/RNA/REF/TruSeq3-PE-2.fa:2:30:10:2:true) (27). Data was then mapped using end-to-end alignment with bowtie version 1.5, allowing multiple binding. Mapping parameters were: -S -t --fr -n 2 -l 28 -e 70 -k 5 --best --strata --allow-contain --no- unal –nomaqround (28). The *P. aeruginosa* PAO1 genome was used as reference (NCBI Reference Sequence NC_002516.2). The output SAM file generated by bowtie was converted to BAM and sorted using SAMtools functions view and sort, with default parameters (29). The quality of the mapped data was assessed using Qualimap 2.2.1 (30). Differentially expressed genes were then obtained using DESeq2 version 3.9 (R, Bioconductor) according to the general pipeline (31–33). Only genes with an absolute fold-change over 2.0 were considered.

NrdR overexpression and purification

The NrdR-H_6 protein from *P. aeruginosa* was overexpressed in BL21(DE3) transformed with plasmid pET- NrdR(PAO). Cells were grown in LB medium with 50 µg/ml ampicillin and 100 µM $ZnSO_4$ and incubated at 37 ºC with vigorous shaking. When cultures reached and OD_{550} of 0.5, protein overexpression was induced by adding IPTG to a concentration of 0.1 mM. Cells were then cultured at 18 ºC over-night (14-16 hours).

To obtain the crude extracts, cells were pelleted by centrifugation (6000 g, 20 min, 4 ºC) and resuspended in 25 ml (per liter of original culture) of NrdR-lysis buffer: 50 mM Tris-HCl (pH 8.5 at 25 ºC), 1 M NaCl, 20 mM imidazole, 1 mM phenylmethylsulphonyl fluoride (PMSF), 100 µM $ZnSO_4$, and 10% glycerol. The suspension was then sonicated until clear (20 pulses of 20 s, with 50 s cooldown between pulses, using a 1/2'' tip in a Branson 450 Digital Sonifier, Marshal Scientific, NH, USA) and centrifuged at high speed (15000 g, 20 min, 4 ºC), keeping the supernatant containing the soluble fraction, which was frozen at -80 ºC for long term storage. To obtain the crude extracts, cells were pelleted, resuspended, sonicated, and centrifuged as described above for NrdR-H_6. The crude extracts then suffered a first step of purification by Immobilized Metal Affinity Chromatography (IMAC1) using a 5 ml Mini-Nuvia IMAC Cartridge (Bio-Rad, CA USA) in an FPLC system (Biologic DuoFlow System, Bio-Rad, CA USA). Protein samples suffered a DNA precipitation step (30 minutes incubation with streptomycin sulfate 1%, at 4 ºC) and were diluted with buffer A1 to a concentration of less than 1 mg/ml of total protein before being injected into the column. The column was equilibrated with 5 column volumes (CV) of Buffer A1 (50 mM Tris-HCl pH 8.5, 1 M NaCl, 20 mM imidazole). A washing step was carried out using 5 CV of Buffer A1. Mixtures with buffer B1 was then introduced to start the

elution (50 mM Tris-HCl pH 8.5, 1 M NaCl, 500 mM imidazole). First, contaminant proteins were removed with a non-specific elution step using 5 CV of buffer with 50 mM imidazole. Then, the protein was recovered in a specific elution step using 5 CV of buffer with 200 mM imidazole. The resulting fractions were analyzed by SDS-PAGE. Fractions containing the protein of interest were concentrated and diafiltrated against buffer 5x NrdR: 100 mM Tris-HCl (pH 9.0 at 25 ºC), 400 mM KCl, 5 mM MgCl2, 5 mM DTT, 250 µM $ZnSO_4$, and 25% glycerol, using VivaSpin 20 10000 MWCO Ultrafiltration units (Sartorius AG, Germany).

The $NrdR_1$ proteins from *E. coli* and *P. aeruginosa* were overexpressed in XCell F' Chemically Competent Cells (Expresso Biotin SUMO Cloning and Protein Expression System, Lucigen, WI, USA) transformed with plasmids pSUMO-NrdR(ECO) and pSUMO-NrdR(PAO), respectively. Cells were grown in 1-liter cultures of LB medium supplemented with 30 µg/ml kanamycin and 50 µM $ZnSO_4$ and incubated at 37 ºC with vigorous shaking. When cultures reached and OD_{550} of 1.0, protein overexpression was induced by adding 0.1% rhamnose. Cells were then cultured at 18 ºC over-night (14-16 hours).

To obtain the crude extracts, cells were pelleted, resuspended, sonicated, and centrifuged as described above for NrdR-H_6. The crude extracts then suffered a first step of purification (IMAC1) using the same procedure described above for NrdR-H_6. The resulting fractions were analyzed by SDS-PAGE. Fractions containing the protein of interest were concentrated and diafiltrated against buffer 4x NrdR-PROT: 100 mM Tris-HCl (pH 8.5 at 25 ºC), 600 mM NaCl, 4 mM DTT, 40 µM $ZnSO_4$ using VivaSpin 20 10000 MWCO Ultrafiltration units (Sartorius AG, Germany).

Before SUMO protease digestion, the protein was diluted with water to a final concentration of 1x NrdR- PROT buffer, and + 2 mM fresh DTT was added. SUMO protease (Lucigen, WI USA) was added (1 unit for each 300 µg of protein) and the reaction mixture was incubated for 3 hours at 30 ºC with gentle mixing. The extra DTT was removed from the digested protein mixture (but not completely, to avoid protein precipitation) by dialysis against 50 mM Tris-HCl (pH 9.0 at 25 ºC), 1 M NaCl, 0.5 mM DTT, using Slide-a-Lyzer Dialysis Cassettes (ThermoFisher, MA, USA).

The digested protein then suffered a second step of purification by a negative IMAC (IMAC2) in the same column and system mentioned above. First, the column was equilibrated with 5 CV of Buffer A2 (50 mM Tris- HCl pH 9.0, 1 M NaCl, 20 mM imidazole).

Protein samples were then injected into the column. The protein was recovered from the flow-through, as the SUMO-tag and SUMO-protease are retained. The resulting fractions were analyzed by SDS-PAGE. Fractions containing the protein of interest were concentrated and diafiltrated as described above, against buffer 5x NrdR: 100 mM Tris-HCl (pH 9.0 at 25 ºC), 400 mM KCl, 5 mM $MgCl_2$, 5 mM DTT, 250 µM $ZnSO_4$, 25% glycerol.

The $NrdR_2$ proteins from *E. coli* and *P. aeruginosa* were purified using the same protocol as the $NrdR_1$ presented above, with the following changes: The first difference is the protein expression step. $NrdR_2$ proteins were overexpressed in BL21 (DE3) transformed with plasmids pCri-NrdR(PAO) or pCri-NrdR(ECO). Cells were grown in LB medium with 30 µg/ml kanamycin and 200 µM $ZnSO_4$ and incubated at 37 ºC with vigorous shaking. After 3 hours of incubation, protein overexpression was induced by adding IPTG to a concentration of 0.2 mM. Cells were then cultured at 18 ºC over-night (16 hours). The second difference is the fusion-protein digestion step. Instead of SUMO protease, recombinant TEV protease produced as previously described (34) was added to the concentrated fusion protein obtained from IMAC-1 at an NrdR:protease molar ratio of 25:1, and digestion occurred for 16 hours at 4 ºC.

All proteins were quantified after every purification step using BIO-RAD Protein Assay (Bio-Rad, CA USA), according to the manufacturer's instructions. If necessary, the concentrated protein was frozen at -80 ºC for long term storage.

SEC and SEC-MALS

For SEC (Size-Exclusion Chromatography) experiments, purified NrdR-H_6 protein from P. aeruginosa, as well as $NrdR_1$ proteins from *E. coli* and *P. aeruginosa*, were used. Protein was pre-incubated with nucleotides, added as 10 mM solutions directly to the concentrated protein to a final molar ratio of 20:1 nucleotide:protein, and incubated for 1 hour at room temperature. We used a Superdex 200 10/300 GL column (20 ml bed volume) (GE Healthcare, IL, USA) in a BioLogic DuoFlow FPLC System (Bio-Rad, CA, USA). All the process occurred at a fixed flow rate of 0.5 ml/min with the following elution buffer: 50 mM Tris-HCl (pH 9.0 at 25 ºC), 250 mM NaCl, 5 mM DTT. When required, nucleotide was added to the column, calculated for a 1:1 molar ratio of nucleotide:protein. The column was equilibrated with 2 column volumes (CV) of elution buffer before injecting the samples, and when protein-nucleotide complexes were to be run it was re-equilibrated with 0.5 CV of elution buffer containing the corresponding nucleotide before their

injections. Sample concentrations were normalized at 0.5 mg/ml, and a fixed injection volume of 220 µl was used. Data was analyzed using BioLogic DuoFlow Software (Bio-Rad, CA, USA).

For SEC-MALS (Size-Exclusion Chromatography – Multi Angle Light Scattering) experiments, purified NrdR 2 proteins from *E. coli* or *P. aeruginosa* were used. When required, protein was pre-incubated with nucleotides, added as 10 mM solution directly to the concentrated protein to a final molar ratio of 20:1 nucleotide:protein, and incubated for 3 hours at room temperature. We used a Superdex 200 10/300 GL column (20 ml bed volume) (GE Healthcare, IL, USA) in an ÄKTA Pure Protein Purification System (GE Healtchare, IL, USA). All the process occurred at a fixed flow rate of 0.5 ml/min with the following elution buffer: 50 mM Tris-HCl (pH 9.0 at 25 ºC), 250 mM NaCl, 1 mM DTT. Fresh nucleotides were added to the elution buffer at a final concentration of 0.025 mM, when needed.

The *E. coli* sample concentrations were normalized at 1 mg/ml before injection. Injection volumes were limited by sample availability, and were as follows: 80 µl NrdR$_2$, 85 µl NrdR$_2$ + AMP, 60 µl NrdR$_2$ + ATP, 60 µl NrdR$_2$ + dATP. The P*. aeruginosa* sample concentrations were normalized at 2 mg/ml, and injection volumes were as follows: 60 µl NrdR$_2$+ AMP, 40 µl NrdR$_2$ + ATP, 40 µl NrdR$_2$ + dATP. SEC data was analyzed using UNICORN 7 (GE Healthcare, IL, USA). MALS data was obtained with a MiniDawn MALS Detector (Wyatt Technology, CA, USA), and analyzed using ASTRA 7 (Wyatt Technology, CA, USA).

Electrophoretic mobility shift assay

Two DNA probes were used for EMSA: an NrdR-sensitive probe containing the full promoter region of *nrdAB* from *E. coli* K-12 substr. MG1655 (P*nrdA* ECO) and a negative-control, NrdR-insensitive probe containing an unrelated internal sequence of the *anr* gene from *P. aeruginosa* PAO1 (*anr*). Probes were generated by a two PCRs method. Briefly, a first PCR is conducted to obtain the corresponding fragments with an arbitrary sequence added at the 3' end of every fragment (M13 complementarity tail); primers 17 and 25 were used for P*nrdA* ECO, and primers 26 and 27 for *anr*. Then, a second PCR uses a WellRED oligo (Millipore Sigma, MA, USA) coupled to the near-infrared fluorophore D3-phosphoramidite (D3- PA); primers 17 and 28 were used for P*nrdA* ECO, and primers 26 and 28 for *anr*. Probes were purified from agarose gels using the GeneJET Gel Extraction

Kit (ThermoFisher, MA, USA) and used in EMSA experiments at a fixed quantity of 100 fmol.

Purified NrdR-H_6, $NrdR_1$, or $NrdR_2$ proteins were used in DNA-protein binding reactions in total amounts of 0, 200 or 400 pmol per reaction, corresponding to 0, 2000 or 4000 protein:DNA molar ratios. Binding reactions (20 µl) also contained BSA (0.2 µg/reaction) and salmon sperm DNA (2 µg/reaction), as well as 4x NrdR-binding buffer, added to a final 1x concentration of 20 mM Tris-HCl (pH 9.0 at 25 ºC), 80 mM KCl, 1 mM $MgCl_2$, 1 mM dithiothreitol, 50 µM $ZnSO_4$, and 5% glycerol. Reactions were incubated at room temperature for 60 minutes before gel electrophoresis.

Electrophoresis was performed in 4% acrylamide gels, prepared with a 37.5:1 proportion acrylamide:bis- acrylamide and using 5% triethylene glycol as an additive for increase DNA-protein complex stability. Gels were casted and run using the PROTEAN II xi system (Bio-Rad, CA, USA), according to the manufacturer's instructions. Gels were run with 25 mA constant current, at 4 ºC, for 4 hours. Final images were obtained by scanning the gels in an Odyssey Imaging System device (LI-COR Biosciences, NE, USA) working in the 700 nm channel.

Other protein techniques

Proteins were routinely examined in pre-cast SDS-PAGE gels (4–20% Mini-PROTEAN TGX Precast Protein Gels, Bio-Rad, CA, USA), and stained with a Coomasie-blue-based stain (PageBlue Protein Staining Solution, ThermoFisher, MA, USA), according to the manufacturer's instructions.

Anti-NrdR western blotting was carried out. A TransBlot-Turbo device and TransBlot-Turbo Mini PVDF Transfer packs (Bio-Rad, CA, USA) were used for transferring the proteins to the membranes, according to the manufacturer's instructions. As primary antibody, we used a rabbit polyclonal anti-NrdR serum (ThermoFisher, MA, USA), applying 2 hours of incubation at 4 ºC with a 1:500 dilution of the serum. The detection of primary antibodies was carried out using a goat anti-rabbit horseradish peroxidase (HRP) conjugate (Bio-Rad, CA, USA), applying 1 hour of incubation at 4 ºC with a 1:5000 dilution of the antibody. The antibody-antigen complex was detected using the Amersham ECL Primer Western Blotting Reagent (GE Healthcare, IL, USA) according to the manufacturer's instructions. Proteins were visualized in an ImageQuant LAS4000 Mini device (GE Healthcare, IL, USA).

Atomic force microscopy

The complexes protein (gsNrdR)-nucleotide (cofactors AMP, ATP, d-ATP) were prepared as follows. The protein was first incubated with a specific cofactor as a concentrated solution, to facilitate cofactor capture, and then diluted in the presence of the cofactor, to prevent the cofactor from being lost during dilution. Three Eppendorf tubes were prepared, the first one containing 0.5 µL of gsNrdR (ECO) (C = 13.6 mg/ml) and 0.8 µL cofactor (C = 10 mM) in AFM buffer 5x (C = 50 mM HEPES pH 8.2, 250 mM NaCl, 25 mM MgCl$_2$ and 5 mM TCEP), the second one containing 10 µL AFM buffer 5x, 38 µL milliQ water and 1 µL cofactor (C = 10 mM) and the third one containing 3.3 µL AFM buffer 5x and 133 µL milliQ water. All reagents ad solutions were kept on ice during sample preparation. The first solution for protein-factor coupling reaction was incubated for 1 hour at room temperature and protected from light, then 1 µL of this solution was mixed to the dilution solution (Eppendorf 2). Finally, 3.4 µL of the solution from Eppendorf 2 was incubated in Eppendorf 3 and left at dark and at room temperature for 1 hour. The final solution for AFM inspection was obtained by mixing 2 µL of the solution from Eppendorf 3 and 18 µL AFM buffer 1x (C = 10 mM HEPES pH 8.2, 50 mM NaCl, 5 mM MgCl$_2$ and 1 mM TCEP). Protein and cofactor reagents were left in ice for the minimum time required for experiments and then put back to the freezer (respectively at -80°C and -20°C). 10 µL of the protein-cofactor complexes were deposited on freshly exfoliated mica discs (diameter: 1 cm). After 2 minutes incubation, samples were washed with 1 mL milliQ water and gently dried under a N$_2$ flow. AFM experiments: AFM measurements were done using a Cypher S AFM (Oxford Instruments, UK). Topographic images were obtained in tapping mode using SSS-FMR cantilevers (Nanoandmore, Switzerland) with nominal k = 2.8 N/m; resonance f = 75 kHz; and tip curvature radius < 5 nm. Imaging was performed in N$_2$ atmosphere using low oscillation amplitudes (< 300 mV) and the highest amplitude setpoint compatible with image quality to guarantee gentle tip-sample interaction. In these conditions, the tip-sample interaction regime was attractive, as confirmed from the value of the phase images, always higher than 90°. More than 70 images of size 512x512 and 1024x1024 pixels were collected in different areas of the samples to verify reproducibility. Data processing and analysis was performed using the commercial software of the Cypher AFM (Igor Pro, WaveMetrix) as well as home-developed scripts for particle characterization (Matlab). The results reported in this work are obtained from the analysis of 5 images for each cofactor used.

Reverse In Vitro Transcription Assay (ReViTA)

All ReViTA experiments included as part of this work were performed using pReViTA-PD, a derivative of pReViTA containing the promoter of the *nrdDG* (P*nrdD*) operon from *E. coli* K-12 substr. MG1655. A single in vitro transcription buffer (IVT buffer) was used for all reactions, with the following composition at a 1x concentration: 40 mM TrisHCl (pH 8.5 at 25 °C), 60 mM KCl, 4 mM $MgCl_2$, 1 mM DTT, 10 µM $ZnSO_4$, 50 ng/µl bovine serum albumin (BSA), 5% glycerol. DTT and $ZnSO_4$ are necessary to keep NrdR functional; BSA and glycerol were included to preserve the protein and facilitate DNA-protein interaction. A ReViTA experiment is comprised of five steps as described previously (Artículo 2):

Step 1: protein-nucleotide incubation. The required amount of NrdR was mixed with the nucleotide cofactors at a 20:1 nucleotide protein ratio. Nucleotides were added directly to the concentrated protein as 10 mM solutions dissolved in 1x IVT buffer, and the mixtures were incubated for 1 hour at room temperature.

Step 2: DNA-protein binding. Protein-nucleotide complexes were added to 15 µl reactions containing 25 fmol of pReViTA-PD, IVT buffer (at a final 1x concentration), and 5 mM of the same nucleotide used to form the complexes. Reactions with a protein:DNA ratio of 200 or higher also included 1 µg of poly(d[I-C]) (Roche LifeScience, Germany) as competition DNA. Reactions were incubated for 1 hour at room temperature.

Step 3: in vitro transcription (IVT). To the previous DNA-protein binding reactions, we added the following components in a total of 4.5 µl: NTPs (ATP, CTP, GTP, UTP) to a final concentration of 5 mM each, spermidine to a final concentration of 1 mM, 20 U (0.5 µl) of Ribolock RNase Inhibitor (ThermoFisher, MA, USA), 0.05 U of yeast inorganic pyrophosphatase (IPPase) (Sigma, Germany), as well as additional nucleotide cofactor and IVT buffer to keep the concentrations at 5 mM and 1x, respectively. Spermidine and IPPase were added to increase the IVT yield. The previous mixes were incubated for 1 hour at room temperature to allow DNA-protein complexes. Then, 0.5 U (0.5 µl) of *E. coli* RNA polymerase saturated with Sigma-70 factor (New England Biolabs, MA, USA) were added to each tube (bringing the volume to 20 µl), and reactions were incubated for 30 min at 37 °C, after which they were stopped by removing the DNA template using TURBO DNase (ThermoFisher, MA, USA), according to the manufacturer's instructions.

Step 4: RNA quantification by two-step qRT-PCR. RNA was reverse transcribed using Maxima Reverse Transcriptase (ThermoFisher, MA, USA), according to the manufacturer's instructions, and using the primers 21 and 24. The resulting cDNAs were diluted 1:50 in

water and quantified in a qPCR reaction using PowerUP SYBR Green Master Mix (ThermoFisher, MA, USA), according to the manufacturer's instructions for absolute quantitation (standard curve). Two independent qPCR reactions were conducted for each cDNA to quantify P*nrdD* (primers 19 and 20) and the control sequences (primers 22 and 23). Standard curves for both sequences were made using purified amplicons as purified PCRs and diluting them to a 1 ng/µl concentration, preparing decimal serial dilutions up to 10^{-7}, and using 10^{-4}, 10^{-6}, 10^{-7}, and 10^{-9} as standard curve points.

Step 5: data treatment. All qRT-PCR data were converted into absolute copy numbers using the standard curves. Then, the P*nrdD* counts were normalized for each sample by dividing by its corresponding control values to capture all unspecific inhibition. Normalized copies of problem reactions (with NrdR) were then divided by the normalized copies of control reactions (without NrdR) to obtain the relative percentage of transcription activity.

Galleria mellonella model of infection

G. mellonella larvae were routinely grown at 35 ºC and 100% humidity. 3 weeks-old larvae were separated for infection and placed in Petri dishes (5 larvae per dish). To prepare bacterial cultures for infection, overnight cultures (in LB medium, with the required antibiotics) of the desired strains were first prepared. Cells were pelleted by centrifugation (5000 g, 10 minutes) and resuspended in sterile PBS, calculated for an OD_{550} of 1.0. The centrifugation-resuspension step was repeated three additional times. Sterile PBS was added to the final suspension to obtain an OD_{550} of 1.0. Decimal serial dilutions of these suspensions in PBS were prepared from 10^{-1} to 10^{-5}, and then a 1:5 dilution to $2·10^{-6}$. 10 µl of the $2·10^{-6}$ dilutions per larva were injected using Hamilton syringes (Hamilton).

10 larvae (2 Petri dishes) per condition were infected, and a control group of 10 larvae injected with sterile PBS was included. Larvae were then incubated at 37 ºC and monitored from 12 h to 24 h after injection every 30 minutes, and a final time 36 h after infection. Kaplan-Meier survival curves were drawn and analyzed using PRISM 9.0 (GraphPad Software).

Results

The established NrdR repression mechanism is limited to ribonucleotide reductases

Although NrdR is well known as a regulator of ribonucleotide reduction, multiple studies have explored the possibility of the NrdR regulon extending beyond ribonucleotide reductases. The first identification of NrdR-boxes (13) considered non-RNR genes potentially regulated by NrdR, such as *dnaA* in *Shewanella* or *topA* in *Pseudomonas*. However, the corresponding promoter regions feature a single NrdR-box instead of the usual pattern found in RNR promoters of two NrdR-boxes separated by an integer number of turns in the DNA helix. The global effects of a *nrdR* mutation have been studied at a transcriptomics level using DNA microarrays in *P. aeruginosa* PAO1 (18) and *E. coli* LF82 (35), as well as at a proteomics level in *B. subtillis* YB955 (36). In all cases, NrdR mutant strains displayed evidence of dozens of dysregulated genes, although only RNR genes were associated with known NrdR-boxes.

In previously unpublished data, our group obtained similar results with *E. coli* K-12, which are included here for reference: a DNA microarray experiment comparing a *nrdR*ΔATPcone strain encoding a non-functional RNR and its isogenic K-12 *susbtr*. MG1655 wild-type strain (from now on, MG1655) under both mid-exponential and stationary growth showed a total of 220 differentially expressed genes (DEGs), including all three RNR operons present in *E. coli* (Supplementary Table S3).

To understand whether the transcriptomic and proteomic effects of the *nrdR* mutation are due to the dysregulation of genes directly controlled by NrdR, we conducted a global search for NrdR-boxes that can be correlated with the observed DEGs. A search for the general γ-proteobacteria NrdR-box consensus (13) using FIMO (25, 26) on the sequences upstream of every translation start codon in the MG1655 genome (see Materials and Methods) revealed 48 putative NrdR-boxes (Supplementary Table S4). These include all six previously identified boxes (13, 17): two upstream of the *nrdAB-yfaE* class I RNR operon, two upstream of *nrdHIEF* (class Ib RNR), and two upstream of *nrdDG* (class III RNR), all separated by three whole turns of the double helix (31-32 bp). Only one more gene (transcriptional regulator *slyA*) presents two NrdR boxes, although they are separated by 6.5 turns in the double helix.

Correlating the presence of NrdR-boxes in the MG1655 genome to differential expression in the *nrdR* mutant strain revealed that, out of 42 upregulated and 46 downregulated genes with a |log (FC)| ≥ 1.5, only *nrdA* and *nrdH* in the whole genome present NrdR-boxes in their promoter regions (Figure 1, left). Expanding the search to all DEGs regardless of log (FC) revealed the anaerobically-active class III RNR gene *nrdD*, which is only weakly derepressed in a Δ*nrdR* background under aerobic conditions, as well as two more hits, *dnaK* and *pdhR*, both featuring a single putative NrdR-box (Supplementary Table S3). All other 211 DEGs were not associated with NrdR-boxes, and all other 40 putative NrdR-boxes were not associated with DEGs.

E. coli (4705 genes)
42 genes log(FC) ≥ 1.5 – 46 genes log(FC) ≤ -1.5
48 putative NrdR-boxes – 2 operons with DEGs and NrdR-boxes

P. aeruginosa (5570 genes)
41 genes log(FC) ≥ 1.5 – 39 genes log(FC) ≤ -1.5
22 putative NrdR-boxes – 3 operons with DEGs and NrdR-boxes

1 *nrdAB-yfaE*
b2234-b2236

2 *nrdHIEF*
b2673-b2676

3 *nrdAB*
PA1156-PA1155

4 *nrdDG*
PA1920-PA1919

5 *nrdJab*
PA5497-PA5496
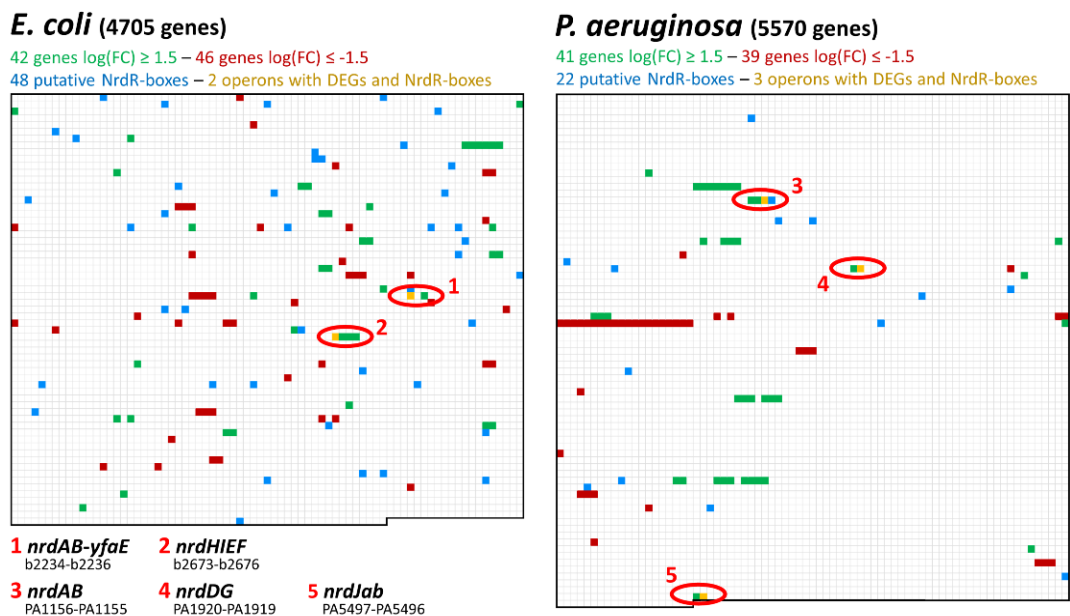
Figure 1. Correlation between DEGs in *nrdR* mutant strains and presence of NrdR-boxes. Data from *E. coli* K-12 *substr*. MG1655 (left) or *P. aeruginosa* PAO1 (right). Each square represents a gene in the genome, from top left (PA0001 *dnaA* in *P. aeruginosa*, b0001 *thrL* in *E. coli*) to bottom right (PA5570 *rpmH* in *P. aeruginosa*, b4705 *mntS* in *E. coli*). Green-coloured squares represent genes upregulated in a *nrdR* mutant strain compared to its isogenic WT strain (DNA microarray data for *E.* coli, see Supplementary Table S3; RNA-seq data for *P. aeruginosa*, see Supplementary Table S5), while red-coloured genes were downregulated. DEGs were only included with |log (FC)| ≥ 1.5. Blue-coloured squares represent genes for which at least one NrdR-box was found within the 450 bp prior to its translation start codon; see Supplementary Table S4. Yellow squares represent the colocalization of DEGs and NrdR-boxes; operons including these genes are circled in red.

An analogous search for NrdR-boxes in the *P. aeruginosa* PAO1 genome revealed 22 putative NrdR-boxes (Supplementary Table S4). These include all eight previously identified boxes (13, 18): three upstream of the *nrdAB* class Ia RNR operon (including an isolated box labelled NrdR-box 3), two upstream of *nrdJab* (class II RNR), two upstream of *nrdDG* (class III RNR), and one upstream of DNA topoisomerase I gene *topA*. Pairs of NrdR-boxes are all separated by three turns of the double helix (31 bp). Additionally, a fourth putative NrdR-box was identified upstream of *nrdA* (NrdR-box 4). No non-RNR gene presented more than one putative NrdR-box.

Correlating the presence of NrdR boxes in the *P. aeruginosa* PAO1 genome to the previously identified DEGs (18) revealed that, out of 143 DEGs identified under aerobic and anaerobic conditions, only *nrdA* and *nrdJa* present NrdR-boxes in their promoter regions. However, as that microarray study failed to detect differential expression in class III RNR operon *nrdDG* (even under anaerobic conditions) or *topA*, potentially due to limitations of the technique or biases of the platform, we decided to conduct a thorough exploration of the effects of *nrdR* inactivation in *P. aeruginosa* PAO1 using RNA-Seq.

Compared to *P. aeruginosa* PAO1 wild type, a Δ*nrdR* mutant strain showed 164 DEGs (104 upregulated and 62 downregulated) (Supplementary Table S5) [UPLOAD TO GEO?]. All RNR operons are significantly upregulated: *nrdA* showed a fold-change of 2.96, *nrdJa* a 13.25, and *nrdD* a 13.65. Other upregulated genes included the whole PQS operon (*pqsABCDE*), responsible for one of the quorum-sensing systems in *P. aeruginosa*, several stress-related genes, such as the heat-shock genes *grpE* and *hslU*, and a total of 14 genes related to the type III secretion system. A Gene Ontology Enrichment Analysis showed hits for type III secretion system, interaction with hots, cellular response to heat, and protein folding (data not shown). On the other hand, the downregulated genes were very disparate, including the arginine deiminase and pyoverdine biosynthetic operon. Most significantly, *topA* was not downregulated. When correlating these results with the presence of putative NrdR-boxes, out of 41 upregulated and 39 downregulated genes with a |log (FC)| ≥ 1.5, only the three RNR operons present NrdR-boxes in their promoter regions (Figure 1, right). Furthermore, expanding the search to all DEGs regardless of log (FC) revealed no other correlations.

The existence of a possible mechanism of direct NrdR transcription regulation based on a single NrdR-box, as well as on binding sites different from the known NrdR-box

consensus, cannot be ruled out. Likewise, the indirect transcriptomic effects of the dysregulation of ribonucleotide reductases are also worth exploring and will be further addressed in the discussion. However, the correlation of genes presenting pairs of NrdR-boxes and differential expression upon *nrdR* inactivation demonstrates that the only genes in both categories are the RNR operons, both in *E. coli* and *P. aeruginosa*. In both strains, NrdR-box2 showed higher scores than NrdR-box1, which is a less conserved sequence. Therefore, we propose that the established mechanism of NrdR repression via binding to pairs of NrdR-boxes overlapping with the base promoter is limited to ribonucleotide reductases.

Recombinant NrdR can be obtained as a fusion protein with solubilization tags

To gain further insight into the mechanism used by NrdR for the repression of RNR expression, we aimed to obtain recombinant NrdR from both *E. coli* and *P. aeruginosa* to conduct *in vitro* studies. NrdR is, however, known to be highly unstable when overexpressed (14, 17, 20, 21). As part of this study, we developed different fusion proteins with varying compromises between yield, purity, and activity.

The simplest strategy was to purify a His_6-tagged version of NrdR. However, this protein was mainly found as inclusion bodies, and its soluble fractions remained highly unstable and prone to precipitation throughout the purification process. For *E. coli*, it was impossible to obtain soluble His_6-tagged NrdR in usable quantities. For *P. aeruginosa*, however, despite the significant losses due to precipitation, it was possible to obtain a significant yield of this protein (NrdR-H_6, Figure 2). When analyzed with PCA precipitation and ion-paired reverse phase HPLC, as-prepared NrdR-H_6 proved to be almost completely nucleotide-free, with only traces of ADP being detected (Supplementary Figure S1). NrdR-H_6 was also proven to be able to bind ATP and dATP when incubated with a 20:1 nucleotide:protein ratio, although a 100% occupancy was never achieved (Supplementary Figure S1).

To keep the protein stable throughout the purification process and preserve its functionality as much as possible (37), we then produced SUMOylated NrdR fusion proteins, coupled to a His-tagged Small Ubiquitin-like Modifier that can be removed later using the SUMO protease, leaving an untagged NrdR with only two a two amino-acid linker appended (NrdR$_1$; see Figure 2). While more stable, NrdR$_1$ protein production produced very low yields, limiting the range of experiments they could be used for. PCA precipitation and HPLC

analysis revealed that the *E. coli* $NrdR_1$ protein was recovered bound to ADP and AMP, with a total nucleotide occupancy over 60%, and able to efficiently bind ATP and dATP when incubated with a 20:1 nucleotide:protein ratio (Supplementary Figure S1). No nucleotides were detected in *P. aeruginosa* $NrdR_1$ preparations.

As the efficiency of the SUMO digestion was deemed to be the most significant bottleneck in the production of $NrdR_1$, a second generation of SUMOylated fusion proteins was developed, including an additional TEV protease cleavage site, thus using the SUMO only for its stabilization/solubilization properties, as well as increasing the peptide linker to six amino-acids, to improve the digestion efficiency ($NrdR_2$; see Figure 2). For *P. aeruginosa*, the $NrdR_2$ protein was never obtained with a high yield and could only be recovered with the addition of AMP throughout the purification process. The *E. coli* $NrdR_2$ protein, however, was obtained with a high yield, and was proven to contain a small amount of AMP (data not shown).

For the following experiments, the $NrdR_2$ protein from *E. coli* was used as the standard, given its superior yield and stability. For *P. aeruginosa* experiments, $NrdR-H_6$ was used regularly, with $NrdR_1$ and $NrdR_2$ used as comparison when necessary.
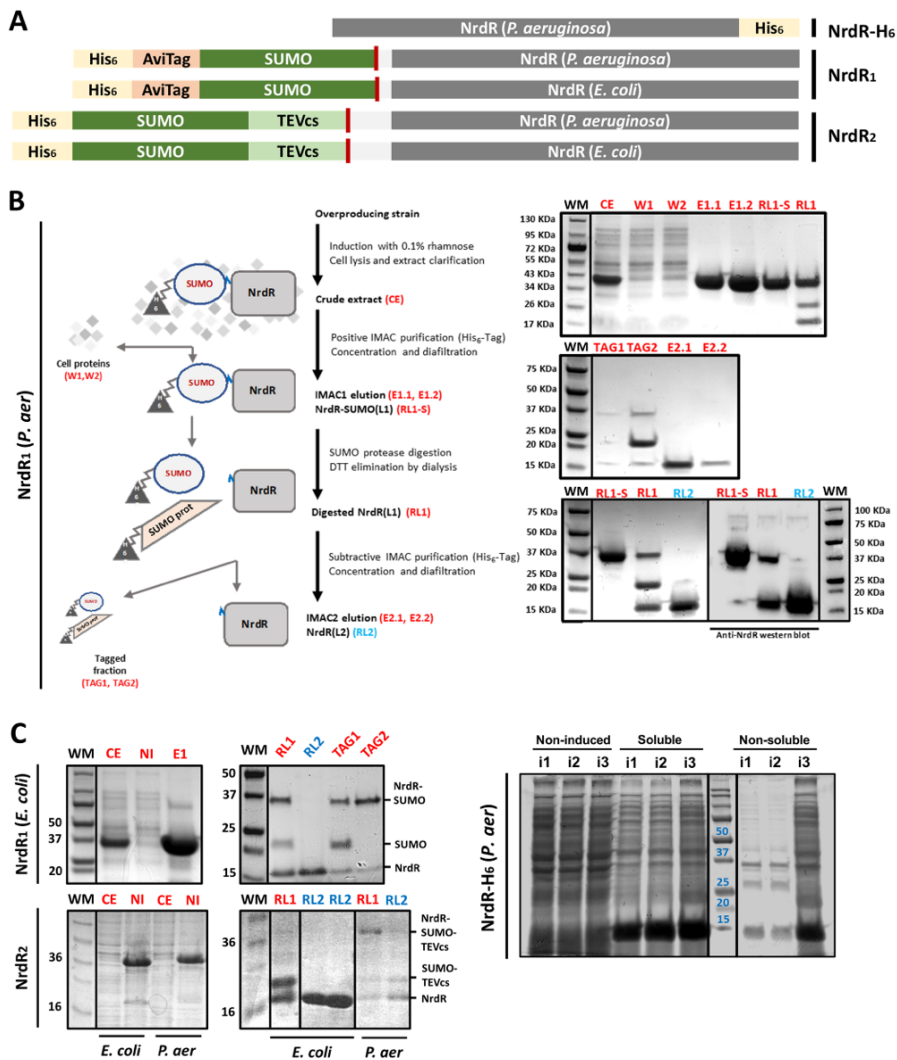
Figure 2. Expression and purification of NrdR fusion proteins.

A; Schematic of the different NrdR fusion proteins used in this study, from N-terminus (left) to C-terminus (right). The following abbreviations are used: His6 (6x histidine tag), SUMO (Small Ubiquitin-like Modifier), AviTag (Protein Biotinylation Tag, not used in this study), TEVcs (Tobacco Etch Virus Cleavage Site). A red vertical line indicates the exact cleavage site after digestion with SUMO protease (NrdR$_1$) or TEV protease (NrdR$_2$). The unlabeled grey box to the right of the cleavage site represents a small linker peptide. **B;** Detailed production of NrdR$_1$ (*P. aer*). The different steps are illustrated on the schematic (left); samples of each step were analyzed on Coomasie Blue-stained SDS-PAGE gels and Anti-NrdR western blots (right). **C**; highlights of the production of all other fusion proteins. Numbers in the weight marker (WM) represent KDa.

NrdR exists as a dynamic population of nucleotide-dependent oligomeric forms

In multiple classes of ribonucleotide reductases, the ATP-cone domain controls the overall enzyme activity by inducing alterations in the quaternary structure of the complex depending on the nucleotide bound to it (4, 12). A similar mechanism has been hypothesized for NrdR since its early discovery (14, 19, 20) as it contains a very similar ATP-cone domain. A more detailed exploration of this mechanism using the NrdR protein from *S. coelicolor* was published during the preparation of this manuscript (37); its implications regarding the findings in this study will be further assessed in the Discussion.

Early size-exclusion chromatography (SEC) experiments using $NrdR_1$ proteins demonstrated that changes in the nucleotide bound to NrdR drastically and reproducibly changed its quaternary structure (Figure 3). In all cases, when pre-incubated with a 20:1 nucleotide:protein ratio of AMP (or without any nucleotides present) NrdR appeared mostly as a low molecular weight peak easy to interpretate as a dimer or a trimer. When bound to dATP or ATP, higher order complexes were detected, with ATP causing the highest apparent molecular weight. The limitations in the yield and purity of the $NrdR_1$ proteins compromise the interpretation of these results. The most reproducible results were obtained using the $NrdR_1$ protein from *P. aeruginosa* (see Figure 3, B), which had proven to be nucleotide-free. In the presence of AMP, NrdR ran as a single peak centered at an apparent molecular weight of 44 KDa (dimer-trimer). When coupled to dATP, two peaks were detected: 34 KDa (dimer) and 129 KDa (approx. hexamer). Finally, when bound to ATP, two peaks were detected: 34 KDa (dimer) and 182 (approx. x10). Most significantly, all peaks were wide, spanning several possible conformations, and their average apparent molecular masses varied with protein concentration and nucleotide incubation time, especially in the case of NrdR-ATP (data not shown). We interpreted this as NrdR forming labile complexes with dynamic protein-protein associations. However, further information was necessary to extract any conclusions.
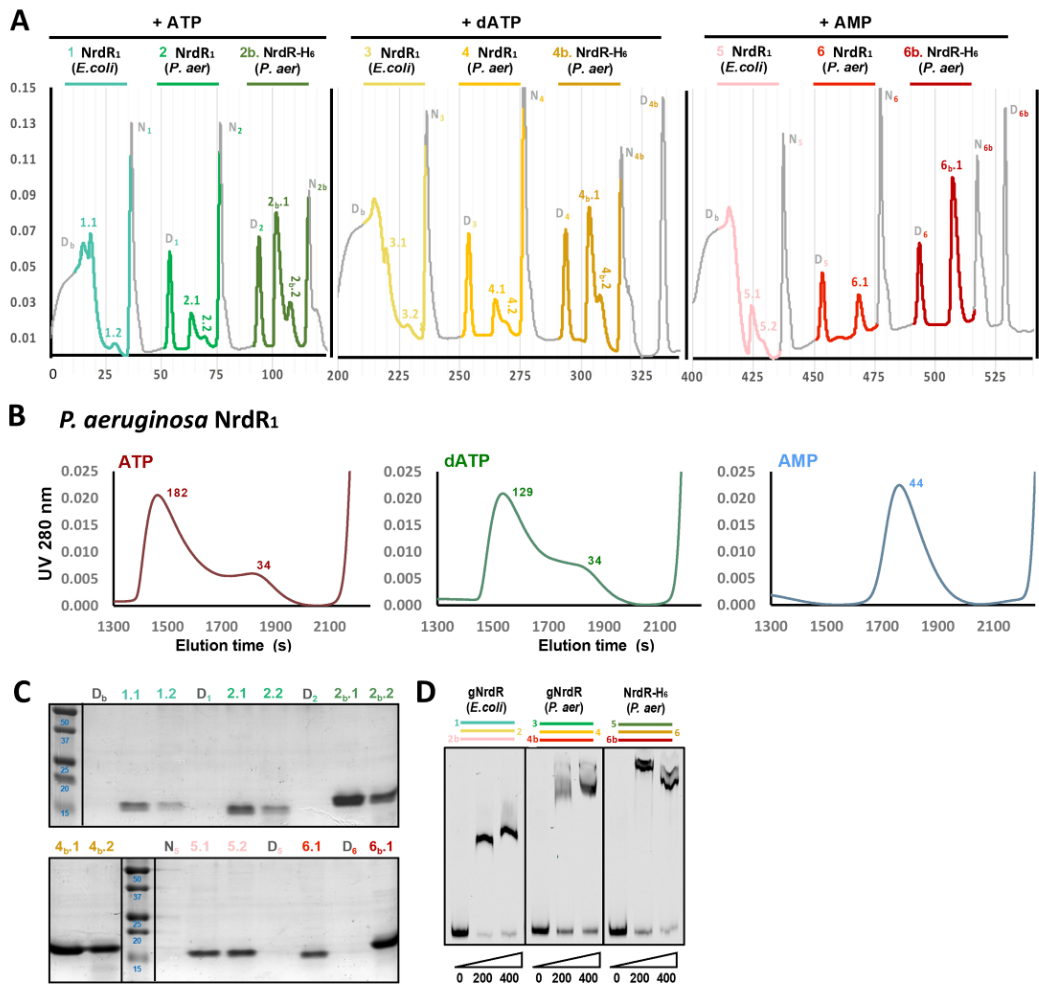
Figure 3. Size-exclusion chromatography of NrdR-nucleotide complexes.

A; SEC chromatogram of $NrdR_1$ (*E. coli*), $NrdR_1$ (*P. aeruginosa*), and NrdR-H_6 (*P. aeruginosa*), pre-incubated with nucleotides at a 20:1 nucleotide:protein ratio and run with the corresponding nucleotide in the elution buffer. Y-axis represents UV absorbance (280 nm), X-axis represent elution time (min). Equilibration and washing steps between nucleotide series have been removed from the chromatogram for clarity. Protein-containing peaks are labeled indicating its injection and peak numbers (e.g., 1.1 for the first peak of the first injection). Other peaks are caused by the free nucleotide in the samples (labeled as N) or the oxidized DTT in the samples (labeled as D). **B**; detailed chromatogram of the peaks corresponding to $NrdR_1$ (*P. aeruginosa*) bound to ATP, dATP and AMP. Numbers near the peaks indicate the average estimated molecular weight of the complex. **C**; SDS-PAGE analysis of representative peaks recovered from the previous SEC experiment. Numbers in the weight marker lane indicate molecular weight in KDa of the band above. **D**; EMSA of the proteins

used for SEC experiments, prior to incubation with nucleotides. Numbers below the images indicate protein amounts in pmol. The DNA fragment used in P*nrdA* (*E. coli*). See Materials and Methods for more details on EMSA conditions.

Using the NrdR$_2$ protein from *E. coli*, we first visualized the effects of nucleotide binding on the quaternary structure of NrdR using atomic force microscopy (AFM). NrdR was pre-incubated with the different nucleotides in a 20:1 ratio and the resulting complexes were deposited on mica, dried, and imaged in conventional dynamic mode (Figure 4A). Measurements of the size and shape of the complexes (Figure 4B,C) detected revealed the wide range of structures present. Protein complexes were determined to be reproducibly smaller when coupled to AMP (Figure 4B), while nucleotide triphosphates produced larger structures. ATP produced a slightly but statistically significantly larger complex than dATP. Looking at the circularity index of the complexes, we could see that, when bound to dATP, NrdR produced significantly more elongated complexes than when bound to ribonucleotides (Figure 4C).
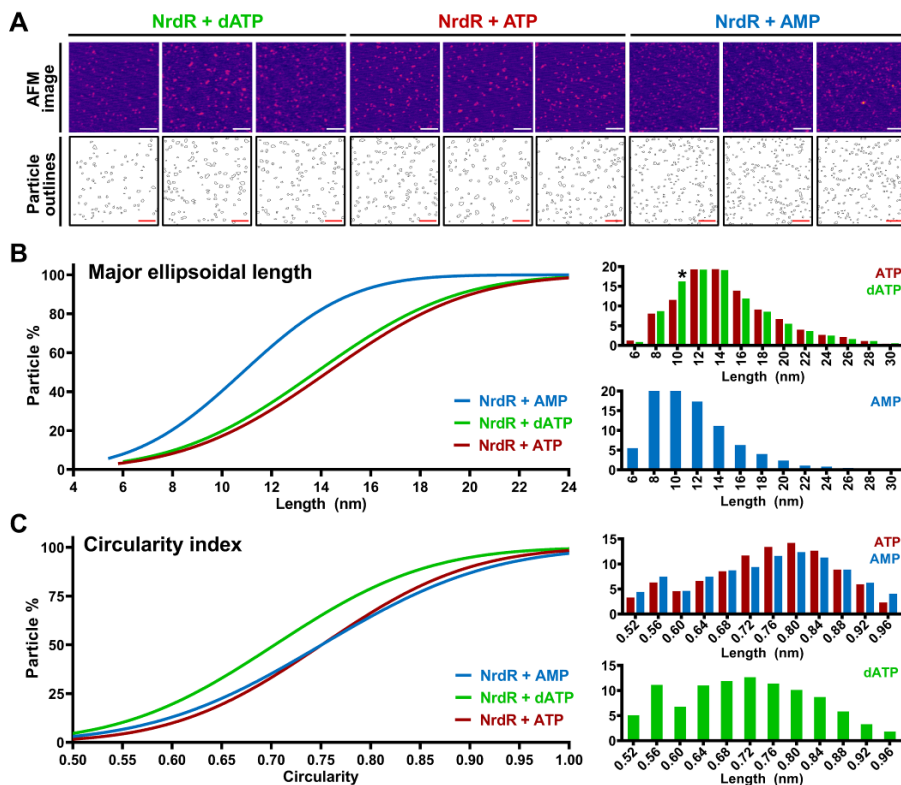
Figure 4. Influence of nucleotide cofactors on the NrdR quaternary structure determined by Atomic Force Microscopy. A; AFM images (top) and particle outlines (bottom) of representative NrdR-nucleotide complexes. NrdR$_2$ (*E. coli*) was incubated with a 20:1 excess of different nucleotides prior to imaging. **B,C;** changes in the frequency of complexes presenting different lengths (B, characterized by the largest length of an ellipse containing the complex) and shapes (C, characterized by the circularity index of the complex, where 1 represents a perfect circle) depending on the nucleotide cofactor used and represented as cumulative frequencies (left) and detailed histograms (right).

To resolve the absolute molecular weight of the complexes and get a clear interpretation of the SEC and AFM results, we then analyzed the NrdR$_2$ proteins using size exclusion chromatography coupled to multiangle light scattering (SEC-MALS). Just as previously observed, complexes proved to be incubation time and protein concentration-dependent, with the most reproducible results obtained when the NrdR$_2$ protein from *E. coli* was just exposed to a fixed concentration of 0.025 mM nucleotide in the running buffer, rather than pre-incubated (see chromatograms in Figure 5A and molecular weight values in Table 1). In the absence of a nucleotide co-factor, NrdR ran as a clear dimer, with a minimum weight-average molar mass (Mw) of 32.78 KDa, and an average of 35.98 KDa. When bound to AMP, the peak presents an average Mw of 44.56 KDa, but with absolute molar mass determination ranging between 50.84 KDa and 30.93 KDa, supporting the dimer/trimer interpretation previously suggested for the *P. aeruginosa* NrdR$_1$ protein. As seen before, the nucleotide triphosphates produced higher-order oligomers: NrdR-ATP presented an average Mw of 140.17 KDa, with an estimated minimum of 81.96 KDa (tetramer) and max of 178.32 KDa (10-mer). NrdR-dATP showed an average Mw of 113.36 KDa, with an estimated minimum of 81.36 KDa (tetramer) and maximum of 133.57 (octamer). ATP and dATP peaks showed a wide range of molar masses and high polydispersity (see black, dashed lanes in Figure 5A), suggesting again dynamic complex interactions. These results agree with all previous observation for NrdR$_1$ (*P. aeruginosa*). Protein-conjugate analysis (Supplementary Table S6) identified the co-factors to be present in higher than 1:1 proportion at the tip of the peak (R$_8$ + ATP$_{9-10}$, R$_6$ + dATP$_{8-9}$).

As NrdR$_2$ from *P. aeruginosa* was highly unstable and could only be obtained when co-purified with AMP, exact interpretations of SEC-MALS experiments with this protein were considered impossible. The results of a single experiment (Supplementary Figure S2) showed the same lower molecular weight peak for NrdR-AMP, and higher order oligomers for dATP and ATP. Although the average molecular weight for NrdR-dATP and NrdR-ATP was lower than that observed for its *E. coli* counterpart, and the dimer characteristic of

AMP contamination was present in all preparations, the relative order of the peaks was the same observed for NrdR$_2$ (*E. coli*) and NrdR$_1$ (*P. aeruginosa*).

Finally, we evaluated the shift in the observed molecular weights observed in SEC-MALS experiments when pre-incubating the protein for 3 hours with the co-factors at a 20:1 nucleotide:protein ratio, rather than just having the co-factor present in the running buffer. This caused further differentiation of the protein-nucleotide complexes (Figure 5B). The NrdR-AMP peak did not vary, with a weight-average molar mass of 44.75, and the NrdR-dATP suffered only a small increase, shifting the center to 121.83 KDa, where the minimum and maximum sizes were still interpreted as tetramer-octamer (Table 1, with pre-incubation). NrdR-ATP, however, suffered a major shift, reaching a weight-average Mw at the center of the peak of 200.31 KDa, and minimum and maximum of 75.11 KDa (tetramer) and 266.47 KDa (15-mer to 16-mer), respectively.
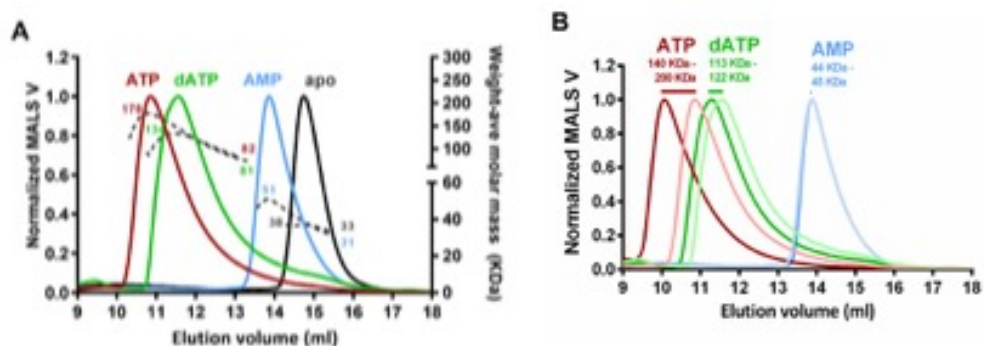
Figure 5. SEC-MALS study of NrdR-nucleotide complexes. **A;** SEC-MALS results of NrdR$_2$ (*E. coli*) exposed to 0.025 mM nucleotide in the running buffer. Left Y axis (solid lines) represents MALS detection data normalized to a maximum signal of 1.0 in each sample. Right OY axis (dashed lines) represents weight-average molar mass (KDa). Numbers near the peaks indicate the minimum and maximum weight-average molar mass for the corresponding peaks. Results are representative of two independent experiments. **B;** comparison of SEC-MALS results of NrdR$_2$ (*E. coli*) only exposed to nucleotides in the running buffer (light colours) or incubated with a 20:1 nucleotide:protein ratio for 3 hours prior to the experiment (dark colours).

Without pre-incubation						
Nucleotide	**Mn**	**Mw**	**Est. min**	**Est. max**	**Polydispersity**	**Interpretation**
+ ATP	131.52 ± 0.32	140.17 ± 0.30	81.96	178.32	1.07 ± 0.00	$R_4 \leftrightarrow R_{10}$
+ dATP	110.83 ± 0.21	113.36 ± 0.21	81.36	133.57	1.02 ± 0.00	$R_4 \leftrightarrow R_8$
+ AMP	43.81 ± 0.09	44.56 ± 0.08	30.93	50.84	1.02 ± 0.00	$R_2 \leftrightarrow R_3$
Apo	35.95 ± 0.08	35.98 ± 0.08	32.78	38.23	1.00 ± 0.00	R_2

With pre-incubation						
Nucleotide	**Mn**	**Mw**	**Est. min**	**Est. max**	**Polydispersity**	**Interpretation**
+ ATP	179.75 ± 0.76	200.31 ± 0.53	75.11	266.47	1.11 ± 0.01	$R_4 \leftrightarrow R_{16}$
+ dATP	118.52 ± 0.22	121.83 ± 0.21	80.06	139.16	1.02 ± 0.00	$R_4 \leftrightarrow R_8$
+ AMP	44.02 ± 0.10	44.75 ± 0.09	31.07	54.53	1.02 ± 0.00	$R_2 \leftrightarrow R_3$

Table 1. Molecular weight and quaternary structure of NrdR-nucleotide complexes determined by SEC-MALS. All data obtained using NrdR$_2$ (*E. coli*). Values for experiments with nucleotide only present in the running buffer (without pre-incubation, top) or pre-incubated with the protein as well (bottom). Mn, number-average molar mass; Mw, weight-average molar mass; Est. min/max, estimated minimum and maximum molar masses. All molar mass values are listed in KDa. The polydispersity index is defined as Mw/Mn. All data correspond to full complexes, including protein and co-factor molecules (see Supplementary Table S6 for protein-conjugate analysis). Error is listed as ± standard deviation.

The activity of NrdR is modulated by its nucleotide cofactor

Once the different quaternary structures of the NrdR-cofactor complexes had been characterized, the next step was to explore the functional meaning of those oligomerization differences. The DNA binding capabilities of NrdR have previously been studied using electrophoretic mobility shift assays (EMSA) in *E. coli* (17, 20), *Chlamydia trachomatis* (21), and *Salmonella typhimurium* (38), although issues with the activity, purity, and specificity of the recombinant NrdR preparations have always made difficult to interpret the results. These problems were avoided when we used the NrdR$_2$ (*E. coli*) protein, with which we obtained a high binding specificity and reproducibility. Early experiments performed using the NrdR-H$_6$ (*P. aeruginosa*) and NrdR$_1$ (*E. coli*) proteins under different binding conditions followed this trend, with significant specificity issues (excessive binding to negative control bands without NrdR-boxes) and protein aggregation observed (data not shown). The highest specificity and reproducibility were obtained with NrdR$_2$ (*E. coli*), adding fresh DTT and Zn to the binding buffer, using 5% triethylene glycol in the EMSA gels for additional stabilization of the complexes, and performing DNA binding in the presence of high

amounts of competition DNA (2 μg of salmon sperm DNA, equivalent to an approximate mass ratio of 65:1 competition:probe DNA).

Under the best conditions established, the EMSA results of an NrdR-sensitive probe (the whole *nrdAB-yfaE* promoter from *E. coli*, P*nrdA*) clearly show the effect of the different nucleotide co-factors (Figure 6, left). Without additional nucleotide or with AMP, NrdR caused only a small shift resulting in an unstable, smeary complex band. NrdR-ATP caused no significant shift, appearing to be inactive. NrdR-dATP, however, produced a clear and intensive shift, consistent with the binding of a large protein oligomer. NrdR-dATP also displayed increased unspecific binding (Figure 6, right), although to a much smaller extent than that observed for the specific probe. ADP caused NrdR to be inactive, just like ATP, while dAMP showed the same unstable shift band observed for AMP (Supplementary Figure S3, top). NrdR$_2$ from *P. aeruginosa* displayed results consistent with those of its *E. coli* counterpart, with a stable shift band only appearing in the presence of dATP, which also caused a smaller increase in unspecific binding (Supplementary Figure S3, bottom), although a large proportion of the protein preparation appeared to be inactive.
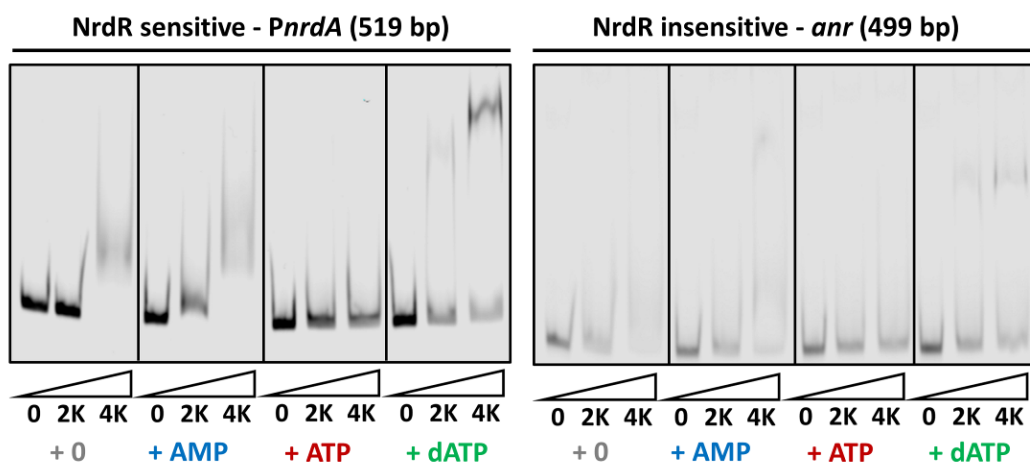
Figure 6. Nucleotide-dependent NrdR DNA binding activity. EMSA performed using NrdR$_2$ (*E. coli*). Two DNA probes were used: P*nrdA*, the promoter of operon *nrdAB*-yfaE from *E. coli,* containing known NrdR-boxes (left) and negative control probe *anr* (right). Numbers below the gels indicate the molar ratio of protein and marked DNA (0:1, 1000:1, 4000:1). Nucleotides indicated below the protein ratios were pre-incubated with NrdR at a fixed 20:1 nucleotide:protein ratio. Data is representative of three individual experiments.

While the differences in DNA binding activity induced by the different nucleotide co-factors have been established, EMSA cannot discern if a DNA-protein complex results in transcriptional repression or not. To address this problem, we employed a recently described *in vitro* transcription-based technique called ReViTA (Artículo 2 *In press*). In this study, the protein was incubated with the desired co-factor at a 20:1 nucleotide:protein ratio to determine the nucleotide-dependent activity of NrdR. Afterward, the DNA template containing the NrdR-sensitive *nrdDG* promoter (P*nrdD*) from *E. coli* was added to proceed with the DNA binding, *in vitro* transcription, DNase treatment, qRT-PCR and data treatment.

Early tests using the ReViTA technique with different NrdR proteins available demonstrated that the NrdR repression of RNR transcription could be easily detected and quantified with this technique. In the absence of competition DNA, high protein:DNA ratios, such as those used in EMSA experiments, would inhibit all NrdR-sensitive and non-NrdR-sensitive transcription (data not shown), so we introduced poly-deoxy-inosinic-deoxy-cytidylic acid, poly[d(I-C)], as a promoter-free competition DNA for reactions with high amounts of protein (higher than 200:1 protein:DNA), while smaller ratios were tested in the absence of competition.

NrdR$_2$ from *E. coli* (Figure 7A) showed specific repression when bound to dATP, with NrdR-dATP repressing P*nrdD* transcription to 54.5% and 34.8% at 2:1 and 4:1 protein:DNA ratios, respectively (averaged over four independent experiments). NrdR-ATP, however, showed low repression rates under those conditions. At higher protein:DNA ratios, NrdR started to cause repression with both dATP and ATP, although dATP reduced transcription further. Importantly, in the range of concentrations where NrdR remained specific (other proportions not shown were tested, such as 6:1, 8:1, 10:1 and 20:1, with similar results), transcription was never fully repressed, which is consistent with the hypothesized biological function of NrdR. NrdR-H$_6$ from *P. aeruginosa* (Figure 7B) did not cause any repression at low protein:DNA ratios, but showed significant specific repression when bound to dATP at 2000:1 and 4000:1 ratios, reducing transcription to 45.7% and 49.8%, respectively (averaged over four independent experiments). NrdR-ATP and NrdR-AMP caused no statistically significant repression. As seen for its *E. coli* counterpart, no concentration of protein was able to fully repress RNR transcription.
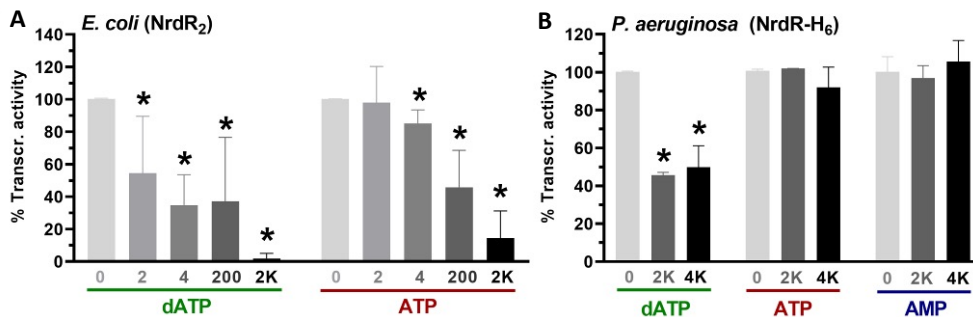
Figure 7. Nucleotide-dependent NrdR repression of *in vitro* transcription using the Regulated *In Vitro* Transcription Assay (ReViTA). A, B; specific repression of the promoter controlling *nrdDG* transcription in *E. coli* K-12 (A) and *P. aeruginosa* PAO1 (B) by NrdR coupled to different nucleotide cofactors. NrdR was incubated with a fixed 20:1 nucleotide:protein ratio, and then added to 100 fmol of DNA template in varying proportions; the numbers under each bar represent the protein:DNA ratio. The transcription of P*nrdD* was normalized using the unregulated control sequence (see Materials and Methods) and expressed as a percentage of the unrepressed (no NrdR) reaction (% transcriptional activity). *: *p*-value less than 0.05 on a two-tailed *t*-test, compared to 0x (no NrdR).

Positive and negative alterations in NrdR production affect fitness and virulence

One of the main driving forces behind the study of NrdR is its potential as a target for antimicrobial therapies, as a bacteria-only general regulator of an essential pathway. However, previous studies in *E. coli* (35), *P. aeruginosa* (18), and *Steptococcus pyogenes* (39) have shown that a *nrdR* mutant strain presents no significant difference in adherence to host cells or host infectivity, despite the significant gene dysregulation observed. Nonetheless, a more detailed exploration of the effects of altered NrdR levels in the fitness and virulence of *E. coli* (40) demonstrated that, while the effects of reduced NrdR amounts are indeed negligible, *nrdR* overexpression results in slower growth speed, reduced proliferation, and fitness, as well as diminished adherence to human epithelial cells. In this study, we extend these observations to *P. aeruginosa*.

First, we compared the growth speed of *P. aeruginosa* PAO1 wild-type, an *nrdR* mutant strain (Δ*nrdR*) and a complementation strain expressing the pUCP20::*nrdR* plasmid (Δ*nrdR* + R$_c$), resulting in a constitutive slight overexpression of *nrdR*. Overexpressing *nrdR* caused an elongated lag phase and a significantly lower growth speed after five hours of culture, finally plateauing at a smaller optical density (Figure 8A).

129

To evaluate the effects of increased *nrdR* expression in the virulence of *P. aeruginosa*, we conducted a series of test infections in *G. mellonella* using the aforementioned strains. We performed two individual experiments, in each one injecting ten larvae per condition with cell suspensions standardized by OD with an average dose of 12 CFU/larva. The results (Figure 8B) show a surprising effect caused by altered *nrdR* levels. In the experiment shown, while the wild-type strain killed its first larva 15 hours after infection, and had killed the whole group after 18 hours, all larvae infected with the *nrdR* mutant strain and the complementation strain were alive at that time point. These strains required more than 24 hours to eliminate half the larva, and the NrdR complementation strain was unable to kill the remaining individuals even 36 hours after infection. Just as previously observed for *E. coli* (40), viable cells of bacterial suspensions standardized by optical density showed a reproducible reduction of CFUs to almost one fourth in the $\Delta nrdR$ + R_c strain.
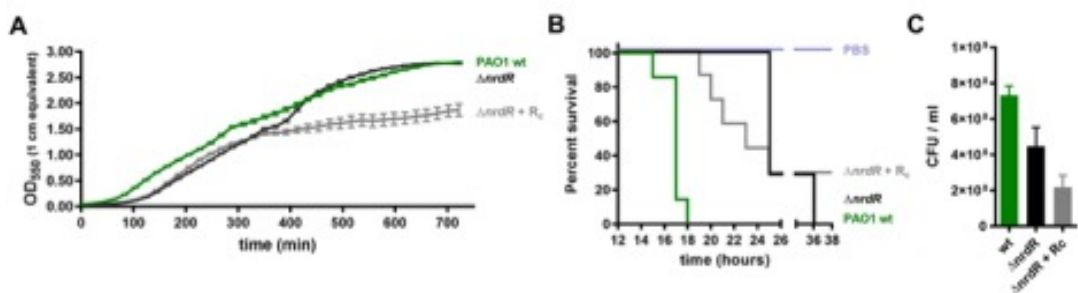
Figure 8. Effects of alterations in *nrdR* expression on bacterial virulence and fitness. A; growth curve of *P. aeruginosa* PAO1 wild-type (wt), its isogenic *nrdR* mutant strain ($\Delta nrdR$), and a complementation strain containing the pUCP20T::*nrdR* plasmid ($\Delta nrdR$ + R_c). OD$_{550}$ values were converted to the equivalent for a 1 cm pathlength for the convenience of the reader. Error bars represent standard deviation. Result is representative of two independent experiments. **B;** Kaplan-Meier survival curve of the previous strains in a *Galleria mellonella* infection assay. Result is representative of two individual experiments. **C;** CFU count of the bacterial suspensions used for *Galleria* infections and growth curve experiments. Error bars represent positive standard deviation. Result is representative of four individual experiments.

Discussion

Since its first description, NrdR has been proposed to be a nucleotide-modulated transcriptional regulator of ribonucleotide reduction (13, 14), given its predicted domains: a DNA-binding domain and an RNR-related nucleotide-binding ATP-cone domain. More assumptions can be made just from considering the position of its cis-elements: NrdR-boxes overlapping with the basal promoters of all RNR operons present in any given bacterial species were found to appear in pairs, separated by an integer number of turns of the DNA helix (13). These findings suggested that NrdR was a repressor, that it relied on protein-protein interactions such as those modulated by ATP-cones in RNRs (4), and, crucially, indicated that its role was a universal one, not related to the specific needs of a particular species or to the differential expression of a single RNR class. The possibility of a single, universal regulator of an essential pathway confined exclusively to bacteria painted NrdR as a potential target for antimicrobial therapies.

While multiple studies have explored the transcriptomic and proteomic effects of *nrdR* inactivation (18, 35, 36), the only identification of NrdR-boxes available is their original description (13). Here, we performed genome-wide searches for NrdR-boxes in *E. coli* and *P. aeruginosa*. Our search using the R-box consensus sequence described for all γ-proteobacteria correctly identified all known NrdR-boxes in both species (13), including the additional NrdR-box3 in *nrdAB* and NrdR-box1 in *topA* for *P. aeruginosa* (Supplementary Table S4), while also identifying 42 and 18 additional putative NrdR-boxes in *E. coli* and *P. aeruginosa*, respectively. Only RNR operons presented pairs of NrdR-boxes separated by an integer number of turns in the DNA helix, strongly suggesting that the oligomerization-based mechanism that has been proposed for NrdR may be limited to RNR regulation. Interestingly, NrdR-box2 of each pair always presents much higher scores than NrdR-box1 (less-conserved). It was described than, in *E. coli*, point-mutations in NrdR-box1 caused no significant reduction in NrdR binding, while mutations in NrdR-box completely disrupted this activity. A plausible interpretation of this fact would be than NrdR-box2 is highly conserved to serve as a central anchor for the NrdR complex, while NrdR-box1 would provide further positioning for the oligomer and could thus be less conserved. Other putative NrdR-boxes could be evidence of an expanded NrdR-regulon requiring a different binding mechanism; however, most identified boxes are likely false positives, as evidenced by the fact that searches using the same consensus sequences on equivalent DNA queries composed of randomly generated DNA (4314 sequences, 470 bp long, with 47.9% GC, for

E. coli; 5678 sequences, 470 bp long, with 64.5% GC. for *P. aeruginosa*) yielded more hits than the real DNA queries (data not shown). Further reducing the *p*-value threshold beyond 5×10^{-5}, however, resulted in some of the known NrdR-boxes not being identified. Therefore, we believe this to be the limit of the identification of NrdR-boxes through motif-based sequence analysis, which then needs to be correlated with transcriptomics data of *nrdR* deletion or overexpression strains.

In this study, we present transcriptomics experiments in *E. coli* and *P. aeruginosa* that correctly identified the upregulation of all RNR operons under *nrdR* inactivation (Supplementary Table S3, Supplementary Table S5), while presenting multiple other upregulated and downregulated genes. The correlation with putative NrdR-boxes (Figure 1), however, demonstrated than only RNR DEGs, as well as two slightly upregulated genes in *E. coli* (chaperone *dnaK* and transcriptional regulator *pdhR*), presented NrdR-boxes in their upstream regions. Nonetheless, given the significant overlap of the DEGs identified in this study with previous observations (18, 35, 36), we believe than the absence of NrdR-boxes does not imply other DEGs to be false positives, but rather that they are caused by the global effects of *nrdR* inactivation, such as reduced fitness and imbalanced NTP/dNTP amounts. While a full exploration of the indirect transcriptomics effects of altered *nrdR* expression would require comparative RNA-seq experiments with both species under both *nrdR* deletion and overexpression, and was considered beyond the boundaries of this study, a limited analysis of the available DEGs reveals interesting trends. The most enriched GO biological processes terms among upregulated genes in both species (Supplementary Figure S4, A), beyond deoxyribonucleotide biosynthesis, include multiple highly associated to stress, such as response to heat (including multiple chaperone genes, such as *dnaK*, *dnaJ*, *hptG*, *clpB*), proteolysis in *P. aeruginosa* (*lon, grepE, hslU*), and nucleotide salvage in *E. coli* (*gsk, tdk*, *udk*, *apt, gpt*), as well as iron transport and siderophore biosynthesis in both species (although pyoverdine synthesis is downregulated in *P. aeruginosa*), and type III protein secretion in *P. aeruginosa*, with multiple whole operons upregulated. Downregulated genes correspond to more varied GO terms and include numerous hypothetical proteins of unknown function, although we can see enriched terms associated to downregulated general anabolic pathways, including several related to ribonucleotide synthesis, and anaerobic respiration in *E. coli*. The correlation between differentially expressed orthologs found in both species (Supplementary Figure S4, B) reveals ribonucleotide reductases, chaperones, heat shock proteins, and siderophore synthesis proteins for enterobactin (*E. coli*) and pyochelin (*P. aeruginosa*), all among the upregulated

genes. These DEGs highlight the significant effects of altered *nrdR* expression, pointing towards its potential use as an antimicrobial target, which is further supported by the recent observation by Wozniak *et al*. that nearly 60% of DEGs caused by RNR repression with hydroxyurea overlap with those observed in *B. subtilis* Δ*nrdR* (41).

The significant effects observed upon *nrdR* inactivation have previously been in conflict with the reported absence of reduction in the infectivity of Δ*nrdR* strains on different infection models (18, 35, 39). However, more recently, it was demonstrated that the overexpression of *nrdR* in *E. coli* causes a significant reduction in fitness and growth speed, as well in adherence to human epithelial cells (40). Here, we extended those findings to *P. aeruginosa*, demonstrating the reduction in viability and growth speed caused by the *nrdR* overexpression, as well as a reduction in infectivity of *G. mellonella* in both the *nrdR* mutant and the overexpression strains, with the latter being unable to kill all larva even after 36 hours (Figure 8). As suggested by Naveen *et al.* (40)*,* we agree that therapy based on targeting NrdR should be directed to its overactivation, rather than its inhibition. These findings highlight the importance of understanding the activation mechanism of NrdR, as well as its structure when bound to different co-factors.

Although multiple studies have explored aspects of NrdR functionality and structure, a full mechanism of action has been elusive. In the first years since its discovery, it was demonstrated that NrdR is indeed a repressor (16, 17), binds nucleotides (16, 42), and forms oligomers in a manner dependent of its nucleotide co-factor, although initially it was only determined that it forms dimers without nucleotide, and higher order oligomers when bound to nucleotide triphosphates (42). No *in vitro* studies could confirm the hypothesized difference in activity between ATP and dATP bound NrdR, and the protein was reported to be highly unstable during purification (14–17, 20, 21). The study published by McKethan *et al.* in 2013 (20) offered important insights into the nucleotide-binding capabilities of NrdR, but did not present any fixed stoichiometry for the NrdR oligomers, and, in apparent conflict with the prevalent hypothesis, only detected DNA binding when NrdR was coupled to monophosphates (AMP/dAMP), and only at very high NrdR:DNA ratios, up to 28000:1. However, a new study using the NrdR protein from *S. coelicolor* published while this manuscript was in preparation (37) finally offered the first structural (cryo-EM) information, providing invaluable information about the NrdR mechanism of action. According to this study, NrdR presents an atypical ATP-cone, able to bind two nucleotides in a similar arrangement as the one previously seen for NrdA in *P. aeruginosa* (43), and forms inactive

tetramers and 12-mers when bound to only ATP, but can form active tetramers, which can further form 8-mers, when simultaneously bound to dATP and ATP/ADP. The findings presented in this present study, aimed towards linking the different oligomerization forms of NrdR to function, must now be viewed in the context of these new crucial discoveries.

Our experiments with *E. coli* NrdR show that, when bound to exclusively ATP, NrdR forms large oligomers visible in AFM (Figure 4) and detectable in size-exclusion chromatography (Figure 3). SEC-MALS studies confirmed a wide range of detectable molar masses, from around 80 KDa to 140 KDa without nucleotide pre-incubation, and to more than 200 KDa when pre-incubated (Figure 5, Table 1). Crucially, while the maximum detectable molecular weight increased with nucleotide pre-incubation and time, the minimum remained constant at the 75-80 KDa range, suggesting a stable form (tetramer) and higher possible aggregations (up to 16-mer with > 200 KDa). These forms showed no DNA binding activity (Figure 6, Supplementary Figure S3) and did not repress RNR transcription *in vitro* at low concentrations, although repression was detected with higher protein:DNA ratios (Figure 7A). However, when dATP was added to NrdR, a significant change was detected. The resultant oligomers were observed as just slightly smaller than the ATP forms in AFM, although with a distinctive lower circularity index (Figure 4), in agreement with the cryo-EM structures published by Grinberg *et al.*, in which the NrdR tetramers containing dATP display a more elongated structure (37). These were demonstrated in SEC experiments to correspond to higher associations than the dimer but smaller than those observed for ATP-bound NrdR (Figure 3) and identified in SEC-MALS to range between the masses of tetramer and octamer, with little variation caused by nucleotide pre-incubation (Figure 5, Table 1). These elongated structures displayed clear specific DNA binding in EMSA experiments (Figure 6, Supplementary Figure S3) and did repress RNR transcription even at low concentrations and presented a higher repression than NrdR-ATP at higher concentrations (Figure 7A). Despite the limited availability and activity of the *P. aeruginosa* protein, the same observations concerning the dATP/ATP-bound forms can be observed for that species, with NrdR-H$_6$ presenting equivalent oligomer sizes in SEC experiments (Figure 3B) and being only active in the presence of dATP at both DNA binding (Supplementary Figure S3) and *in vitro* transcription levels (Figure 7B).
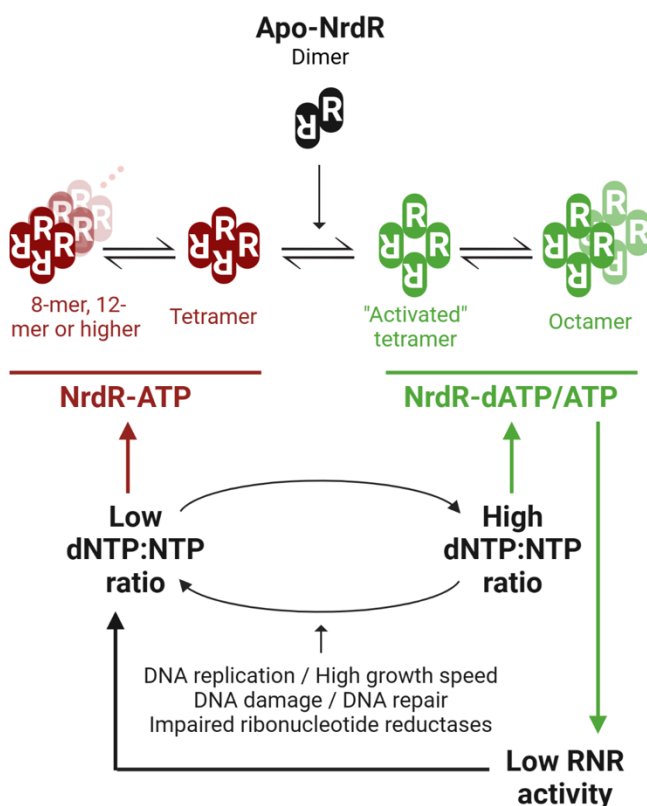
Figure 9. Model of the NrdR mechanism of action. NrdR bound to no nucleotide co-factor is dimeric. When bound to only ATP, in the presence of a low dNTP:NTP ratio, it forms "inactive" tetramers, which can further associate to form 8-mer, 12-mer or higher forms, as an inactive NrdR storage. When bound to dATP on top of ATP/ADP, in the presence of higher dNTP:NTP ratios, the structure of the tetramer changes to an "activated" form, which can associate to form octamers. The activated tetramer form represses RNR transcription, eventually reducing the dNTP:NTP ratio.

Given the recent discovery that NrdR from *S. coelicolor* requires ATP or ADP, in addition to dATP, to bind DNA (37), it now becomes apparent that the activity we detected for both the *E. coli* and *P. aeruginosa* proteins when adding dATP relied in the presence of small amounts of contaminant ADP in both preparations, specially at it has been demonstrated using PCA precipitation and ion-paired reverse phase HPLC that ATP and dATP incubated NrdR from both species presented traces of ADP (Supplementary Figure S1). The inactivity of dATP-bound NrdR in *E. coli* NrdR observed McKethan *et al.* (20) is, incidentally, also explainable this way; as part of that study, NrdR was thoroughly deprived of all nucleotides using a process of controlled denaturalization and reconstitution.

All these facts can be summarized in a model for the NrdR mechanism of action (Figure 9). In this model, NrdR is only found as a dimer without a co-factor as a transitory state, as it exists normally *in vivo* in an equilibrium between an "inactive" ATP-only tetramer and a more elongated, "active" dATP + ribonucleotide tetramer. The inactive tetramer can further aggregate into octamer, 12-mer, 16-mer, or presumably even higher oligomer forms, while dATP-containing NrdR only forms tetramers and octamers. The balance between the active and inactive forms of NrdR can be affected by the intracellular dNTP:NTP ratio, despite the difference in orders of magnitude in which dATP and ATP are present in the cell (44, 45) through the already described negative-cooperative mechanism (20), which grants NrdR a much higher affinity for dATP in the presence of ATP. This model explicitly does not grant any biological function to NrdR bound to nucleotide monophosphates, which simultaneously are present at lower concentrations and are not preferentially bound by NrdR (44, 45), and proposes that detected NrdR-AMP and NrdR-dAMP forms are the result of nucleotide dephosphorylation, either *in vivo* or during treatment. The unique structure caused by AMP observable in AFM, SEC, and SEC-MALS experiments, however, remains unexplored, and is potentially of the utmost interest for its implications in the potential development of drugs targeting NrdR.

Overall, the results reported as part of this work expand the ATP/dATP based oligomerization mechanism reported in *S. coelicolor* by Grinberg *et al*. (37) to *E. coli* and *P. aeruginosa* and, for the first time, link these differences in quaternary structure to the functional repression of RNR transcription using ReViTA, as well as establish the limits of this oligomerization-based mechanism to RNR operons using transcriptomics data and motif-based genome-wide identification of NrdR binding sites. This work, however, also highlights the importance of certain further studies, such as a full exploration of the *in vitro* activity of NrdR previously devoid of all nucleotide contaminants and bound to combinations of nucleotides to confirm and expand the dATP/ATP based mechanism, as well as full comparative RNA-Seq studies to explore the indirect effects of NrdR overexpression, and structural studies of NrdR bound to different nucleotide co-factors to better understand how to take advantage of this crucial regulator as an antimicrobial target.

References

1. Greene BL, Kang G, Cui C, Bennati M, Nocera DG, Drennan CL, Stubbe JA. 2020. Ribonucleotide Reductases: Structure, Chemistry, and Metabolism Suggest New Therapeutic Targets. Annu Rev Biochem 89:45–75.
2. Stubbe J, Nocera DG. 2021. Radicals in Biology: Your Life Is in Their Hands. J Am Chem Soc 143:13463–13472.
3. Ruskoski TB, Boal AK. 2021. The periodic table of ribonucleotide reductases. J Biol Chem 297:101137–101138.
4. Torrents E. 2014. Ribonucleotide reductases: Essential enzymes for bacterial life. Front Cell Infect Microbiol 4:1–9.
5. Wheeler LJ, Rajagopal I, Mathews CK. 2005. Stimulation of mutagenesis by proportional deoxyribonucleoside triphosphate accumulation in *Escherichia coli*. DNA Repair (Amst) 4:1450–1456.
6. Mathews CK. 2006. DNA precursor metabolism and genomic stability. The FASEB Journal 20:1300–1314.
7. Torrents E, Sahlin M, Sjöberg B-Marie. 2014. Ribonucleotide Reductase Family: Genetics and Genomics., p. 1–99. *In* Ribonucleotide Reductase.
8. Herrick J, Sclavi B. 2007. Ribonucleotide reductase and the regulation of DNA replication: An old story and an ancient heritage. Mol Microbiol 63:22–34.
9. Reichard P. 2002. Ribonucleotide reductases. The evolution of allosteric regulation. Arch Biochem Biophys 397:149–155.
10. Larsson KM, Jordan A, Eliasson R, Reichard P, Logan DT, Nordlund P. 2004. Structural mechanism of allosteric substrate specificity regulation in a ribonucleotide reductase. Nat Struct Mol Biol 11:1142–1149.
11. Pai C-C, Kearsey SE. 2017. A Critical Balance: dNTPs and the Maintenance of Genome Stability. Genes (Basel) 8.
12. Eriksson M, Uhlin U, Ramaswamy S, Ekberg M, Regnström K, Sjöberg BM, Eklund H. 1997. Binding of allosteric effectors to ribonucleotide reductase protein R1: Reduction of active-site cysteines promotes substrate binding. Structure 5:1077–1092.
13. Rodionov DA, Gelfand MS. 2005. Identification of a bacterial regulatory system for ribonucleotide reductases by phylogenetic profiling. Trends in Genetics 21:385–389.
14. Borovok I, Gorovitz B, Yanku M, Schreiber R, Gust B, Chater K, Aharonowitz Y, Cohen G. 2004. Alternative oxygen-dependent and oxygen-independent ribonucleotide reductases in *Streptomyces*: Cross-regulation and physiological role in response to oxygen limitation. Mol Microbiol 54:1022–1035.
15. Borovok I, Kreisberg-Zakarin R, Yanko M, Schreiber R, Myslovati M, Åslund F, Holmgren A, Cohen G, Aharonowitz Y. 2002. *Streptomyces* spp. contain class Ia and class II ribonucleotide reductases: Expression analysis of the genes in vegetative growth. Microbiology (N Y) 148:391–404.
16. Grinberg I, Shteinberg T, Gorovitz B, Aharonowitz Y, Cohen G, Borovok I. 2006. The *Streptomyces* NrdR transcriptional regulator is a Zn ribbon/ATP cone protein that binds to the promoter regions of class Ia and class II ribonucleotide reductase operons. J Bacteriol 188:7635–7644.

17. Torrents E, Grinberg I, Gorovitz-Harris B, Lundström H, Borovok I, Aharonowitz Y, Sjöberg BM, Cohen G. 2007. NrdR controls differential expression of the *Escherichia coli* ribonucleotide reductase genes. J Bacteriol 189:5012–5021.

18. Crespo A, Pedraz L, Torrents E. 2015. Function of the *Pseudomonas aeruginosa* NrdR transcription factor: Global transcriptomic analysis and its role on ribonucleotide reductase gene expression. PLoS One 10:1–19.

19. Borovok I, Gorovitz B, Schreiber R, Aharonowitz Y, Cohen G. 2006. Coenzyme B12 controls transcription of the *Streptomyces* class Ia ribonucleotide reductase *nrdABS* operon via a riboswitch mechanism. J Bacteriol 188:2512–2520.

20. Mckethan BL, Spiro S. 2013. Cooperative and allosterically controlled nucleotide binding regulates the DNA binding activity of NrdR. Mol Microbiol 90:278–289.

21. Case EDR, Akers JC, Tan M. 2011. CT406 encodes a chlamydial ortholog of NrdR, a repressor of ribonucleotide reductase. J Bacteriol 193:4396–4404.

22. Li H, Handsaker B, Wysoker A, Fennell T, Ruan J, Homer N, Marth G, Abecasis G, Durbin R. 2009. The Sequence Alignment/Map format and SAMtools. Bioinformatics 25:2078–2079.

23. Quinlan AR, Hall IM. 2010. BEDTools: a flexible suite of utilities for comparing genomic features. Bioinformatics 26:841–842.

24. Bailey TL, Elkan C. 1994. Fitting a mixture model by expectation maximization to discover motifs in biopolymers.

25. Bailey TL, Johnson J, Grant CE, Noble WS. 2015. The MEME Suite. Nucleic Acids Res 43:W39–W49.

26. Grant CE, Bailey TL, Noble WS. 2011. FIMO: Scanning for occurrences of a given motif. Bioinformatics 27:1017–1018.

27. Bolger AM, Lohse M, Usadel B. 2014. Trimmomatic: a flexible trimmer for Illumina sequence data. Bioinformatics 30:2114–2120.

28. Langmead B, Trapnell C, Pop M, Salzberg SL. 2009. Ultrafast and memory-efficient alignment of short DNA sequences to the human genome. Genome Biol 10.

29. Li H, Handsaker B, Wysoker A, Fennell T, Ruan J, Homer N, Marth G, Abecasis G, Durbin R. 2009. The Sequence Alignment/Map format and SAMtools. Bioinformatics 25:2078–2079.

30. Okonechnikov K, Conesa A, García-Alcalde F. 2016. Qualimap 2: advanced multi-sample quality control for high-throughput sequencing data. Bioinformatics 32:292–294.

31. Love MI, Huber W, Anders S. 2014. Moderated estimation of fold change and dispersion for RNA-seq data with DESeq2. Genome Biol 15.

32. Huber W, Carey VJ, Gentleman R, Anders S, Carlson M, Carvalho BS, Bravo HC, Davis S, Gatto L, Girke T, Gottardo R, Hahne F, Hansen KD, Irizarry RA, Lawrence M, Love MI, MaCdonald J, Obenchain V, Oleš AK, Pagès H, Reyes A, Shannon P, Smyth GK, Tenenbaum D, Waldron L, Morgan M. 2015. Orchestrating high-throughput genomic analysis with Bioconductor. Nat Methods 12:115–121.

33. Love M, Anders S, Huber W. 2014. Beginner's guide to using the DESeq2 package https://doi.org/10.1101/002832.

34. Goulas T, Cuppari A, Garcia-Castellanos R, Snipas S, Glockshuber R, Arolas JL, Gomis-Rüth FX. 2014. The pCri System: A Vector Collection for Recombinant Protein Expression and Purification. PLoS One 9:e112643.

35. Dreux N, Cendra M del M, Massier S, Darfeuille-Michaud A, Barnich N, Torrents E. 2015. Ribonucleotide reductase NrdR as a novel regulator for motility and chemotaxis during adherent-invasive Escherichia coli infection. Infect Immun 83:1305–1317.

36. Castro-Cerritos KV, Lopez-Torres A, Obregón-Herrera A, Wrobel K, Wrobel K, Pedraza-Reyes M. 2018. LC–MS/MS proteomic analysis of starved *Bacillus subtilis* cells overexpressing ribonucleotide reductase (*nrdEF*): implications in stress-associated mutagenesis. Curr Genet 64:215–222.

37. Rozman Grinberg I, Martínez-Carranza M, Bimai O, Nouaïria G, Shahid S, Lundin D, Logan DT, Sjöberg BM, Stenmark P. 2022. A nucleotide-sensing oligomerization mechanism that controls NrdR-dependent transcription of ribonucleotide reductases. Nature Communications 2022 13:1 13:1–10.

38. Panosa A, Roca I, Gibert I. 2010. Ribonucleotide Reductases of *Salmonella Typhimurium*: Transcriptional Regulation and Differential Role in Pathogenesis. PLoS One 5:11328.

39. Zhang Y, Okada R, Isaka M, Tatsuno I, Isobe KI, Hasegawa T. 2015. Analysis of the roles of NrdR and DnaB from *Streptococcus pyogenes* in response to host defense. APMIS 123:252–259.

40. Naveen V, Hsiao CD. 2016. NrdR Transcription Regulation: Global Proteome Analysis and Its Role in *Escherichia coli* Viability and Virulence. PLoS One 11:e0157165.

41. Wozniak KJ, Simmons LA. 2021. Hydroxyurea Induces a Stress Response That Alters DNA Replication and Nucleotide Metabolism in *Bacillus subtilis*. J Bacteriol 203:171–192.

42. Grinberg I, Shteinberg T, Hassan AQ, Aharonowitz Y, Borovok I, Cohen G. 2009. Functional Analysis of the *Streptomyces coelicolor* NrdR ATP-Cone Domain: Role in Nucleotide Binding, Oligomerization, and DNA Interactions †. J Bacteriol 191:1169–1179.

43. Johansson R, Jonna VR, Kumar R, Nayeri N, Lundin D, Sjöberg BM, Hofer A, Logan DT. 2016. Structural Mechanism of Allosteric Activity Regulation in a Ribonucleotide Reductase with Double ATP Cones. Structure 24:906–917.

44. Bennett BD, Kimball EH, Gao M, Osterhout R, Van Dien SJ, Rabinowitz JD. 2009. Absolute metabolite concentrations and implied enzyme active site occupancy in *Escherichia coli*. Nat Chem Biol 5:593–599.

45. Buckstein MH, He J, Rubin H. 2008. Characterization of Nucleotide Pools as a Function of Physiological State in Escherichia coli. J Bacteriol 190:718–726.

46. Bailey TL, Boden M, Buske FA, Frith M, Grant CE, Clementi L, Ren J, Li WW, Noble WS. 2009. MEME Suite: Tools for motif discovery and searching. Nucleic Acids Res 37:202–208.

47. Thomas PD, Campbell MJ, Kejariwal A, Mi H, Karlak B, Daverman R, Diemer K, Muruganujan A, Narechania A. 2003. PANTHER: A Library of Protein Families and Subfamilies Indexed by Function. Genome Res 13:2129–2141.

48. Mi H, Dong Q, Muruganujan A, Gaudet P, Lewis S, Thomas PD. 2010. PANTHER version 7: improved phylogenetic trees, orthologs and collaboration with the Gene Ontology Consortium. Nucleic Acids Res 38:D204–D210.

49. Supek F, Bošnjak M, Škunca N, Šmuc T. 2011. REVIGO Summarizes and Visualizes Long Lists of Gene Ontology Terms. PLoS One 6:e21800.

50. Tennekes M. 2021. treemap: Treemap Visualization.

51. Whiteside MD, Winsor GL, Laird MR, Brinkman FSL. 2013. OrtholugeDB: a bacterial and archaeal orthology resource for improved comparative genomic analysis. Nucleic Acids Res 41:D366.

Material Suplementario

Supplementary Table S1. Strains and plasmids in this study.

Strains and plasmids are listed with simplified names (referred to as), commonly used in the text. Antibiotic resistance is indicated with the following abbreviations: Amp (ampicillin), Kn (kanamycin), Tc (tetracycline), and Gm (gentamicin). The origin species of each *nrdR* gene is specified: *P. aeruginosa* (*P.* aer*) or E. coli*.

Item	Referred to as	(Strain) Genotype	Description	Source
Strains				
PAO1	PAO1 (WT)	Wild-type (ATCC 15692 / CECT 4122)	Wild-type *P. aeruginosa* lab strain	ATCC
PW7855	PAO1 Δ*nrdR*	PAO1 *nrdR*::ISlacZ/hah, **Tc^R**	PAO1 derivative with a transposon interrupting *nrdR*	*Jacobs et al.* [1]
K-12	K12 MG1655	F$^-$ λ^- *ilvG rfb*-50 *rph*-1 (ATCC 700926)	Wild-type *E. coli* lab strain	Laboratory stock
BL21(DE3)	BL21	F$^-$ *ompT gal dcm lon hsdSB*(r$_B^-$ m$_B^-$) λ(DE3 [*lacI lacUV5-T7p07 ind1 sam7 nin5*]) [malB$^+$]$_{K-12}$(λ^S)	*E. coli* strain for IPTG-induced T7 protein overexpression	Lucigen, WI USA
DH5α	DH5α	*recA1 endA1 hdsR17 supE44 thi-1 relA1 Δ(lacZYA-argF)U169 deoR Φ80dlacZM15*	*E. coli* strain for cloning procedures	Lucigen, WI USA
Plasmids				
pJET1.2-blunt	pJET1.2		General carrier vector for cloning procedures, **Amp^R**	ThermoFisher, MA USA
pET22b$^+$	pET22b+		Vector for IPTG-induced T7 protein overexpression of His$_6$-fusion proteins, **Amp^R**	Millipore Sigma, MA USA
pET22b$^+$::*nrdR*(P.a er)	pET-NrdR(PAO)		pET22b+ derivative producing an NrdR-His6 (*P. aer*) fusion protein, **Amp^R**	This work
pAviTag-NN-His SUMO Kan	pSUMO		Vector for Rhamnose-induced overexpression of SUMO-fusion proteins, **Kn^R**	Lucigen, WI USA
pAviTag-NN-His SUMO Kan::*nrdR*(P. aer)	pSUMO-NrdR(PAO)		pSUMO derivative producing a His$_6$-AviTag-SUMO-NrdR (*P. aer*) fusion protein, **Kn^R**	This work
pAviTag-NN-His SUMO Kan::*nrdR*(E. coli)	pSUMO-NrdR(ECO)		pSUMO derivative producing a His$_6$-AviTag-SUMO-NrdR (*E. coli*) fusion protein, **Kn^R**	This work
pCri11a	pCri11a		Vector for IPTG-induced overexpression of His$_6$-SUMO-His$_6$ fusion proteins, **Kn^R**	*Goulas et al.* [2]
pCri11a::*nrdR*(P. aer)	pCri-NrdR(PAO)		pCri derivative producing a His$_6$-SUMO-TEVcs-NrdR (*P. aer*) fusion protein, **Kn^R**	This work
pCri11a::*nrdR*(E. coli)	pCri-NrdR(ECO)		pCri derivative producing a His$_6$-SUMO-TEVcs-NrdR (*E. coli*) fusion protein, **Kn^R**	Work
pETS130-GFP	pETS130		Broad-host range, promoterless GFP, Gm^R, **Gm^R**	*Sjoberg et al.* [3]
pReViTA	pReViTA		pETS130 derivative, *in vitro* transcription template plasmid for ReViTA, **Gm^R**	This work
pReViTA-P*nrdA* (E. coli)	pReViTA-PA		pReViTA derivative, carrying the promoter region of *nrdAB* in *E. coli*, **Gm^R**	This work
pETS176	pUCP20T::nrdR		pUC2P0T derivative, complementation plasmid for *nrdR*, **Amp^R**	*Crespo et al.* [4]

1. Jacobs MA, Alwood A, Thaipisuttikul I, Spencer D, Haugen E, Ernst S, et al. Comprehensive transposon mutant library of Pseudomonas aeruginosa. Proceedings of the National Academy of Sciences of the United States of America. 2003;100(24):14339-44.

2. Goulas T, Cuppari A, Garcia-Castellanos R, Snipas S, Glockshuber R, Arolas JL, et al. The pCri System: a vector collection for recombinant protein expression and purification. PloS one. 2014;9(11):e112643.

3. Sjoberg BM, Torrents E. Shift in ribonucleotide reductase gene expression in *Pseudomonas aeruginosa* during infection. Infection and immunity. 2011;79(7):2663-9.

4. Crespo A, Pedraz L, Torrents E. Function of the *Pseudomonas aeruginosa* NrdR Transcription Factor: Global Transcriptomic Analysis and Its Role on Ribonucleotide Reductase Gene Expression. PloS one. 2015;10(4):e0123571.

Supplementary table S2. Sequence and application of the primers used in this study

Primers are commonly referred to in the text by their numbers as listed here. [D3-PA] in 28 indicates D3-phosphoramidite

Number	Name	Sequence	Application
1	NrdR_NdeI_fw	CATATGCATTGTCCCTTCTGCGGTG	Cloning, pET-NrdR(PAO)
2	NrdR_XhoI_rv	CTCGAGTTCCTTGGCCGGCTCGCG	Cloning, pET-NrdR(PAO)
3	T7-promoter_fw	TAATACGACTCACTATAGGG	PCR test, pET-NrdR / pCri-NrdR
4	T7-terminator_rv	CTAGTTATTGCTCAGCGGTG	PCR test, pET-NrdR / pCri-NrdR
5	NrdR-PAO_SUMO_fw	CGCGAACAGATTGGAGGTGGCAGCATGCATTGTCCCTTCTGCGGT	Cloning, pSUMO-NrdR(PAO)
6	NrdR-PAO_SUMO_rv	GTGGCGGCCGCTCTATTACGTTCATTCCTTGGCCGGCTC	Cloning, pSUMO-NrdR(PAO)
7	NrdR-ECO_SUMO_fw	CGCGAACAGATTGGAGGTGGATCCATGCATTGTCTGTTTCG	Cloning, pSUMO-NrdR(ECO)
8	NrdR-ECO_SUMO_rv	GTGGCGGCCGCTCTATTAGGCTTAGTCCTCCAGGCGC	Cloning, pSUMO-NRdR(ECO)
9	SUMO_fw	ATTCAAGCTGATCAGACCCCTGAA	PCR test, pSUMO-NrdR
10	pETite_rv	CTCAAGACCCGTTTAGAGGC	PCR test, pSUMO-NrdR
11	NrdR-PAO_TEV_fw	ATTACCATGGGCGAGAACCTTTACTTTCAAGGCAGCGGCAGCGGCAGCATGCATTGTCCCTTCTGC	Cloning, pCri-NrdR(PAO)
12	NrdR-PAO_TEV_rv	TATATACTCGAGTCATTCCTTGGCCGGCTCGCG	Cloning, pCri-NrdR(PAO)
13	NrdR-ECO_TEV_fw	TATACCATGGGCGAGAACCTTTACTTTCAAGGATCCGGATCCGGATCCATGCATTGCCCATTCTGTTTCGC	Cloning, pCri-NrdR(ECO)
14	NrdR-ECO_TEV_rv	TATATACTCGAGTTAGTCCTCCAGGCGCGCGATCT	Cloning, pCri-NrdR(ECO)
15	pETS130-backB_fw	AATCTAGATGCCCATGGACGCACAC	Cloning, pReViTA
16	pETS130-backB_rv	AAGACGTCCGGGGAGGCAGACAAGGTATA	Cloning, pReViTA
17	PnrdA-ECO_BamHI_fw	AAAGGATCCATCATTTTCTATAAGACGG	Cloning, pReViTA-PA / EMSA probes
18	PnrdA-ECO_SpeI_rv	AACTAGTAGCAGATTCTGATTCATG	Cloning, pReViTA-PA
19	ReViTA_TEST_fw	AGCACAAGTTTTATCCGGCC	ReViTA, qPCR
20	ReViTA_TEST_rv	CATATCACCAGCTCACCGTC	ReViTA, qPCR
21	ReViTA_TEST_rt	TGCTCATGGAAAACGGTGTAAC	ReViTA, rev. transcription
22	ReViTA_CTRL_fw	TTTCGGTCGTGAGTTCGGAG	ReViTA, qPCR
23	ReViTA_CTRL_rv	GCAAGCGCGATGAATGTCTT	ReViTA, qPCR
24	ReViTA_CTRL_rt	CGCCAACAACCGCTTCTTG	ReViTA, rev. transcription
25	PnrdA-ECO_m13_rv	CTGGGCGTCGTTTTACAAACTGAATGTGGGAGCG	EMSA probes
26	Anr-ctrlNEG_fw	GAATTCATGGCCGAAACCATCAAG	EMSA probes
27	Anr-ctrlNEG_m13_rv	CTGGGCGTCGTTTTACCTTCTTCGACAGCAGCAG	EMSA probes
28	WellRed M13	[D3-PA]GTCACTGGGCGTCGTTTTAC	EMSA probes, infrared dye

Supplementary Table S3 Transcriptomic effects of *nrdR* inactivation, DNA microarray assay in *E. coli*.

Differentially expressed genes (DEGs) in a *nrdR*-ATPcone mutant *E. coli* strain compared to its isogenic wild-type K-12 *substr*. MG1655 strain. DEGs were only accepted with a p-value lower than 0.01 and a log(fold-change) higher than 1.0 in at least either exponential or stationary phase. Genes are listed by locus-tag; when available, gene name and a short functional description are also included. Genes in operons displaying putative NrdR-boxes in their upstream region (see Supplementary Table S4) are indicated. Genes in the *nrd* operons are highlighted in bold.

Upregulated genes							
Gene			Exponential phase		Stationary phase		NrdR-box
Locus	Name	Function/Product	LogFC	P-value	LogFC	P-value	Comments
b0014	dnaK	Chaperone protein DnaK	1.31	3.63E-06			Single NrdR-box
b0015	dnaJ	Chaperone protein DnaJ	1.39	3.10E-06			
b0068	thiB	Thiamine ABC transp., periplasmic binding protein			1.07	5.22E-03	
b0071	leuD	3-isopropylmalate dehydratase subunit LeuD	1.06	1.07E-03			
b0113	pdhR	DNA-binding transcriptional dual regulator PdhR			1.42	1.46E-04	Single NrdR-box
b0150	fhuA	Ferrichrome outer membrane transp.			2.78	2.54E-03	
b0151	fhuC	Fe(III) hydroxamate ABC transp., ATP binding subunit			2.09	7.93E-03	
b0195	trmO	tRNA m(6)t(6)A37 methyltransferase			1.21	7.55E-04	
b0199	metN	L-methionine/D-methionine ABC transp.			1.00	8.95E-05	
b0224	yafK	L,D-transpeptidase domain-containing protein			1.08	1.07E-04	
b0238	gpt	Xanthine-guanine phsophoribosyltransferase			1.43	8.43E-03	
b0314	betT	Choline:H(+) symporter			1.25	9.30E-03	
b0315	pdeL	c-di-GMP phosphodiesterase PdeL			1.27	2.00E-03	
b0405	queA	TRNA preQ1(34) SAM ribosyltransferase-isomerase			1.37	4.24E-03	
b0433	ampG	Muropeptide:H(+) symporter			1.24	7.34E-03	
b0468	ybaN	DUF454 domain-containing inner membrane protein			1.75	2.48E-03	
b0469	apt	Adenine phosphoribosyltransferase			1.31	6.51E-03	
b0473	htpG	Chaperone protein HtpG	1.11	7.52E-05			
b0477	gsk	Inosine/guanosine kinase			1.09	4.60E-03	
b0524	lpxH	UDP-2,3-diacylglucosamine diphosphatase			1.04	8.03E-03	
b0592	fepB	Fe-enterobactin ABC transp., perip. binding protein			2.08	2.98E-03	
b0593	entC	Isochorismate synthase EntC			4.26	6.92E-03	
b0594	entE	2,3-dihydroxybenzoate-AMP ligase			3.67	8.13E-03	
b0595	entB	Enterobactin synthase component B			2.75	8.26E-03	
b0596	entA	2,3-dihydro-2,3-dihydroxybenzoate dehydrogenase			2.32	8.85E-03	
b0597	entH	Proofreading thioesterase, enterobactin biosynthesis			2.34	9.91E-03	
b0630	lipB	Lipoyl(octanoyl) transferase			1.26	1.87E-03	
b0636	rlmH	23S rRNA m(3)psi1915 methyltransferase			1.17	5.40E-03	
b0737	tolQ	Tol-Pal system protein TolQ			1.40	4.11E-03	
b0813	rhtA	L-threonine/L-homoserine exporter			1.01	6.35E-03	
b0819	ldtB	L,D-transpeptidase LdtB			1.37	3.25E-03	
b0822	ybiV	Sugar phosphatase YbiV			1.25	6.59E-04	
b0841	ybjG	Undecaprenyl pyrophosphate phosphatase			1.76	3.77E-03	
b0874	lysO	L-lysine exporter			1.39	4.72E-03	
b0877	ybjX	DUF535 domain-containing protein YbjX			1.06	7.37E-04	
b0931	pncB	Nicotinate phosphoribosyltransferase			1.09	2.90E-04	
b0946	zapC	Cell division protein ZapC	1.05	8.72E-03			
b1018	efeO	Ferrous iron transport system protein EfeO			2.28	1.48E-03	
b1019	efeB	Heme-containing peroxidase/deferrochelatase			1.66	4.07E-03	
b1074	flgC	Flagellar basal-body rod protein FlgC			1.12	7.84E-03	
b1133	mnmA	TRNA-specific 2-thiouridylase			1.15	7.96E-03	
b1203	ychF	Redox-responsive ATPase YchF			1.02	4.69E-03	
b1204	pth	Peptidyl-tRNA hydrolase			1.40	3.58E-03	
b1216	chaA	Na(+)/K(+):H(+) antiporter ChaA			1.41	6.18E-03	
b1238	tdk	Thymidine/deoxyuridine kinase			1.21	5.06E-03	
b1253	yciA	Acyl-CoA thioesterase YciA			1.61	3.83E-03	
b1295	ymjA	DUF2543 domain-containing protein YmjA			1.30	5.47E-03	
b1321	ycjX	DUF463 domain-containing protein YcjX	1.61	2.61E-03			
b1322	ycjF	DUF697 domain-containing inner membrane protein	1.67	3.31E-04			
b1439	ydcR	Putative DNA-binding transcriptional regulator			1.03	7.78E-04	
b1452	yncE	PQQ-like domain-containing protein YncE			1.91	8.46E-04	
b1494	pqqL	Periplasmic metalloprotease			1.12	4.85E-03	
b1495	yddB	Putative TonB-dependent receptor YddB			1.47	5.36E-05	
b1496	yddA	ABC transp. family protein YddA			2.22	3.45E-03	
b1524	glsB	Glutaminase 2			1.01	2.64E-03	
b1615	uidC	Outer membrane porin family protein UidC	1.05	2.52E-03			
b1626	ydgK	DUF2569 domain-containing inner membrane protein			1.36	6.18E-04	
b1627	rsxA	SoxR [2Fe-2S] reducing system protein RsxA			1.70	2.48E-03	

b1628	rsxB	SoxR [2Fe-2S] reducing system protein RsxB			1.55	9.96E-03	
b1652	rnt	RNase T			1.21	9.02E-03	
b1660	ydhC	Putative transp. YdhC			1.21	5.40E-04	
b1704	aroH	3-deoxy-7-phosphoheptulonate synthase, Trp-sensitive			1.29	3.50E-03	
b1759	nudG	5-hydroxy-CTP diphosphatase			1.02	1.93E-03	
b1786	dgcJ	Putative diguanylate cyclase DgcJ			1.44	2.21E-03	
b1796	yoaG	DUF1869 domain-containing protein YoaG	1.30	9.53E-03	1.59	9.21E-04	
b1797	yeaR	DUF1971 domain-containing protein YeaR			1.77	7.87E-03	
b1828	yebQ	Putative transp. YebQ			1.38	9.76E-03	
b1870	cmoA	Carboxy-S-adenosyl-L-methionine synthase			1.10	2.20E-03	
b1888	cheA	Chemotaxis protein CheA			1.08	2.49E-03	
b1890	motA	Motility protein A			1.40	7.24E-04	
b1905	ftnA	Ferritin iron storage protein	1.13	6.78E-03			
b1921	fliZ	DNA-binding transcriptional regulator FliZ			1.57	6.28E-03	
b1922	fliA	RNA polymerase, sigma 28 (sigma F) factor			1.60	4.91E-03	
b1925	fliS	Flagellar biosynthesis protein FliS			1.03	4.17E-03	
b2022	hisB	Imidazoleglycerol-phosphate dehydratase	1.04	1.25E-03			
b2066	udk	Uridine/cytidine kinase			1.46	5.63E-03	
b2155	cirA	Iron-catecholate outer membrane transp. CirA			3.95	7.87E-03	
b2173	yeiR	Zinc-binding GTPase YeiR			1.08	4.61E-04	
b2182	bcr	Multidrug efflux pump Bcr			1.40	7.28E-03	
b2187	yejL	DUF1414 domain-containing protein YejL			1.00	8.81E-03	
b2211	yojI	Microcin J25 efflux protein			3.06	7.83E-03	
b2234	**nrdA**	**RNR class Ia, α subunit**			**1.90**	**4.78E-06**	NrdR-box pair
b2235	**nrdB**	**RNR class Ia, β subunit**			**1.45**	**4.35E-06**	NrdR-box pair
b2236	yfaE	2Fe-tyrosyl radical cofactor maintenance protein			1.71	3.38E-06	
b2273	yfbN	Uncharacterized protein			1.14	1.82E-03	
b2350	yfdG	CPS-53 prophage; putative glucose translocase			1.32	2.60E-03	
b2392	mntH	Mn(2(+))/Fe(2(+)): H(+) symporter MntH			1.02	7.42E-03	
b2393	nupC	Nucleoside:H(+) symporter NupC			1.21	2.19E-03	
b2509	xseA	Exodeoxyribonuclease VII subunit XseA			1.37	2.06E-04	
b2567	rnc	RNase III			1.23	2.37E-03	
b2575	yfiC	TRNA m(6)A37 methyltransferase			1.21	1.72E-03	
b2592	clpB	Chaperone protein ClpB	1.95	4.22E-04			
b2669	stpA	DNA-binding transcriptional repressor StpA			1.34	1.58E-03	
b2673	**nrdH**	**RNR class Ib, associated glutarredoxin**	**3.19**	**2.36E-08**	**6.52**	**2.12E-09**	NrdR-box pair
b2674	**nrdI**	**RNR class Ib, maintenance flavodoxin**	**3.17**	**1.80E-07**	**6.34**	**6.33E-09**	NrdR-box pair
b2675	**nrdE**	**RNR class Ib, α subunit**	**2.85**	**3.02E-07**	**4.87**	**7.37E-08**	NrdR-box pair
b2676	**nrdF**	**RNR class Ib, β subunit**	**2.67**	**1.94E-05**	**5.98**	**1.95E-07**	NrdR-box pair
b2749	ygbE	DUF3561 domain-containing inner membrane protein			1.25	6.99E-03	
b2807	ygdD	DUF423 domain-containing inner membrane protein			1.11	4.72E-03	
b2817	amiC	N-acetylmuramoyl-L-alanine amidase C			1.01	1.08E-04	
b2832	ygdQ	UPF0053 inner membrane protein YgdQ			1.18	6.20E-03	
b2838	lysA	Diaminopimelate decarboxylase			1.02	3.68E-03	
b2845	yqeG	Putative transp. YqeG			1.10	5.33E-03	
b2944	yggI	Protein YggI			1.54	1.16E-03	
b3064	tsaD	N(6)-L-threonylcarbamoyladenine synthase subunit			1.00	2.70E-03	
b3190	ibaG	Acid stress protein IbaG			1.01	4.17E-03	
b3212	gltB	Glutamate synthase subunit GltB	1.30	5.26E-05			
b3213	gltD	Glutamate synthase subunit GltD	1.01	2.01E-03	1.11	8.35E-04	
b3424	glpG	Rhomboid protease GlpG			1.47	2.30E-03	
b3425	glpE	Thiosulfate sulfurtransferase GlpE			1.78	7.92E-03	
b3541	dppD	Dipeptide ABC transp. ATP binding subunit DppD	2.05	6.69E-03			
b3542	dppC	Dipeptide ABC transp. membrane subunit DppC	1.39	3.72E-03			
b3543	dppB	Dipeptide ABC transp. membrane subunit DppB	2.66	2.23E-03			
b3643	rph	Truncated RNase PH			1.18	8.57E-03	
b3661	nlpA	Lipoprotein-28	1.24	3.44E-03			
b3670	ilvN	Acetohydroxy acid synthase I subunit IlvN	1.79	5.89E-05			
b3671	ilvB	Acetohydroxy acid synthase I subunit IlvB	1.78	2.90E-04			
b3687	ibpA	Small heat shock protein IbpA			1.01	9.58E-03	
b3702	dnaA	Chromosomal replication initiator protein DnaA			1.01	4.84E-03	

b3707	tnaC	TnaAB operon leader peptide	3.65	8.96E-04			
b3708	tnaA	Tryptophanase	2.84	2.60E-04			
b3742	mioC	Flavoprotein MioC			1.09	1.06E-03	
b3766	ilvL	IlvXGMEDA operon leader peptide	1.47	3.77E-03			
b3778	rep	ATP-dependent DNA helicase Rep			1.17	6.44E-03	
b4049	dusA	TRNA-dihydrouridine synthase A			1.11	4.63E-03	
b4238	**nrdD**	**RNR class III, α subunit**	**1.26**	**6.35E-03**			NrdR-box pair
b4312	fimB	Regulator for fimA	1.08	3.28E-03			
b4367	fhuF	Hydroxamate siderophore iron reductase			2.67	9.19E-04	
b4372	holD	DNA polymerase III subunit			1.06	7.48E-03	
b4511	ybdZ	Enterobactin biosynthesis protein YbdZ			3.70	5.19E-04	

Downregulated genes							
Gene			Exponential phase		Stationary phase		NrdR-box
Locus	Name	Function/Product	LogFC	P-value	LogFC	P-value	Comments
b0007	yaaJ	Putative transp. YaaJ			-1.22	6.31E-03	
b0034	caiF	DNA-binding transcriptional activator CaiF			-1.90	2.98E-03	
b0119	yacL	UPF0231 family protein YacL			-1.02	1.45E-03	
b0129	yadI	Putative PTS enzyme IIA component YadI			-1.32	3.66E-03	
b0336	codB	Cytosine transp.	-1.69	1.02E-03			
b0337	codA	Cytosine/isoguanine deaminase	-1.23	4.68E-06			
b0509	glxR	Tartronate semialdehyde reductase 2			-1.18	9.60E-03	
b0798	ybiA	N-glycosidase YbiA			-1.96	2.80E-03	
b0895	dmsB	Dimethyl sulfoxide reductase subunit B			-2.04	2.31E-03	
b0896	dmsC	Dimethyl sulfoxide reductase subunit C			-1.62	1.37E-04	
b0953	rmf	Ribosome modulation factor			-1.40	4.38E-03	
b0994	torT	Periplasmic trimethylamine-N-oxide binding protein			-1.20	9.57E-03	
b1131	purB	Adenylosuccinate lyase	-1.21	6.15E-03			
b1182	hlyE	Hemolysin E			-1.06	8.05E-03	
b1225	narH	Nitrate reductase A subunit beta			-3.10	7.89E-03	
b1226	narJ	Nitrate reductase 1, Mo-cofactor assembly chaperone			-3.35	8.73E-03	
b1227	narI	Nitrate reductase A subunit gamma			-3.17	4.35E-03	
b1420	mokB	Putative regulatory protein MokB			-1.55	3.05E-03	
b1426	ydcH	Protein YdcH			-2.33	6.00E-03	
b1462	yddH	Flavin reductase-like protein YddH			-1.51	7.38E-03	
b1475	fdnH	Formate dehydrogenase N subunit beta			-2.53	2.43E-03	
b1752	ydjZ	DedA family protein YdjZ			-1.82	5.07E-03	
b1849	purT	Phosphoribosylglycinamide formyltransferase 2	-2.50	6.17E-03			
b2000	flu	CP4-44 prophage; Ag43 autotransp.	-2.20	1.15E-05	-2.69	1.58E-06	
b2001	yeeR	CP4-44 prophage; inner membrane protein	-2.69	2.86E-07	-2.45	2.66E-07	
b2002	yeeS	CP4-44 prophage; JAB domain-containing protein	-1.94	7.38E-05	-1.39	3.87E-05	
b2003	yeeT	CP4-44 prophage; DUF987 domain-containing protein	-1.01	1.02E-04			
b2009	sbmC	DNA gyrase inhibitor			-1.51	6.94E-03	
b2197	ccmE	Periplasmic heme chaperone			-1.33	1.30E-03	
b2198	ccmD	Cytochrome C maturation protein D			-1.30	1.26E-03	
b2199	ccmC	Cytochrome C maturation protein C			-1.23	6.38E-03	
b2201	ccmA	Cytochrome C maturation protein A			-1.40	9.78E-03	
b2202	napC	Periplasmic nitrate reductase cytochrome C protein			-1.65	7.79E-03	
b2203	napB	Periplasmic nitrate reductase cytochrome C550 protein			-1.88	2.91E-03	
b2204	napH	Ferredoxin-type protein NapH			-1.94	2.68E-03	
b2205	napG	Ferredoxin-type protein NapG			-2.31	4.14E-03	
b2292	yfbS	Putative transp. YfbS			-1.88	9.29E-03	
b2312	purF	Amidophosphoribosyltransferase	-2.33	5.29E-03			
b2398	yfeC	Putative DNA-binding transcriptional regulator YfeC			-1.67	5.24E-03	
b2399	yfeD	Putative DNA-binding transcriptional regulator YfeD			-1.45	2.06E-03	
b2419	yfeK	DUF5329 domain-containing protein YfeK	-1.87	9.32E-04			
b2476	purC	Pi-ribosylaminoimidazole-succinocarboxamide synth.	-1.89	8.48E-04			
b2500	purN	Phosphoribosylglycinamide formyltransferase 1	-2.14	5.71E-03			

b2507	guaA	GMP synthetase	-1.62	5.09E-04		
b2508	guaB	Inosine 5'-monophosphate dehydrogenase	-1.80	6.96E-03		
b2557	purL	Phosphoribosylformylglycinamide synthetase	-2.40	1.12E-04		
b2685	emrA	Multidrug efflux pump membrane fusion protein EmrA	-1.22	8.83E-03		
b2686	emrB	Multidrug efflux pump membrane subunit EmrB	-1.16	5.56E-03		
b2730	hypE	Hydrogenase maturation protein, carbamoyl deH.			-1.19	1.38E-03
b2768	ygcP	Putative anti-terminator regulatory protein			-1.16	9.18E-03
b2902	ygfF	Putative oxidoreductase YgfF	-1.26	1.39E-04		
b2971	yghG	Lipoprotein YghG	-1.55	5.46E-03		
b2994	hybC	Hydrogenase 2 large subunit			-1.25	1.32E-03
b2995	hybB	Hydrogenase 2 membrane subunit			-1.70	7.53E-04
b2996	hybA	Hydrogenase 2 iron-sulfur protein			-2.19	8.71E-03
b3055	ygiM	Putative signal transduction protein (SH3 domain)	-1.31	3.26E-03		
b3091	uxaA	D-altronate dehydratase			-1.43	9.65E-03
b3115	tdcD	Propionate kinase			-1.48	3.30E-04
b3116	tdcC	Threonine/serine:H(+) symporter			-2.04	1.02E-03
b3350	kefB	K(+) : H(+) antiporter KefB			-1.04	2.09E-03
b3478	nikC	Ni(2(+)) ABC transp. membrane subunit NikC			-2.26	2.44E-04
b3479	nikD	Ni(2(+)) ABC transp. ATP binding subunit NikD			-2.28	4.51E-04
b3480	nikE	Ni(2(+)) ABC transp. ATP binding subunit NikE			-1.65	3.42E-05
b3481	nikR	DNA-binding transcriptional repressor NikR			-1.07	1.60E-04
b3571	malS	Alpha-amylase			-2.09	1.24E-03
b3573	ysaA	Putative electron transport protein YsaA			-2.07	8.53E-03
b3612	gpmM	2,3-BPG-independent phosphoglycerate mutase			-1.03	9.97E-03
b3645	dinD	DNA damage-inducible protein D			-1.37	4.50E-05
b3715	yieH	6-phosphogluconate phosphatase	-1.01	7.25E-03		
b3755	yieP	DNA-binding transcriptional regulator YieP			-1.08	9.97E-03
b3774	ilvC	Ketol-acid reductoisomerase (NADP(+))			-2.12	2.23E-03
b3924	fpr	Flavodoxin/ferredoxin-NADP(+) reductase			-1.02	9.95E-03
b4005	purD	Phosphoribosylamine--glycine ligase	-2.91	1.33E-04		
b4006	purH	Bifunctional AICAR transformylase/IMP cyclohydrolase	-2.31	7.36E-03		
b4064	ghxP	Guanine/hypoxanthine transp. GhxP	-2.70	9.56E-03		
b4065	yjcE	Putative transp. YjcE			-1.05	8.91E-03
b4072	nrfC	Putative menaquinol-cytochrome C reductase subunit			-2.17	4.95E-03
b4073	nrfD	Putative menaquinol-cytochrome C reductase subunit			-1.11	6.73E-04
b4079	fdhF	Formate dehydrogenase H			-1.34	6.68E-03
b4217	ytfK	Stringent response modulator YtfK			-1.28	5.79E-03
b4224	chpS	ChpS antitoxin, ChpB-ChpS toxin-antitoxin system			-1.06	6.65E-03
b4244	pyrI	Aspartate carbamoyltransferase, PyrI subunit	-1.26	2.02E-04		
b4245	pyrB	Aspartate carbamoyltransferase catalytic subunit	-1.30	5.30E-05		
b4334	yjiL	Activator of (R)-hydroxyglutaryl-CoA dehdratase			-1.85	4.06E-03
b4428	hokB	Toxin HokB			-1.43	7.05E-03

Supplementary Table S4. Bioinformatic prediction of NrdR-boxes in *E. coli* and *P. aeruginosa*.
Putative NrdR-boxes identified in a FIMO (26) (MEME Suite (46)) search on promoter-enriched whole-genome queries containing the sequences 450 bp upstream and 20 bp downstream of the translation start codon for each in gene in the *P. aeruginosa* PAO1 and *E. coli* K-12 *substr*. MG1655 genomes. Only hits with a p-value lower than $1 \cdot 10^{-4}$ were included. Results were deduplicated and assigned to the gene with the closest translation start. *nrd* operons are highlighted in bold.

Escherichia coli

			Distance to ATG		Putative NrdR-box		
		Closest gene					
Locus	Name	Function/Product	Start	Stop	P-value	Sequence	Comments
b0014	dnaK	Chaperone protein DnaK	-26	-11	1.98E-05	ACCGAATATATAGTGG	dnaKJ - Single NrdR box
b0055	djlA	Co-chaperone protein DjlA	-55	-40	2.85E-06	CACCTTTATATTGTGG	
b0098	secE	Protein translocation ATPase	-238	-223	4.45E-05	GCGCAACATCTTGCAT	
b0113	pdhR	DNA-binding transcriptional dual regulator PdhR	-312	-297	2.30E-05	TCTCAATATGTAGAAT	pdhR-aceEF-lpd - Single NrdR box
b0213	yafS	Putative SAM-dependent methyltransferase	-286	-271	1.59E-05	TTCCCTTATCTTGTGT	
b0382	iraP	Anti-adaptor protein, sigma stabilization	-173	-158	1.56E-05	AGCCTATATTTTGTGT	
b0460	hha	Hemolysin expression-modulating protein Hha	-155	-140	4.48E-05	CACCTTTATGTTGTTC	
b0583	entD	Phosphopantetheinyl transferase EntD	-88	-73	4.01E-05	ATTCAATATATTGCAG	
b0645	ybeR	Uncharacterized protein YbeR	-257	-242	9.71E-06	CAACAATATATTGAGC	
b0720	gltA	Citrate synthase	-449	-434	2.88E-06	AACCTACATATAGTTT	
b0721	sdhC	Succinate:quinone oxidoreductase	-275	-260	1.57E-05	AAACTATATGTAGGTT	
b0815	opgE	Phosphoethanolamine transferase	-335	-320	2.84E-05	GCTCTCTATGTTGTGC	
b1000	cbpA	Curved DNA-binding protein	-267	-252	9.48E-06	TACCCATATATAGCGT	
b1089	rpmF	50S ribosomal subunit protein L32	-320	-305	3.36E-05	ACACAACGTATTGTTT	
b1114	mfd	Transcription-repair coupling factor	-45	-30	1.11E-05	CCCCCATATGTTGAGG	
b1128	roxA	Ribosomal protein-arginine oxygenase	-315	-300	8.90E-06	CATCTCTATATTGTGG	
b1298	puuD	γ-glutamyl-γ-aminobutyrate hydrolase	-335	-320	1.02E-05	CATCAACATATTGCGT	
b1443	ydcV	Putative ABC transporter membrane subunit	-359	-344	3.48E-05	TCTCTATATCTGGTTG	
b1466	narW	Putative private chaperone for NarZ nitrate reductase	-375	-360	3.24E-05	CGCCAATATGTTGAGT	
b1487	ddpA	2CD-dipep. ABC transporter, periplasmic bind. protein	-340	-325	1.22E-05	CCGCAATATGTTGTTG	
b1491	yddW	Divisome-localized glycosyl hydrolase	-166	-151	2.73E-06	CCACACTATATTGTGA	
b1642	slyA	DNA-binding transcriptional dual regulator SlyA	-249	-234	2.06E-05	ACACCAGATCTTGTAA	
b1642	slyA	DNA-binding transcriptional dual regulator SlyA	-182	-167	3.63E-05	ACCGAATATATTGCGT	
b1791	yeaN	2-nitroimidazole exporter	-301	-286	3.75E-05	AAACCGCATATTGTGG	
b2025	hisF	Imidazole glycerol phosphate synthase	-398	-383	4.27E-05	TCACAAGATATGGTGA	
b2159	nfo	Endonuclease IV	-72	-57	1.06E-05	CCACTACATCTTGCTC	
b2234	**nrdA**	**RNR class Ia, α subunit**	**-93**	**-78**	**5.42E-09**	**CCCCTATATATAGTGT**	**nrdAB - NrdR box 2**
b2234	**nrdA**	**RNR class Ia, α subunit**	**-125**	**-110**	**2.45E-05**	**TCACACTATCTTGCAG**	**nrdAB - NrdR box 1**
b2348	argW	tRNA-Arg	-297	-282	3.45E-05	ATCCTCTATCTGGTGT	
b2351	gtrB	CPS-53 prophage, 3B bactoprenol glucosyl transferase	-158	-143	2.49E-05	ATGCTATATGTTGGGT	
b2543	yphA	Putative inner membrane protein	-27	-12	4.94E-05	TCACATTATCTTGCAA	
b2593	yfiH	Polyphenol oxidase YfiH	-74	-59	1.16E-05	CCACAAGATATGGTGG	
b2673	**nrdH**	**RNR class Ib, associated glutarredoxin**	**-89**	**-74**	**8.63E-07**	**CAACTACATCTAGTAT**	**nrdHIEF - NrdR box 2**
b2673	**nrdH**	**RNR class Ib, associated glutarredoxin**	**-120**	**-105**	**2.75E-06**	**TTGCTATATATTGTGT**	**nrdHIEF - NrdR box 1**
b3052	hldE	Heptose 7-P kinase/heptose 1-P adenyltransferase	-314	-299	1.33E-06	ACCCAATATCTGGTGT	
b3155	yhbQ	DNA damage response nuclease YhbQ	-102	-87	3.22E-05	TGACAACATGTTGTTT	
b3180	yhbY	Ribosome assembly factor YhbY	-336	-321	3.56E-05	TGACCACATATTGTGA	
b3186	rplU	50S ribosomal subunit protein L21	-304	-289	2.36E-05	CCGCCATATCTTGCGC	
b3210	arcB	Sensor histidine kinase ArcB	-383	-368	4.65E-05	CCGCTGCATATTGTGA	
b3454	livF	Branched chain aa/phenylalanine ABC transporter	-158	-143	3.54E-05	CACCACTATCTTGTTG	
b3647	ligB	DNA ligase B	-285	-270	3.52E-05	AAACAATATAAAGCGT	
b3745	viaA	Putative ATPase cofactor	-242	-227	3.26E-05	GCCCAACATCTTGTCG	
b4177	purA	Adenylosuccinate synthetase	-134	-119	2.28E-05	CTACTACATGTTGAGG	
b4180	rlmB	23S rRNA 2'-O-ribose G2251 methyltransferase	-76	-61	4.01E-05	ATTCAATATATTGCAG	
b4238	**nrdD**	**RNR class III**	**-177**	**-162**	**3.18E-07**	**ACCCAATATGTTGTAT**	**nrdDG - NrdR box 2**
b4238	**nrdD**	**RNR class III**	**-208**	**-193**	**2.99E-06**	**GCACTATATATAGACT**	**nrdDG - NrdR box 1**
b4270	leuX	tRNA-Leu	-292	-277	9.03E-06	CTTCAACATCTTGTGG	
b4684	yqfG	Uncharacterized protein YqfG	-277	-262	3.71E-06	AACCTCTATATTGTGG	

Pseudomonas aeruginosa

			Distance to ATG		Putative NrdR-box		
		Closest gene					
Locus	Name	Function/Product	Start	Stop	P-value	Sequence	Comments
PA0254	hudA	Virulence attenuating factor HudA	-23	-8	3.11E-05	CACCTATATGGAGTGG	
PA1156	**nrdA**	**RNR class Ia, α subunit**	**-398**	**-383**	**2.88E-07**	**CCCCTATATCTTGGGT**	**nrdAB - NrdR-box 2**
PA1156	**nrdA**	**RNR class Ia, α subunit**	**-194**	**-179**	**1.70E-05**	**CCACTAGGTATTGTGT**	**nrdDG - NrdR-box 4**
PA1156	**nrdA**	**RNR class Ia, α subunit**	**-429**	**-414**	**2.70E-05**	**GCGCATTACTTGTTAT**	**nrdAB - NrdR-box 1**
PA1157		**Probable TCS response regulator**	**-125**	**-110**	**4.86E-08**	**CCACAATATGTAGTT**	**nrdAB - NrdR-box 3**
PA1157		Probable TCS response regulator	-350	-335	1.27E-05	ACCCAAGATATAGGGG	
PA1383		Hypothetical protein	-181	-166	2.25E-06	CCACTTCATGTAGTGG	
PA1388		Hypothetical protein	-32	-17	2.72E-05	CCACTACGTCTTGTAG	
PA1802	clpX	ClpX protease	-42	-27	1.94E-05	TGCCTTCATCTTGTGT	
PA1884		Probable transcriptional regulator	-56	-41	4.27E-05	TTCCAATATATTGGAC	
PA1920	**nrdD**	**RNR class III**	**-57**	**-42**	**1.15E-06**	**CCACAACATATTGTTG**	**nrdDG - NrdR-box 1**
PA1920	**nrdD**	**RNR class III**	**-26**	**-11**	**3.37E-06**	**ACACATCATGTTGTGG**	**nrdDG - NrdR-box 2**
PA2167		Hypothetical protein	-250	-235	4.60E-05	CCCCTCCATCTAGAAG	
PA2229		Conserved hypothetical protein	-53	-38	3.39E-05	GGACTCTATTGTAT	
PA2523	czcR	Heavy metal resp., TCS response regulator	-21	-6	2.35E-05	ATACTTTATATAGGGG	
PA3011	topA	DNA topoisomerase I	-76	-61	3.72E-07	CCACTATATATAGCGG	topA - Single NrdR-box
PA4210	phzA1	Phenazine biosynthesis protein PhzA1	-388	-373	3.86E-05	CTACCAGATCTTGTAG	
PA4280	birA	BirA bifunctional protein	-38	-23	3.54E-05	CCTCTATATGATGCGT	
PA4523		Hypothetical protein	-152	-137	3.11E-05	ACCCTCTATCTAGATT	
PA5325	sphA	Sphingosine-dependent virulence factor	-156	-141	1.04E-05	TCCCATCATATAGCGT	
PA5497	**nrdJa**	**RNR class II, polypeptide A**	**-7**	**8**	**2.25E-05**	**TAACTAGATGTTGCGT**	**nrdJab - NrdR-box 2**
PA5497	**nrdJa**	**RNR class II, polypeptide A**	**-38**	**-23**	**2.41E-05**	**ACACAAGATATTGATT**	**nrdJab - NrdR-box 1**

Supplementary Table S5. Transcriptomic effects of *nrdR* inactivation, RNA-seq study in *P. aeruginosa*.

DEGs in a Δ*nrdR* mutant strain in *P. aeruginosa* compared to its isogenic wild-type PAO1 strain. DEGs were only accepted with a false discovery rate (FDR) lower than 0.01 and a log(fold-change) higher than 1.0. Low quality mapping hits and poorly expressed genes were filtered out. Genes are listed by locus-tag; when available, gene name and a short functional description are also included. Genes in operons displaying putative NrdR-boxes in their upstream region (see Supplementary Table S4) are indicated. Genes in the *nrd* operons are highlighted in bold.

Upregulated genes					
Gene			Δ*nrdR* vs WT		NrdR-box
Locus	Name	Function/Product	LogFC	FDR	Comments
PA0201		Hypothetical protein	1.22	2.20E-41	
PA0526		Hypothetical protein	1.27	8.62E-34	
PA0527	*dnr*	Transcriptional regulator Dnr	1.26	2.54E-71	
PA0604		ABC transporter	1.20	4.56E-85	
PA0605		ABC transporter permease	1.40	5.82E-42	
PA0606		ABC transporter permease	1.41	5.60E-61	
PA0779		ATP-dependent protease	1.43	3.80E-90	
PA0839		Transcriptional regulator	2.60	2.79E-223	
PA0996	*pqsA*	Anthranilate-CoA ligase	2.54	0.00E+00	
PA0997	*pqsB*	Hypothetical protein	2.44	3.21E-268	
PA0998	*pqsC*	Hypothetical protein	2.29	2.64E-163	
PA0999	*pqsD*	3-oxoacyl-ACP synthase	1.95	1.58E-93	
PA1000	*pqsE*	Thioesterase PqsE	1.77	8.17E-111	
PA1001	*phnA*	Anthranilate synthase component I	1.86	1.19E-100	
PA1002	*phnB*	Anthranilate synthase component II	1.82	2.98E-117	
PA1154		Hypothetical protein	2.31	1.40E-53	
PA1155	***nrdB***	**RNR class Ia, β subunit**	**1.78**	**3.63E-156**	**NrdR-box pair (+2)**
PA1156	***nrdA***	**RNR class Ia, α subunit**	**1.63**	**4.63E-93**	**NrdR-box pair (+2)**
PA1331		Hypothetical protein	1.46	5.16E-135	
PA1429		Cation-transporting P-type ATPase	1.24	2.16E-65	
PA1546	*hemN*	Oxygen-independent coproporphyrinogen-III oxidase	1.24	1.13E-95	
PA1596	*htpG*	Chaperone protein HtpG	1.32	3.89E-74	
PA1597		Hypothetical protein	1.97	8.81E-184	
PA1600		Cytochrome C	1.92	1.01E-108	
PA1601		Aldehyde dehydrogenase	1.83	6.93E-202	
PA1602		Oxidoreductase	1.81	5.83E-140	
PA1649		Short-chain dehydrogenase	1.54	2.87E-67	
PA1690	*pscU*	Translocation protein in type III secretion	1.06	6.33E-39	
PA1691	*pscT*	Translocation protein in type III secretion	1.12	1.06E-31	
PA1692		Translocation protein in type III secretion	1.07	1.23E-33	
PA1694	*pscQ*	Type III secretion system protein	1.27	2.11E-71	
PA1695	*pscP*	Translocation protein in type III secretion	1.28	1.50E-46	
PA1696	*pscO*	Translocation protein in type III secretion	1.15	1.27E-51	
PA1698	*popN*	Type III secretion outer membrane protein PopN	1.03	5.26E-50	
PA1700		Hypothetical protein	1.01	3.78E-39	
PA1701		Hypothetical protein	1.22	2.29E-31	
PA1702		Hypothetical protein	1.26	4.50E-28	
PA1703	*pcrD*	Type III secretory apparatus protein PcrD	1.08	5.05E-79	
PA1707	*pcrH*	Regulatory protein PcrH	1.24	3.67E-48	
PA1708	*popB*	Translocator protein PopB	1.11	2.74E-86	
PA1709	*popD*	Translocator outer membrane protein PopD	1.03	5.57E-70	
PA1715	*pscB*	Type III export apparatus protein	1.04	6.56E-56	
PA1721	*pscH*	Type III export protein PscH	1.06	8.49E-45	

PA1722	*pscI*	Type III export protein PscI	1.01	3.34E-44	
PA1896		Hypothetical protein	1.12	1.68E-08	
PA1919	***nrdG***	**RNR class III activating protein**	**4.89**	**1.05E-155**	**NrdR-box pair**
PA1920	***nrdD***	**RNR class III**	**6.33**	**0.00E+00**	**NrdR-box pair**
PA2018		Multidrug efflux protein	1.37	1.01E-126	
PA2019		Multidrug efflux lipoprotein	1.57	1.36E-48	
PA2193	*hcnA*	Hydrogen cyanide synthase subunit HcnA	1.20	1.09E-24	
PA2194	*hcnB*	Hydrogen cyanide synthase subunit HcnB	1.11	4.54E-33	
PA2322		Gluconate permease	1.42	9.49E-60	
PA2403		Hypothetical protein	1.35	2.47E-99	
PA2404		Hypothetical protein	1.42	1.36E-89	
PA2405		Hypothetical protein	1.41	1.09E-80	
PA2406		Hypothetical protein	1.53	1.95E-78	
PA2407		Adhesion protein	1.66	4.85E-135	
PA2408		ABC transporter ATP-binding protein	1.53	6.27E-43	
PA2409		ABC transporter permease	1.41	2.08E-84	
PA2410		Hypothetical protein	1.22	1.83E-67	
PA2550		Acyl-CoA dehydrogenase	2.77	5.73E-261	
PA2593	*qteE*	Quorum threshold expression protein QteE	1.23	5.65E-18	
PA3126	*ibpA*	Heat-shock protein IbpA	1.08	9.59E-51	
PA3327		Non-ribosomal peptide synthetase	1.79	1.25E-88	
PA3328		FAD-dependent monooxygenase	2.28	1.45E-37	
PA3329		Hypothetical protein	1.73	1.59E-19	
PA3330		Short-chain dehydrogenase	1.46	1.02E-13	
PA3331		Cytochrome P450	1.66	1.67E-26	
PA3332		Hypothetical protein	1.88	2.05E-19	
PA3333	*fabH2*	3-oxoacyl-ACP synthase III	1.60	1.93E-17	
PA3334		Acyl carrier protein	1.26	1.80E-12	
PA3427		Short-chain dehydrogenase	1.17	2.47E-58	
PA3449		Hypothetical protein	1.35	7.50E-11	
PA3479	*rhlA*	Rhamnosyltransferase subunit A	1.03	4.83E-14	
PA3661		Hypothetical protein	1.11	4.11E-09	
PA3912		Hypothetical protein	1.08	9.41E-35	
PA4056	*ribD*	Riboflavin-specific deaminase/reductase	1.49	4.54E-64	
PA4057	*nrdR*	Transcriptional regulator NrdR	1.34	6.56E-127	
PA4218		Transporter	2.22	2.14E-56	
PA4219		Hypothetical protein	1.63	2.85E-60	
PA4220		Hypothetical protein	1.36	2.25E-21	
PA4221	*fptA*	Fe(III)-pyochelin outer membrane receptor	1.41	1.83E-72	
PA4222		ABC transporter ATP-binding protein	1.27	1.38E-26	
PA4223		ABC transporter ATP-binding protein	1.05	2.03E-32	
PA4224	*pchG*	Pyochelin biosynthetic protein PchG	1.74	2.11E-47	
PA4225	*pchF*	Pyochelin synthetase	1.81	2.22E-89	
PA4226	*pchE*	Dihydroaeruginoic acid synthetase	1.86	1.97E-108	
PA4228	*pchD*	2%2C3-dihydroxybenzoate-AMP ligase	1.61	1.60E-39	
PA4229	*pchC*	Pyochelin biosynthetic protein PchC	1.63	2.94E-22	
PA4230	*pchB*	Isochorismate-pyruvate lyase	1.84	8.25E-17	

Locus	Name	Function/Product	LogFC	P-value	Comments
PA4231	pchA	Salicylate biosynthesis isochorismate synthase	1.58	5.14E-40	
PA4542	clpB	Chaperone protein ClpB	1.12	2.39E-89	
PA4759	dapB	4-hydroxy-tetrahydrodipicolinate reductase	1.29	2.96E-123	
PA4760	dnaJ	Molecular chaperone DnaJ	1.22	1.73E-69	
PA4761	dnaK	Molecular chaperone DnaK	1.28	3.15E-84	
PA4762	grpE	Heat shock protein GrpE	1.05	1.44E-64	
PA5020		Acyl-CoA dehydrogenase	2.01	1.51E-169	
PA5054	hslU	ATP-dependent protease ATP-binding subunit HslU	1.33	1.71E-112	
PA5055		Hypothetical protein	1.28	3.59E-77	
PA5207		Phosphate transporter	1.12	5.07E-52	
PA5496	**nrdJb**	**RNR class II, polypeptide B**	**3.29**	**0.00E+00**	**NrdR-box pair**
PA5497	**nrdJa**	**RNR class II, polypeptide A**	**3.66**	**0.00E+00**	**NrdR-box pair**

Downregulated genes					
Gene			ΔnrdR vs WT		NrdR-box
Locus	Name	Function/Product	LogFC	P-value	Comments
PA0132		Beta alanine--pyruvate transaminase	-1.28	1.46E-54	
PA0887	acsA	Acetyl-CoA synthetase	-1.10	5.72E-57	
PA1744		Hypothetical protein	-2.19	2.44E-12	
PA1942		Hypothetical protein	-3.21	7.98E-75	
PA1970		Hypothetical protein	-1.16	2.14E-11	
PA2394	pvdN	Pyoverdine biosynthesis protein PvdN	-1.15	9.20E-19	
PA2395	pvdO	Pyoverdine biosynthesis protein PvdO	-1.40	7.52E-39	
PA2400	pvdJ	Pyoverdine biosynthesis protein PvdJ	-1.05	5.63E-47	
PA2402		Peptide synthase	-1.13	5.03E-91	
PA2411		Thioesterase	-1.10	4.98E-38	
PA2412		Hypothetical protein	-1.16	5.01E-22	
PA2413	pvdH	Diaminobutyrate--2-oxoglutarate aminotransferase	-1.22	1.53E-37	
PA2424		Peptide synthase	-1.50	5.89E-86	
PA2425	pvdG	Pyoverdine biosynthesis protein PvdG	-1.14	7.54E-09	
PA2426	pvdS	Extracytoplasmic-function sigma-70 factor	-1.59	5.25E-31	
PA2474		Hypothetical protein	-7.32	3.82E-16	
PA2475		Cytochrome P450	-10.89	1.29E-159	
PA2476	dsbG	Thiol:disulfide interchange protein DsbG	-12.30	0.00E+00	
PA2477		Thiol:disulfide interchange protein	-11.36	8.12E-170	
PA2478		Thiol:disulfide interchange protein DsbD	-9.25	9.89E-282	
PA2479		Two-component response regulator	-7.52	2.69E-101	
PA2480		Two-component sensor	-9.43	1.35E-146	
PA2481		Hypothetical protein	-11.86	0.00E+00	
PA2482		Cytochrome C	-11.52	0.00E+00	
PA2483		Hypothetical protein	-10.81	0.00E+00	
PA2484		Hypothetical protein	-10.45	9.10E-297	
PA2485		Hypothetical protein	-10.56	1.19E-137	
PA2486		Hypothetical protein	-10.18	3.95E-102	
PA2487		Hypothetical protein	-10.20	2.51E-105	
PA2488		Transcriptional regulator	-8.54	4.36E-116	

PA2489		Transcriptional regulator	-10.55	5.12E-100
PA2490		Hypothetical protein	-8.40	2.87E-29
PA2491		Oxidoreductase	-11.09	0.00E+00
PA2492	*mexT*	Transcriptional regulator MexT	-9.61	0.00E+00
PA2493	*mexE*	Multidrug efflux membrane fusion protein MexE	-7.95	0.00E+00
PA2494	*mexF*	Multidrug efflux transporter MexF	-6.51	0.00E+00
PA2495	*oprN*	Multidrug efflux outer membrane protein OprN	-5.32	0.00E+00
PA2754a		Hypothetical protein	-1.05	4.27E-14
PA2759		Hypothetical protein	-1.23	2.71E-20
PA2811		ABC transporter permease	-1.58	8.53E-127
PA2812		ABC transporter ATP-binding protein	-1.85	5.49E-219
PA2813		Glutathione S-transferase	-3.14	0.00E+00
PA3038		Porin	-1.09	1.81E-49
PA3189		Sugar ABC transporter permease	-1.06	4.68E-53
PA3229		Hypothetical protein	-4.13	0.00E+00
PA3234		Acetate permease	-1.25	9.17E-77
PA3235		Hypothetical protein	-1.31	9.68E-73
PA3268		TonB-dependent receptor	-1.20	3.79E-96
PA3496		Hypothetical protein	-1.23	2.68E-30
PA3530		Hypothetical protein	-1.30	4.77E-66
PA3568		Propionyl-CoA synthetase	-1.12	8.31E-37
PA3901	*fecA*	Fe(III) dicitrate transporter FecA	-2.51	1.53E-299
PA4354		Hypothetical protein	-2.32	1.08E-183
PA4355		Major facilitator superfamily transporter	-1.84	1.59E-161
PA4356	*xenB*	Xenobiotic reductase	-1.72	5.29E-134
PA4514		Iron transport outer membrane receptor	-2.10	1.15E-214
PA4623		Hypothetical protein	-1.36	5.05E-17
PA4710	*phuR*	Heme/hemoglobin uptake outer membrane receptor	-1.32	1.04E-44
PA4881		Hypothetical protein	-5.03	1.00E-161
PA5171	*arcA*	Arginine deiminase	-1.71	4.53E-140
PA5172	*arcB*	Ornithine carbamoyltransferase	-2.50	1.29E-231
PA5173	*arcC*	Carbamate kinase	-2.46	0.00E+00

Supplementary Table S6. SEC-MALS protein-conjugate analysis.

Protein-conjugate analysis (ASTRA 7, Wyatt Technology) applied to SEC-MALS data of NrdR-nucleotide complexes (see Table 1 and Figure 4). Data corresponding to $NrdR_2$ (*E. coli*) assayed with nucleotide only present in the running buffer (without pre-incubation) or pre-incubated with the protein as well. Molecular weight (weight-average molar mass) of the complex (total), the NrdR fraction (protein), and the nucleotide fraction (co-factor). All values in KDa; errors listed as ± standard deviation. All data, as well as the interpretation given in the composition column, correspond to the center of peaks encompassing multiple quaternary structures.

	Without pre-incubation			With pre-incubation		
Nucleotide	**Mw (protein)**	**Mw (co-factor)**	**Composition**	**Mw (protein)**	**Mw (co-factor)**	**Composition**
+ ATP	135.59 ± 0.29	4.98 ± 0.30	R_8 + $ATP_{9\text{-}10}$	193.80 ± 0.51	7.09 ± 0.53	R_{10}+$ATP_{13\text{-}15}$
+ dATP	109.36 ± 0.21	4.36 ± 0.22	R_6 + $dATP_{8\text{-}9}$	117.49 ± 0.22	4.73 ± 0.22	R_6 + $dATP_{9\text{-}10}$

Supplementary Figure S1. Ion-paired reverse phase HPLC quantification of nucleotides bound to NrdR.

A; Nucleotide quantification in the supernatant of PCA-precipitated protein samples, expressed as percentages of nucleotide-bound protein. Supernatants of as-prepared NrdR$_1$ protein from *E. coli* (top) and NrdR-H$_6$ protein from *P. aeruginosa* (bottom) are represented in the first column. The next two columns correspond to proteins pre-incubated with the desired nucleotide co-factor, treated with size-exclusion desalting columns to remove non-bound nucleotides, and finally precipitated with PCA. dADP was not included in this analysis. **B-I**; raw chromatograms, representing absorbance units (260 nm). Peaks are labeled with their elution time and colour-coded for convenience. (**B**) is a control experiment without protein in which 20 µM of ATP and 20 µM of dATP were subject to the PCA precipitation protocol to evaluate the stability of the nucleotide themselves under acid treatment. The pie chart details the effects for ATP: 87.62% of ATP was recovered as ATP, 8.77% as ADP and 1.07% as AMP; 2.54% was not recovered. (**C**) is a control experiment without protein in which 20 µmol of ATP were eliminated from the sample using a size-exclusion desalting column. The pie chart details the effects of the procedure: 97.57% of nucleotide was successfully eliminated. (**D,E,F**) correspond to the experiments using NrdR$_1$ from *E. coli*, summarized in panel A. (**G,H,I**) correspond to the experiments using NrdR-H$_6$ from *P. aeruginosa*, summarized in panel A.
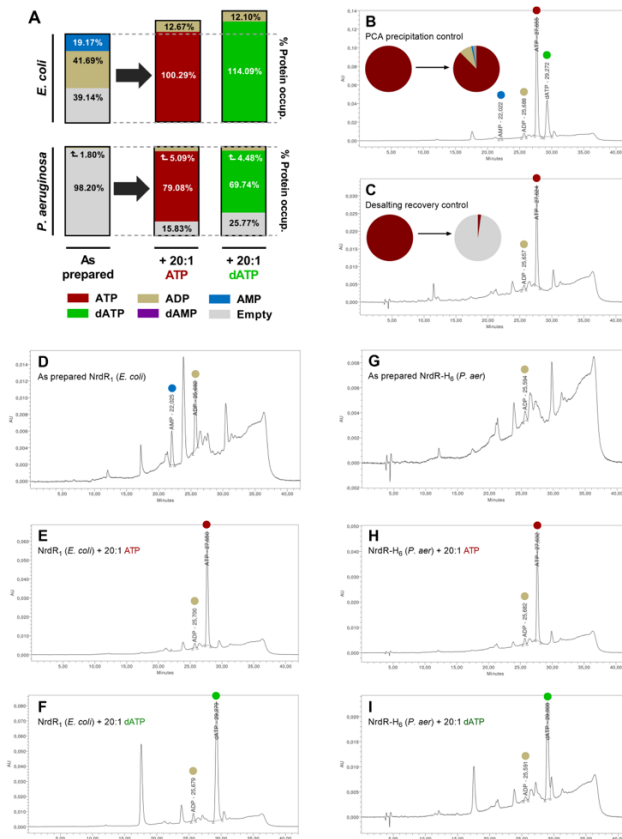
Supplementary Figure S2. SEC-MALS study of NrdR-nucleotide complexes (*P. aeruginosa*).

SEC-MALS results of NrdR$_2$ (*P. aeruginosa*) exposed to 0.025 mM nucleotide in the running buffer. Left Y axis (solid lines) represents MALS detection data normalized to a maximum signal of 1.0 in each sample. Right OY axis (dashed lines) represents weight-average molar mass (KDa). Numbers near the peaks indicate the minimum and maximum weight-average molar mass for the corresponding peaks. Results are representative of two independent experiments.
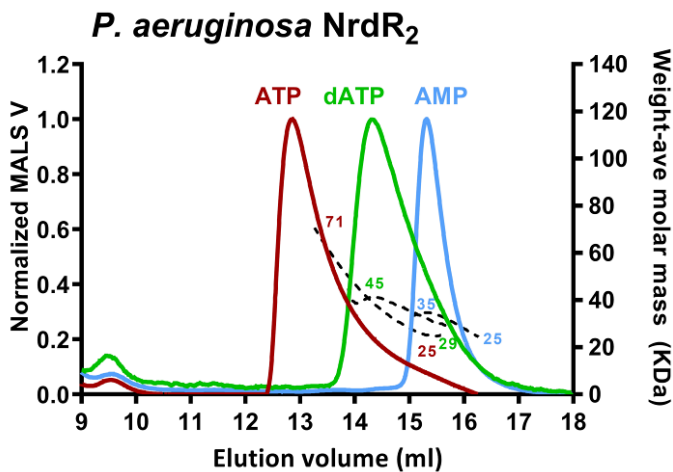
Supplementary Figure S3. Full images of EMSA gels.

Full, unedited images of EMSA gels performed using NrdR$_2$ proteins from *E. coli* and *P. aeruginosa*. Two DNA probes were used: P*nrdA*, containing the promoter from the *nrdAB-yfaE* operon in *E. coli* (NrdR sensitive, labeled P*nrdA* (ECO)) and an NrdR-insensitive negative control labeled Ctrl(-). Numbers below the gels indicate the molar ratio of NrdR protein and marked DNA (0:1, 2000:1, and 4000:1 for *E. coli*, 0:1, 2500:1, and 5000:1 for *P. aeruginosa*). Nucleotides indicated below the protein ratios were pre-incubated with NrdR at a fixed 20:1 nucleotide:protein ratio. Two replicate experiments are provided for both protein sources.
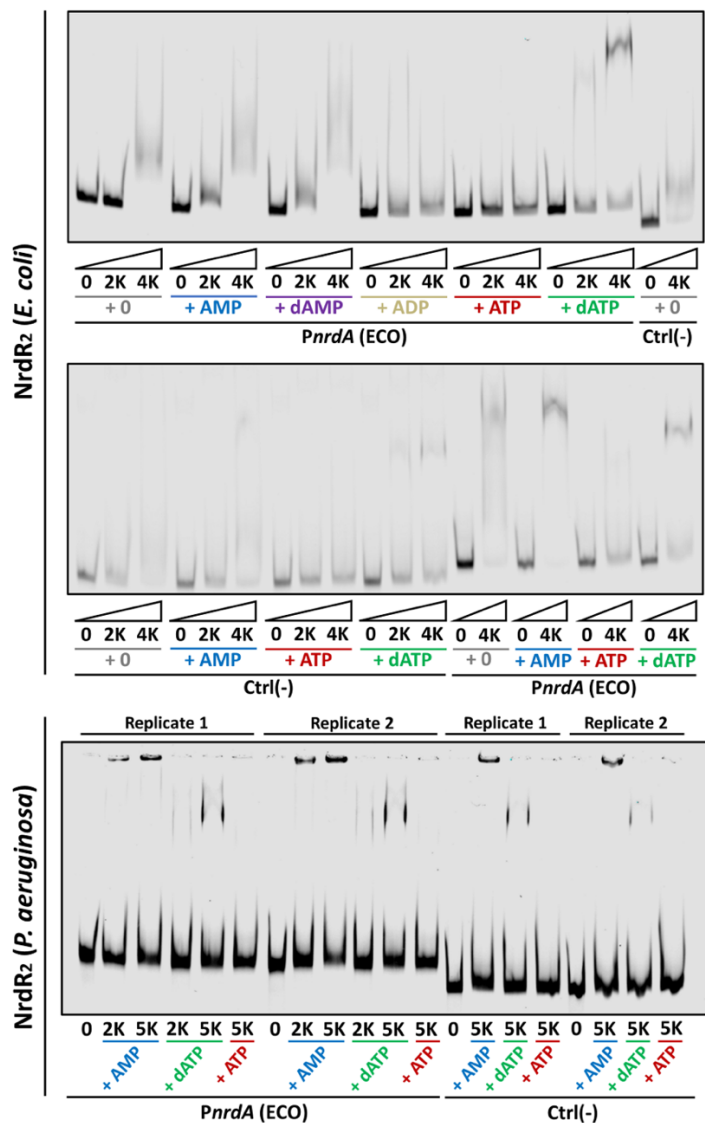
Supplementary Figure S4. Comparative analysis of Δ*nrdR* transcriptomics data.

A; Comparison of enriched gene ontology (GO) biological processes in the DEGs determined from *nrdR* mutant strains of *E. coli* K-12 *substr*. MG1655 (see Supplementary Table S2) and *P. aeruginosa* PAO1 (see Supplementary Table S4), compared to their corresponding wild-type strains. Lists of enriched GO IDs were produced using PANTHER (47, 48), summarized and analyzed with REVIGO (49) and plotted using R Treemap (50). **B;** Representation of the correlation between DEGs in *P. aeruginosa* and its corresponding orthologs in *E. coli*, as determined by the aforementioned studies. Each square represents a gene in the *P. aeruginosa* genome, from top left (PA0001 *dnaA*) to bottom right (PA5570 *rpmH*). Green-coloured squares represent genes upregulated in PAO Δ*nrdR*, while red-coloured genes were downregulated. Blue-coloured squares represent genes for which at least one ortholog was found to be differentially expressed in *E. coli*. Yellow squares represent genes differentially expressed in both species; operons including these genes are circled in red and detailed to the right. Orthologous genes were determined using OrtholugeDB (51).
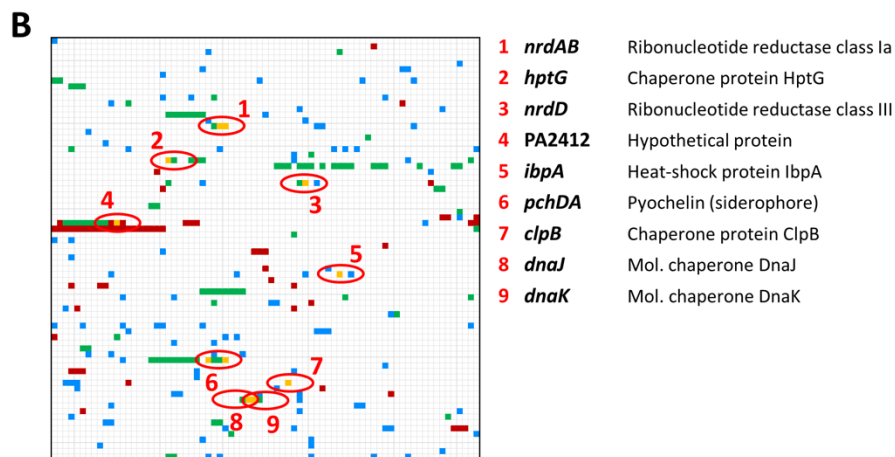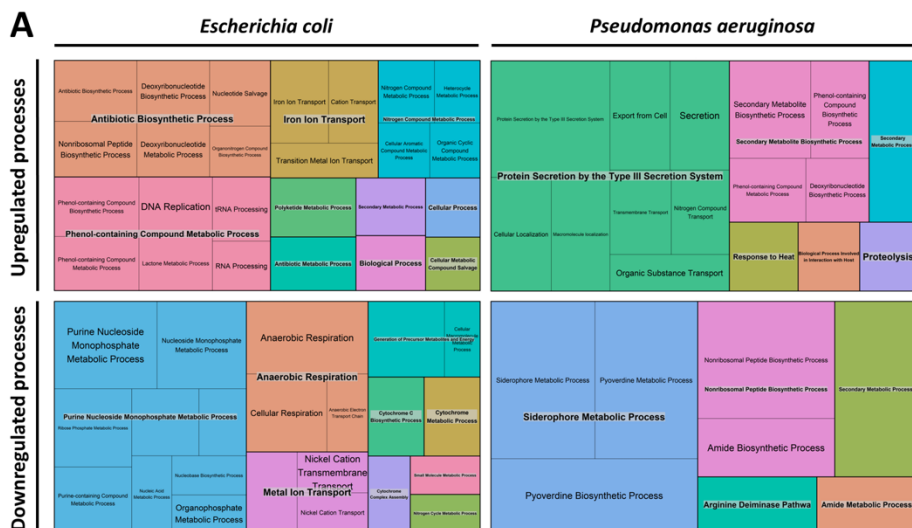
Artículo 4: 3D spatial organization and improved antibiotic treatment of a *Pseudomonas aeruginosa–Staphylococcus aureus* wound biofilm by nanoparticle enzyme delivery.

Alba Rubio-Canalejas, Aida Baelo, Sara Herbera, Núria Blanco-Cabra, Marija Vukomanovic and Eduard Torrents

Resumen

Las heridas y su tratamiento suponen un elevado gasto para la salud pública entre materiales, profesionales y hospitalización (271). Además, las heridas rompen la barrera protectora de la piel haciendo que aumente la susceptibilidad a infecciones y lo que dificulta la cicatrización. *P. aeruginosa* y *S. aureus* son dos patógenos que se encuentran comúnmente infectando heridas (243). La coexistencia de ambas especies bacterianas en una infección aumenta su resistencia y/o tolerancia a los antimicrobianos debido a la relación sinérgica que se desarrollan entre ellas (229). Además, durante la infección estas bacterias crecen embebidas dentro de un biofilm formado por polisacáridos, proteínas, lípidos y eDNA tal y como se desarrolló el en sección 2 de la introducción de esta tesis. El crecimiento en biofilm y la matriz extracelular generada protege a las bacterias del sistema inmune del hospedador y de agentes externos como antibióticos, haciendo que la infección se vuelva mucho más recalcitrante con un estado inflamatorio persistente que aumenta el daño en los tejidos (272). Entre las heridas crónicas infectadas están incluidas las infecciones de heridas quirúrgicas, las quemaduras, las úlceras de pie, pierna o de cúbito (216). La aparición de heridas infectadas y su difícil eliminación ponen de manifiesto la imperiosa necesidad de encontrar nuevas estrategias que ayuden a romper el biofilm formado para eliminar este tipo de infecciones.

Uno de los objetivos principales de este proyecto era evaluar la capacidad antibiofilm de terapias combinatorias de antibióticos con enzimas que degradan distintos componentes de la EPS del biofilm (que se relaciona con el objetivo 4 de esta tesis). De esta forma, lo que se buscaba era romper la matriz del biofilm usando enzimas específicas para

favorecer la disgregación de éste y la penetrabilidad de los antibióticos y así aumentar su eficacia. En este trabajo se probaron cuatro enzimas distintas, dos hidrolasas, (celulasa y α-amilasa), una nucleasa (DNasa I) y una proteasa (proteinasa K). Además, las enzimas se inmovilizaron sobre nanopartículas de plata y se evaluó el efecto antimicrobiano sobre la viabilidad bacteriana y la penetrabilidad de los antibióticos. El otro objetivo era estudiar la localización de las especies bacterianas *P. aeruginosa* y *S. aureus* dentro del biofilm para entender su relación e interacciones. Para abordar los objetivos de este proyecto hemos utilizado un modelo *in vitro* de herida (wound-like biofilm, WLB) infectada que describe el comportamiento, la fisiología y el microambiente de un biofilm bajo estas condiciones.

En el artículo publicado se muestran los resultados que cumplen con el Objetivos 4 de esta tesis. En una infección dual por *P. aeruginosa* y *S. aureus* es importante usar una combinación de antibióticos, como por ejemplo gentamicina y ciprofloxacina, para que la terapia sea efectiva contra ambos patógenos. En nuestro trabajo pudimos ver que el uso de un único antibiótico, gentamicina o ciprofloxacina era efectivo contra ambas especies en cultivo planctónico, pero no cuando las bacterias crecían dentro del biofilm, donde su tolerancia antimicrobiana es mayor (Figura 1 del Artículo 4). También se evaluó la capacidad antimicrobiana de nanopartículas de plata (AgNP) en el WLB, observando que las AgNP ejercían un efecto visible contra *P. aeruginosa,* pero no contra *S. aureus* (Figura 3 del Artículo 4)*.* Finalmente se estudió el efecto de diferentes estrategias antibiofilm y antimicrobianas contra *P. aeruginosa* y *S. aureus* en el WLB. Se combinó el uso de los antibióticos gentamicina y ciprofloxacina con enzimas que rompen y disgregan los componentes de la EPS (celulasa, α-amilasa, DNasa I y proteinasa K) en su forma soluble o inmovilizadas en AgNP. Los ensayos antimicrobianos mostraron que la combinación de antibióticos y las enzimas celulasa y α-amilasa tenían una mayor actividad antibiofilm contra *P. aeruginosa* que contra *S. aureus.* La enzima DNasa I es la que mostró mayor actividad antimicrobiana, y con este tratamiento se consiguió la mayor reducción del mayor número de células viables de *P. aeruginosa*, y aumentó el número de células libres de *S. aureus.* Al usar proteinasa K como terapia antibiofilm no se observó un aumento de la efectividad de los antibióticos, por lo que se podría decir que esta enzima tiene una baja actividad antibiofilm en comparación con el resto de los tratamientos utilizados. En general se observó que en todas las estrategias de disgregación la actividad de las enzimas inmovilizadas sobre AgNP era mayor que la enzima soluble (Figura 4 del Artículo 4).

Seguidamente evaluamos la disposición espacial de las bacterias infectantes en este modelo. Para ello, el WLB se cortó transversalmente para obtener tres partes, Superior, Media e Inferior. Cada una de las partes se observó con el microscopio electrónico de barrido (FE-SEM) y con el microscopio confocal (CLSM) para analizar la matriz del biofilm y la distribución espacial de *P. aeruginosa* y *S. aureus* dentro de este sistema. Se observó que cada especie bacteriana forma microcolonias y que las microcolonias de una especie bacteriana están separadas físicamente de las otras. Las microcolonias de *P. aeruginosa* se encuentran mayoritariamente en las regiones Superior e Inferior, en cambio *S. aureus* se encuentra en todo el WLB formando agregados bacterianos compactos. También se estudió el efecto de los antibióticos gentamicina y ciprofloxacina sobre la matriz y en la distribución bacteriana. Con la microscopía SEM se observó que el uso de antibióticos convirtió a la matriz en una malla de porosa con agujeros y menor cantidad de EPS. Las imágenes con CLSM muestran una menor viabilidad bacteriana, especialmente en *P. aeruginosa* (Figura 5 del Artículo 4)*.* El efecto de la DNasa I sobre el WLB también se observó con CLSM. El uso de DNasa I aumentó la actividad de los antibióticos ya que se observó una disminución en el número de células de *P. aeruginosa* en comparación a las muestras sin enzima*.* También se observó un aumento en el número de células libres de *S. aureus*, mayoritariamente en las zonas Superior e Inferior del WLB*.* El uso de DNasa I inmovilizada sobre AgNP mejoró actividad de la enzima libre, observando una mayor cantidad de células de *S. aureus* disgregadas (Figura 6 del Artículo 4). Finalmente, se analizó el eDNA del WLB utilizando CLSM. El uso de DNasa I disminuyó notablemente el eDNA presente en el WLB, especialmente cuando la enzima se encontraba inmovilizada sobre AgNP (Figura 7 del Artículo 4).

Publicación

🔄 Check for updates

3D spatial organization and improved antibiotic treatment of a *Pseudomonas aeruginosa–Staphylococcus aureus* wound biofilm by nanoparticle enzyme delivery

Alba Rubio-Canalejas[1], Aida Baelo[1], Sara Herbera[1],
Núria Blanco-Cabra[1,2], Marija Vukomanovic[3] and
Eduard Torrents[1,2]*

[1]Bacterial Infections and Antimicrobial Therapies Group, Institute for Bioengineering of Catalonia, The Barcelona Institute of Science and Technology, Barcelona, Spain, [2]Microbiology Section, Department of Genetics, Microbiology and Statistics, Faculty of Biology, University of Barcelona, Barcelona, Spain, [3]Advanced Materials Department, Institute Jozef Stefan, Ljubljana, Slovenia

Chronic wounds infected by *Pseudomonas aeruginosa* and *Staphylococcus aureus* are a relevant health problem worldwide because these pathogens grow embedded in a network of polysaccharides, proteins, lipids, and extracellular DNA, named biofilm, that hinders the transport of antibiotics and increases their antimicrobial tolerance. It is necessary to investigate therapies that improve the penetrability and efficacy of antibiotics. In this context, our main objectives were to study the relationship between *P. aeruginosa* and *S. aureus* and how their relationship can affect the antimicrobial treatment and investigate whether functionalized silver nanoparticles can improve the antibiotic therapy. We used an optimized *in vitro* wound model that mimics an *in vivo* wound to co-culture *P. aeruginosa* and *S. aureus* biofilm. The *in vitro* wound biofilm was treated with antimicrobial combinatory therapies composed of antibiotics (gentamycin and ciprofloxacin) and biofilm-dispersing free or silver nanoparticles functionalized with enzymes (α-amylase, cellulase, DNase I, or proteinase K) to study their antibiofilm efficacy. The interaction and colocalization of *P. aeruginosa* and *S. aureus* in a wound-like biofilm were examined and detailed characterized by confocal and electronic microscopy. We demonstrated that antibiotic monotherapy is inefficient as it differentially affects the two bacterial species in the mixed biofilm, driving *P. aeruginosa* to overcome *S. aureus* when using ciprofloxacin and the contrary when using gentamicin. In contrast, dual-antibiotic therapy efficiently reduces both species while maintaining a balanced population. In addition, DNase I nanoparticle treatment had a potent antibiofilm effect, decreasing *P. aeruginosa* and *S. aureus* viability to 0.017 and 7.7%, respectively, in combined antibiotics. The results showed that using nanoparticles functionalized with DNase I enhanced the antimicrobial treatment, decreasing the bacterial viability more than using the antibiotics alone. The enzymes α-amylase and

159

cellulase showed some antibiofilm effect but were less effective compared to the DNase I treatment. Proteinase K showed insignificant antibiofilm effect. Finally, we proposed a three-dimensional colocalization model consisting of *S. aureus* aggregates within the biofilm structure, which could be associated with the low efficacy of antibiofilm treatments on bacteria. Thus, designing a clinical treatment that combines antibiofilm enzymes and antibiotics may be essential to eliminating chronic wound infections.

KEYWORDS

biofilm, wound healing, chronic infection, antimicrobial therapies, nanoparticle

Introduction

Wounds and wound management represent a relevant but sometimes unrecognized, growing challenge for healthcare and the economic system worldwide. Only wound management accounts for 3% of the total healthcare expenses such as materials, professionals, and hospitalization costs, among others (Lindholm and Searle, 2016). Wound features entail susceptibility to microbial colonization and proliferation, leading to infection and wound-healing difficulties (Zhao et al., 2016).

Commonly, infected wounds have an acute or a chronic etiology depending on their healing time frame and healing capacity (Zhao et al., 2016). However, a remarkable 80% of chronic wounds contain biofilms (Malone et al., 2017), and 1.5–2 million people in Europe and around 6.5 million people in the USA are affected by this condition (Lindholm and Searle, 2016). Many dermal infections, including surgical, burn, or bite wound infections and other skin abrasions, are classified as acute and are solved in a timely fashion. Nonetheless, some patients suffer from pathologic conditions such as diabetes, obesity, immunosuppression, or drug treatments, which predispose the delayed or failed healing of infected wounds. Foot, leg, and decubitus ulcers are the most representative examples of chronic infections (Zhao et al., 2016). Indeed, chronic wounds are also associated with a persistent host inflammatory state and an incomplete antimicrobial response against treatments (Zhao et al., 2016).

Free bacteria irreversibly attach to the surface of wounds and rapidly divide and recruit other microorganisms to form microcolonies (Fleming and Rumbaugh, 2017), a process regulated by environmental or physiological cues (Liu et al., 2016). Eventually, microcolonies evolve into a tridimensional, generally polymicrobial community known as biofilm (Liu et al., 2019). Biofilm presence in wounds is associated with chronicity and wound complications. Nevertheless, proper biofilm-based wound care and management strategies can minimize wound-healing impact in our society. Currently, wound debridement, systemic antibiotics, biocides, and antibiofilm agents are the main strategies against wound biofilms (Hrynyshyn et al., 2022). However, it is imperative to develop new effective strategies that are tested prospectively and employed in chronic wounds to support the healing process and reduce infection rates (Percival et al., 2012).

Pseudomonas aeruginosa and *Staphylococcus aureus* are two ubiquitous opportunistic pathogens most frequently isolated from biofilm-based chronic infections (DeLeon et al., 2014). These bacteria have a complex relationship in nature where they can show a competitive interplay as the exoproducts produced by *P. aeruginosa* suppress *S. aureus* growth and even provoke the appearance of small colony variants in the staphylococcal population (Kumar and Ting, 2015; Cendra et al., 2019; Cendra and Torrents, 2021). However, the polymicrobial nature of most biofilms allows bacteria to exploit synergistic relationships and therefore favors their cooperation and virulent traits (Dalton et al., 2011). Interestingly, the dual infection of these bacteria increases their resistance and/or tolerance to antimicrobials, prevalence, tissue colonization, and their ability to delay healing (DeLeon et al., 2014; Brothers et al., 2015).

Bacteria in biofilms are protected by a self-synthesized extracellular polymeric matrix formed by polysaccharides, proteins, lipids, and extracellular DNA (eDNA), commonly called extracellular polymeric substance (EPS) (Fleming and Rumbaugh, 2017). The encapsulation of bacteria inside the biofilm provides the acquisition of new features different from their planktonic states, such as a dormant state, the host immune system avoidance, or resistance/tolerance to some antimicrobial treatments. The biofilm is a mechanical barrier against endogenous and exogenous antimicrobial strategies that impedes the reepithelization process (Fleming et al., 2017).

Notwithstanding, mature biofilms are dynamic. The bacteria forming the biofilm can actively modify it during their lifecycle in response to environmental changes (i.e., nutrient starvation and oxygen depletion, accumulation of toxic products, immune system challenges, quorum sensing, and others) (Fleming and Rumbaugh, 2017). Eventually, planktonic cells are released from

the biofilm and migrate to more favorable environments, always promoting bacterial survival (Fleming and Rumbaugh, 2017). In nature, the dispersion of bacteria can be accomplished through the segregation of bacterial biofilm-dispersing enzymes that act on the EPS. Some studies have already evaluated the capacity of various biofilm-dispersing enzymes such as glycolytic hydrolases, proteases, and DNases to increase biofilm disaggregation and the number of free bacteria (Tetz and Tetz, 2010; Fleming et al., 2017). Interestingly, the use of biofilm-dispersing enzymes is a potential pre-treatment as they increase the susceptibility of the biofilm-forming bacteria (Redman et al., 2021). In addition, the dual infection of chronic wounds with *P. aeruginosa* and *S. aureus* in the clinical setting shows the importance of using a combinatory therapy of antibiotics to target both bacterial pathogens (Serra et al., 2015). The antibiotic combination may depend on the patient and the clinical outcome of the chronic wound. There are treatments with different classes of antibiotics, such as penicillin, cephalosporins, aminoglycosides, and fluoroquinolones (Garner et al., 2020).

Due to the complexity of the biofilm and the wound-healing process, it is difficult to find an *in vivo* or *in vitro* model that appropriately describes the biofilm's behavior, physiology, and microenvironment in the skin (Klein et al., 2018). Here, we use an optimized wound-like biofilm *in vitro* model previously described (Sun et al., 2008; DeLeon et al., 2014) that allows *P. aeruginosa* and *S. aureus* co-culture in the wound environment, similar to *in vivo* conditions.

In this study, we used a convenient and reliable *in vitro* wound-like biofilm model to evaluate the efficacy of different antibiofilm strategies. We used four biofilm-dispersing enzymatic treatments combined with antibiotics to test their effect on bacterial viability. Also, we aim to better understand the *P. aeruginosa* and *S. aureus* synergistic relationship by studying their interactions and colocalization inside the biofilm.

Materials and methods

Bacterial strains and growth conditions

Pseudomonas aeruginosa PAO1 (ATCC 15692) and *Staphylococcus aureus* SA31 (ATCC 29213) were maintained in initial cryo-stock cultures at $-80°C$, and they resuscitated in Luria-Bertani (LB) agar (Scharlab, S.L., Spain) and Tryptic Soy Agar (TSA) (Scharlab, S.L., Spain) plates, respectively. Isolated colonies were grown overnight in LB broth and Tryptic Soy Broth (TSB) (Scharlab, S.L., Spain), respectively, at $37°C$ with shaking at 200 rpm. Unless otherwise specified, all reagents were purchased from Sigma, Spain.

Antibiotics and matrix-degrading enzymes

The antibiotics gentamicin sulfate (Gm) (PanReac AppliChem, Spain) and ciprofloxacin hydrochloride (Cip) (Cayman Chemical, USA) were employed simultaneously at a final concentration of $13.5 \mu g/ml$ according to the values shown in Supplementary Figure S1. α-amylase from *Bacillus subtilis* (MP Biomedicals, USA), cellulase from *Aspergillus niger* (MP Biomedicals, USA), deoxyribonuclease I from bovine pancreas (DNase I), and proteinase K from *Tritirachium album* (PanReac AppliChem, Spain) were used as biofilm-dispersing enzymes at different concentrations. The enzymes were tested alone or with gentamicin and ciprofloxacin.

Antibacterial susceptibility testing and MIC_{50}

P. aeruginosa PAO1 and *S. aureus* SA31 grew on LB and TSB, respectively, until they reached an optical density (OD_{550} nm) of 0.1, which corresponds to 10^7 CFU/ml for each bacterial species. The bacteria were plated in a microtiter plate (Corning 3596 Polystyrene Flat Bottom 96 Well, Corning, USA) using several concentrations of gentamicin (from 0.0613 to 64 $\mu g/ml$), ciprofloxacin (from 0.0613 to 64 $\mu g/ml$), or silver nanoparticles (AgNP, from 0.03125 to 1 mg/ml). Bacterial growth at $37°C$ and 150 rpm was monitored for 16 h, measuring the absorbance at 550 nm every 15 min in a SPARK Multimode microplate reader (Tecan, Switzerland). The minimum inhibitory concentration of 50% (MIC_{50}) corresponds with the concentration of the antibiotics that inhibited bacterial growth by 50%.

Nanoparticle synthesis and characterization

AgNP immobilized with enzymes were formed using α-amylase, cellulase, DNase I, and proteinase K. The nanoparticles were synthesized using the chemical reduction method (Kandarp Mavani, 2013). Different options were investigated to functionalize the enzymes on the nanoparticles. (1) Aqueous solutions of silver nitrate ($AgNO_3$) (50 ml, 4 mM) and enzyme (25 ml, 0.4 mg/ml) were premixed for 10 min (200 rpm, $25°C$). It was followed by the addition of sodium borohydride ($NaBH_4$) (50 ml, 6 mM), which resulted in instant nanoparticle formation. (2) For forming bare AgNP, silver precursor was premixed with water following $NaBH_4$ reduction. Reaction mixtures were kept for 2 h at 200 rpm and then centrifuged at 8,000 rpm for 20 min to collect formed AgNP. In the next step, AgNP were re-dispersed in fresh enzyme solutions in Tris-buffer (50 mM Tris-HCl, pH = 8) and mixed for 2 days (200 rpm, $25°C$). The

Artículo 4: 3D spatial organization and improved antibiotic treatment of a *Pseudomonas aeruginosa-Staphylococcus aureus* wound biofilm by nanoparticle enzyme delivery

Rubio-Canalejas et al.   10.3389/fmicb.2022.959156

maximum enzymatic activity was obtained with the two-step approach. The resulting dispersions were precipitated by centrifugation at 8,000 rpm, washed in fresh Tris-HCl, frozen in liquid nitrogen, and freeze-dried. All syntheses were done using lab-made ultra-pure water (Purelab Option-Q7, ELGA, UK).

Nanoparticle-enzyme activity quantification

The α-amylase and cellulase activities in the grafted AgNP were quantified by calculating the amount of reducing sugars produced in the polysaccharides' hydrolysis by DNS (3,5 dinitrosalicylic acid) method (Miller, 1959) following the protocol of Bernfeld (1955) for the α-amylase enzymatic activity and the protocol described by Wood and Bhat (1988) for the cellulase activity. Briefly, 10 mg/ml of starch was diluted in 400 μl of 0.02 M phosphate buffer and mixed with 400 μl of the α-amylase-AgNP for 3 min at 20°C. On the contrary, 20 mg/ml of sodium carboxymethyl cellulose (Acros Organics, Spain) diluted in 200 μl of 0.05 M citrate buffer was mixed with 200 μl of the cellulase-AgNP for 30 min at 50°C. Both reactions were stopped by adding the color reagent solution (1.06 M potassium sodium tartrate tetrahydrate and 43 mM DNS) and then boiled (400 μl of color reagent solution added and then boiled for 15 min in the α-amylase reaction, and 600 μl of color reagent solution added and then boiled for 5 min in the cellulase reaction). Standard curves of the reducing sugars produced in the reaction (maltose for α-amylase and glucose for cellulase) were performed by mixing different concentrations of the reducing sugars with the color reagent solution at the same volume ratio as with the AgNP. Colorimetric quantification of reducing sugars was performed by absorbance measurement at 540 nm. One unit is defined as the amount of enzyme which liberated 1 μmole of a reducing sugar per minute under the assay conditions.

To calculate the NP DNase I activity, 100 ng of *P. aeruginosa* genomic DNA was mixed with known concentrations of AgNP containing DNase I (up to 20 μl final volume). The mixtures were incubated for 30 min at 37°C, then loaded into a 0.8% agarose gel stained with ethidium bromide, and visualized under the UV light in a Gel Doc[TM] XR+ (Bio-Rad Laboratories, Spain). The DNase I activity was calculated by quantifying DNA degradation with Quantity One (Bio-Rad Laboratories, Spain) software. One unit is defined as the enzyme that degrades 1 μg of DNA per hour.

Proteinase K-AgNP activity was determined by quantifying tyrosine released from denatured hemoglobin proteolysis by the Folin–Ciocalteu assay (Anson, 1938). Briefly, 2.5 ml of a hemoglobin substrate solution (2% hemoglobin and 6 M urea in 100 mM potassium phosphate buffer) was mixed with 0.5 ml of the Proteinase K-AgNP and incubated at 37°C for 10 min. The reaction was stopped by adding 5 ml of 5% trichloroacetic acid,

and the solution was filtered through a 0.45 μm filter. About 1.5 ml of 1 N of Folin and Ciocalteu's phenol reagent was then added to 2.5 ml of the filtered product of the proteolysis reaction or the standard tyrosine solution (1.1 mM L-Tyr). The solutions were incubated for 30 min at room temperature, and the tyrosine was quantified by absorbance measurement at 750 nm. One unit of enzyme will produce 1 μmole of tyrosine per minute.

The commercial enzymes at known concentrations were used as a control to determine the activity of the enzyme-coated nanoparticles in each activity quantification assay.

In vitro wound-like biofilm model

The wound-like medium (WLM) was made by combining 45% Bolton broth (Scharlab, S.L., Spain), 50% bovine plasma (VWR, Biowest SAS, France), and 5% lacked horse red blood cells (hemolyzed RBCs, Thermo Scientific Oxoid Ltd., UK) as described previously to a final 1 ml volume per WLB experiment (Sun et al., 2008; Dalton et al., 2011; DeLeon et al., 2014). About 1 ml of the WLM was placed in a 12 × 75 mm glass tube, inoculated with ~10^4 CFU/mL of fresh *S. aureus* and *P. aeruginosa* cultures, and grown at 37°C for 24 h in static conditions until forming the wound-like biofilm clot.

Wound-like biofilm antimicrobial assays

Antibiotics, enzymes, or nanoparticle-coated enzymes were freshly diluted in sterile 1x phosphate-buffered saline (PBS) (Fisher Scientific, Spain) to a final concentration of 13.5 μg/ml for gentamycin and ciprofloxacin, 20 and 40 μg/ml for α-amylase, 100 and 200 μg/ml for cellulase, 0.2 and 0.4 μg/ml for DNase I, 20 and 40 μg/ml for proteinase K, and 1 and 2 mg/ml for the AgNP. The wound-like biofilms (WLBs) were gently mixed avoiding biofilm disruption with 1 ml of the disaggregating solutions to be tested and left at 37°C for 16 h in static conditions. After incubation, WLBs were rinsed once with 1 ml of 1x PBS and weighted in an Entris Precision Balance (Sartorius, Goettingen, Germany). The WLBs were weighed inside a tube, and afterward, the weight of the tube was subtracted. Washed WLBs were resuspended with 1 ml of 1x PBS + 0.05% Tween20 (Sigma-Aldrich, Spain) and dispersed using a homogenizer T 10 basic ULTRA TURRAX (IKA-Werke GmbH & Co. KG, Germany) with an 8 mm diameter probe. The samples were diluted in PBS + 0.05% Tween 20, plated on *Staphylococcus* isolation agar [TSA containing 7.5% (w/v) of NaCl] and *Pseudomonas* isolation agar (LB agar containing 2 mg/ml of crystal violet), and incubated overnight at 37°C (Supplementary Figure S2). The total counts of each bacterial strain were used to determine the colony-forming units per gram of WLB clot (CFU/g).

Wound-like biofilm staining and confocal microscopy imaging

The WLB clot was cut into three slices, top, middle, and bottom, to study the structure and spatial organization of *P. aeruginosa* and *S. aureus* inside the biofilm using the Bacterial Viability and Gram Stain Kit (Biotium, Fremont, USA). This kit combines the dye DAPI, which binds to the bacterial DNA, and the wheat germ agglutinin (WGA) coupled to a CFTM-488A fluorophore that binds the N-acetylglucosamine present in the peptidoglycan of gram-positive bacteria; thus, *P. aeruginosa* was stained with DAPI, and *S. aureus* was stained with DAPI and WGA. After staining, the samples were incubated for 60 min on ice. To discriminate between genomic bacterial DNA and eDNA, two dyes were used: SYTO60 (Thermo Scientific Oxoid Ltd., UK), which stains the genomic bacterial DNA, and TOTO-1 (Thermo Scientific Oxoid Ltd., UK), which stains the eDNA. The samples were incubated for 15 min on ice after staining. A Zeiss LSM 800 confocal laser scanning microscope (CSLM, Zeiss, Germany) was used to scan the samples. ImageJ and COMSTAT 2 software were used to measure clusters areas, analyze the images, and quantify eDNA (Heydorn et al., 2000).

Scanning electron microscopy imaging of the clots

Field-emission scanning electron microscopy (FE-SEM) was used to visualize the structure and distributions of bacterial species in the mixed-species WLB. WLB clots were cut into slices and introduced into a 3% glutaraldehyde solution. After 3 h, the solution was replaced by fresh glutaraldehyde solution and incubated overnight at 4°C. Clot samples were subsequently washed three times with $1 \times$ PBS, and dehydration was later performed by immersing the samples in increased ethanol concentrations (30, 50, 70, 90, and 100% v/v) for 30 min. The clots were afterward dried with a Critical Point Dryer (CPD BalTec 030, BalTec AG, Liechtenstein), covered with gold, and visualized using the field-emission scanning microscope Nova NanoSEM 230 (FEI Company, USA).

Transmission electron microscopy

Transmission electron microscopy (TEM) investigation was performed at Tecnai Spirit 120 kV microscope. Nanoparticles were dispersed in water using an ultrasonic bath for a couple of minutes and deposited on copper lacey carbon grids.

Statistical analysis

GraphPad Prism 9.0 (GraphPad Software, USA) was used to perform statistical analyses and generate histograms. Data values were expressed as the mean ± standard deviation. Significant differences between conditions were determined using unpaired Student's *t*-tests.

Results

Different antibiotic resistance of *P. aeruginosa* and *S. aureus* growing in a wound-like biofilm

The aminoglycoside gentamicin (Gm) and the fluoroquinolone ciprofloxacin (Cip) are broad-spectrum antibiotics commonly used to treat wounds containing *P. aeruginosa* and *S. aureus* infections (Serra et al., 2015; Negut et al., 2018). These antibiotics display high activity against non-resistant strains of both species. In this work, we determined the MIC_{50} values of gentamicin and ciprofloxacin in planktonic cultures of *P. aeruginosa* and *S. aureus* (Figure 1A). We used the previously described WLB model (see Materials and methods) that mimics an infected wound with a co-culture of *P. aeruginosa* and *S. aureus* to evaluate the local treatment efficacy of gentamicin and ciprofloxacin.

Although the *P. aeruginosa* and *S. aureus* monomicrobial planktonic cultures are susceptible to gentamicin and ciprofloxacin (MIC_{50} ranges from 0.25 to 1 µg/ml, Figure 1A), the biofilm structure found in the WLB confers protection to the bacteria, favoring the appearance of tolerance traits against antimicrobial treatments (Fazli et al., 2009). Figures 1B–E reflects the different bactericidal effects of gentamicin and ciprofloxacin when *P. aeruginosa* and *S. aureus* grew on polymicrobial WLB for 24 h. After 24 h, we observed that ciprofloxacin reduced *P. aeruginosa* cell number by 3.5 logs, while less than one log was reduced for *S. aureus*. The gentamicin treatment produced the opposite effect and reduced 1.5 log number for *S. aureus* and by less than a log for *P. aeruginosa* cells (Figures 1B–D). Considering both bacteria (*P. aeruginosa* plus *S. aureus*), the treatment with gentamicin reduced the total cell number by 0.83 logs, and ciprofloxacin reduced around 2.1 logs of the bacteria. Only when both antibiotics were used simultaneously, the whole cell number was reduced by more than 3.2 log number (Figures 1B,E).

Immobilization and characterization of biofilm disaggregate silver nanoparticles

To target the matrix of polymicrobial biofilms more effectively, we designed nanosized particles with enzymes (α-amylase, cellulase, DNase I, and proteinase K) immobilized

FIGURE 1
Bactericidal effect of ciprofloxacin and gentamicin. **(A)** MIC$_{50}$ values of ciprofloxacin (Cip) and gentamicin (Gm) on *P. aeruginosa* (*P. aer*) and *S. aureus* (*S. aur*) in planktonic culture. **(B)** Log number of bacterial cell of *P. aeruginosa*, *S. aureus*, and total bacteria comparing treated (with ciprofloxacin and gentamicin at 13.5 μg/ml) to untreated samples after 24 h in a dual-species WLB. **(C–E)** Bacterial cell number in the clot (CFU/g) measured over 24 h without treatment, with ciprofloxacin, gentamicin, and gentamicin + ciprofloxacin at a final concentration of 13.5 μg/ml. **(C)** Cell number of *P. aeruginosa*, **(D)** *S. aureus*, and **(E)** total bacteria (*P. aeruginosa* and *S. aureus*).

TABLE 1 Composition, encapsulation efficiency, and properties of drug-loaded nanoparticles.

	Enzyme coupled	Enzyme activity (U/mg NP)	Effective diameter (nm)	Polydispersity index	Z-potential (mV)
AgNP	–	–	1,172 ± 28	0.304 ± 0.025	−3.5 ± 9
AgNP-α-amylase	α-amylase	55.89	101.9 ± 1.0	0.320 ± 0.004	−17.1 ± 0.6
AgNP-Cellulase	Cellulase	0.15	28.4 ± 0.2	0.365 ± 0.004	−20.1 ± 1.4
AgNP-DNase I	DNase I	276	39.3 ± 0.2	0.233 ± 0.005	−16.1 ± 12
AgNP-Proteinase K	Proteinase K	0.37	356.1 ± 17	0.324 ± 0.009	−20.0 ± 1.5

on their surface (see specifications in Table 1). Along with the potential improvement in antibacterial treatment obtained by decomposing the matrix, the enzymes were meant to point toward the most relevant components that keep the stability of the matrix preventing the activity of antibiotics. Formed AgNP were nanospheres with cubic crystalline structure (JCPDS No. 4-0783) (Figures 2A,B). Without the enzyme, they were unstable aggregates with almost neutral zeta potential and high effective diameter (Table 1). These aggregates were formed of nanoparticles with broad size distribution (Figure 2B). Once the enzymes were immobilized to the AgNP surface, their

stability improved significantly. It was observed an increase of up to 5.7 times in the magnitude of their zeta potentials and a significant reduction of up to 41 times in their effective diameters (Table 1). TEM analysis revealed that different enzymes protected particle growth and stability differently. The most effective were DNase I and cellulase, which kept the primary grains to a few tens of nanometers, while α-amylase and proteinase K protected AgNP from growing larger (Figure 2B). Another proof for immobilization-affected stability was the changes detected in AgNP optical spectra (Figure 2C). Due to intensive agglomeration, non-immobilized AgNP did not show

FIGURE 2

Characterization of silver nanoparticles (AgNP). **(A)** X-ray diffraction patterns of bare AgNP and AgNP with immobilized α-amylase, DNase I, proteinase K, and cellulase. **(B)** TEM images of AgNP with different surfaces: bare AgNP without enzyme (a), AgNP with proteinase K (b), DNase I (c), α-amylase (d), and cellulase (e). Images on the left present particle size and agglomeration, while those on the right look closely at the organic coating immobilized on their surface. **(C)** UV-vis spectra showing the stability of AgNP without and with different enzymes (DNase I, α-amylase, cellulase, and proteinase K) immobilized to their surface based on the presence or absence of surface plasmon resonance maximum (SPR), its position, and width.

any surface plasmon resonance maximum (SPR), which was detected for all the enzyme immobilized AgNP. The narrowest SPR, which shifted to lower wavelengths, was detected for the most stable DNase I and cellulase-protected AgNP. Although immobilization of the enzymes protected AgNP growth most effectively in the case of DNase I and cellulase, the activity of enzymes immobilized to their surface differs significantly. While DNase I immobilized to AgNP retained high enzymatic activity (276 U/mg NP), the activity obtained for cellulase on AgNP was much lower (0.15 U/mg NP) (see detailed characterization in Table 1). According to the highest morphological stability

and enzymatic activity, it could be expected that AgNP-DNase I would be the most effective in disaggregating EPS matrix and in penetration inside its volume.

Silver nanoparticles have a different effect on bacteria in the wound-like biofilm

Our kinetics assays reveal that the silver released from the AgNP had a differential antibacterial effect

FIGURE 3

Antimicrobial capacity of silver nanoparticles (AgNP) on *P. aeruginosa* and *S. aureus*. Antimicrobial kinetic assay of silver nanoparticles (AgNP) on *P. aeruginosa* and *S. aureus* planktonic cultures **(A,B)** and dual-species WLB **(C,D)**. Different AgNP concentrations were used to determine the best antimicrobial concentration. The statistical analysis to determine significance was performed using the Student Unpaired t-test (*$0.01 < p < 0.05$; **$p < 0.01$; vs. non-treated WLB).

on planktonic cultures of *P. aeruginosa* and *S. aureus*. The antimicrobial activity of silver was higher against *P. aeruginosa*, whose growth was affected by low concentrations of AgNP (>0.03125 mg/ml) (Figure 3A) compared to the inhibition of *S. aureus,* which needed increased concentrations of AgNP (>0.25 mg/ml) (Figure 3B).

Figures 3C,D shows the antibacterial activity of the silver released from different AgNP concentrations on a WLB antimicrobial assay. When both strains grew together in a WLB, the biofilm structure protected *S. aureus* from the bactericidal action of the AgNP. The AgNP showed a bactericidal effect in WLB against *P. aeruginosa* when using a concentration of at least 1 mg/mL (Figure 3C). However, the

FIGURE 4

Differential response of antibiofilm treatments on *P. aeruginosa* and *S. aureus* polymicrobial WLB. WLB antimicrobial assays show the effect of the antibiofilm treatments consisting of ciprofloxacin (Cip) and gentamicin (Gm) antibiotics at a final concentration of 13.5 µg/ml each, along with a biofilm-dispersing enzyme in solution or functionalized on AgNP at a final concentration of 1 or 2 mg/ml. The concentration of enzyme indicated above the concentration of AgNP corresponds to the amount of enzyme functionalized on AgNP. Percentage of viability corresponds

(Continued)

167

FIGURE 4 (Continued)
to counts of CFU on plate from the bacteria in WLB. **(A,B)** α-amylase, **(C,D)**, cellulase **(E,F)**, DNase I, and **(G,H)** proteinase K. In each antimicrobial assay, three biological replicates were used, and two technical replicates were performed for each biological sample. The statistical analysis to determine significance was performed using the Student Unpaired *t*-test (■, $0.01 < p < 0.05$; ■■, $p < 0.01$, vs. non-treated WLB. *$0.01 < p < 0.05$; **$p < 0.01$; ***$p < 0.001$; vs. antibiotic-treated WLB. *$0.01 < p < 0.05$; **$p < 0.01$; ***$p < 0.001$; functionalized AgNP vs. enzyme in solution at the same conditions).

tested concentrations did not modify the *S. aureus* cell numbers (Figure 3D).

Effect of biofilm-dispersing strategies and antimicrobial therapies against *P. aeruginosa* and *S. aureus in vitro* wound-like biofilm model

We tested the ability of four enzymes that target different EPS components to disrupt the matrix structure of a *P. aeruginosa*–*S. aureus* polymicrobial biofilm. The biofilm-dispersing activity of these enzymes was tested using free enzymes or immobilized on AgNP at the same working concentration. In addition, the enzymes were tested alone or with gentamicin and ciprofloxacin to evaluate whether the combined treatment enhanced antibiotic efficacy against the dual-species wound biofilm.

The WLB antimicrobial assays using α-amylase and cellulase showed higher antibiofilm activity against *P. aeruginosa* than against *S. aureus* (Figures 4A–D). Regarding the general efficacy of these two enzymes, their impact on the biofilm was low. However, higher concentrations of α-amylase and cellulase could have been used to test whether the disruptive effect of the enzymes was increased. Besides, the results show that the activity of the immobilized enzyme AgNP was higher than the enzyme in its soluble form. Nonetheless, this outcome could be due to the antimicrobial effect of the silver rather than from the enzyme *per se*, just as is observed in Figure 3.

The use of DNase I combined with antibiotics had a remarkable effect against *P. aeruginosa* (Figure 4E). This effect was significantly higher when the enzyme was immobilized on AgNP and applied with antibiotics. Indeed, we and others already showed the outstanding ability of DNase I to inhibit and disperse *P. aeruginosa* biofilms (Baelo et al., 2015). The use of DNase I against *S. aureus* increased their cell number when using free and immobilized enzymes on AgNP. This increase was probably due to the bacterial disaggregation of *S. aureus* inside the biofilm (Figure 4F). Besides, as mentioned before, DNase I showed the highest stability and activity of all the enzymes immobilized to the AgNP surface. In addition, to study the behavior of single antibiotics and DNase I, we experimented using gentamicin or ciprofloxacin monotherapy with the same concentration of dispersing enzyme (Supplementary Figure S3). We observed that the viability of *P. aeruginosa* was higher

with gentamycin than with ciprofloxacin and that its viability decreased when the enzyme DNase I was used. On the contrary, the viability of *S. aureus* was higher when using ciprofloxacin than gentamycin, and the addition of DNase I increased the number of bacterial cells.

Finally, it was observed that none of the different proteinase K concentrations used in the biofilm assay dispersed the biofilm independently of the free or conjugated state of the enzyme (Figures 4G,H). This could be explained by the combination of low AgNP stability and low activity of enzymes immobilized at their surface. Higher enzyme concentrations could have been used to test whether the activity of proteinase K improved.

Spatial bacterial organization in the *P. aeruginosa*–*S. aureus* mixed *in vitro* wound reflects their different antibiotic resistance

We used the *in vitro* WLB model to analyze the microscopic structure and spatial distribution of *P. aeruginosa* and *S. aureus* polymicrobial wound biofilm. After wound biofilm-forming, we divided the wound biofilm clots into three different transversal parts (top, middle, and bottom) to analyze the localization of the different bacterial species, how they relate to each other, and if each species formed single-species aggregates inside the WLB (see scheme in Figure 5A). As the conditions inside the wound should be different, especially considering oxygen concentration in the different layers of the biofilm, we expected to see differences in the bacterial distribution, such as finding *P. aeruginosa* in the more aerobic parts of the biofilm. Each part was observed with FE-SEM (Figure 5B) and CLSM (Figure 5C). Both microscopy techniques showed that inside the untreated clot (PBS), each bacteria species was forming one-species clusters or microcolonies embedded in a highly dense matrix, which allowed the compartmentalization and physical separation of the different bacterial species. The images show that *P. aeruginosa* (PA) [in blue dashed circles in FE-SEM images and dyed with DAPI (blue) in the CSLM images] formed microcolonies located throughout the outside areas, mainly being present in the top and the bottom regions of the clot. However, *S. aureus* (SA) [in green dashed circles in FE-SEM images and dyed with DAPI and WGA (green) in the CSLM images] aggregated compactly, forming clusters placed mainly in the inside part of the clot. The size of the clusters increased as

Artículo 4: 3D spatial organization and improved antibiotic treatment of a *Pseudomonas aeruginosa-Staphylococcus aureus* wound biofilm by nanoparticle enzyme delivery

Rubio-Canalejas et al. 10.3389/fmicb.2022.959156

FIGURE 5
Spatial bacterial distribution in the *in vitro* wound biofilm system before and after antibiotic treatment. Analysis of the transversal parts of the WLB (top, middle, and bottom) **(A)** using FE-SEM **(B)** and CSLM **(C)**. In the FE-SEM images, blue and green dashed circles surround *P. aeruginosa* and *S. aureus* bacterial aggregates, respectively. In CSLM images, *P. aeruginosa* PAO1 (PA) is dyed with DAPI (blue), and *S. aureus* SA31 (SA) is stained with WGA (green). **(A)** Scheme of the three-dimensional WLB colocalization model proposed. **(B)** FE-SEM and **(C)** CSLM representative images of the transversal parts of *P- aeruginosa*–*S. aureus* two-species biofilm in the clots under the effect of a 16-h treatment of ciprofloxacin (Cip) and gentamicin (Gm) and left untreated (PBS). In each region of the clot (top, middle, and bottom), two biological replicates were used, and at least five technical replicates per sample were taken. The scale bar corresponds to 10 μm.
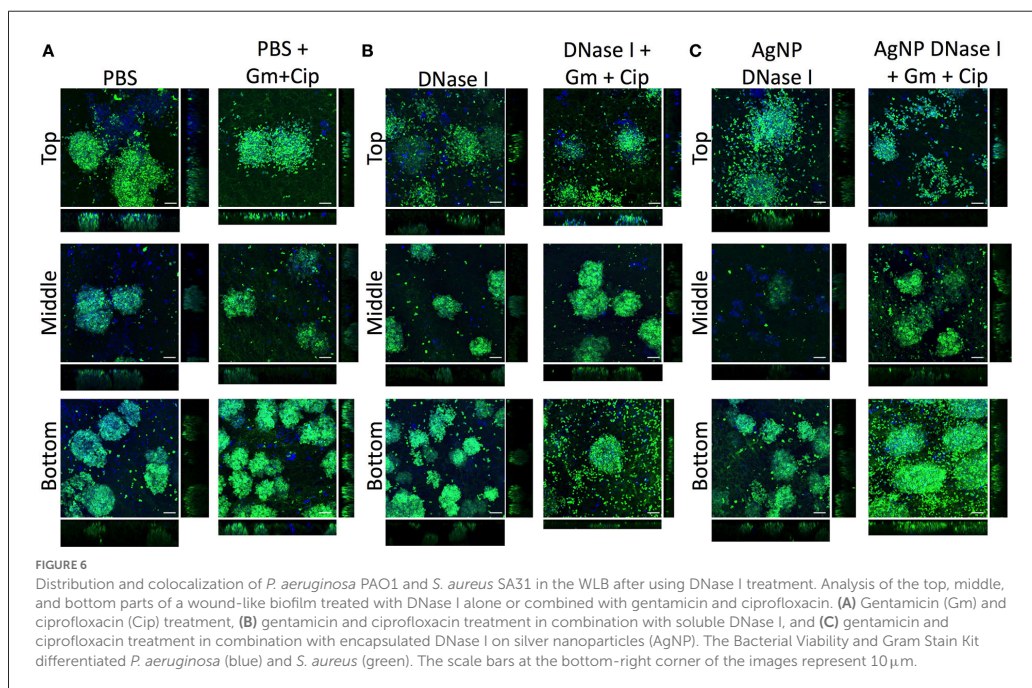
the layers deepened inside the clot, finding the largest *S. aureus* aggregates in the bottom region (Figures 5B,C). The size of the *S. aureus* clusters in each region was quantified and plotted in histograms. The histograms confirmed the cluster distribution observed in the WLB (Supplementary Figure S4).

Since we detected different responses to gentamicin and ciprofloxacin treatments in the wound biofilm environment that directly depended on the bacterial species (Figure 1), we hypothesized that the differential effect would depend on the location and distribution of each bacterium in the wound biofilm environment. The three-dimensional bacterial species organization and matrix composition of the clot might cause differential penetration of the antibiotics in different geographical areas of the biofilm. We used FE-SEM and CLSM to analyze the outcome of the transversal regions of the mixed wound biofilm after the antibiotic treatment. The FE-SEM images (Figure 5B) show that the overall biofilm structural appearance was modified after the antibiotic treatment. The images show that the biofilm matrix was changed completely, becoming a mesh of porous fibrin fibers with low EPS and a matrix with holes that included much bacterial debris. The CSLM (Figure 5C) images show the bacterial viability reductions observed in previous experiments (Figure 1). The combined use of gentamicin and ciprofloxacin resulted in a bacterial reduction load, especially for *P. aeruginosa*, throughout the different traversal parts of the WLB.

However, the bacterial reduction load for *S. aureus* seemed less clear.

DNase I degrade eDNA favoring bacterial dispersion and enhancing antibiotic penetration in the wound-like biofilm

The EPS in the WLB forms a complex structure that helps to protect the bacterial species from different antimicrobials or the host immune response. eDNA is a key element that forms part of the EPS and the structure of the WLB. The antibiofilm assays (Figure 4) showed that the enzyme DNase I increased the antimicrobial activity of combined gentamicin and ciprofloxacin against *P. aeruginosa* when used in combination, especially when the enzyme was immobilized on AgNP. However, the combination of DNase I and antibiotics increased the bacterial cell number of *S. aureus*. Therefore, we used CLSM to analyze the effect of DNase I on the bacterial structure inside the WLB (Figure 6). The first images show the bacterial structure inside the WLB without treatment and after treatment with gentamicin and ciprofloxacin (Figure 6A). It can be seen that each bacterial species (*P. aeruginosa* dyed with DAPI, in blue; and *S. aureus* dyed with DAPI and WGA, in green) was forming one-species microcolonies that were embedded inside the biofilm matrix.

FIGURE 6
Distribution and colocalization of *P. aeruginosa* PAO1 and *S. aureus* SA31 in the WLB after using DNase I treatment. Analysis of the top, middle, and bottom parts of a wound-like biofilm treated with DNase I alone or combined with gentamicin and ciprofloxacin. **(A)** Gentamicin (Gm) and ciprofloxacin (Cip) treatment, **(B)** gentamicin and ciprofloxacin treatment in combination with soluble DNase I, and **(C)** gentamicin and ciprofloxacin treatment in combination with encapsulated DNase I on silver nanoparticles (AgNP). The Bacterial Viability and Gram Stain Kit differentiated *P. aeruginosa* (blue) and *S. aureus* (green). The scale bars at the bottom-right corner of the images represent 10 μm.

After the antibiotic treatment, the cell number of both bacteria was reduced; however, the decrease of *S. aureus* was not as notable. The use of soluble DNase I (Figure 6B) resulted in the breakdown of the microcolonies of both bacteria.

The dissemination was more notable in the clusters of *S. aureus*, as the number of free single cells increased. The cluster dissemination was mainly observed in the top and bottom regions of the WLB, where single *S. aureus* cells were unattached from the primary aggregates. The use of gentamicin and ciprofloxacin mixed with DNase I decreased the viability of both species in the three transversal parts of the WLB (top, middle, and bottom). The decrease of *P. aeruginosa* in the bottom part of the clot was highly notable. In addition, AgNP coated with DNase I boosted the bacterial disaggregation from their microcolonies (Figure 6C). A similar outcome was observed in the *S. aureus* clusters. The dispersion observed after the use of DNase I-coated AgNP was higher compared to the soluble DNase I. The use of AgNP almost completely broke down the compact *S. aureus* clusters in the top region, and the number of *S. aureus* single cells found in the bottom region increased. The microcolony dissemination was enhanced when the enzyme was combined with antibiotics. The combination of enzyme-antibiotics reduced the total bacterial cell number, being more evident in *P. aeruginosa*.
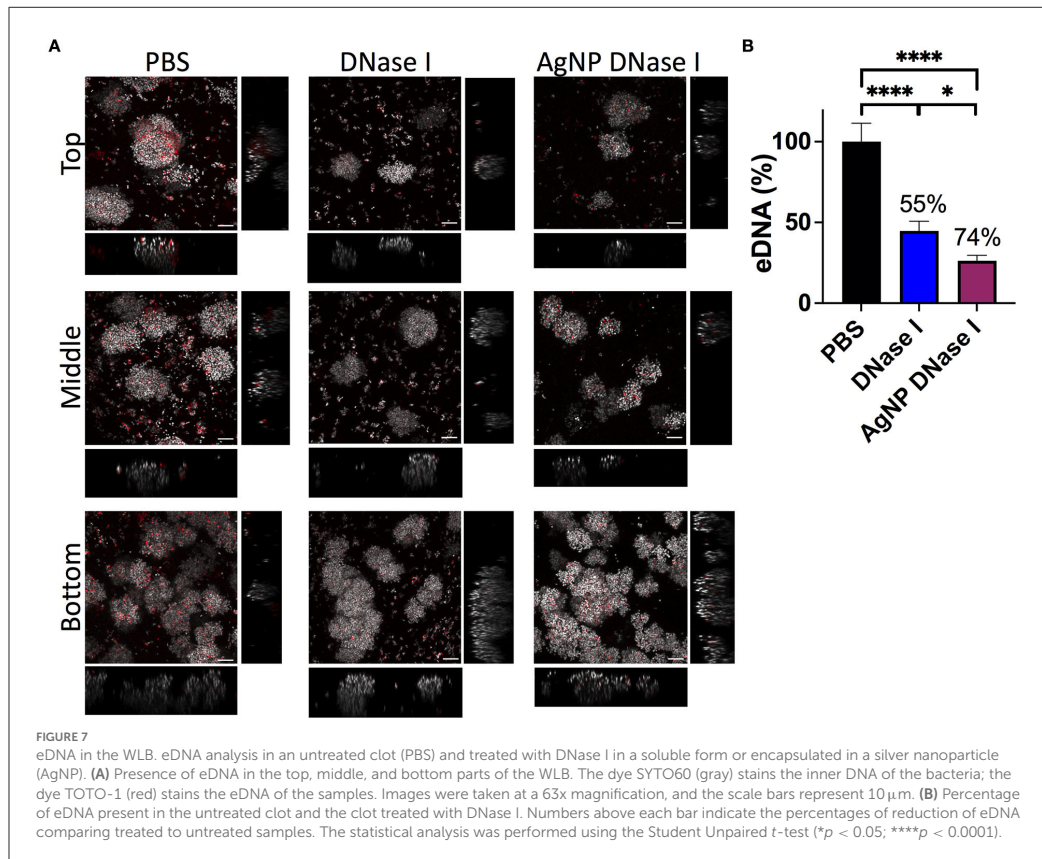
In addition, we deeply analyzed the eDNA present in the WLB with CLSM using an untreated clot and a clot treated with DNase I and AgNP coated with DNase I (Figure 7). The images show that the eDNA present in the WLB (stained with TOTO-1 in red) notably decreased when the clot was treated with DNase I (Figure 7A). It seems that eDNA degradation was more efficient where fewer bacteria were present, such as in the top and middle parts of the clot. We quantified the eDNA present in each sample (PBS, DNase I, and AgNP-DNase I) and calculated the percentage of eDNA reduction in the WLB after the treatments (Figure 7B). We determined that eDNA significantly decreased in the clot after treatment with DNase I in its soluble form and immobilized in AgNP by 55 and 74%, respectively. Moreover, the reduction observed when using AgNP-DNase I was significantly higher than the soluble and non-encapsulated DNase I.

Discussion

A particular biofilm's spatial structure and composition determine its pathogenicity and therapeutic responses. Thus, we deepened into an *in vitro* wound-like biofilm that contained a stable community of two of the most frequent bacteria found in wounds, *P. aeruginosa* and *S. aureus*. We explored how gentamicin and ciprofloxacin, two common broad-spectrum antibiotics, affected the viability of *P. aeruginosa* and *S. aureus* when growing as a dual-species wound biofilm. We expected

170

FIGURE 7
eDNA in the WLB. eDNA analysis in an untreated clot (PBS) and treated with DNase I in a soluble form or encapsulated in a silver nanoparticle (AgNP). **(A)** Presence of eDNA in the top, middle, and bottom parts of the WLB. The dye SYTO60 (gray) stains the inner DNA of the bacteria; the dye TOTO-1 (red) stains the eDNA of the samples. Images were taken at a 63x magnification, and the scale bars represent $10\,\mu m$. **(B)** Percentage of eDNA present in the untreated clot and the clot treated with DNase I. Numbers above each bar indicate the percentages of reduction of eDNA comparing treated to untreated samples. The statistical analysis was performed using the Student Unpaired t-test (*$p < 0.05$; ****$p < 0.0001$).

a reduced antibiotic susceptibility compared with monoculture biofilms since previous investigations already reported this behavior in the wound biofilm model (DeLeon et al., 2014). Besides, the antibiotics' effect on the species dynamics has not been previously analyzed. Here, we demonstrate that gentamicin and ciprofloxacin shift the population distribution in the wound biofilm environment, driving a particular bacterial species to outcompete the other. Whereas, *P. aeruginosa* remained unaffected by a 24-h treatment with gentamicin, its viability was reduced by 3.5 logs when ciprofloxacin was used.

On the contrary, *S. aureus* viability decreased by 1.5 logs when using gentamicin and nearly unchanged when using ciprofloxacin (Figure 1). The increased gentamicin tolerance of *P. aeruginosa* in the wound biofilm may be due to alginate, one of the main components of the EPS matrix, among other factors (DeLeon et al., 2014). The mechanism by which ciprofloxacin lacked activity against *S. aureus* in the wound biofilm has not yet been investigated. Still, other investigations have detected that *S. aureus* showed low susceptibility against ciprofloxacin

in a multispecies wound biofilm in which *P. aeruginosa* is co-cultured (DeLeon et al., 2014; Townsend et al., 2017). Recently, it was described that *S. aureus* was more tolerant to ciprofloxacin due to the inhibition of its respiration, which reduced ATP levels (Radlinski et al., 2017). However, ciprofloxacin possesses low solubility and permeability, leading to restricted diffusion into *S. aureus* cells. Whether *S. aureus* enhanced tolerance to ciprofloxacin due to *P. aeruginosa,* a restricted penetration into the wound biofilm structure, or both remains unexplored.

These outcomes show that only the use of both antibiotics combined had an additive effect and reduced the viability of *P. aeruginosa* and *S. aureus* by 3.2 logs. Other studies have shown that therapies combining different antibiotics are useful tools for treating biofilm-related infections (Ciofu et al., 2017). The response to antibiotic chemotherapies may be considered when treating biofilm infections since choosing the inappropriate antibiotic could lead to an unbalanced microbial population and enhance the growth of the more pathogenic bacteria. The dual-antibiotic therapy reduced the viability of

Artículo 4: 3D spatial organization and improved antibiotic treatment of a *Pseudomonas aeruginosa-Staphylococcus aureus* wound biofilm by nanoparticle enzyme delivery

Rubio-Canalejas et al.   10.3389/fmicb.2022.959156

both bacteria, improved the overall antibiotic efficacy, and maintained a more balanced population distribution, improving infection resolution.

One of the main biofilm treatment problems is some antibiotics' poor penetration. Therefore, there is an urgent need to find high penetrability antimicrobial compounds against chronic wound infections. Silver-containing creams are extensively used to treat burns and wounds as they reduce the viability of *P. aeruginosa* and *S. aureus* by 99% (Wu et al., 2014; Zhou et al., 2016). AgNP is an outstanding therapy against wound infections due to its enhanced inhibitory effect against bacteria and its ability to encapsulate large amounts of enzyme (Radulescu et al., 2016; Kumar et al., 2018). In this study, we produced AgNP with enzymes immobilized on their surface. We observed that the enzyme immobilization reduced the particle size and changed its zeta potential, increasing its penetrability (Figure 2). We determined the antimicrobial activity of AgNP on *P. aeruginosa* and *S. aureus* planktonic cultures and in WLB. The use of AgNP at low concentrations reduced the viability of *P. aeruginosa* and *S. aureus* when growing on planktonic cultures. When AgNP was used against a dual-species biofilm, the viability of *P. aeruginosa* decreased 10 times, whereas the total cell number of *S. aureus* was maintained (Figure 3). This result indicates that the AgNP cannot eliminate the bacteria embedded in the biofilm, probably because it does not penetrate completely into the EPS matrix.

Here, we explored the use of α-amylase, cellulase, DNase I, and proteinase K to disrupt EPS components that may be relevant in the polymicrobial wound model. In addition, we hypothesized that the viability of *P. aeruginosa* and *S. aureus* would decrease more using the enzymes immobilized on AgNP than in their free soluble form due to the silver antibacterial effect already observed (Figure 3).

α-amylase and cellulase have previously been shown to disperse the EPS in wound biofilms; thus, we hypothesized that these enzymes were promising to be used in combination therapies (Fleming et al., 2017; Fleming and Rumbaugh, 2018; Redman et al., 2020). Our results indicate that the viability of *P. aeruginosa* decreased when using α-amylase and cellulase, and this decrease was higher when the enzymes were immobilized on AgNP (Figures 4A,C). However, the viability of *S. aureus* increased when using these enzymes (Figures 4B,D), possibly due to the enzymatic dispersion of cells from the defined cluster increasing the bacterial cell number counts. Therefore, we believe that α-amylase and cellulase have an excellent potential to be used as antibiofilm compounds in combination therapies. Fleming et al. (2020) already observed the ability of glycoside hydrolase treatments to break the bacterial clusters of *P. aeruginosa* and *S. aureus*.

DNase I has been widely tested as an antibiofilm agent because of its ability to degrade eDNA, which is the major component of most single-species biofilms formed by *P. aeruginosa* and *S. aureus* (Sugimoto et al., 2018). Our results

indicate that DNase I was the most promising enzyme to be used because *P. aeruginosa* viability was significantly reduced when used in combination with gentamicin and ciprofloxacin. This decrease was more remarkable when the enzyme was immobilized on AgNP. This observation lines with Modak and Fox (1973). They observed that silver binds to DNA, interfering with bacterial replication, so the use of DNase I attached to AgNP may enhance the degradation of eDNA (Figure 4E) and possibly inhibit bacterial proliferation.

On the contrary, the number of viable cells of *S. aureus* increased when using DNase I, especially when the enzyme was immobilized. eDNA has been described to accumulate mainly in *S. aureus* aggregates in a wound biofilm model like we employed (Kucera et al., 2014). We hypothesized that the aggregated bacterial cells were disseminated when the eDNA was degraded, increasing the number of bacterial cells observed in the biofilm viability test (Figure 4F). This indicated that eDNA might have a role in reducing antibiotic susceptibility on the *S. aureus* aggregates surrounded by eDNA. These results support the idea that DNase I may be a strong antibiofilm compound, especially when linked to AgNP. Thus, the combination therapy of DNase I with antibiotics may be an important strategy for the future. In addition, the results using single antibiotics as monotherapy showed that using both antibiotics simultaneously is a better approach to target both bacterial species inside the wound.

Proteinase K is an unspecific serine endopeptidase that possesses hydrolytic activity in a wide range of protein substrates. Since proteinaceous fibrin fibers mainly form the matrix derived from the wound environment, protein degradation may improve the destabilization of the biofilm. However, we could not demonstrate that proteinase K enzymatic treatment improves the antibiotic efficacy on the wound biofilm by increasing antibiotic activity against the two bacterial species (Figures 4G,H). This outcome may be due to the low AgNP stability and low activity of the enzyme (Table 1).

It is essential to highlight that the high heterogeneity observed for *S. aureus* was possible because the bacterial clusters observed inside the wound also present high-sizeheterogenicity. Depending on the efficacy of dispersing bacterial aggregations, the releasing bacteria would form viable counts (increasing CFU). Thus, the data obtained were more heterogeneous than those from *P. aeruginosa*.

Although these treatments seemed promising, it would probably be necessary to combine several dispersing enzymes to eliminate the biofilm, as the EPS degrading efficiency depends on the EPS composition (Redman et al., 2021).

In this work, we also studied the interaction, colocalization, and synergic relationship between *P. aeruginosa* and *S. aureus* in a dual-species wound biofilm. In concordance with other authors that have analyzed *in vivo* and *in vitro* polymicrobial wound biofilms (Kirketerp-Moller et al., 2008; Fazli et al., 2009; Dalton et al., 2011; Woods et al., 2012; Kucera et al., 2014; Brackman et al., 2016), we found that bacteria segregated in

single-species aggregates are covered by matrix depositions. Despite a detailed description of the structure and bacterial distribution that has not been depicted before, some of these investigations analyzed the distribution of *S. aureus* and *P. aeruginosa* based on their relative distance to the wound surface. However, whereas some authors indicate that *S. aureus* aggregates locate closer to the surface and *P. aeruginosa* penetrates deeply in the wound bed (Kirketerp-Moller et al., 2008; Fazli et al., 2009), others differ and found *P. aeruginosa* near the surface and more aerobic areas (Dalton et al., 2011; Woods et al., 2012; Kucera et al., 2014). In this study, we analyzed different transversal areas of the wound biofilms and represented for the first time an overall distribution scheme. We observed that *P. aeruginosa* bacterial aggregates extend throughout the biofilm but with a preference for the outer regions (top and bottom areas) (Figure 5A), which may be due to a *P. aeruginosa* preference for the aerobic or completely anaerobic environments like other investigations indicated (Woods et al., 2012; Brackman et al., 2016). As for *S. aureus*, bacterial aggregates were located in the central parts of the biofilm-forming compact bacterial aggregates, being the bottom part where the most extensive aggregates were found, and surrounded by a dense matrix layer, probably following the abscess formation process in which the created fibrin meshwork protects bacteria from the immune cell attack and prevents antibiotic penetration (Vanassche et al., 2013; Dastgheyb et al., 2015). We think these results may be relevant when designing specific antibacterial treatments against wound biofilms since the bacterial location and physical features of a particular biofilm in the infection site may influence the effect of local antimicrobials and their ability to reach bacterial cells.

Besides affecting bacterial viability and overall species distribution within the biofilm (Figures 5B,C), decreasing the amount of *P. aeruginosa* cells, and increasing the number of free *S. aureus* cells, antibiotic treatment notably modified the overall wound biofilm structure and matrix composition (Figure 5B). Gentamicin and ciprofloxacin increased the porosity of the biofilm through changes in the EPS matrix production, as other antimicrobials do (Schilcher et al., 2016; Andre et al., 2019). We believe that bacteria may alter the composition of the matrix as an adaptive mechanism to enhance protection against antibiotics.

The overall species distribution within the biofilm changed after using DNase I. Other authors have already observed the outstanding ability that DNase I presents, breaking the eDNA of the EPS in biofilms (Baelo et al., 2015). Our results indicate that the degradation of the eDNA triggered the dissemination of single cells from the bacterial aggregates (Figure 6). It seemed that the number of free cells from

S. aureus was higher than those from *P. aeruginosa*. These results would indicate that the clusters of *S. aureus* stuck together using eDNA, and when it was degraded, the cells were disaggregated from the cluster. The cell dissemination was more notable on the top and bottom parts of the WLB, especially when the DNase I was immobilized on AgNP (Figure 6). We hypothesize that bacterial aggregates protect single bacteria against antibiotics, being disseminated cells more susceptible to them. The use of enzymes, especially DNase I, that favor cell dispersion from the bacterial clusters would increase the number of disseminated bacteria and thus their susceptibility (Figure 4).

Finally, in our results, we observed and quantified a significant reduction of eDNA inside the WLB after using DNase I (Figure 7). eDNA reduction seemed more efficient on the top and bottom parts of the WLB, just as is observed in Figure 6. Besides, the graph showed that eDNA reduction was significantly higher when using DNase I immobilized on AgNP (Figure 7B). This increased effect could be explained due to the DNA binding proprieties of the silver ions present on the nanoparticles (Modak and Fox, 1973). Silver ions would facilitate the binding of DNase I to the eDNA and enhance its degradation, the dissemination of the cells, and finally, the bacterial elimination with antibiotics.

The question of applying the functionalized AgNP with antibiotics for *in vivo* wound treatment should be addressed for future perspectives. Other authors have already dealt with this issue and pointed out new insights in the field (Blanco-Fernandez et al., 2021; Ndlovu et al., 2022).

Conclusion

Our findings may provide valuable information about how biofilm's architecture and matrix composition, shaped by both microorganisms and the environment, may influence antibiotic susceptibility and population dynamics in a multispecies wound biofilm. By determining the effect of matrix-degrading enzymes, we have demonstrated that polysaccharides and eDNA play a key role in wound biofilm stability. Furthermore, the colocalization and species distribution studies have provided a broader vision of the species interrelation inside the wound biofilm. Altogether, these results may help to improve current antibacterial therapies in wound infections. Future studies combining several enzymes should be carried out to test whether it increases the enzymes' dispersing activity and the antibiotics' antimicrobial effect. In addition, these treatments should be tested against multidrug-resistant bacteria and clinically isolated bacteria to assure their efficacy and possible future clinical use.

Artículo 4: 3D spatial organization and improved antibiotic treatment of a *Pseudomonas aeruginosa-Staphylococcus aureus* wound biofilm by nanoparticle enzyme delivery

Rubio-Canalejas et al.   10.3389/fmicb.2022.959156

Data availability statement

The raw data supporting the conclusions of this article will be made available by the authors, without undue reservation.

Author contributions

AR-C, AB, SH, and NB-C performed biological assays and wrote the manuscript. MV performed the NP synthesis and characterization. ET directed the research, revised the experimental data, and wrote the manuscript. The manuscript was written through the contributions of all authors. All authors have approved the final version of the manuscript.

Funding

Acknowledgments

Conflict of interest

The authors declare that the research was conducted in the absence of any commercial or financial relationships that could be construed as a potential conflict of interest.

Publisher's note

All claims expressed in this article are solely those of the authors and do not necessarily represent those of their affiliated organizations, or those of the publisher, the editors and the reviewers. Any product that may be evaluated in this article, or claim that may be made by its manufacturer, is not guaranteed or endorsed by the publisher.

Supplementary material

The Supplementary Material for this article can be found online at: https://www.frontiersin.org/articles/10.3389/fmicb.2022.959156/full#supplementary-material

References

Andre, C., de Jesus Pimentel-Filho, N., de Almeida Costa, P. M., and Vanetti, M. C. D. (2019). Changes in the composition and architecture of staphylococcal biofilm by nisin. *Braz. J. Microbiol.* 50, 1083–1090. doi: 10.1007/s42770-019-00135-w

Anson, M. L. (1938). The estimation of pepsin, trypsin, papain, and cathepsin with hemoglobin. *J. Gen. Physiol.* 22, 79–89. doi: 10.1085/jgp.22.1.79

Baelo, A., Levato, R., Julian, E., Crespo, A., Astola, J., Gavalda, J., et al. (2015). Disassembling bacterial extracellular matrix with DNase-coated nanoparticles to enhance antibiotic delivery in biofilm infections. *J. Control. Release* 209, 150–158. doi: 10.1016/j.jconrel.2015.04.028

Bernfeld, P. (1955). Amylases, α and β. *Method Enzymol.* 1, 149–115. doi: 10.1016/0076-6879(55)01021-5

Blanco-Fernandez, B., Castano, O., Mateos-Timoneda, M. A., Engel, E., and Perez-Amodio, S. (2021). Nanotechnology approaches in chronic wound healing. *Adv. Wound Care* 10, 234–256. doi: 10.1089/wound.2019.1094

Brackman, G., Garcia-Fernandez, M. J., Lenoir, J., De Meyer, L., Remon, J. P., De Beer, T., et al. (2016). Dressings loaded with cyclodextrin-hamamelitannin complexes increase *Staphylococcus aureus* susceptibility toward antibiotics both in single as well as in mixed biofilm communities. *Macromol. Biosci.* 16, 859–869. doi: 10.1002/mabi.201500437

Brothers, K. M., Stella, N. A., Hunt, K. M., Romanowski, E. G., Liu, X., Klarlund, J. K., et al. (2015). Putting on the brakes: bacterial impediment of wound healing. *Sci. Rep.* 5, 14003. doi: 10.1038/srep14003

Cendra, M. D. M., Blanco-Cabra, N., Pedraz, L., and Torrents, E. (2019). Optimal environmental and culture conditions allow the *in vitro* coexistence of *Pseudomonas aeruginosa* and *Staphylococcus aureus* in stable biofilms. *Sci. Rep.* 9, 16284. doi: 10.1038/s41598-019-52726-0

Cendra, M. D. M., and Torrents, E. (2021). *Pseudomonas aeruginosa* biofilms and their partners in crime. *Biotechnol. Adv.* 49, 107734. doi: 10.1016/j.biotechadv.2021.107734

Ciofu, O., Rojo-Molinero, E., Macia, M. D., and Oliver, A. (2017). Antibiotic treatment of biofilm infections. *APMIS* 125, 304–319. doi: 10.1111/apm.12673

Dalton, T., Dowd, S. E., Wolcott, R. D., Sun, Y., Watters, C., Griswold, J. A., et al. (2011). An *in vivo* polymicrobial biofilm wound infection model to study interspecies interactions. *PLoS ONE* 6, e27317. doi: 10.1371/journal.pone.0027317

Dastgheyb, S., Parvizi, J., Shapiro, I. M., Hickok, N. J., and Otto, M. (2015). Effect of biofilms on recalcitrance of staphylococcal joint infection to antibiotic treatment. *J. Infect. Dis.* 211, 641–650. doi: 10.1093/infdis/jiu514

DeLeon, S., Clinton, A., Fowler, H., Everett, J., Horswill, A. R., and Rumbaugh, K. P. (2014). Synergistic interactions of *Pseudomonas aeruginosa* and *Staphylococcus aureus* in an *in vitro* wound model. *Infect. Immun.* 82, 4718–4728. doi: 10.1128/IAI.02198-14

Fazli, M., Bjarnsholt, T., Kirketerp-Moller, K., Jorgensen, B., Andersen, A. S., Krogfelt, K. A., et al. (2009). Nonrandom distribution of *Pseudomonas aeruginosa* and *Staphylococcus aureus* in chronic wounds. *J. Clin. Microbiol.* 47, 4084–4089. doi: 10.1128/JCM.01395-09

Fleming, D., Chahin, L., and Rumbaugh, K. (2017). Glycoside hydrolases degrade polymicrobial bacterial biofilms in wounds. *Antimicrob. Agents Chemother.* 61, e01998-16. doi: 10.1128/AAC.01998-16

Fleming, D., Redman, W., Welch, G. S., Mdluli, N. V., Rouchon, C. N., Frank, K. L., et al. (2020). Utilizing glycoside hydrolases to improve the quantitation and visualization of biofilm bacteria. *Biofilm* 2, 100037. doi: 10.1016/j.bioflm.2020.100037

174

Artículo 4: 3D spatial organization and improved antibiotic treatment of a *Pseudomonas aeruginosa-Staphylococcus aureus* wound biofilm by nanoparticle enzyme delivery

Rubio-Canalejas et al.

10.3389/fmicb.2022.959156

Fleming, D., and Rumbaugh, K. (2018). The consequences of biofilm dispersal on the host. *Sci. Rep.* 8, 10738. doi: 10.1038/s41598-018-29121-2

Fleming, D., and Rumbaugh, K. P. (2017). Approaches to dispersing medical biofilms. *Microorganisms* 5, 15. doi: 10.3390/microorganisms5020015

Garner, M. R., Sethuraman, S. A., Schade, M. A., and Boateng, H. (2020). Antibiotic prophylaxis in open fractures: evidence, evolving issues, and recommendations. *J. Am. Acad. Orthop. Surg.* 28, 309–315. doi: 10.5435/JAAOS-D-18-00193

Heydorn, A., Nielsen, A. T., Hentzer, M., Sternberg, C., Givskov, M., Ersboll, B. K., et al. (2000). Quantification of biofilm structures by the novel computer program COMSTAT. *Microbiology* 146 (Pt 10), 2395–2407. doi: 10.1099/00221287-146-10-2395

Hrynyshyn, A., Simoes, M., and Borges, A. (2022). Biofilms in surgical site infections: recent advances and novel prevention and eradication strategies. *Antibiotics.* 11, 69. doi: 10.3390/antibiotics11010069

Kandarp Mavani, M. S. (2013). Synthesis of silver nanoparticles by using sodium borohydride as a reducing agent. *Int J Eng Res Technol.* 2. doi: 10.13140/2.1.3116.8648

Kirketerp-Moller, K., Jensen, P. O., Fazli, M., Madsen, K. G., Pedersen, J., Moser, C., et al. (2008). Distribution, organization, and ecology of bacteria in chronic wounds. *J. Clin. Microbiol.* 46, 2717–2722. doi: 10.1128/JCM.00501-08

Klein, P., Sojka, M., Kucera, J., Matonohova, J., Pavlik, V., Nemec, J., et al. (2018). A porcine model of skin wound infected with a polybacterial biofilm. *Biofouling* 34, 226–236. doi: 10.1080/08927014.2018.1425684

Kucera, J., Sojka, M., Pavlik, V., Szuszkiewicz, K., Velebny, V., and Klein, P. (2014). Multispecies biofilm in an artificial wound bed–A novel model for in vitro assessment of solid antimicrobial dressings. *J. Microbiol. Methods* 103, 18–24. doi: 10.1016/j.mimet.2014.05.008

Kumar, A., and Ting, Y. P. (2015). Presence of *Pseudomonas aeruginosa* influences biofilm formation and surface protein expression of *Staphylococcus aureus*. *Environ. Microbiol.* 17, 4459–4468. doi: 10.1111/1462-2920.12890

Kumar, M., Curtis, A., and Hoskins, C. (2018). Application of nanoparticle technologies in the combat against anti-microbial resistance. *Pharmaceutics* 10. doi: 10.3390/pharmaceutics10010011

Lindholm, C., and Searle, R. (2016). Wound management for the 21st century: combining effectiveness and efficiency. *Int Wound J.* 13(Suppl. 2), 5–15. doi: 10.1111/iwj.12623

Liu, W., Jacquiod, S., Brejnrod, A., Russel, J., Burmolle, M., and Sorensen, S. J. (2019). Deciphering links between bacterial interactions and spatial organization in multispecies biofilms. *ISME J.* 13, 3054–3066. doi: 10.1038/s41396-019-0494-9

Liu, W., Roder, H. L., Madsen, J. S., Bjarnsholt, T., Sorensen, S. J., and Burmolle, M. (2016). Interspecific bacterial interactions are reflected in multispecies biofilm spatial organization. *Front. Microbiol.* 7, 1366. doi: 10.3389/fmicb.2016.01366

Malone, M., Bjarnsholt, T., McBain, A. J., James, G. A., Stoodley, P., Leaper, D., et al. (2017). The prevalence of biofilms in chronic wounds: a systematic review and meta-analysis of published data. *J. Wound Care* 26, 20–25. doi: 10.12968/jowc.2017.26.1.20

Miller, G. L. (1959). Use of dinitrosalicylic acid reagent for determination of reducing sugar. *Anal. Chem.* 31, 426–428. doi: 10.1021/ac60147a030

Modak, S. M., and Fox, C. L. (1973). Binding of silver sulfadiazine to the cellular components of *Pseudomonas aeruginosa*. *Biochem. Pharmacol.* 22, 2391–2404. doi: 10.1016/0006-2952(73)90341-9

Ndlovu, S. P., Fonkui, T. Y., Ndinteh, D. T., and Aderibigbe, B. A. (2022). Dissolvable wound dressing loaded with silver nanoparticles together with ampicillin and ciprofloxacin. *Ther. Deliv.* 13, 295–311. doi: 10.4155/tde-2021-0087

Negut, I., Grumezescu, V., and Grumezescu, A. M. (2018). Treatment strategies for infected wounds. *Molecules* 23. doi: 10.3390/molecules23092392

Percival, S. L., Hill, K. E., Williams, D. W., Hooper, S. J., Thomas, D. W., and Costerton, J. W. (2012). A review of the scientific evidence for biofilms in wounds. *Wound Repair Regen.* 20, 647–657. doi: 10.1111/j.1524-475X.2012.00836.x

Radlinski, L., Rowe, S. E., Kartchner, L. B., Maile, R., Cairns, B. A., Vitko, N. P., et al. (2017). *Pseudomonas aeruginosa* exoproducts determine antibiotic efficacy against *Staphylococcus aureus*. *PLoS Biol.* 15, e2003981. doi: 10.1371/journal.pbio.2003981

Radulescu, M., Andronescu, E., Dolete, G., Popescu, R. C., Fuf,ă, O., Chifiriuc, M. C., et al. (2016). Silver nanocoatings for reducing the exogenous microbial colonization of wound dressings. *Materials* 9, 11. doi: 10.3390/ma9050345

Redman, W. K., Welch, G. S., and Rumbaugh, K. P. (2020). Differential efficacy of glycoside hydrolases to disperse biofilms. *Front. Cell. Infect. Microbiol.* 10, 379. doi: 10.3389/fcimb.2020.00379

Redman, W. K., Welch, G. S., Williams, A. C., Damron, A. J., Northcut, W. O., and Rumbaugh, K. P. (2021). Efficacy and safety of biofilm dispersal by glycoside hydrolases in wounds. *Biofilm* 3, 100061. doi: 10.1016/j.bioflm.2021.100061

Schilcher, K., Andreoni, F., Dengler Haunreiter, V., Seidl, K., Hasse, B., and Zinkernagel, A. S. (2016). Modulation of *Staphylococcus aureus* biofilm matrix by subinhibitory concentrations of clindamycin. *Antimicrob. Agents Chemother.* 60, 5957–5967. doi: 10.1128/AAC.00463-16

Serra, R., Grande, R., Butrico, L., Rossi, A., Settimio, U. F., Caroleo, B., et al. (2015). Chronic wound infections: the role of *Pseudomonas aeruginosa* and *Staphylococcus aureus*. *Expert Rev. Anti Infect. Ther.* 13, 605–613. doi: 10.1586/14787210.2015.1023291

Sugimoto, S., Sato, F., Miyakawa, R., Chiba, A., Onodera, S., Hori, S., et al. (2018). Broad impact of extracellular DNA on biofilm formation by clinically isolated methicillin-resistant and -sensitive strains of *Staphylococcus aureus*. *Sci. Rep.* 8, 2254. doi: 10.1038/s41598-018-20485-z

Sun, Y., Dowd, S. E., Smith, E., Rhoads, D. D., and Wolcott, R. D. (2008). *In vitro* multispecies Lubbock chronic wound biofilm model. *Wound Repair Regen.* 16, 805–813. doi: 10.1111/j.1524-475X.2008.00434.x

Tetz, V. V., and Tetz, G. V. (2010). Effect of extracellular DNA destruction by DNase I on characteristics of forming biofilms. *DNA Cell Biol.* 29, 399–405. doi: 10.1089/dna.2009.1011

Townsend, E. M., Sherry, L., Kean, R., Hansom, D., Mackay, W. G., Williams, C., et al. (2017). Implications of antimicrobial combinations in complex wound biofilms containing fungi. *Antimicrob. Agents Chemother.* 61, e00672-17. doi: 10.1128/AAC.00672-17

Vanassche, T., Peetermans, M., Van Aelst, L. N., Peetermans, W. E., Verhaegen, J., Missiakas, D. M., et al. (2013). The role of staphylothrombin-mediated fibrin deposition in catheter-related *Staphylococcus aureus* infections. *J. Infect. Dis.* 208, 92–100. doi: 10.1093/infdis/jit130

Wood, T. M., and Bhat, K. M. (1988). Methods for measuring cellulase activities. *Meth. Enzymol.* 160, 87–112. doi: 10.1016/0076-6879(88)60109-1

Woods, J., Boegli, L., Kirker, K. R., Agostinho, A. M., Durch, A. M., Delancey Pulcini, E., et al. (2012). Development and application of a polymicrobial, *in vitro*, wound biofilm model. *J. Appl. Microbiol.* 112, 998–1006. doi: 10.1111/j.1365-2672.2012.05264.x

Wu, J., Zheng, Y., Song, W., Luan, J., Wen, X., Wu, Z., et al. (2014). In situ synthesis of silver-nanoparticles/bacterial cellulose composites for slow-released antimicrobial wound dressing. *Carbohydr. Polym.* 102, 762–771. doi: 10.1016/j.carbpol.2013.10.093

Zhao, R., Liang, H., Clarke, E., Jackson, C., and Xue, M. (2016). Inflammation in chronic wounds. *Int. J. Mol. Sci.* 17, 2085. doi: 10.3390/ijms17122085

Zhou, Y., Chen, R., He, T., Xu, K., Du, D., Zhao, N., et al. (2016). Biomedical potential of ultrafine Ag/AgCl nanoparticles coated on graphene with special reference to antimicrobial performances and burn wound healing. *ACS Appl. Mater. Interfaces* 8, 15067–15075. doi: 10.1021/acsami.6b03021

Material Suplementario

FIGURE S1. Optimization of gentamicin and ciprofloxacin concentration in dual-species WLB. *P. aeruginosa* and *S. aureus* bacterial cell number in the clot (CFU/g) after 24 h treatment of different concentrations (µg/ml) of gentamicin and ciprofloxacin used simultaneously. The statistical analysis to determine significance between the untreated control (0 µg/ml) and the different antibiotic concentrations was performed using the Student Unpaired *t*-test (*, $p < 0.05$).
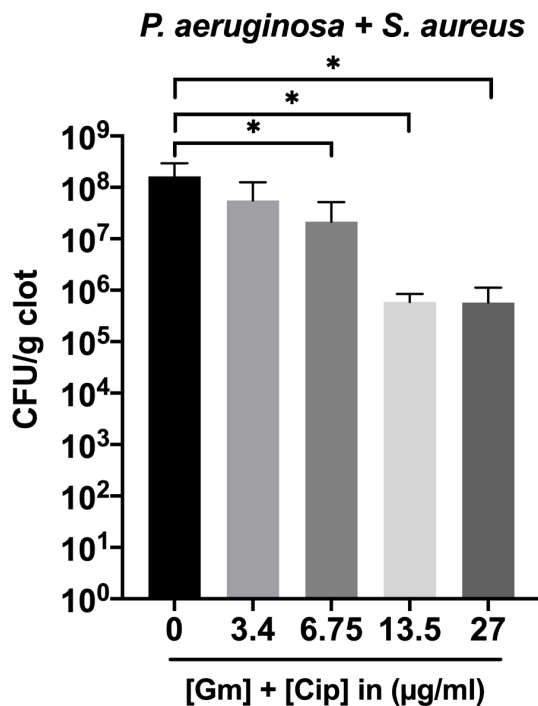

FIGURE S2. Growth of *P. aeruginosa* and *S. aureus* on different media. Growth of *P. aeruginosa* PAO1 and *S. aureus* SA31 on LB agar containing 2 mg/ml of crystal violet and TSA containing 7.5 % (w/v) of NaCl.
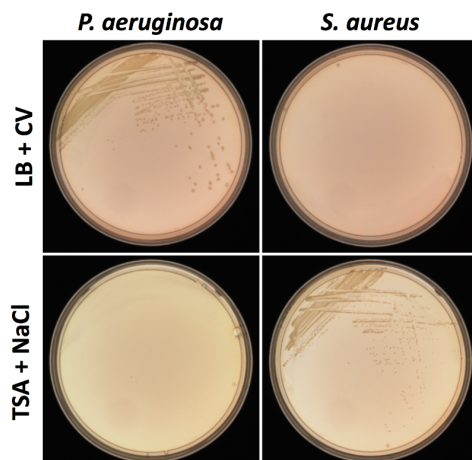
FIGURE S3. Antimicrobial assays on *P. aeruginosa* and *S. aureus* polymicrobial WLB. Effect of the antibiofilm treatments consisting of single use of gentamicin (Gm) or ciprofloxacin (Cip) at a final concentration of 13.5 µg/ml each, along with DNase I. Percentage of viability corresponds to counts of CFU on plate from the bacteria in WLB. The statistical analysis to determine significance was performed using the Student Unpaired *t*-test (*, $p < 0.05$; **, $p < 0.01$).
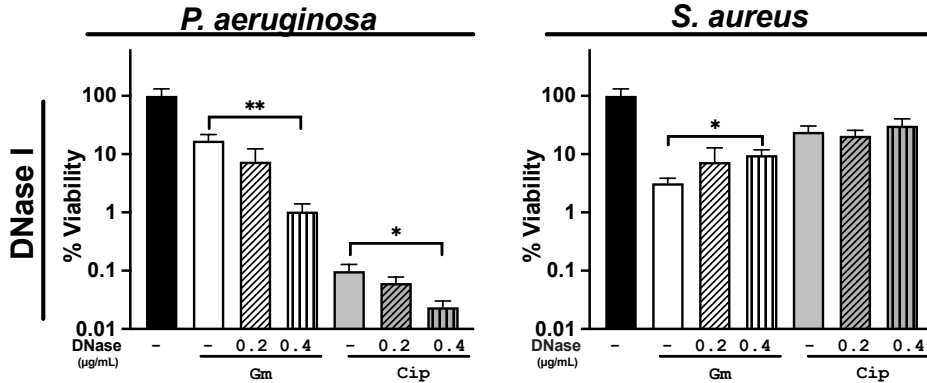
FIGURE. S4. **Histograms of the area of the *S. aureus* clusters to evaluate their distribution in the different traversal parts of the clot (top, middle, and bottom).**
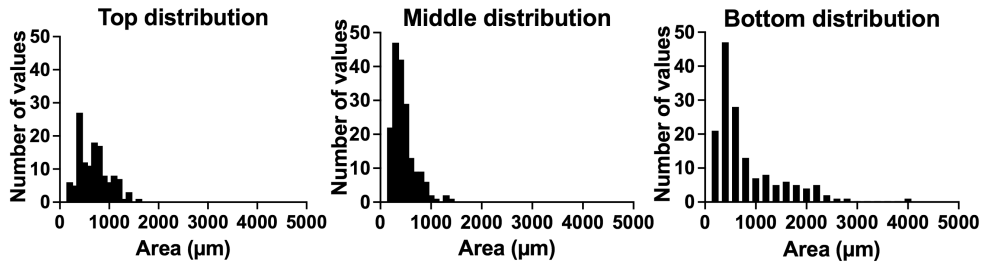
FIGURE S5. Enlarged CSLM images from the wound biofilm. The figures correspond to the Figures 5 and 6 from the main text.
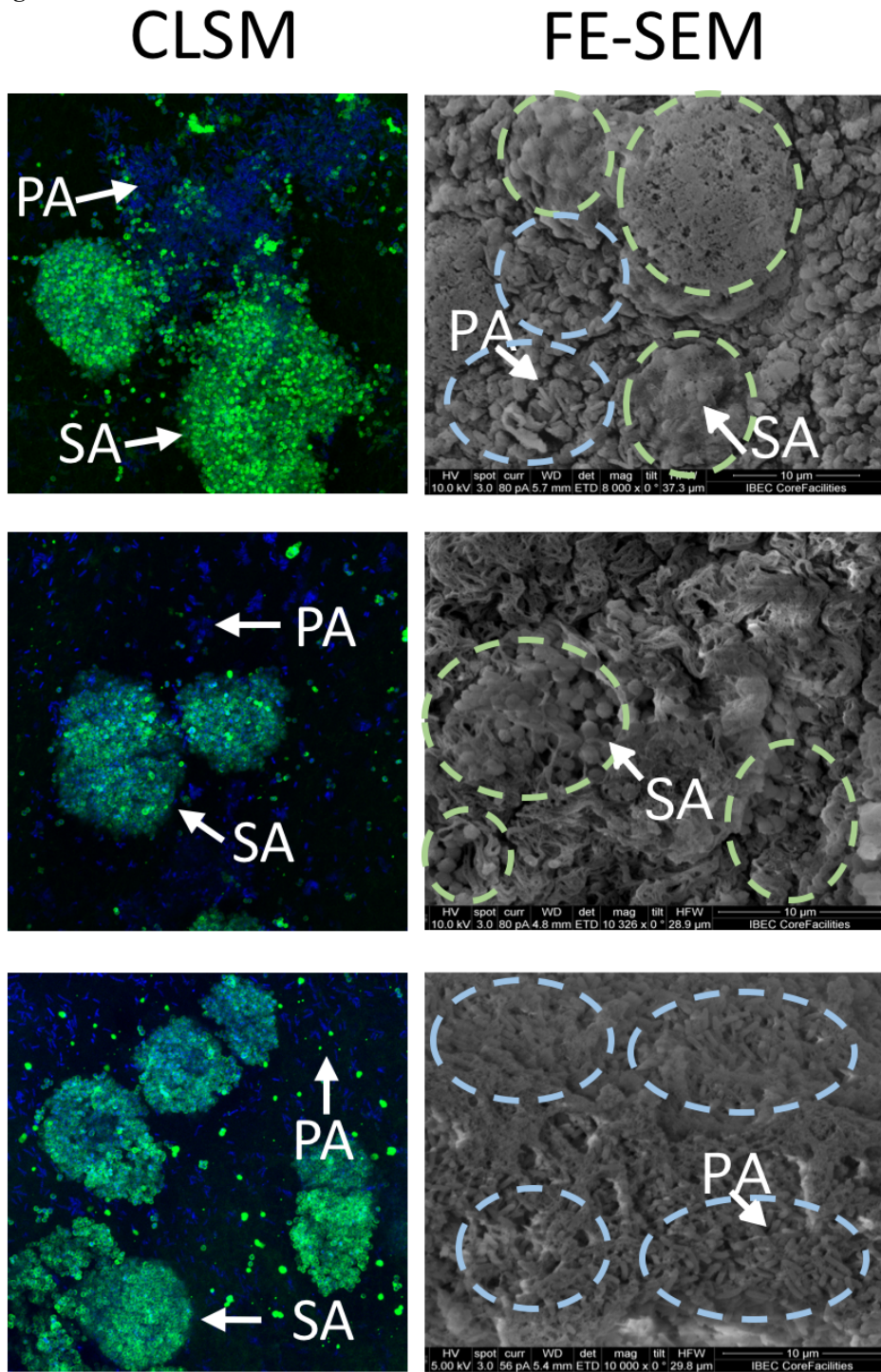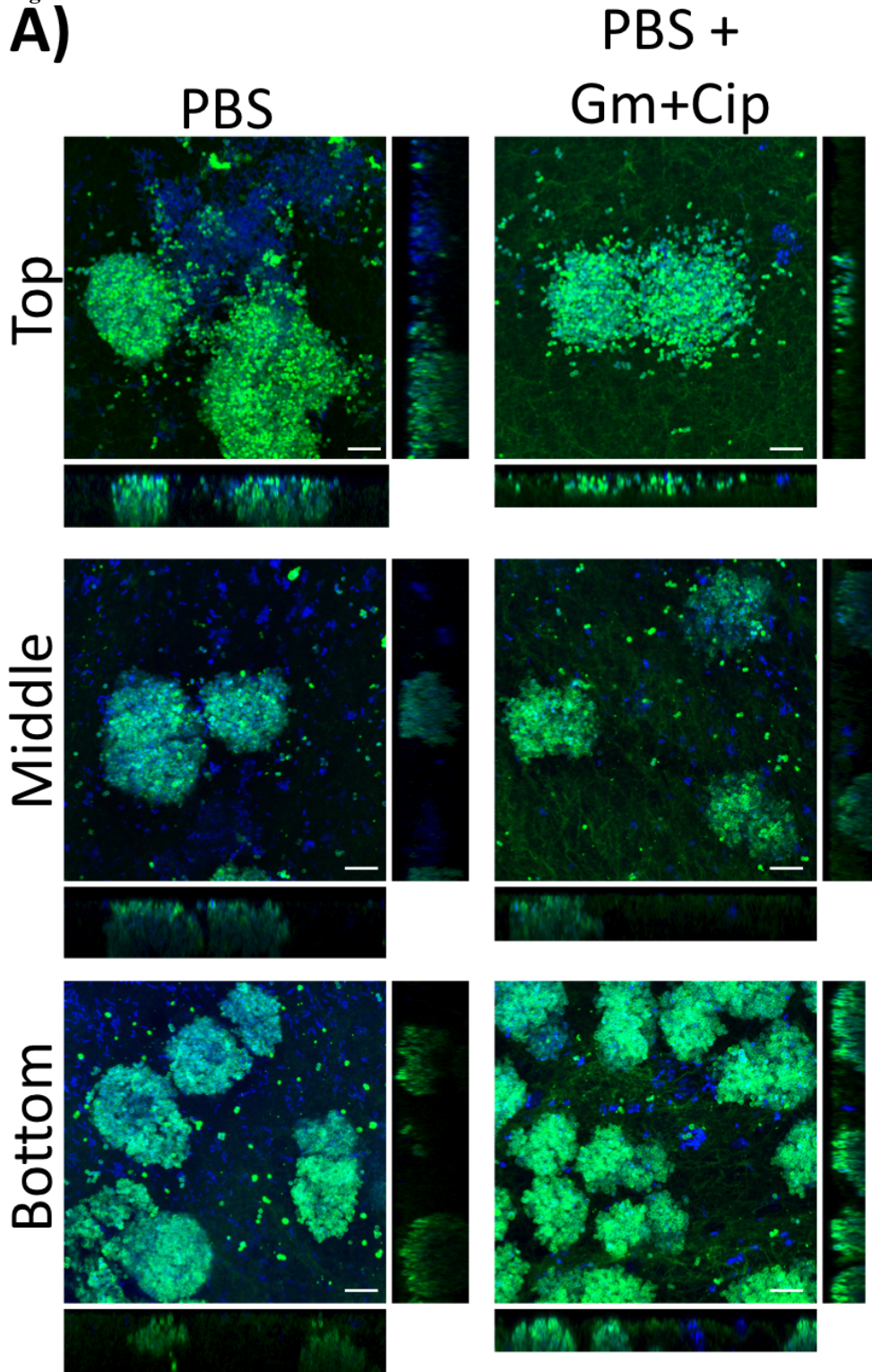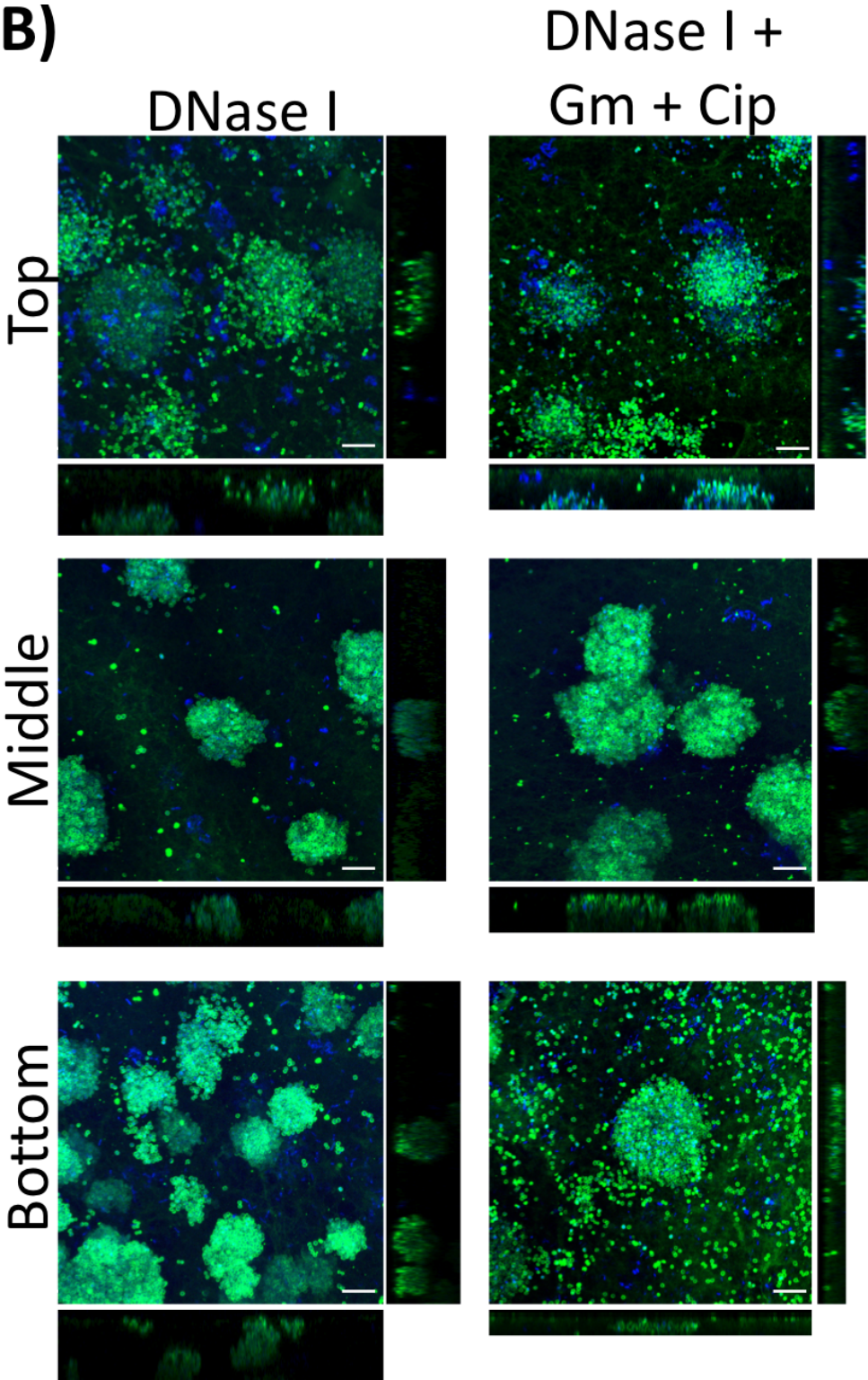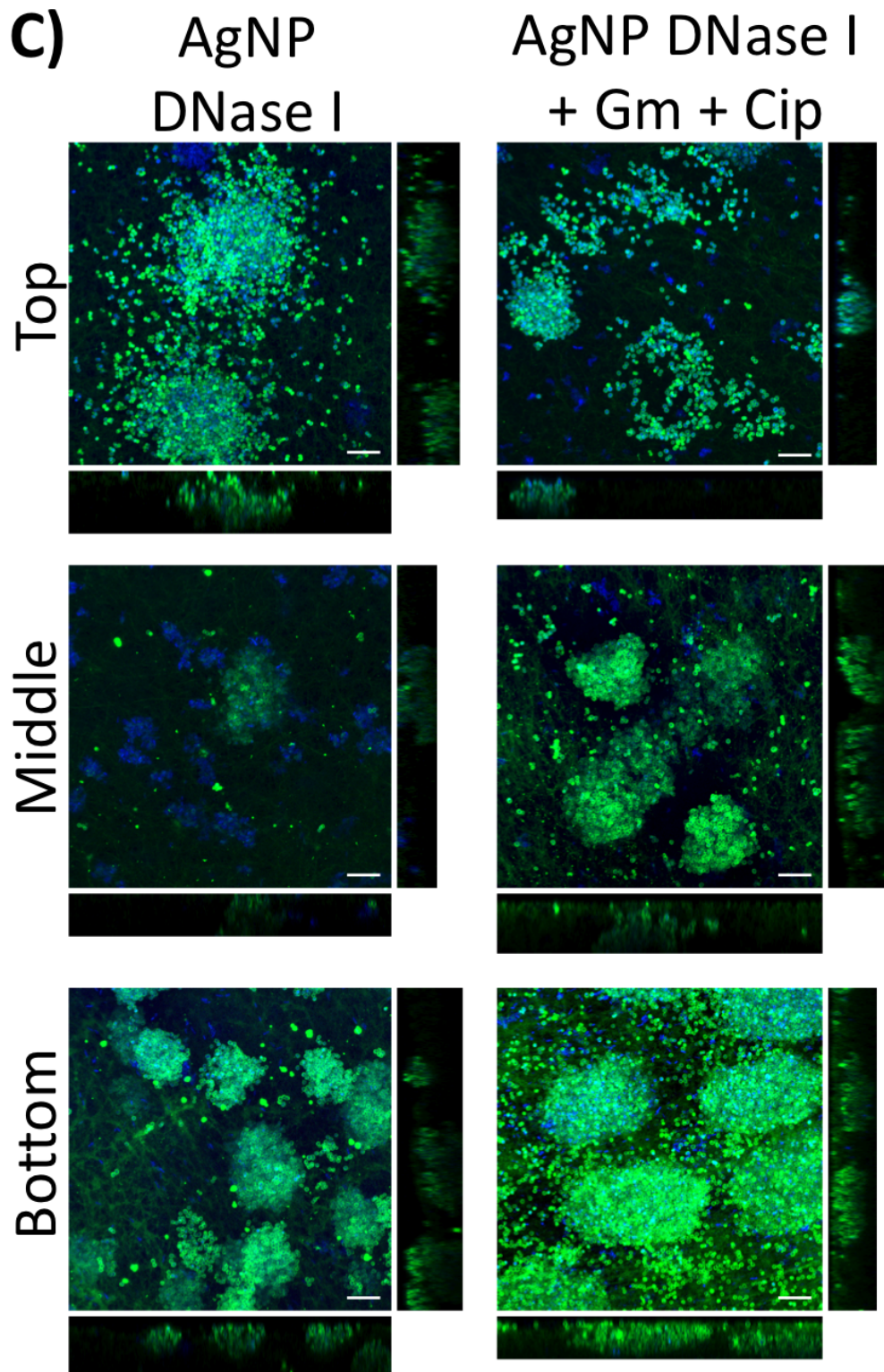**Figure 5:**

Figure 6:

A)

Discusión global de los resultados obtenidos

Los artículos presentados en esta tesis bajo la sección "Resultados" abordan distintos aspectos de las infecciones de *P. aeruginosa*. Hemos estudiado, desde la red regulatoria de las enzimas esenciales para la síntesis de ADN, las RNR, hasta el uso de nuevas terapias contra las coinfecciones de *P. aeruginosa* y *S. aureus* en heridas, pasando por el desarrollo de un nuevo sistema para medir la expresión génica utilizando técnicas de transcripción *in vitro.*

A continuación, se describe una discusión general de los resultados obtenidos, para una versión más extensa pueden acudir a la sección "discussion" de cada una de las publicaciones o trabajos.

Factores transcripcionales para regular la expresión de las RNR

En los Artículos 1 y 3, "*Pseudomonas aeruginosa* nonphosphorylated AlgR induces ribonucleotide reductase expression under oxidative stress infectious conditions" (273) y "Regulon and mechanism of action of NrdR, a global regulator of ribonucleotide reduction" se estudia la regulación transcripcional de las enzimas esenciales ribonucleótido reductasas por los FT AlgR y NrdR. Entender las interacciones entre FT ayuda a comprender su regulación génica y los mecanismos que se desencadenan para dar respuesta a situaciones ambientales concretas a través del metabolismo bacteriano, como por ejemplo condiciones de escasez de nutrientes, estrés, niveles de oxígeno o el desarrollo de una infección o la formación de un biofilm(175, 274). En estos artículos hemos explorado el mecanismo de regulación de AlgR (Artículo 1) y de acción de NrdR (Artículo 3) sobre las diferentes RNR.

AlgR es un regulador global del metabolismo de *P. aeruginosa* que forma parte del sistema de dos componentes FimS-AlgR donde FimS es una quinasa transmembrana que cataliza la fosforilación de AlgR para activar o inactivar vías metabólicas específicas (81, 166). La transcripción de *algR* se lleva a cabo a través de dos promotores diferentes que dependen de FT específicos (171). En una infección, la producción de especies reactivas del oxígeno (ROS) es uno de los principales mecanismos de defensa que tiene el organismo contra las bacterias (275). La Figura 1 del Artículo 1 muestra que la expresión de *algR* se activa bajo condiciones de estrés oxidativo y especialmente durante la fase de crecimiento estacionaria a través del promotor P*algR*. Esto puede indicar que AlgR puede ser activada

en presencia de ROS sin depender de FimS. lo que puede indicar que AlgR no depende de FimS para ser activa en presencia de ROS. Aunque hay estudios que relacionan a AlgR con el sistema de defensa frente al estrés oxidativo, su función no está clara. Se ha sugerido que la función de protección de AlgR puede estar relacionada con la producción de alginato, ya que este polímero participa en la protección bacteriana frente a las ROS (275).

En relación con las RNR, AlgR regula las RNR de clase II (*nrdJ*) y de clase I (*nrdA*), participando en el control de la reserva total de dNTPs. En condiciones de estrés oxidativo, AlgR induce la expresión de *nrdJ* y *nrdA* a partir de la proteína en su estado no fosforilado (Figuras 2 y 3 del Artículo 1). Este mismo patrón de activación transcripcional se observó en la cepa de laboratorio *P. aeruginosa* PA14 y en el aislado clínico *P. aeruginosa* PAET1, lo que corrobora la importancia de AlgR en presencia de ROS. También observamos una menor inducción basal de las RNR en estas cepas en comparación con la cepa *P. aeruginosa* PAO1.

Debido a la relevancia que tiene el estudio del crecimiento bacteriano dentro del biofilm, medimos la expresión de las RNR en biofilm bajo condiciones de estrés oxidativo para simular una infección (Figuras 4 y 5 del Artículo 1) (274, 276). En este estudio observamos que la expresión de *nrdJ* y *nrdA* dependía directamente de AlgR y que la inducción era debida específicamente a AlgR en su estado no fosforilado. También estudiamos Anr, un FT que regula genes implicados en condiciones anaeróbicas, mostrando que también interviene en la regulación de *nrdJ* durante la formación de biofilm (142). Estos resultados concuerdan con lo observado en las Figuras 2 y 3 del Artículo 1.

Finalmente, estudiamos la expresión de las RNR *in vivo* en el modelo de infección de *G. mellonella* cuyos hemocitos producen ROS en el interior de las larvas (277). Observamos que *algR* se inducía durante todo el proceso de infección mayoritariamente a través de P*algR*, y que la ribonucleótido reductasa *nrdJ* mostraba la mayor inducción a 18 h tras la infección, lo que parece indicar que la RNR de clase II cumple un papel relevante durante los procesos infectivos (Figura 6 del Artículo 1). Esto concuerda con lo observado para los FT AlgR y Anr que regulan la transcripción de dicha enzima (81, 142).

Basándonos en los resultados obtenidos, hemos formulado una hipótesis sobre lo que puede estar sucediendo en la célula cuando se producen ROS (Figura 7 del Artículo 1). En condiciones de estrés oxidativo, se observa un aumento en la expresión de *algR* a través del promotor P*algR*, y las RNR de clase I y II inducen su expresión a través de la proteína AlgR no fosforilada en diferentes condiciones, tanto en planctónico como en biofilm, así

como durante la infección en *G. mellonella* (Figuras 1-6 del Artículo 1). Según nuestra hipótesis, AlgU y/o RpoS son los responsables de detectar las ROS, ya que los factores sigma AlgU y RpoS activan la expresión de *algR*, lo que resulta en la producción mayoritaria de proteína no fosforilada (171). Aunque AlgU y otras proteínas relacionadas como AlgW y MucP se han relacionado con estrés oxidativo, su papel no está completamente claro (275, 278). Proponemos que, en condiciones de estrés oxidativo, AlgW y/o MucP escinden AlgU de MucA, y el factor AlgU liberado activa la expresión de *algR* para que AlgR active a su vez la expresión de *nrdA* y *nrdJ*, y así se produzcan los dNTPs necesarios para reparar el ADN dañado por las ROS. Una vez que se eliminan las ROS, AlgU volvería a ser secuestrado por MucA. Por otro lado, si bien se sabe que RpoS detecta el estrés en *E. coli*, no hay estudios concluyentes que confirmen su relación con el estrés oxidativo en *P. aeruginosa* (279). Esto parece indicar que AlgU es el factor sigma implicado en la activación de *algR*, aunque esto no es concluyente y deberían realizarse experimentos utilizando cepas Δ*algU* y Δ*rpoS* para determinar el método de acción del sistema de defensa de la bacteria frente al estrés oxidativo y su relación con la red que regula las RNR (Figura 7 del Artículo 1).

Además de AlgR, hay otros FT que regulan la transcripción de las RNR para activar su expresión en condiciones específicas. El regulador transcripcional NrdR cumple una función clave a la hora de controlar la síntesis de las distintas RNR codificadas por el genoma de *P. aeruginosa*. Una interacción estrechamente regulada entre los distintos FT que regulan las RNR es clave para mantener un buen equilibrio de dNTPs que favorezcan el crecimiento microbiano evitando la aparición de mutaciones (3).

Tras explorar de forma bioinformática y transcriptómica la relación de NrdR con el genoma de *E. coli* y *P. aeruginosa* se identificaron varias cajas NrdR en las regiones promotoras de las RNR en ambas especies (Figura 1 del Artículo 3). La distancia entre las cajas sugiere que la regulación por NrdR puede llevarse a cabo mediante la oligomerización de la proteína. Aun así, el mecanismo funcional y la estructura de NrdR todavía no se ha caracterizado completamente. Aunque se sabía que NrdR es un represor cuya funcionalidad depende de la unión a cofactores nucleotídicos, todavía estaba claro si su actividad dependía de la unión a ATP o a dATP (280). Gracias a los últimos estudios publicados se ha obtenido la primera información estructural de NrdR (89). Esta proteína tiene un cono-ATP, y según Grinberg et al., al cono-ATP se pueden unir dos nucleótidos cuya naturaleza determina la formación de formas oligoméricas específicas: tetrámeros y docecámeros inactivos al unirse ATP; y tetrámeros y octámeros activos al unirse dATP y ATP/ADP

simultáneamente (89). Resultados similares se obtuvieron en nuestros experimentos utilizando la proteína NrdR de *E. coli*. En nuestro estudio observamos que la unión de NrdR a ATP desencadenaba la formación de grandes oligómeros (>200 Da) sin capacidad de unión al ADN ni de represión de la transcripción de las RNR (Figuras 3-7 del Artículo 3). No obstante, al incubar la proteína NrdR con dATP se observó la formación de formas más pequeñas que al añadir ATP. Al unirse dATP se obtenía una población dinámica entre tetrámeros y octámeros con una unión clara y específica al ADN en experimentos EMSA (Figuras 3-6 del Artículo 3). Estos oligómeros reprimieron activamente la transcripción de las RNR (Figura 7 del Artículo 3). Resultados similares se han obtenido tras utilizar la proteína NrdR de *P. aeruginosa* (Figura 7 del Artículo 3).

Nuestra hipótesis de funcionamiento de NrdR se esquematiza en la Figura 9 del Artículo 3. Según nuestro modelo, la proteína NrdR se encontraría en equilibrio formando entre un tetrámero inactivo con ATP (que puede agregar formando oligómeros más grandes) y un tetrámero activo con dATP (que puede llegar a gormar octámeros).

Además de su funcionalidad, es de gran importancia que la expresión de NrdR esté altamente regulada, ya que, niveles desregulados de NrdR en *E. coli* dieron lugar a desequilibrios entre NTPs y dNTPs, lo que sugiere que NrdR puede considerarse como diana antimicrobiana. Estudios previos que analizaron la virulencia de cepas con el gen *nrdR* mutado no observaron una elevada infectividad de las cepas (82, 281, 282). Sin embargo, una alta producción de NrdR redujo la fitness y velocidad de crecimiento de las cepas de *E. coli* (283)*.* Los resultados mostrados en la Figura 8 del Artículo 3 indican que las cepas de *P. aeruginosa* con el gen *nrdR* mutado y con la proteína sobreexpresada presentan una menor virulencia, ya que se observó un aumento en la viabilidad de las larvas de *G. mellonella* en ambos casos.

En general, hemos obtenido una mayor comprensión del mecanismo de oligomerización y funcionalidad de NrdR *in vivo* en función de su unión a ATP y dATP. Esto nos ha permitido relacionar las estructuras cuaternarias de NrdR con su actividad utilizando el sistema ReViTA (Artículo 2) (89). Asimismo, hemos identificado la posible utilización de NrdR como diana antimicrobiana.

Desarrollo de una nueva técnica para estudiar la expresión génica mediante transcripción *in vitro*

En el Artículo 2, "ReViTA: A novel *in vitro* transcription system to study gene regulation", desarrollamos una nueva técnica para estudiar la expresión transcripcional de genes cuando éstos están regulados por FT mediante experimentos de transcripción *in vitro.*

El estudio genético de patógenos microbianos ayuda a comprender su estilo de vida y los factores que activan la expresión de genes que contribuyen al desarrollo de la infección. Por lo tanto, es prioritario desarrollar técnicas novedosas que faciliten el estudio de los genes y su regulación. Debido a esto y para dar respuesta a la necesidad observada en el Artículo 3 de estudiar la transcripción de las RNR *in vitro*, se desarrolló esta tecnología*.* En este artículo presentamos una técnica denominada ReViTA (**Re**verse *in **V**itro* **T**ranscription **A**ssay), que permite estudiar la expresión transcripcional y la regulación génica utilizando la IVT*.* Con el sistema ReViTA se puede evaluar el papel de un FT cuando se une a un gen específico mediante IVT (Figura 1 del Artículo 2).

El uso del sistema ReViTA ofrece numerosas ventajas, como la eliminación de la necesidad de modificar genéticamente el organismo de estudio, la obtención resultados específicos para el FT estudiado sin que haya modificaciones producidas por otros factores presentes *in vivo*, la eliminación de la necesidad de radiomarcar el ARN y la protección de la muestra frente a 5' exonucleasas al estar dentro de un plásmido (284). Sin embargo, la técnica ReViTA también presenta algunas limitaciones. La RNAP utilizada en el estudio está saturada con σ^{70}, por lo que es necesario utilizar otra RNAP con su factor sigma correspondiente si el promotor a estudiar no es σ^{70}. Además, la formación del complejo RNAP-promotor está influenciada por diversos parámetros como la concentración de sal, la temperatura y el tiempo de incubación, así como la concentración de RNAP, que se deben optimizarse empíricamente si es necesario. También es necesario purificar el FT de interés, lo que puede presentar algunos problemas adicionales (284).

Para valorar el sistema ReViTA evaluamos la expresión de dos promotores de *P. aeruginosa*, *nrdA* y *dinB*, a través de los FT AlgR y LexA. La Figura 2 del Artículo 2 muestra los geles de purificación de cada proteína y los geles de retardo (EMSA) tras incubarse con los promotores a los que se unen. En estos geles observamos que la proteína LexA forma un dímero, que corresponde con la forma activa de la proteína cuando se une al promotor

dinB (270, 285–287). Los geles de EMSA mostraron que cada FT se une de forma específica a su promotor, encontrando una pequeña unión inespecífica entre la proteína LexA y la región control de nuestro sistema ReViTA.

Los promotores y factores de transcripción seleccionados se sometieron al procedimiento IVT para estudiar su función en la regulación génica. Los resultados obtenidos con el sistema ReViTA y con fragmentos lineales de PCR se compararon entre sí para comprobar la adecuación de nuestro sistema (Figura 3 del Artículo 2). En ambos tipos de experimentos, la incubación con el FT modificó la expresión transcripcional a partir de los promotores seleccionados. AlgR incrementó la expresión de *nrdA* de manera proporcional a la cantidad de FT utilizado, lo que sugiere que los resultados son coherentes. Sin embargo, al utilizar el FT LexA con el promotor *dinB*, la expresión se redujo, pero no disminuyó más a medida que aumentaba la cantidad de proteína. Nuestra hipótesis es que la falta de relación directa entre cantidad de proteína y reducción de expresión es debida a que la proteína LexA se une de forma inespecífica a la secuencia control del sistema ReViTA, tal como se observa en la Figura 2 del Artículo 2. Los resultados muestran que el sistema ReViTA es útil para determinar la función de FT específicos y se convierte en una excelente opción para medir expresión génica y utilizarse en el estudio de la regulación transcripcional de genes.

Estudio de las infecciones en heridas y su posible tratamiento

En el Artículo 4, "3D spatial organization and improved antibiotic treatment of a *Pseudomonas aeruginosa–Staphylococcus aureus* wound biofilm by nanoparticle enzyme delivery" (288), nos hemos centrado en el estudio de terapias antimicrobianas para eliminar la infección producida por *P. aeruginosa* y *S. aureus* y de la localización espacial de estas bacterias dentro de un modelo de herida *in vitro*.

En estudios anteriores se ha determinado que el uso de antibióticos de amplio espectro, como gentamicina y ciprofloxacina, por separado no fue capaz de eliminar una infección doble de *P. aeruginosa* y *S. aureus* cuando crecían formando un biofilm en heridas *in vitro* (243)*.* En la Figura 1 del Artículo 4 de esta publicación se muestra que el uso de gentamicina y ciprofloxacina por separado modifica la distribución de la población bacteriana en el biofilm. Mientras que la viabilidad de *P. aeruginosa* solo se vio afectada tras el tratamiento con ciprofloxacina con una reducción de 3.5 logs, la vialidad de *S. aureus* solo disminuyó 1.5 logs tras el uso de gentamicina. En otras ocasiones se ha observado

tolerancia a gentamicina por *P. aeruginosa* y a ciprofloxacina por *S. aureus* y se ha hipotetizado que en el caso de *P. aeruginosa* se debe a la producción de alginato y en *S. aureus* a su capacidad para inhibir la respiración (243, 289). La terapia antibiótica dual redujo la viabilidad de ambas especies bacterianas 3.2 logs. En este trabajo proponemos el uso de terapias combinadas para el tratamiento de estas infecciones polimicrobianas. Anteriormente ya se han utilizado como herramientas útiles para tratar infecciones (290).

Debido a que la composición de la EPS dificulta la penetración de algunos antibióticos a las capas más profundas del biofilm, es necesario desarrollar nuevos tratamientos con alta capacidad de penetración. El uso de AgNP es una terapia excepcional para tratar biofilms debido a su efector inhibidor del crecimiento (Figura 3 del Artículo 4) y porque sobre ellas se pueden inmovilizar enzimas que disgreguen la EPS, lo que permite una mayor penetración y difusión de los antibióticos (134, 291). En esta publicación exploramos el uso de α-amilasa, celulasa, DNasa I y proteinasa K como agentes disgregadores del biofilm, ya sea en su forma soluble o inmovilizadas sobre AgNP.

El uso de α-amilasa y la celulasa como agentes para dispersar los agregados bacterianos de *P. aeruginosa* y *S. aureus* ha generado resultados prometedores en estudios previos de otros autores (223, 292). Nuestros resultados mostraron que la viabilidad de *P. aeruginosa* disminuyó al utilizar estas enzimas junto con antibióticos y que la disminución fue mayor cuando las enzimas estaban inmovilizadas sobre AgNP (Figura 4A, C del Artículo 4). Sin embargo, tras usar α-amilasa y la celulasa los resultados mostraron un aumento en la viabilidad de *S. aureus* (Figura 4B, D del Artículo 4), probablemente debido a la dispersión de las células previamente agrupadas. El uso de DNasa I como agente antibiofilm se ha probado previamente debido a su capacidad para degradar el eDNA que forma parte de la EPS (162, 209). Con la DNasa I se observó la mayor reducción de la viabilidad de *P. aeruginosa* (Figura 4E del Artículo 4). Aunque la viabilidad de *S. aeruginosa* aumentó (Figura 4F del Artículo 4), nuestra hipótesis apunta a que el aumento de las células viables se debe a que la eliminación del eDNA hace que se liberen las bacterias embebidas en los agregados, ya que el eDNA se acumula principalmente en agregados de *S. aureus* (235). Esto parece indicar que el eDNA juega un papel esencial en el aumento de la tolerancia a los antibióticos por parte de *S. aureus*, pudiendo ser un potente agente antibiofilm cuando se usa inmovilizada en AgNP junto a antibióticos. Al utilizar la proteinasa K no se observó una mejora de la actividad antibiótica contra las dos especies tras el tratamiento enzimático (Figura 4G-H del Artículo 4), probablemente debido a las características fisicoquímicas de

las nanopartículas funcionalizadas (Tabla 1 del Artículo 4). Una posible limitación de estos estudios puede ser la necesidad de utilizar varias enzimas simultáneamente para degradar distintos componentes de la EPS (293). Aun así, se deben realizar experimentos para confirmar esta hipótesis.

Al estudiar la interacción, colocalización y relación entre *P. aeruginosa* y *S. aureus,* observamos que dentro de las heridas se generan agregados de una sola especie que se rodean de componentes de la matriz. Cabe destacar que nuestros resultados coinciden con lo mostrado por otros autores que han analizado biofilms en heridas *in vivo* e *in vitro* (232–235). Sin embargo, al analizar la localización de estos agregados bacterianos hay disonancias entre diversos estudios. Por un lado, mientras que algunos autores indican que *P. aeruginosa* crece en las zonas más profundas del biofilm y *S. aureus* se sitúa en la parte más cercana a la superficie (232, 233), otros defienden que *P. aeruginosa* se localiza cerca de la superficie en las zonas con más oxígeno (234, 235). En nuestro trabajo observamos que los agregados de *P. aeruginosa* se encuentran mayoritariamente en zonas más superficiales o las más profundas, y los agregados de *S. aureus* se localizan en toda la herida, formando grandes aglomeraciones en la zona más profunda del biofilm y rodeados de matriz, probablemente como medida de protección (Figura 5 del Artículo 4) (294, 295). En el estudio de la matriz extracelular observamos que el uso de gentamicina y ciprofloxacina aumentó la porosidad del biofilm, tal y como hacen otros antimicrobianos (296, 297).

En este trabajo utilizamos la enzima DNasa I debido a su alta capacidad para romper el eDNA de la EPS (162, 298, 299). Nuestros resultados muestran que el uso de la enzima desencadenó la liberación bacteriana de los agregados, lo que llevó a la dispersión de bacterias por todo el biofilm (Figura 6 del Artículo 4). La elevada reducción de la viabilidad bacteriana observada al utilizar esta enzima en la Figura 4 del Artículo 4 es posiblemente debida a que las bacterias liberadas son más susceptibles a los antibióticos y la DNasa I es muy eficaz para romper el eDNA de la matriz, lo que conduce a una mayor liberación. Finalmente, la Figura 7 del Artículo 4 muestra la reducción del eDNA en la herida tras utilizar la enzima DNasa I, y su eficacia es mayor cuando se encuentra inmovilizada en las AgNP. En el futuro, se debería estudiar el uso de las terapias combinadas y de estas nanopartículas en ensayos *in vivo*, tal como han indicado otros autores (300, 301).

Conclusiones

1. En *Pseudomonas aeruginosa*, la expresión del gen *algR* se induce a través del promotor P*algR* bajo condiciones de estrés oxidativo durante el crecimiento plantónico (fase exponencial y estacionaria) y durante el proceso de infección en *G. mellonella*.

2. En *P. aeruginosa*, y bajo condiciones de estrés oxidativo, el factor de transcripción AlgR sin fosforilar activa de forma directa la transcripción de las RNR de clase I y clase II. Esta activación tiene lugar durante el crecimiento planctónico, en biofilm y en la infección en *G. mellonella*, donde la RNR de clase II juega un papel crucial*.*

3. Las RNR de clase I y II presentan patrones de expresión similares en las cepas de *P. aeruginosa* PAO1 y PA14 y en la cepa del aislado clínico PAET1. La mayor expresión de las RNR se produce en la cepa de *P. aeruginosa* PAO1 bajo las mismas condiciones de crecimiento.

4. La técnica ReViTA (Reverse *in vitro* Transcription Assay) permite estudiar la regulación génica mediada por factores de transcripción y caracterizar *in vitro* la función biológica de factores de transcripción de interés.

5. NrdR regula los genes de las RNR en *Escherichia coli* y *P. aeruginosa* a través de su unión a cofactores nucleotídicos. La unión de NrdR a ATP forma grandes oligómeros inactivos. La unión a dATP forma tetrámeros y octámeros que son activos y funcionales y se unen al ADN reprimiendo la transcripción de las RNR.

6. En *P. aeruginosa*, una expresión alterada de NrdR afecta negativamente el fitness de la bacteria durante la infección en *Galleria mellonella*, presentándose como una posible diana antimicrobiana.

7. Las terapias combinadas que utilizan enzimas aumentan la eficacia de los antibióticos gentamicina y ciprofloxacina al disgregar el biofilm y reducir la viabilidad de *P. aeruginosa* y *Staphylococcus aureus*. En la mayoría de los casos, las enzimas inmovilizadas sobre nanopartículas de plata reducen significativamente la viabilidad bacteriana global en comparación con las enzimas solubles.

8. La terapia combinatoria de DNasa I con gentamicina y ciprofloxacina presenta el mayor potencial para ser utilizada como tratamiento en heridas crónicas contra *P. aeruginosa* y *S. aureus*.

9. *P. aeruginosa* y *S. aureus* forman agregados separados dentro del biofilm en herida. Los agregados de *P. aeruginosa* se localizan en todo el biofilm, siendo menos numerosos en la zona intermedia. Por otro lado, *S. aureus* predomina en la zona inferior del biofilm, donde se encuentran agregados grandes y numerosos.

Bibliografía

1. Lindahl T. 1993. Instability and decay of the primary structure of DNA. Nature 362:709–715.
2. Crick F. 1970. Central dogma of molecular biology. Nature 227:561–563.
3. Greene BL, Kang G, Cui C, Bennati M, Nocera DG, Drennan CL, Stubbe JA. 2020. Ribonucleotide Reductases: Structure, Chemistry, and Metabolism Suggest New Therapeutic Targets. Annu Rev Biochem 89:45–75.
4. Torrents E. 2014. Ribonucleotide reductases: Essential enzymes for bacterial life. Front Cell Infect Microbiol 4.
5. Ruskoski TB, Boal AK. 2021. The periodic table of ribonucleotide reductases. J Biol Chem 297:101137–101138.
6. Stubbe J, Nocera DG. 2021. Radicals in Biology: Your Life Is in Their Hands. J Am Chem Soc 143:13463–13472.
7. Mulliez E, Ollagnier S, Fontecave M, Eliasson R, Reichard P. 1995. Formate is the hydrogen donor for the anaerobic ribonucleotide reductase from *Escherichia coli*. Proc Natl Acad Sci U S A 92:8759–8762.
8. Wei Y, Li B, Prakash D, Ferry JG, Elliott SJ, Stubbe JA. 2015. A Ferredoxin Disulfide Reductase Delivers Electrons to the *Methanosarcina barkeri* Class III Ribonucleotide Reductase. Biochemistry 54:7019–7028.
9. Torrents E, Sahlin M, Sjöberg BM, 2008 undefined. 2008. The Ribonucleotide Reductase Family-Genetics and Genomics. Ribonucleotides Reductases 17–177.
10. Reichard P, Rutberg L. 1960. Formation of deoxycytidine 5'-phosphate from cytidine 5'-phosphate with enzymes from *Escherichia coli*. BBA - Biochimica et Biophysica Acta 37:554–555.
11. Cotruvo JA, Stubbe J. 2011. Class I ribonucleotide reductases: Metallocofactor assembly and repair *in vitro* and *in vivo*. Annu Rev Biochem 80:733–767.
12. Levitz TS, Drennan CL. 2022. Starting a new chapter on class Ia ribonucleotide reductases. Curr Opin Struct Biol 77.
13. Nordlund P, Reichard P. 2006. Ribonucleotide reductases. Annu Rev Biochem 75:681–706.
14. Rose HR, Maggiolo AO, McBride MJ, Palowitch GM, Pandelia ME, Davis KM, Yennawar NH, Boal AK. 2019. Structures of Class Id Ribonucleotide Reductase Catalytic Subunits Reveal a Minimal Architecture for Deoxynucleotide Biosynthesis. Biochemistry 58:1845–1860.
15. Rose HR, Ghosh MK, Maggiolo AO, Pollock CJ, Blaesi EJ, Hajj V, Wei Y, Rajakovich LJ, Chang WC, Han Y, Hajj M, Krebs C, Silakov A, Pandelia ME, Bollinger JM, Boal AK. 2018. Structural Basis for Superoxide Activation of *Flavobacterium johnsoniae* Class I Ribonucleotide Reductase and for Radical Initiation by Its Dimanganese Cofactor. Biochemistry 57:2679–2693.
16. Blaesi EJ, Palowitch GM, Hu K, Kim AJ, Rose HR, Alapati R, Lougee MG, Kim HJ, Taguchi AT, Tan KO, Laremore TN, Griffin RG, Krebs C, Matthews ML, Silakov A, Bollinger JM, Allen BD, Boal AK. 2018. Metal-free class Ie ribonucleotide reductase from pathogens initiates catalysis with a tyrosinederived dihydroxyphenylalanine radical. Proc Natl Acad Sci U S A 115:10022–10027.

17. Srinivas V, Lebrette H, Lundin D, Kutin Y, Sahlin M, Lerche M, Eirich J, Branca RMM, Cox N, Sjöberg BM, Högbom M. 2018. Metal-free ribonucleotide reduction powered by a DOPA radical in *Mycoplasma* pathogens. Nature 563:416–420.

18. Jordan A, Pontis E, Atta M, Krook M, Gibert I, Barbé J, Reichard P. 1994. A second class I ribonucleotide reductase in Enterobacteriaceae: characterization of the *Salmonella typhimurium* enzyme. Proceedings of the National Academy of Sciences 91:12892–12896.

19. Jordan A, Aragall E, Gibert I, Barbé J. 1996. Promoter identification and expression analysis of *Salmonella typhimurium* and *Escherichia coli nrdEF* operons encoding one of two class I ribonucleotide reductases present in both bacteria. Mol Microbiol 19:777–790.

20. Cotruvo JA, Stubbe J. 2010. An active dimanganese(III)-tyrosyl radical cofactor in *Escherichia coli* class Ib ribonucleotide reductase. Biochemistry 49:1297–1309.

21. Cotruvo JA, Stubbe J. 2011. *Escherichia coli* Class Ib ribonucleotide reductase contains a dimanganese(III)-tyrosyl radical cofactor *in vivo*. Biochemistry 50:1672–1681.

22. Cotruvo JA, Stich TA, Britt RD, Stubbe J. 2013. Mechanism of assembly of the dimanganese-tyrosyl radical cofactor of class Ib ribonucleotide reductase: Enzymatic generation of superoxide is required for tyrosine oxidation via a Mn(III)Mn(IV) intermediate. J Am Chem Soc 135:4027–4039.

23. Stubbe J. 2003. Di-iron-tyrosyl radical ribonucleotide reductases. Curr Opin Chem Biol 7:183–8.

24. Roshick C, Iliffe-Lee ER, McClarty G. 2000. Cloning and Characterization of Ribonucleotide Reductase from *Chlamydia trachomatis*. Journal of Biological Chemistry 275:38111–38119.

25. Högbom M, Stenmark P, Voevodskaya N, McClarty G, Gräslund A, Nordlund P. 2004. The radical site in chlamydial ribonucleotide reductase defines a new R2 subclass. Science (1979) 305:245–248.

26. Jiang W, Yun D, Saleh L, Barr EW, Xing G, Hoffart LM, Maslak M-A, Krebs C, Bollinger JM. 2007. A manganese(IV)/iron(III) cofactor in *Chlamydia trachomatis* ribonucleotide reductase. Science 316:1188–91.

27. Stubbe JA, Seyedsayamdost MR. 2019. Discovery of a New Class i Ribonucleotide Reductase with an Essential DOPA Radical and NO Metal as an Initiator of Long-Range Radical Transfer. Biochemistry 58:435–437.

28. Blakley RL, Barker HA. 1964. Cobamide stimulation of the reduction of ribotides to deoxyribotides in *Lactobacillus leichmannii*. Biochem Biophys Res Commun 16:391–397.

29. Torrents E, Trevisiol C, Rotte C, Hellman U, Martin W, Reichard P. 2006. *Euglena gracilis* Ribonucleotide Reductase. Journal of Biological Chemistry 281:5604–5611.

30. Lundin D, Gribaldo S, Torrents E, Sjöberg BM, Poole AM. 2010. Ribonucleotide reduction - horizontal transfer of a required function spans all three domains. BMC Evol Biol 10:383.

31. Torrents E, Poplawski A, Sjöberg BM. 2005. Two proteins mediate class II ribonucleotide reductase activity in *Pseudomonas aeruginosa*: Expression and transcriptional analysis of the aerobic enzymes. Journal of Biological Chemistry 280:16571–16578.

32. Eliasson R, Pontis E, Jordan A, Reichard P. 1999. Allosteric control of three B12-dependent (class II) ribonucleotide reductases: Implications for the evolution of ribonucleotide reduction. Journal of Biological Chemistry 274:7182–7189.

33. Sintchak MD, Arjara G, Kellogg BA, Stubbe JA, Drennan CL. 2002. The crystal structure of class II ribonucleotide reductase reveals how an allosterically regulated monomer mimics a dimer. Nat Struct Biol 9:293–300.

34. Tamao Y, Blakley RL. 1973. Direct spectrophotometric observation of an intermediate formed from deoxyadenosylcobalamin in ribonucleotide reduction. Biochemistry 12:24–34.

35. Larsson K-M, Logan DT, Nordlund P. 2010. Structural basis for adenosylcobalamin activation in AdoCbl-dependent ribonucleotide reductases. ACS Chem Biol 5:933–42.

36. Lawrence CC, Gerfen GJ, Samano V, Nitsche R, Robins MJ, Rétey J, Stubbe JA. 1999. Binding of Cob(II)alamin to the adenosylcobalamin-dependent ribonucleotide reductase from *Lactobacillus leichmannii*. Identification of dimethylbenzimidazole as the axial ligand. J Biol Chem 274:7039–7042.

37. Licht S, Gerfen GJ, Stubbe J. 1996. Thiyl radicals in ribonucleotide reductases. Science (1979) 271:477–481.

38. Booker S, Licht S, Broderick J, Stubbe JA. 1994. Coenzyme B12-dependent ribonucleotide reductase: evidence for the participation of five cysteine residues in ribonucleotide reduction. Biochemistry 33:12676–12685.

39. Fontecave M, Eliasson R, Reichard P. 1989. Enzymatic Regulation of the Radical Content of the Small Subunit of *Escherichia coli* Ribonucleotide Reductase Involving Reduction of Its Redox Centers. Journal of Biological Chemistry 264:9164–9170.

40. Reichard P. 2002. Ribonucleotide reductases: the evolution of allosteric regulation. Arch Biochem Biophys 397:149–55.

41. Logan DT, Andersson J, Sjöberg BM, Nordlund P. 1999. A glycyl radical site in the crystal structure of a class III ribonucleotide reductase. Science 283:1499–1504.

42. Torrents E, Buist G, Liu A, Eliasson R, Kok J, Gibert I, Gräslund A, Reichard P. 2000. The Anaerobic (Class III) Ribonucleotide Reductase from *Lactococcus lactis*. Journal of Biological Chemistry 275:2463–2471.

43. Torrents E, Eliasson R, Wolpher H, Gräslund A, Reichard P. 2001. The Anaerobic Ribonucleotide Reductase from *Lactococcus lactis*. Journal of Biological Chemistry 276:33488–33494.

44. Tamarit J, Mulliez E, Meier C, Trautwein A, Fontecave M. 1999. The anaerobic ribonucleotide reductase from *Escherichia coli*. The small protein is an activating enzyme containing a [4fe-4s](2+) center. J Biol Chem 274:31291–31296.

45. Sun X, Eliasson R, Pontis E, Andersson J, Buist G, Sjöberg BM, Reichard P. 1995. Generation of the glycyl radical of the anaerobic *Escherichia coli* ribonucleotide reductase requires a specific activating enzyme. J Biol Chem 270:2443–2446.

46. Ollagnier S, Mulliez E, Schmidt PP, Eliasson R, Gaillard J, Deronzier C, Bergman T, Gräslund A, Reichard P, Fontecavet M. 1997. Activation of the anaerobic ribonucleotide reductase from *Escherichia coli*. The essential role of the iron-sulfur center for S-adenosylmethionine reduction. Journal of Biological Chemistry 272:24216–24223.

47. Eliasson R, Fontecave M, Jornvall H, Krook M, Pontis E, Reichard P. 1990. The anaerobic ribonucleoside triphosphate reductase from *Escherichia coli* requires S-adenosylmethionine as a cofactor. Proc Natl Acad Sci U S A 87:3314–3318.

48. Harder J, Eliasson R, Pontis E, Ballinger MD, Reichard P. 1992. Activation of the anaerobic ribonucleotide reductase from *Escherichia coli* by S-adenosylmethionine. Journal of Biological Chemistry 267:25548–25552.

49. Sun X, Ollagnier S, Schmidt PP, Atta M, Mulliez E, Lepape L, Eliasson R, Gräslund A, Fontecave M, Reichard P, Sjöberg BM. 1996. The free radical of the anaerobic ribonucleotide reductase from *Escherichia coli* is at glycine 681. Journal of Biological Chemistry 271:6827–6831.

50. Andersson J, Westman MA, Sahlin M, Sjöberg BM. 2000. Cysteines involved in radical generation and catalysis of class III anaerobic ribonucleotide reductase: A protein engineering study of bacteriophage T4 NrdD. Journal of Biological Chemistry 275:19449–19455.

51. King DS, Reichard P. 1995. Mass spectrometric determination of the radical scission site in the anaerobic ribonucleotide reductase of *Escherichia coli*. Biochem Biophys Res Commun 206:731–5.

52. Torrents E, Eliasson R, Wolpher H, Gräslund A, Reichard P. 2001. The anaerobic ribonucleotide reductase from *Lactococcus lactis*. Interactions between the two proteins NrdD and NrdG. Journal of Biological Chemistry 276:33488–33494.

53. Torrents E, Aloy P, Gibert I, Rodríguez-Trelles F. 2002. Ribonucleotide reductases: Divergent evolution of an ancient enzyme. J Mol Evol 55:138–152.

54. Mulliez E, Ollagnier S, Fontecave M, Eliasson R, Reichard P. 1995. Formate is the hydrogen donor for the anaerobic ribonucleotide reductase from *Escherichia coli*. Proc Natl Acad Sci U S A 92:8759–8762.

55. Wheeler LJ, Rajagopal I, Mathews CK. 2005. Stimulation of mutagenesis by proportional deoxyribonucleoside triphosphate accumulation in *Escherichia coli*. DNA Repair (Amst) 4:1450–1456.

56. Pai C-C, Kearsey SE. 2017. A Critical Balance: dNTPs and the Maintenance of Genome Stability. Genes (Basel) 8.

57. Kumar D, Abdulovic AL, Viberg J, Nilsson AK, Kunkel TA, Chabes A. 2011. Mechanisms of mutagenesis *in vivo* due to imbalanced dNTP pools. Nucleic Acids Res 39:1360–1371.

58. Herrick J, Sclavi B. 2007. Ribonucleotide reductase and the regulation of DNA replication: an old story and an ancient heritage. Mol Microbiol 63:22–34.

59. Mathews CK. 2006. DNA precursor metabolism and genomic stability. The FASEB Journal 20:1300–1314.

60. Larsson KM, Jordan A, Eliasson R, Reichard P, Logan DT, Nordlund P. 2004. Structural mechanism of allosteric substrate specificity regulation in a ribonucleotide reductase. Nat Struct Mol Biol 11:1142–1149.

61. Brown NC, Reichard P. 1969. Role of effector binding in allosteric control of ribonucleoside diphosphate reductase. J Mol Biol 46:39–55.

62. Reichard P. 1993. From RNA to DNA, Why So Many Ribonucleotide Reductases? Science (1979) 260:1773–1777.

63. Eriksson M, Uhlin U, Ramaswamy S, Ekberg M, Regnström K, Sjöberg BM, Eklund H. 1997. Binding of allosteric effectors to ribonucleotide reductase protein R1: Reduction of active-site cysteines promotes substrate binding. Structure 5:1077–1092.

64. Rofougaran R, Vodnala M, Hofer A. 2006. Enzymatically active mammalian ribonucleotide reductase exists primarily as an $\alpha_6\beta_2$ octamer. Journal of Biological Chemistry 281:27705–27711.

65. Ormö M, Sjöberg BM. 1990. An ultrafiltration assay for nucleotide binding to ribonucleotide reductase. Anal Biochem 189:138–141.

66. Ingemarson R, Thelander L. 1996. A kinetic study on the influence of nucleoside triphosphate effectors on subunit interaction in mouse ribonucleotide reductase. Biochemistry 35:8603–8609.

67. Lundin D, Berggren G, Logan DT, Sjöberg B-M. 2015. The origin and evolution of ribonucleotide reduction. Life (Basel) 5:604–36.

68. Augustin LB, Jacobson BA, Fuchs JA. 1994. *Escherichia coli* Fis and DnaA proteins bind specifically to the *nrd* promoter region and affect expression of an nrd-lac fusion. J Bacteriol 176:378–387.

69. Davies BW, Kohanski MA, Simmons LA, Winkler JA, Collins JJ, Walker GC. 2009. Hydroxyurea Induces Hydroxyl Radical-Mediated Cell Death in *Escherichia coli*. Mol Cell 36:845–860.

70. Han JS, Kwon HS, Yim JB, Hwang DS. 1998. Effect of IciA protein on the expression of the *nrd* gene encoding ribonucleoside diphosphate reductase in *E. coli*. Mol Gen Genet 259:610–614.

71. Zheng D, Constantinidou C, Hobman JL, Minchin SD. 2004. Identification of the CRP regulon using *in vitro* and *in vivo* transcriptional profiling. Nucleic Acids Res 32:5874–5893.

72. Cendra M del M, Juárez A, Madrid C, Torrents E. 2013. H-NS is a novel transcriptional modulator of the ribonucleotide reductase genes in *Escherichia coli*. J Bacteriol 195:4255–4263.

73. Tuggle CK, Fuchs JA. 1986. Regulation of the operon encoding ribonucleotide reductase in *Escherichia coli*: evidence for both positive and negative control. EMBO J 5:1077–1085.

74. Jacobson BA, Fuchs JA. 1998. Multiple cis-acting sites positively regulate *Escherichia coil nrd* expression. Mol Microbiol 28:1315–1322.

75. Sun L, Jacobson BA, Dien BS, Srienc F, Fuchs JA. 1994. Cell cycle regulation of the *Escherichia coli nrd* operon: requirement for a cis-acting upstream AT-rich sequence. J Bacteriol 176:2415–2426.

76. Lee YS, Kim H, Hwang DS. 1996. Transcriptional activation of the *dnaA* gene encoding the initiator for *oriC* replication by IciA protein, an inhibitor of *in vitro oriC* replication in *Escherichia coli*. Mol Microbiol 19:389–396.

77. Borovok I, Gorovitz B, Schreiber R, Aharonowitz Y, Cohen G. 2006. Coenzyme B_{12} controls transcription of the *Streptomyces* class Ia ribonucleotide reductase *nrdAB*S operon via a riboswitch mechanism. J Bacteriol 188:2512–2520.

78. Vassinova N, Kozyrev D. 2000. A method for direct cloning of Fur-regulated genes: identification of seven new fur-regulated loci in *Escherichia coli*. Microbiology (Reading) 146 Pt 12:3171–3182.

79. Tolla DA, Savageau MA. 2010. Regulation of aerobic-to-anaerobic transitions by the FNR cycle in *Escherichia coli*. J Mol Biol 397:893–905.

80. Boston T, Atlung T. 2003. FNR-mediated oxygen-responsive regulation of the *nrdDG* operon of *Escherichia coli*. J Bacteriol 185:5310–5313.

81. Crespo A, Pedraz L, van der Hofstadt M, Gomila G, Torrents E. 2017. Regulation of ribonucleotide synthesis by the *Pseudomonas aeruginosa* two-component system AlgR in response to oxidative stress. Scientific Reports 2017 7:1 7:1–15.

82. Crespo A, Pedraz L, Torrents E. 2015. Function of the *Pseudomonas aeruginosa* NrdR Transcription Factor: Global Transcriptomic Analysis and Its Role on Ribonucleotide Reductase Gene Expression. PLoS One 10.

83. Torrents E, Westman MA, Sahlin M, Sjöberg BM. 2006. Ribonucleotide reductase modularity: Atypical duplication of the ATP-cone domain in *Pseudomonas aeruginosa*. Journal of Biological Chemistry 281:25287–25296.

84. Sjöberg BM, Torrents E. 2011. Shift in ribonucleotide reductase gene expression in *Pseudomonas aeruginosa* during infection. Infect Immun 79:2663–2669.

85. Crespo A, Pedraz L, Astola J, Torrents E. 2016. *Pseudomonas aeruginosa* Exhibits Deficient Biofilm Formation in the Absence of Class II and III Ribonucleotide Reductases Due to Hindered Anaerobic Growth. Front Microbiol 7.

86. Crespo A, Gavaldà J, Julián E, Torrents E. 2017. A single point mutation in class III ribonucleotide reductase promoter renders *Pseudomonas aeruginosa* PAO1 inefficient for anaerobic growth and infection. Scientific Reports 2017 7:1 7:1–10.

87. Borovok I, Kreisberg-Zakarin R, Yanko M, Schreiber R, Myslovati M, Åslund F, Holmgren A, Cohen G, Aharonowitz Y. 2002. *Streptomyces spp.* contain class Ia and class II ribonucleotide reductases: Expression analysis of the genes in vegetative growth. Microbiology (N Y) 148:391–404.

88. Rodionov DA, Gelfand MS. 2005. Identification of a bacterial regulatory system for ribonucleotide reductases by phylogenetic profiling. Trends in Genetics 21:385–389.

89. Rozman Grinberg I, Martínez-Carranza M, Bimai O, Nouaïria G, Shahid S, Lundin D, Logan DT, Sjöberg BM, Stenmark P. 2022. A nucleotide-sensing oligomerization mechanism that controls NrdR-dependent transcription of ribonucleotide reductases. Nat Commun 13.

90. Rodionov DA, Gelfand MS. 2005. Identification of a bacterial regulatory system for ribonucleotide reductases by phylogenetic profiling. Trends Genet 21:385–389.

91. Borovok I, Gorovitz B, Yanku M, Schreiber R, Gust B, Chater K, Aharonowitz Y, Cohen G. 2004. Alternative oxygen-dependent and oxygen-independent ribonucleotide reductases in *Streptomyces*: cross-regulation and physiological role in response to oxygen limitation. Mol Microbiol 54:1022–1035.

92. Torrents E, Grinberg I, Gorovitz-Harris B, Lundström H, Borovok I, Aharonowitz Y, Sjöberg BM, Cohen G. 2007. NrdR controls differential expression of the *Escherichia coli* ribonucleotide reductase genes. J Bacteriol 189:5012–5021.

93. Grinberg I, Shteinberg T, Gorovitz B, Aharonowitz Y, Cohen G, Borovok I. 2006. The *Streptomyces* NrdR transcriptional regulator is a Zn ribbon/ATP cone protein that binds to the promoter regions of class Ia and class II ribonucleotide reductase operons. J Bacteriol 188:7635–7644.

94. Mckethan BL, Spiro S. 2013. Cooperative and allosterically controlled nucleotide binding regulates the DNA binding activity of NrdR. Mol Microbiol 90:278–289.

95. Naveen V, Hsiao CD. 2016. NrdR Transcription Regulation: Global Proteome Analysis and Its Role in *Escherichia coli* Viability and Virulence. PLoS One 11.

96. Aravind L, Wolf YI, Koonin E v. 2000. The ATP-cone: An evolutionarily mobile, ATP-binding regulatory domain. J Mol Microbiol Biotechnol 2:191–194.

97. Costerton JW, Geesey GG, Cheng KJ. 1978. How bacteria stick. Sci Am 238:86–95.

98. Stewart PS, Franklin MJ. 2008. Physiological heterogeneity in biofilms. Nat Rev Microbiol 6:199–210.

99. Flemming HC, van Hullebusch ED, Neu TR, Nielsen PH, Seviour T, Stoodley P, Wingender J, Wuertz S. 2022. The biofilm matrix: multitasking in a shared space. Nat Rev Microbiol https://doi.org/10.1038/S41579-022-00791-0.

100. Tseng BS, Zhang W, Harrison JJ, Quach TP, Song JL, Penterman J, Singh PK, Chopp DL, Packman AI, Parsek MR. 2013. The extracellular matrix protects *Pseudomonas aeruginosa* biofilms by limiting the penetration of tobramycin. Environ Microbiol 15:2865–2878.

101. Pezzoni M, Lemos M, Pizarro RA, Costa CS. 2022. UVA as environmental signal for alginate production in *Pseudomonas aeruginosa*: role of this polysaccharide in the protection of planktonic cells and biofilms against lethal UVA doses. Photochem Photobiol Sci 21:1459–1472.

102. O'Toole G, Kaplan HB, Kolter R. 2000. Biofilm formation as microbial development. Annu Rev Microbiol 54:49–79.

103. Gordon V, Bakhtiari L, Kovach K. 2019. From molecules to multispecies ecosystems: The roles of structure in bacterial biofilms. Phys Biol 16.

104. Hogardt M, Hoboth C, Schmoldt S, Henke C, Bader L, Heesemann J. 2007. Stage-specific adaptation of hypermutable *Pseudomonas aeruginosa* isolates during chronic pulmonary infection in patients with cystic fibrosis. Journal of Infectious Diseases 195:70–80.

105. Stewart PS, Costerton JW. 2001. Antibiotic resistance of bacteria in biofilms. Lancet 358:135–138.

106. Davies D. 2003. Understanding biofilm resistance to antibacterial agents. Nat Rev Drug Discov 2:114–122.

107. Lebeaux D, Ghigo J-M, Beloin C. 2014. Biofilm-Related Infections: Bridging the Gap between Clinical Management and Fundamental Aspects of Recalcitrance toward Antibiotics. Microbiology and Molecular Biology Reviews 78:510–543.

108. Percival SL, Suleman L, Vuotto C, Donelli G. 2015. Healthcare-associated infections, medical devices and biofilms: risk, tolerance and control. J Med Microbiol 64:323–334.

109. Kaplan JB. 2011. Antibiotic-induced biofilm formation. International Journal of Artificial Organs 34:737–751.

110. Stoodley P, Sauer K, Davies DG, Costerton JW. 2002. Biofilms as complex differentiated communities. Annu Rev Microbiol 56:187–209.

111. Funari R, Shen AQ. 2022. Detection and Characterization of Bacterial Biofilms and Biofilm-Based Sensors. ACS Sens 7:347–357.

112. Sauer K, Stoodley P, Goeres DM, Hall-Stoodley L, Burmølle M, Stewart PS, Bjarnsholt T. 2022. The biofilm life cycle: expanding the conceptual model of biofilm formation. Nature Reviews Microbiology 2022 20:10 20:608–620.

113. Romeo T. 2008. Bacterial Biofilms: Preface. Curr Top Microbiol Immunol 322.

114. Guttenplan SB, Kearns DB. 2013. Regulation of flagellar motility during biofilm formation. FEMS Microbiol Rev 37:849–871.

115. Flemming HC, Wingender J, Szewzyk U, Steinberg P, Rice SA, Kjelleberg S. 2016. Biofilms: an emergent form of bacterial life. Nat Rev Microbiol 14:563–575.

116. Sakuragi Y, Kolter R. 2007. Quorum-sensing regulation of the biofilm matrix genes (*pel*) of *Pseudomonas aeruginosa*. J Bacteriol 189:5383–5386.

117. Jensen P, Bjarnsholt T, Phipps R, Rasmussen TB, Calum H, Christoffersen L, Moser C, Williams P, Pressler T, Givskov M, Høiby N. 2007. Rapid necrotic killing of polymorphonuclear leukocytes is caused by quorum-sensing-controlled production of rhamnolipid by *Pseudomonas aeruginosa*. Microbiology (Reading) 153:1329–1338.

118. Flemming HC, Wingender J. 2010. The biofilm matrix. Nat Rev Microbiol 8:623–633.

119. Koo H, Allan RN, Howlin RP, Stoodley P, Hall-Stoodley L. 2017. Targeting microbial biofilms: current and prospective therapeutic strategies. Nat Rev Microbiol 15:740–755.

120. Danese PN, Pratt LA, Kolter R. 2000. Exopolysaccharide production is required for development of *Escherichia coli* K-12 biofilm architecture. J Bacteriol 182:3593–3596.

121. Ma L, Conover M, Lu H, Parsek MR, Bayles K, Wozniak DJ. 2009. Assembly and development of the *Pseudomonas aeruginosa* biofilm matrix. PLoS Pathog 5.

122. Kaplan JB. 2010. Biofilm dispersal: mechanisms, clinical implications, and potential therapeutic uses. J Dent Res 89:205–218.

123. Vacca I. 2017. Biofilms: Building up the matrix. Nat Rev Microbiol 15:512–513.

124. Whitchurch CB, Tolker-Nielsen T, Ragas PC, Mattick JS. 2002. Extracellular DNA required for bacterial biofilm formation. Science (1979) 295:1487.

125. Blanco-Cabra N, Movellan J, Marradi M, Gracia R, Salvador C, Dupin D, Loinaz I, Torrents E. 2022. Neutralization of ionic interactions by dextran-based single-chain nanoparticles improves tobramycin diffusion into a mature biofilm. NPJ Biofilms Microbiomes 8.

126. Allesen-Holm M, Barken KB, Yang L, Klausen M, Webb JS, Kjelleberg S, Molin S, Givskov M, Tolker-Nielsen T. 2006. A characterization of DNA release in *Pseudomonas aeruginosa* cultures and biofilms. Mol Microbiol 59:1114–1128.

127. Alhede M, Alhede M, Qvortrup K, Kragh KN, Jensen PØ, Stewart PS, Bjarnsholt T. 2020. The origin of extracellular DNA in bacterial biofilm infections *in vivo*. Pathog Dis 78.

128. Davey ME, Caiazza NC, O'Toole GA. 2003. Rhamnolipid surfactant production affects biofilm architecture in *Pseudomonas aeruginosa* PAO1. J Bacteriol 185:1027–1036.

129. Molin S. 2009. *Pseudomonas*: Model Organism, Pathogen, Cell Factory . Edited by Bernd H. A. Rehm. Weinheim (Germany): Wiley-VCH . $270.00. xxi + 402 p.; ill.; index. 978-3-527-31914-5. 2008. Q Rev Biol 84:204–205.

130. Green SK, Schroth MN, Cho JJ, Kominos SD, Vitanza-Jack VB. 1974. Agricultural plants and soil as a reservoir for *Pseudomonas aeruginosa*. Appl Microbiol 28:987–991.

131. Wagner VE, Iglewski BH. 2008. *P. aeruginosa* Biofilms in CF Infection. Clin Rev Allergy Immunol 35:124–134.

132. Bassetti M, Vena A, Russo A, Croxatto A, Calandra T, Guery B. 2018. Rational approach in the management of *Pseudomonas aeruginosa* infections. Curr Opin Infect Dis 31:578–586.

133. Azam MW, Khan AU. 2019. Updates on the pathogenicity status of *Pseudomonas aeruginosa*. Drug Discov Today 24:350–359.

134. Redman WK, Welch GS, Rumbaugh KP. 2021. Assessing Biofilm Dispersal in Murine Wounds. J Vis Exp https://doi.org/10.3791/62136.

135. Aloush V, Navon-Venezia S, Seigman-Igra Y, Cabili S, Carmeli Y. 2006. Multidrug-resistant *Pseudomonas aeruginosa*: risk factors and clinical impact. Antimicrob Agents Chemother 50:43–48.

136. Gellatly SL, Hancock REW. 2013. *Pseudomonas aeruginosa*: new insights into pathogenesis and host defenses. Pathog Dis 67:159–173.

137. Klockgether J, Cramer N, Wiehlmann L, Davenport CF, Tümmler B. 2011. *Pseudomonas aeruginosa* Genomic Structure and Diversity. Front Microbiol 2:150.

138. Moradali MF, Ghods S, Rehm BHA. 2017. *Pseudomonas aeruginosa* Lifestyle: A Paradigm for Adaptation, Survival, and Persistence. Front Cell Infect Microbiol 7.

139. Hancock REW, Speert DP. 2000. Antibiotic resistance in *Pseudomonas aeruginosa*: Mechanisms and impact on treatment. Drug Resistance Updates 3:247–255.

140. Galán-Vásquez E, Luna B, Martínez-Antonio A. 2011. The Regulatory Network of *Pseudomonas aeruginosa*. Microb Inform Exp 1:3.

141. Arai H. 2011. Regulation and function of versatile aerobic and anaerobic respiratory metabolism in *Pseudomonas aeruginosa*. Front Microbiol 2.

142. Pedraz L, Blanco-Cabra N, Torrents E. 2020. Gradual adaptation of facultative anaerobic pathogens to microaerobic and anaerobic conditions. FASEB J 34:2912–2928.

143. Eschbach M, Schreiber K, Trunk K, Buer J, Jahn D, Schobert M. 2004. Long-term anaerobic survival of the opportunistic pathogen *Pseudomonas aeruginosa* via pyruvate fermentation. J Bacteriol 186:4596–4604.

144. Yoon MY, Lee KM, Park Y, Yoon SS. 2011. Contribution of cell elongation to the biofilm formation of *Pseudomonas aeruginosa* during anaerobic respiration. PLoS One 6.

145. Drenkard E, Ausubel FM. 2002. *Pseudomonas* biofilm formation and antibiotic resistance are linked to phenotypic variation. Nature 416:740–743.

146. King JD, Kocíncová D, Westman EL, Lam JS. 2009. Lipopolysaccharide biosynthesis in *Pseudomonas aeruginosa*. Innate Immun 15:261–312.

147. Vallis AJ, Yahr TL, Barbieri JT, Frank DW. 1999. Regulation of ExoS production and secretion by *Pseudomonas aeruginosa* in response to tissue culture conditions. Infect Immun 67:914–920.

148. Martin DW, Schurr MJ, Mudd MH, Govan JRW, Holloway BW, Deretic V. 1993. Mechanism of conversion to mucoidy in *Pseudomonas aeruginosa* infecting cystic fibrosis patients. Proc Natl Acad Sci U S A 90:8377–8381.

149. Costerton JW, Stewart PS, Greenberg EP. 1999. Bacterial biofilms: A common cause of persistent infections. Science (1979) 284:1318–1322.

150. Lee J, Zhang L. 2015. The hierarchy quorum sensing network in *Pseudomonas aeruginosa*. Protein Cell 6:26–41.

151. Kuchma SL, O'Toole GA. 2022. Surface-Induced cAMP Signaling Requires Multiple Features of the *Pseudomonas aeruginosa* Type IV Pili. J Bacteriol https://doi.org/10.1128/jb.00186-22.

152. Colvin KM, Irie Y, Tart CS, Urbano R, Whitney JC, Ryder C, Howell PL, Wozniak DJ, Parsek MR. 2012. The Pel and Psl polysaccharides provide *Pseudomonas aeruginosa* structural redundancy within the biofilm matrix. Environ Microbiol 14:1913–1928.

153. Nivens DE, Ohman DE, Williams J, Franklin MJ. 2001. Role of alginate and its O acetylation in formation of *Pseudomonas aeruginosa* microcolonies and biofilms. J Bacteriol 183:1047–1057.

154. Damron FH, Goldberg JB. 2012. Proteolytic regulation of alginate overproduction in *Pseudomonas aeruginosa*. Mol Microbiol 84:595–607.

155. Deretic V, Dikshit R, Konyecsni WM, Chakrabarty AM, Misra TK. 1989. The algR gene, which regulates mucoidy in *Pseudomonas aeruginosa*, belongs to a class of environmentally responsive genes. J Bacteriol 171:1278–1283.

156. Hentzer M, Teitzel GM, Balzer GJ, Heydorn A, Molin S, Givskov M, Parsek MR. 2001. Alginate overproduction affects *Pseudomonas aeruginosa* biofilm structure and function. J Bacteriol 183:5395–5401.

157. Reichhardt C, Parsek MR. 2019. Confocal Laser Scanning Microscopy for Analysis of *Pseudomonas aeruginosa* Biofilm Architecture and Matrix Localization. Front Microbiol 10:677.

158. van Schaik EJ, Giltner CL, Audette GF, Keizer DW, Bautista DL, Slupsky CM, Sykes BD, Irvin RT. 2005. DNA binding: A novel function of *Pseudomonas aeruginosa* type IV pili. J Bacteriol 187:1455–1464.

159. Blanco-Cabra N, Paetzold B, Ferrar T, Mazzolini R, Torrents E, Serrano L, LLuch-Senar M. 2020. Characterization of different alginate lyases for dissolving *Pseudomonas aeruginosa* biofilms. Sci Rep 10.

160. Wang S, Liu X, Liu H, Zhang L, Guo Y, Yu S, Wozniak DJ, Ma LZ. 2015. The exopolysaccharide Psl-eDNA interaction enables the formation of a biofilm skeleton in *Pseudomonas aeruginosa*. Environ Microbiol Rep 7:330–340.

161. Wilton M, Wong MJQ, Tang L, Liang X, Moore R, Parkins MD, Lewenza S, Dong TG. 2016. Chelation of Membrane-Bound Cations by Extracellular DNA Activates the Type VI Secretion System in *Pseudomonas aeruginosa*. Infect Immun 84:2355–2361.

162. Baelo A, Levato R, Julian E, Crespo A, Astola J, Gavalda J, Engel E, Mateos-Timoneda MA, Torrents E. 2015. Disassembling bacterial extracellular matrix with DNase-coated nanoparticles to enhance antibiotic delivery in biofilm infections. J Control Release 209:150–158.

163. Yu H, He X, Xie W, Xiong J, Sheng H, Guo S, Huang C, Zhang D, Zhang K. 2014. Elastase LasB of *Pseudomonas aeruginosa* promotes biofilm formation partly through rhamnolipid-mediated regulation. Can J Microbiol 60:227–235.

164. Govan JRW, Deretic V. 1996. Microbial pathogenesis in cystic fibrosis: Mucoid *Pseudomonas aeruginosa* and *Burkholderia cepacia*. Microbiol Rev 60:539–574.

165. Sriramulu DD, Lünsdorf H, Lam JS, Römling U. 2005. Microcolony formation: A novel biofilm model of *Pseudomonas aeruginosa* for the cystic fibrosis lung. J Med Microbiol 54:667–676.

166. Okkotsu Y, Little AS, Schurr MJ. 2014. The *Pseudomonas aeruginosa* AlgZR two-component system coordinates multiple phenotypes. Front Cell Infect Microbiol 4.

167. Leid JG, Willson CJ, Shirtliff ME, Hassett DJ, Parsek MR, Jeffers AK. 2005. The Exopolysaccharide Alginate Protects *Pseudomonas aeruginosa* Biofilm Bacteria from IFN-γ-Mediated Macrophage Killing . The Journal of Immunology 175:7512–7518.

168. Lizewski SE, Schurr JR, Jackson DW, Frisk A, Carterson AJ, Schurr MJ. 2004. Identification of AlgR-regulated genes in *Pseudomonas aeruginosa* by use of microarray analysis. J Bacteriol 186:5672–5684.

169. Mena A, Smith EE, Burns JL, Speert DP, Moskowitz SM, Perez JL, Oliver A. 2008. Genetic adaptation of *Pseudomonas aeruginosa* to the airways of cystic fibrosis patients is catalyzed by hypermutation. J Bacteriol 190:7910–7917.

170. Wozniak DJ, Ohman DE. 1994. Transcriptional analysis of the *Pseudomonas aeruginosa* genes *algR, algB,* and *algD* reveals a hierarchy of alginate gene expression which is modulated by *algT*. J Bacteriol 176:6007–6014.

171. Pritchett CL, Little AS, Okkotsu Y, Frisk A, Cody WL, Covey CR, Schurr MJ. 2015. Expression analysis of the *Pseudomonas aeruginosa* AlgZR two-component regulatory system. J Bacteriol 197:736–748.

172. Leitão JH, Sá-Correia I. 1995. Growth-phase-dependent alginate synthesis, activity of biosynthetic enzymes and transcription of alginate genes in *Pseudomonas aeruginosa*. Arch Microbiol 163:217–222.

173. Whitchurch CB, Alm RA, Mattick JS. 1996. The alginate regulator AlgR and an associated sensor FimS are required for twitching motility in *Pseudomonas aeruginosa*. Proc Natl Acad Sci U S A 93:9839–9843.

174. Whitchurch CB, Erova TE, Emery JA, Sargent JL, Harris JM, Semmler ABT, Young MD, Mattick JS, Wozniak DJ. 2002. Phosphorylation of the *Pseudomonas aeruginosa* response regulator AlgR is essential for type IV fimbria-mediated twitching motility. J Bacteriol 184:4544–4554.

175. Okkotsu Y, Tieku P, Fitzsimmons LF, Churchill ME, Schurr MJ. 2013. *Pseudomonas aeruginosa* AlgR phosphorylation modulates rhamnolipid production and motility. J Bacteriol 195:5499–5515.

176. Wertheim HFL, Melles DC, Vos MC, van Leeuwen W, van Belkum A, Verbrugh HA, Nouwen JL. 2005. The role of nasal carriage in *Staphylococcus aureus* infections. Lancet Infectious Diseases 5:751–762.

177. Tong SYC, Davis JS, Eichenberger E, Holland TL, Fowler VG. 2015. *Staphylococcus aureus* infections: Epidemiology, pathophysiology, clinical manifestations, and management. Clin Microbiol Rev 28:603–661.

178. van Belkum A, Melles DC, Nouwen J, van Leeuwen WB, van Wamel W, Vos MC, Wertheim HFL, Verbrugh HA. 2009. Co-evolutionary aspects of human colonisation and infection by *Staphylococcus aureus*. Infection, Genetics and Evolution 9:32–47.

179. Archer GL. 1998. *Staphylococcus aureus:* A well-armed pathogen. Clinical Infectious Diseases 26:1179–1181.

180. Schlievert PM, Davis CC. 2020. Device-Associated Menstrual Toxic Shock Syndrome. Clin Microbiol Rev 33.

181. Moormeier DE, Bayles KW. 2017. *Staphylococcus aureus* biofilm: a complex developmental organism. Mol Microbiol 104:365–376.

182. Brooks JL, Jefferson KK. 2012. *Staphylococcal* biofilms: quest for the magic bullet. Adv Appl Microbiol 81:63–87.

183. Thomer L, Schneewind O, Missiakas D. 2016. Pathogenesis of *Staphylococcus aureus* Bloodstream Infections. Annual Review of Pathology: Mechanisms of Disease 11:343–364.

184. Mahdally NH, George RF, Kashef MT, Al-Ghobashy M, Murad FE, Attia AS. 2021. Staquorsin: A Novel *Staphylococcus aureus* Agr-Mediated Quorum Sensing Inhibitor Impairing Virulence in vivo Without Notable Resistance Development. Front Microbiol 12:700494.

185. Kong KF, Vuong C, Otto M. 2006. *Staphylococcus* quorum sensing in biofilm formation and infection. International Journal of Medical Microbiology 296:133–139.

186. Zecconi A, Piccinini R, Fox LK. 2003. Epidemiologic study of intramammary infections with *Staphylococcus aureus* during a control program in nine commercial dairy herds. J Am Vet Med Assoc 223:684–688.

187. Balasubramanian D, Harper L, Shopsin B, Torres VJ. 2017. *Staphylococcus aureus* pathogenesis in diverse host environments. Pathog Dis 75.

188. Oliveira D, Borges A, Simões M. 2018. *Staphylococcus aureus* toxins and their molecular activity in infectious diseases. Toxins (Basel) 10.

189. Kane TL, Carothers KE, Lee SW. 2018. Virulence Factor Targeting of the Bacterial Pathogen *Staphylococcus aureus* for Vaccine and Therapeutics. Curr Drug Targets 19:111–127.

190. Gómez MI, O'Seaghdha M, Magargee M, Foster TJ, Prince AS. 2006. *Staphylococcus aureus* protein A activates TNFR1 signaling through conserved IgG binding domains. Journal of Biological Chemistry 281:20190–20196.

191. Fournier B, Philpott DJ. 2005. Recognition of *Staphylococcus aureus* by the innate immune system. Clin Microbiol Rev 18:521–540.

192. Bohach GA, Fast DJ, Nelson RD, Schlievert PM. 1990. Staphylococcal and streptococcal pyrogenic toxins involved in toxic shock syndrome and related illnesses. Crit Rev Microbiol 17:251–272.

193. Clarke SR, Foster SJ. 2006. Surface Adhesins of *Staphylococcus aureus*. Adv Microb Physiol 51:187–224.

194. Cheng AG, McAdow M, Kim HK, Bae T, Missiakas DM, Schneewind O. 2010. Contribution of coagulases towards *Staphylococcus aureus* disease and protective immunity. PLoS Pathog 6:19–20.

195. Jin T, Bokarewa M, Foster T, Mitchell J, Higgins J, Tarkowski A. 2004. *Staphylococcus aureus* resists human defensins by production of staphylokinase, a novel bacterial evasion mechanism. J Immunol 172:1169–1176.

196. Sieprawska-Lupa M, Mydel P, Krawczyk K, Wójcik K, Puklo M, Lupa B, Suder P, Silberring J, Reed M, Pohl J, Shafer W, McAleese F, Foster T, Travis J, Potempa J. 2004. Degradation of human antimicrobial peptide LL-37 by *Staphylococcus aureus*-derived proteinases. Antimicrob Agents Chemother 48:4673–4679.

197. Mandell GL. 1975. Catalase, superoxide dismutase, and virulence of *Staphylococcus aureus*. In vitro and in vivo studies with emphasis on staphylococcal--leukocyte interaction. J Clin Invest 55:561–566.

198. Rooijakkers SHM, Ruyken M, Roos A, Daha MR, Presanis JS, Sim RB, van Wamel WJB, van Kessel KPM, van Strijp JAG. 2005. Immune evasion by a staphylococcal complement inhibitor that acts on C3 convertases. Nat Immunol 6:920–927.

199. Turner NA, Sharma-Kuinkel BK, Maskarinec SA, Eichenberger EM, Shah PP, Carugati M, Holland TL, Fowler VG. 2019. Methicillin-resistant *Staphylococcus aureus:* an overview of basic and clinical research. Nat Rev Microbiol 17:203–218.

200. Levine DP. 2006. Vancomycin: A history. Clinical Infectious Diseases 42.

201. Idrees M, Sawant S, Karodia N, Rahman A. 2021. *Staphylococcus aureus* Biofilm: Morphology, Genetics, Pathogenesis and Treatment Strategies. Int J Environ Res Public Health 18.

202. Cramton SE, Gerke C, Schnell NF, Nichols WW, Götz F. 1999. The intercellular adhesion (*ica*) locus is present in *Staphylococcus aureus* and is required for biofilm formation. Infect Immun 67:5427–5433.

203. Izano EA, Amarante MA, Kher WB, Kaplan JB. 2008. Differential roles of poly-N-acetylglucosamine surface polysaccharide and extracellular DNA in *Staphylococcus aureus* and Staphylococcus epidermidis biofilms. Appl Environ Microbiol 74:470–476.

204. Otto M. 2018. Staphylococcal Biofilms. Microbiol Spectr 6.

205. Joo HS, Otto M. 2012. Molecular basis of *in vivo* biofilm formation by bacterial pathogens. Chem Biol 19:1503–1513.

206. Dengler V, Foulston L, DeFrancesco AS, Losick R. 2015. An Electrostatic Net Model for the Role of Extracellular DNA in Biofilm Formation by *Staphylococcus aureus*. J Bacteriol 197:3779–3787.

207. Kaplan JB. 2010. Biofilm dispersal: mechanisms, clinical implications, and potential therapeutic uses. J Dent Res 89:205–218.

208. Zapotoczna M, McCarthy H, Rudkin JK, O'Gara JP, O'Neill E. 2015. An Essential Role for Coagulase in *Staphylococcus aureus* Biofilm Development Reveals New Therapeutic Possibilities for Device-Related Infections. J Infect Dis 212:1883–1893.

209. Sugimoto S, Sato F, Miyakawa R, Chiba A, Onodera S, Hori S, Mizunoe Y. 2018. Broad impact of extracellular DNA on biofilm formation by clinically isolated Methicillin-resistant and -sensitive strains of *Staphylococcus aureus*. Sci Rep 8.

210. Harris-Tryon TA, Grice EA. 2022. Microbiota and maintenance of skin barrier function. Science 376:940–945.

211. Tomic-Canic M, Burgess JL, O'Neill KE, Strbo N, Pastar I. 2020. Skin Microbiota and its Interplay with Wound Healing. Am J Clin Dermatol 21:36–43.

212. Carvalho AR, Diniz RM, Suarez MAM, Figueiredo CSSS, Zagmignan A, Grisotto MAG, Fernandes ES, da Silva LCN. 2018. Use of some asteraceae plants for the treatment of wounds: From ethnopharmacological studies to scientific evidences. Front Pharmacol 9:784.

213. Zhu J, Zhou H, Gerhard EM, Zhang S, Parra Rodríguez FI, Pan T, Yang H, Lin Y, Yang J, Cheng H. 2023. Smart bioadhesives for wound healing and closure. Bioact Mater 19:360.

214. Wilkinson HN, Hardman MJ. 2020. Wound healing: cellular mechanisms and pathological outcomes: Cellular Mechanisms of Wound Repair. Open Biol 10.

215. Pinto AM, Cerqueira MA, Bañobre-Lópes M, Pastrana LM, Sillankorva S. Bacteriophages for Chronic Wound Treatment: From Traditional to Novel Delivery Systems https://doi.org/10.3390/v12020235.

216. Zhao R, Liang H, Clarke E, Jackson C, Xue M. 2016. Inflammation in chronic wounds. Int J Mol Sci 17.

217. Ladhani HA, Yowler CJ, Claridge JA. 2021. Burn Wound Colonization, Infection, and Sepsis. Surg Infect (Larchmt) 22:44–48.

218. Dowd SE, Delton Hanson J, Rees E, Wolcott RD, Zischau AM, Sun Y, White J, Smith DM, Kennedy J, Jones CE. 2011. Survey of fungi and yeast in polymicrobial infections in chronic wounds. J Wound Care 20:40–47.

219. Rahim K, Saleha S, Zhu X, Huo L, Basit A, Franco OL. 2017. Bacterial Contribution in Chronicity of Wounds. Microb Ecol 73:710–721.

220. Serra R, Grande R, Butrico L, Rossi A, Settimio UF, Caroleo B, Amato B, Gallelli L, de Franciscis S. 2015. Chronic wound infections: The role of *Pseudomonas aeruginosa* and *Staphylococcus aureus*. Expert Rev Anti Infect Ther 13:605–613.

221. Bahamondez-Canas TF, Heersema LA, Smyth HDC. 2019. Current Status of In Vitro Models and Assays for Susceptibility Testing for Wound Biofilm Infections. Biomedicines 7.

222. Attinger C, Wolcott R. 2012. Clinically Addressing Biofilm in Chronic Wounds. Adv Wound Care (New Rochelle) 1:127–132.

223. Fleming D, Chahin L, Rumbaugh K. 2017. Glycoside hydrolases degrade polymicrobial bacterial biofilms in wounds. Antimicrob Agents Chemother2016/11/23. 61.

224. Tognon M, Köhler T, Luscher A, van Delden C. 2019. Transcriptional profiling of *Pseudomonas aeruginosa* and *Staphylococcus aureus* during in vitro co-culture. BMC Genomics 20.

225. Kumar A, Ting YP. 2015. Presence of *Pseudomonas aeruginosa* influences biofilm formation and surface protein expression of *Staphylococcus aureus*. Environ Microbiol2015/05/01. 17:4459–4468.

226. Biswas L, Biswas R, Schlag M, Bertram R, Götz F. 2009. Small-colony variant selection as a survival strategy for *Staphylococcus aureus* in the presence of *Pseudomonas aeruginosa*. Appl Environ Microbiol 75:6910–6912.

227. Orazi G, O'Toole GA. 2017. *Pseudomonas aeruginosa* alters *Staphylococcus aureus* sensitivity to vancomycin in a biofilm model of cystic fibrosis infection. mBio 8.

228. Cendra MDM, Blanco-Cabra N, Pedraz L, Torrents E. 2019. Optimal environmental and culture conditions allow the *in vitro* coexistence of *Pseudomonas aeruginosa* and *Staphylococcus aureus* in stable biofilms. Sci Rep2019/11/11. 9:16284.

229. Cendra MDM, Torrents E. 2021. *Pseudomonas aeruginosa* biofilms and their partners in crime. Biotechnol Adv2021/04/01. 49:107734.

230. Trizna EY, Yarullina MN, Baidamshina DR, Mironova A v., Akhatova FS, Rozhina E v., Fakhrullin RF, Khabibrakhmanova AM, Kurbangalieva AR, Bogachev MI, Kayumov AR. 2020. Bidirectional alterations in antibiotics susceptibility in *Staphylococcus aureus-Pseudomonas aeruginosa* dual-species biofilm. Sci Rep 10.

231. Armbruster CR, Wolter DJ, Mishra M, Hayden HS, Radey MC, Merrihew G, MacCoss MJ, Burns J, Wozniak DJ, Parsek MR, Hoffman LR. 2016. *Staphylococcus aureus* Protein A Mediates Interspecies Interactions at the Cell Surface of *Pseudomonas aeruginosa*. mBio 7.

232. Kirketerp-Moller K, Jensen PO, Fazli M, Madsen KG, Pedersen J, Moser C, Tolker-Nielsen T, Hoiby N, Givskov M, Bjarnsholt T. 2008. Distribution, organization, and ecology of bacteria in chronic wounds. J Clin Microbiol2008/05/30. 46:2717–2722.

233. Fazli M, Bjarnsholt T, Kirketerp-Moller K, Jorgensen B, Andersen AS, Krogfelt KA, Givskov M, Tolker-Nielsen T. 2009. Nonrandom distribution of *Pseudomonas aeruginosa* and *Staphylococcus aureus* in chronic wounds. J Clin Microbiol2009/10/09. 47:4084–4089.

234. Woods J, Boegli L, Kirker KR, Agostinho AM, Durch AM, Delancey Pulcini E, Stewart PS, James GA. 2012. Development and application of a polymicrobial, *in vitro*, wound biofilm model. J Appl Microbiol2012/02/23. 112:998–1006.

235. Kucera J, Sojka M, Pavlik V, Szuszkiewicz K, Velebny V, Klein P. 2014. Multispecies biofilm in an artificial wound bed--A novel model for *in vitro* assessment of solid antimicrobial dressings. J Microbiol Methods2014/06/01. 103:18–24.

236. Gude S, Pinçe E, Taute KM, Seinen AB, Shimizu TS, Tans SJ. 2020. Bacterial coexistence driven by motility and spatial competition. Nature 578:588–592.

237. Dalton T, Dowd SE, Wolcott RD, Sun Y, Watters C, Griswold JA, Rumbaugh KP. 2011. An *in vivo* polymicrobial biofilm wound infection model to study interspecies interactions. PLoS One2011/11/15. 6:e27317.

238. Smith AC, Rice A, Sutton B, Gabrilska R, Wessel AK, Whiteley M, Rumbaugh KP. 2017. Albumin inhibits *Pseudomonas aeruginosa* quorum sensing and alters polymicrobial interactions. Infect Immun 85.

239. Price CE, Brown DG, Limoli DH, Phelan V v., O'Toole GA. 2020. Exogenous Alginate Protects *Staphylococcus aureus* from Killing by *Pseudomonas aeruginosa*. J Bacteriol 202.

240. Pallett R, Leslie LJ, Lambert PA, Milic I, Devitt A, Marshall LJ. 2019. Anaerobiosis influences virulence properties of *Pseudomonas aeruginosa* cystic fibrosis isolates and the interaction with *Staphylococcus aureus*. Sci Rep 9.

241. Thaarup IC, Bjarnsholt T. 2021. Current *In Vitro* Biofilm-Infected Chronic Wound Models for Developing New Treatment Possibilities. Adv Wound Care (New Rochelle) 10:91–102.

242. Sun Y, Dowd SE, Smith E, Rhoads DD, Wolcott RD. 2008. In vitro multispecies Lubbock chronic wound biofilm model. Wound Repair Regen2009/01/09. 16:805–813.

243. DeLeon S, Clinton A, Fowler H, Everett J, Horswill AR, Rumbaugh KP. 2014. Synergistic interactions of </i>Pseudomonas aeruginosa</i> and </i>Staphylococcus aureus</i> in an *in vitro* wound model. Infect Immun2014/08/27. 82:4718–4728.

244. Terry J, Neethirajan S. 2014. A novel microfluidic wound model for testing antimicrobial agents against *Staphylococcus pseudintermedius* biofilms. J Nanobiotechnology 12.

245. Crone S, Garde C, Bjarnsholt T, Alhede M. 2015. A novel *in vitro* wound biofilm model used to evaluate low-frequency ultrasonic-assisted wound debridement. J Wound Care 24:64–72.

246. Pabst B, Pitts B, Lauchnor E, Stewart PS. 2016. Gel-Entrapped *Staphylococcus aureus* Bacteria as Models of Biofilm Infection Exhibit Growth in Dense Aggregates, Oxygen Limitation, Antibiotic Tolerance, and Heterogeneous Gene Expression. Antimicrob Agents Chemother 60:6294–6301.

247. Oates A, Lindsay S, Mistry H, Ortega F, McBain AJ. 2018. Modelling antisepsis using defined populations of facultative and anaerobic wound pathogens grown in a basally perfused biofilm model. Biofouling 34:507–518.

248. Townsend EM, Sherry L, Rajendran R, Hansom D, Butcher J, Mackay WG, Williams C, Ramage G. 2016. Development and characterisation of a novel three-dimensional inter-kingdom wound biofilm model. Biofouling 32:1259–1270.

249. Calum H, Trøstrup H, Laulund AS, Thomsen K, Christophersen L, Høiby N, Moser C. 2022. Murine burn lesion model for studying acute and chronic wound infections. APMIS 130:477–490.

250. Zomer HD, Trentin AG. 2018. Skin wound healing in humans and mice: Challenges in translational research. J Dermatol Sci 90:3–12.

251. Grada A, Mervis J, Falanga V. 2018. Research Techniques Made Simple: Animal Models of Wound Healing. Journal of Investigative Dermatology 138:2095-2105.e1.

252. Williamson DA, Carter GP, Howden BP. 2017. Current and Emerging Topical Antibacterials and Antiseptics: Agents, Action, and Resistance Patterns. Clin Microbiol Rev 30:827.

253. Aslam S. 2008. Effect of antibacterials on biofilms. Am J Infect Control 36:S175.e9-S175.e11.

254. Srivastava P, Sivashanmugam K. 2020. Combinatorial Drug Therapy for Controlling *Pseudomonas aeruginosa* and Its Association With Chronic Condition of Diabetic Foot Ulcer. International Journal of Lower Extremity Wounds 19:7–20.

255. Aguilera-Correa JJ, Gisbert-Garzarán M, Mediero A, Fernández-Aceñero MJ, de-Pablo-Velasco D, Lozano D, Esteban J, Vallet-Regí M. 2022. Antibiotic delivery from bone-targeted mesoporous silica nanoparticles for the treatment of osteomyelitis caused by methicillin-resistant *Staphylococcus aureus*. Acta Biomater https://doi.org/10.1016/J.ACTBIO.2022.10.039.

256. Sharma A, Pócsi I, Weindl G, Pfalzgraff A, Brandenburg K. 2018. Antimicrobial Peptides and Their Therapeutic Potential for Bacterial Skin Infections and Wounds. Frontiers in Pharmacology | www.frontiersin.org 1:281.

257. Redman WK, Welch GS, Rumbaugh KP. 2020. Differential efficacy of glycoside hydrolases to disperse biofilms. Front Cell Infect Microbiol, 20200724th ed. 10:379.

258. Givskov M, de Nys R, Manefield M, Gram L, Maximilien R, Eberl L, Molin Sø, Steinberg PD, Kjelleberg S. 1996. Eukaryotic interference with homoserine lactone-mediated prokaryotic signalling. J Bacteriol 178:6618–6622.

259. Danquah CA, Osei-Djarbeng S, Appiah T, Boakye YD, Adu F, Danquah CA, Osei-Djarbeng S, Appiah T, Boakye YD, Adu F. 2019. Combating Biofilm and Quorum Sensing: A New Strategy to Fight Infections. Bacterial Biofilms https://doi.org/10.5772/INTECHOPEN.89227.

260. Warrier A, Satyamoorthy K, Murali TS. 2021. Quorum-sensing regulation of virulence factors in bacterial biofilm. Future Microbiol 16:1003–1021.

261. Brackman G, Breyne K, de Rycke R, Vermote A, van Nieuwerburgh F, Meyer E, van Calenbergh S, Coenye T. 2016. The Quorum Sensing Inhibitor Hamamelitannin Increases Antibiotic Susceptibility of *Staphylococcus aureus* Biofilms by Affecting Peptidoglycan Biosynthesis and eDNA Release. Sci Rep 6.

262. McVay CS, Velásquez M, Fralick JA. 2007. Phage therapy of *Pseudomonas aeruginosa* infection in a mouse burn wound model. Antimicrob Agents Chemother 51:1934–1938.

263. Moghadam MT, Khoshbayan A, Chegini Z, Farahani I, Shariati A. 2020. Bacteriophages, a New Therapeutic Solution for Inhibiting Multidrug-Resistant Bacteria Causing Wound Infection: Lesson from Animal Models and Clinical Trials. Drug Des Devel Ther 14:1867–1883.

264. Moghadam MT, Khoshbayan A, Chegini Z, Farahani I, Shariati A. 2020. Bacteriophages, a New Therapeutic Solution for Inhibiting Multidrug-Resistant Bacteria Causing Wound Infection: Lesson from Animal Models and Clinical Trials. Drug Des Devel Ther 14:1867.

265. Pires DP, Melo LDR, Vilas Boas D, Sillankorva S, Azeredo J. 2017. Phage therapy as an alternative or complementary strategy to prevent and control biofilm-related infections. Curr Opin Microbiol 39:48–56.

266. Halstead FD, Thwaite JE, Burt R, Laws TR, Raguse M, Moeller R, Webber MA, Oppenheim BA. 2016. Antibacterial Activity of Blue Light against Nosocomial Wound Pathogens Growing Planktonically and as Mature Biofilms. Appl Environ Microbiol 82:4006–4016.

267. Masurkar SA, Chaudhari PR, Shidore VB, Kamble SP. 2012. Effect of biologically synthesised silver nanoparticles on *Staphylococcus aureus* biofilm quenching and prevention of biofilm formation. IET Nanobiotechnol 6:110.

268. Yang X, Ma C. 2016. *In Vitro* Transcription Assays and Their Application in Drug Discovery. J Vis Exp2016/09/30. https://doi.org/10.3791/54256.

269. Kanwal F, Chen T, Zhang Y, Zhang Y, Simair A, Rujie C, Sadaf Zaidi NUS, Guo X, Wei X, Siegel G, Lu C. 2018. Large-Scale *in Vitro* Transcription, RNA Purification and Chemical Probing Analysis. Cell Physiol Biochem2018/08/10. 48:1915–1927.

270. Sanders LH, Rockel A, Lu H, Wozniak DJ, Sutton MD. 2006. Role of *Pseudomonas aeruginosa dinB*-encoded DNA polymerase IV in mutagenesis. J Bacteriol2006/10/17. 188:8573–8585.

271. Lindholm C, Searle R. 2016. Wound management for the 21st century: combining effectiveness and efficiency. Int Wound J2016/07/28. 13 Suppl 2:5–15.

272. Fleming D, Rumbaugh KP. 2017. Approaches to dispersing medical biofilms. Microorganisms 5.

273. Rubio-Canalejas A, Admella J, Pedraz L, Torrents E. 2023. *Pseudomonas aeruginosa* Nonphosphorylated AlgR Induces Ribonucleotide Reductase Expression under Oxidative Stress Infectious Conditions. mSystems https://doi.org/10.1128/MSYSTEMS.01005-22.

274. Blanco-Cabra N, López-Martínez MJ, Arévalo-Jaimes BV, Martin-Gómez MT, Samitier J, Torrents E. 2021. A new BiofilmChip device for testing biofilm formation and antibiotic susceptibility. NPJ Biofilms Microbiomes 7.

275. da Cruz Nizer WS, Inkovskiy V, Versey Z, Strempel N, Cassol E, Overhage J. 2021. Oxidative Stress Response in *Pseudomonas aeruginosa*. Pathogens 10.

276. Rossi F, Cattò C, Mugnai G, Villa F, Forlani F. 2021. Effects of the Quinone Oxidoreductase WrbA on *Escherichia coli* Biofilm Formation and Oxidative Stress. Antioxidants (Basel) 10.

277. Grizanova E v., Semenova AD, Komarov DA, Chertkova EA, Slepneva IA, Dubovskiy IM. 2018. Maintenance of redox balance by antioxidants in hemolymph of the greater wax moth *Galleria mellonella* larvae during encapsulation response. Arch Insect Biochem Physiol 98.

278. Yu H, Boucher JC, Hibler NS, Deretic V. 1996. Virulence properties of *Pseudomonas aeruginosa* lacking the extreme-stress sigma factor AlgU (sigmaE). Infect Immun 64:2774–2781.

279. Hou S, Zhang J, Ma X, Hong Q, Fang L, Zheng G, Huang J, Gao Y, Xu Q, Zhuang X, Song X. 2021. Role of *rgsA* in Oxidative Stress Resistance in *Pseudomonas aeruginosa*. Curr Microbiol 78:3133–3141.

280. Grinberg I, Shteinberg T, Hassan Q, Aharonowitz Y, Borovok I, Cohen G. 2009. Functional analysis of the *Streptomyces coelicolor* NrdR ATP-cone domain: role in nucleotide binding, oligomerization, and DNA interactions. J Bacteriol 191:1169–1179.

281. Dreux N, Cendra M del M, Massier S, Darfeuille-Michaud A, Barnich N, Torrents E. 2015. Ribonucleotide reductase NrdR as a novel regulator for motility and chemotaxis during adherent-invasive *Escherichia coli* infection. Infect Immun 83:1305–1317.

282. Zhang Y, Okada R, Isaka M, Tatsuno I, Isobe KI, Hasegawa T. 2015. Analysis of the roles of NrdR and DnaB from *Streptococcus pyogenes* in response to host defense. APMIS 123:252–259.

283. Naveen V, Hsiao CD. 2016. NrdR Transcription Regulation: Global Proteome Analysis and Its Role in *Escherichia coli* Viability and Virulence. PLoS One 11:e0157165.

284. Ross W, Gourse RL. 2009. Analysis of RNA polymerase-promoter complex formation. Methods2008/10/28. 47:13–24.

285. Giese KC, Michalowski CB, Little JW. 2008. RecA-dependent cleavage of LexA dimers. J Mol Biol2008/02/01. 377:148–161.

286. Groban ES, Johnson MB, Banky P, Burnett PG, Calderon GL, Dwyer EC, Fuller SN, Gebre B, King LM, Sheren IN, von Mutius LD, O'Gara TM, Lovett CM. 2005. Binding of the *Bacillus subtilis* LexA protein to the SOS operator. Nucleic Acids Res2005/11/05. 33:6287–6295.

287. Chandran A v, Srikalaivani R, Paul A, Vijayan M. 2019. Biochemical characterization of *Mycobacterium tuberculosis* LexA and structural studies of its C-terminal segment. Acta Crystallogr D Struct Biol2019/01/16. 75:41–55.

288. Rubio-Canalejas A, Baelo A, Herbera S, Blanco-Cabra N, Vukomanovic M, Torrents E. 2022. 3D spatial organization and improved antibiotic treatment of a *Pseudomonas aeruginosa-Staphylococcus aureus* wound biofilm by nanoparticle enzyme delivery. Front Microbiol 13:959156.

289. Radlinski L, Rowe SE, Kartchner LB, Maile R, Cairns BA, Vitko NP, Gode CJ, Lachiewicz AM, Wolfgang MC, Conlon BP. 2017. Pseudomonas aeruginosa exoproducts determine antibiotic efficacy against Staphylococcus aureus. PLoS Biol2017/11/28. 15:e2003981.

290. Ciofu O, Rojo-Molinero E, Macia MD, Oliver A. 2017. Antibiotic treatment of biofilm infections. APMIS2017/04/14. 125:304–319.

291. Wu J, Zheng Y, Song W, Luan J, Wen X, Wu Z, Chen X, Wang Q, Guo S. 2014. In situ synthesis of silver-nanoparticles/bacterial cellulose composites for slow-released antimicrobial wound dressing. Carbohydr Polym, 20131106th ed. 102:762–771.

292. Fleming D, Redman W, Welch GS, Mdluli N v, Rouchon CN, Frank KL, Rumbaugh KP. 2020. Utilizing glycoside hydrolases to improve the quantitation and visualization of biofilm bacteria. Biofilm, 20200901st ed. 2:100037.

293. Redman WK, Welch GS, Williams AC, Damron AJ, Northcut WO, Rumbaugh KP. 2021. Efficacy and safety of biofilm dispersal by glycoside hydrolases in wounds. Biofilm, 20211113th ed. 3:100061.

294. Vanassche T, Peetermans M, van Aelst LNL, Peetermans WE, Verhaegen J, Missiakas DM, Schneewind O, Hoylaerts MF, Verhamme P. 2013. The role of staphylothrombin-mediated fibrin deposition in catheter-related *Staphylococcus aureus* infections. Journal of Infectious Diseases 208:92–100.

295. Dastgheyb S, Parvizi J, Shapiro IM, Hickok NJ, Otto M. 2015. Effect of biofilms on recalcitrance of staphylococcal joint infection to antibiotic treatment. J Infect Dis2014/09/13. 211:641–650.

296. Andre C, de Jesus Pimentel-Filho N, de Almeida Costa PM, Vanetti MCD. 2019. Changes in the composition and architecture of staphylococcal biofilm by nisin. Braz J Microbiol2019/08/29. 50:1083–1090.

297. Schilcher K, Andreoni F, Dengler Haunreiter V, Seidl K, Hasse B, Zinkernagel AS. 2016. Modulation of *Staphylococcus aureus* biofilm matrix by subinhibitory concentrations of clindamycin. Antimicrob Agents Chemother2016/07/28. 60:5957–5967.

298. Nijland R, Hall MJ, Burgess JG. 2010. Dispersal of biofilms by secreted, matrix degrading, bacterial DNase. PLoS One2010/12/24. 5:e15668.

299. Tetz V v, Tetz G v. 2010. Effect of extracellular DNA destruction by DNase I on characteristics of forming biofilms. DNA Cell Biol2010/05/25. 29:399–405.

300. Blanco-Fernandez B, Castano O, Mateos-Timoneda MA, Engel E, Perez-Amodio S. 2021. Nanotechnology Approaches in Chronic Wound Healing. Adv Wound Care (New Rochelle)2020/04/23. 10:234–256.

301. Ndlovu SP, Fonkui TY, Ndinteh DT, Aderibigbe BA. 2022. Dissolvable wound dressing loaded with silver nanoparticles together with ampicillin and ciprofloxacin. Ther Deliv2022/08/05. 13:295–311.